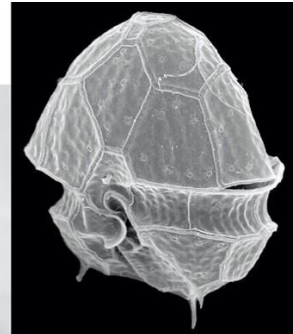Mariana Sofia Oliveira Pandeirada

Evolução de caracteres em dinoflagelados peridinióides: clarificação filogenética para uma classificação estável

Unveiling character evolution in peridinioid dinoflagellates: clarifying phylogeny towards a stable classification
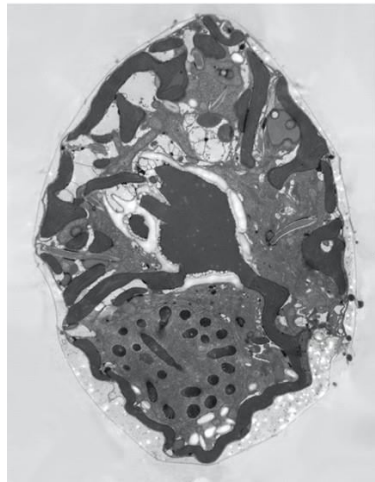
Universidade de Aveiro
2022

Mariana Sofia Oliveira Pandeirada

Evolução de caracteres em dinoflagelados peridinióides: clarificação filogenética para uma classificação estável

Unveiling character evolution in peridinioid dinoflagellates: clarifying phylogeny towards a stable classification

Tese apresentada à Universidade de Aveiro para cumprimento dos requisitos necessários à obtenção do grau de Doutor em Biologia, realizada sob a orientação científica do Doutor António José de Brito Fonseca Mendes Calado, Professor Auxiliar do Departamento de Biologia da Universidade de Aveiro, da Doutora Sandra Carla Fernandes Craveiro Mendes Calado, Investigadora da GeoBioTec – Geobiociências, Geotecnologias e Geoengenharias, Unidade de Investigação da Universidade de Aveiro, e do Doutor Øjvind Moestrup, Professor do Departamento de Biologia da Universidade de Copenhaga

À irmã, pais e avós

o júri/ the jury

presidente/ president

Doutor Tito da Silva Trindade
professor catedrático da Universidade de Aveiro

vogais/ members

Doutor João António de Almeida Serôdio
professor auxiliar com agregação da Universidade de Aveiro

Doutora Lília Maria Antunes dos Santos
professora auxiliar da Universidade de Coimbra

Doutora Ana de Jesus Branco de Melo de Amorim Ferreira
professora auxiliar da Universidade de Lisboa

Doutor António José de Brito Fonseca Mendes Calado (Orientador)
professor auxiliar da Universidade de Aveiro

Doutor Albert Reñé Vicente
investigador, ICM – Institut de Ciènces del Mar – CSIC

resumo

Os dinoflagelados são protistas com características comportamentais e celulares muito particulares, que ocorrem tanto em sistemas marinhos como de água doce. A classificação tradicional dos dinoflagelados, baseada na morfologia celular externa, não é apoiada pelas características ultrastruturais conhecidas actualmente nem pelas filogenias obtidas com base em sequências de DNA. A aplicação conjunta da informação filogenética e ultrastrutural ao grupo dos dinoflagelados com teca organizados conceptualmente à volta do género *Peridinium*, os chamados peridinióides, resultou na alteração da visão da filogenia do grupo, com algumas modificações inesperadas. É necessário o estudo detalhado da ultrastrutura de mais espécies de peridinióides para identificar características do grupo que sejam relevantes no nível filogenético e que possam ajudar a identificar cenários realísticos da evolução de características em dinoflagelados. Neste trabalho, a ultrastrutura de vários dinoflagelados de água doce foi examinada e as respectivas sequências do gene que codifica o ribossoma foram adicionadas em análises filogenéticas. Um dos organismos examinados representa uma nova espécie de *Tovellia*, descrita com o nome *T. rubescens* sp. nov., em alusão à alteração regular da cor destes organismos em cultura, de amarelo-esverdeada para avermelhada (Capítulo 2). A análise detalhada da ultrastrutura de *T. rubescens* sp. nov. permitiu confirmar a estabilidade de várias características ultrastruturais associadas com as Tovelliaceae, um grupo relevante para o conhecimento das características do ancestral dos peridinióides. A descoberta em Portugal de uma espécie de *Sphaerodinium* diferente da anteriormente examinada em detalhe, constituiu a primeira demonstração com técnicas modernas da existência de várias espécies neste género e permitiu confirmar a presença de várias características pouco comuns, estabelecendo-as como características deste género; as características de *Sphaerodinium* são também relevantes para o nosso conhecimento das plesiomorfias em peridinió́dies (Capítulo 3). A observação de um representante de *Parvodinium*, um género proposto em 2008 para reunir organismos anteriormente classificados em *Peridinium* somente com base no tipo de tabulação, possibilitou a caracterização ultrastrutural do género, o que permitirá fazer comparações com outros dinoflagelados da família Peridiniopsidaceae. O estudo detalhado das características ultrastruturais de espécimes do complexo de espécies de *Parvodinium umbonatum*– *P. inconspicuum* (que inclui a espécie tipo do género) permitiu o reconhecimento de características potencialmente típicas de *Parvodinium* que não estão correlacionadas com o arranjo das placas (Capítulo 4). A

Resumo (continuação)

descoberta, num lago da região de Aveiro, de duas populações ligeiramente diferentes de dinoflagelados identificáveis como *Peridiniopsis cunningtonii* permitiram fazer uma re-avaliação das afinidades desta espécie, que revelaram uma maior afinidade com o género *Parvodinium* do que com o género *Peridiniopsis*; é proposta a nova combinação *Parvodinium cunningtonii* comb. nov. e faz-se a descrição de uma nova variedade, *Parvodinium cunningtonii* var. *inerme* var. nov. (Capítulo 5). Estas novas afinidades encontradas para esta espécie destacam a incerteza que ainda permanece em todas as espécies de *Peridinium*, *Peridiniopsis* e *Parvodinium* que ainda não foram examinadas por métodos modernos. No Capítulo 6 são apresentados cenários possíveis de evolução de características em peridinióides, incorporando as características ultrastruturais descritas neste trabalho e destacando a necessidade de estabilização das classificações ao nível de género, família e ordem, e ainda a necessidade de uma revisão sistemática de toda a informação ultrastrutural sobre dinoflagelados que foi adquirida durante os últimos 20 anos.

abstract

Dinoflagellates are a group of protists with unusual behavioural and cellular features, found in both marine and fresh water. The traditional dinoflagellate classification, based mainly on external morphology and features of the cell surface, is not supported by current knowledge on detailed cell ultrastructure combined with DNA-sequence based phylogenies. The application of this combined approach to the group of armoured dinoflagellates traditionally organized around the genus *Peridinium*, the so-called peridinioids, has induced changes in our understanding of the phylogeny of this group, some of them quite unexpected. Detailed ultrastructural examination of further peridinioid species is necessary to identify phylogenetically relevant characters in the group, and to provide realistic scenarios of character evolution in dinoflagellates. In the present work, the fine structure of several freshwater dinoflagellates was examined and rRNA gene sequences added to DNA-based phylogenetic hypotheses. One proved to be a new species of the woloszynskioid genus *Tovellia*, described as *T. rubescens* sp. nov., a name that aludes to the regular colour changes from yellowish-green to reddish observed in cultures of this organism (Chapter 2). The detailed analysis of the ultrastructure of *T. rubescens* afforded the opportunity to confirm the stability of several fine-structural features associated with the Tovelliaceae, a group relevant for the understanding of the features of the ancestral to the peridinioids. The discovery in Portugal of a species of *Sphaerodinium* different from the one previously examined in detail represented the first demonstration of species-level diversity in the genus obtained by modern techniques and allowed the verification of significant, unusual characters that appear to be characteristic of the genus, again with relevance to our understanding of plesiomorphic characters in peridinioids (Chapter 3). The examination of a representative of typical *Parvodinium*, a genus segregated in 2008 from the genus *Peridinium* solely on the basis of amphiesmal plate arrangement, resulted in the addition of a fine-structural identity to the genus that will allow further comparisons to be made within the family Peridiniopsidaceae. Detailed fine-structural examination of specimens of the *Parvodinium umbonatum–P. inconspicuum* species complex (which includes the type of the genus) afforded the recognition of characters potentially typical of the genus, which do not correlate with amphiesmal plate arrangements (Chapter 4). The finding in a nearby lake of two somewhat different populations identifiable as *Peridiniopsis cunningtonii* led to the reassessment of the affinities of this species, which was found to be more related to *Parvodinium* than *Peridiniopsis*; a new combination, *Parvodinium cunningtonii* comb. nov., was proposed, and a new variety was

Abstract (continuation)

described, *Parvodinium cunningtonii* var. *inerme* var. nov. (Chapter 5). These observed affinities highlight the current uncertainty about all species of *Peridinium*, *Peridiniopsis* and *Parvodinium* that have not yet been examined by modern methods. In Chapter 6 tentative scenarios of character evolution in peridinioids are presented, incorporating the newly obtained fine-structural information and highlighting the need for further stabilization of genus, family and order level classifications, and the necessity for a reavaluation of the wealth of fine-structural dinoflagellate features uncovered during the past 20 years.

This thesis includes the following articles:

Pandeirada, M.S., Craveiro, S.C., Daugbjerg, N., Moestrup, Ø., Domingues, P. & Calado, A.J. 2019. Studies on woloszynskioid dinoflagellates X: ultrastructure, phylogeny and color variation in *Tovellia rubescens* n. sp. (Dinophyceae). *Journal of Eukaryotic Microbiology* 66: 937–953 (DOI: 10.1111/jeu.12745) – Chapter 2

Pandeirada, M.S., Craveiro, S.C., Daugbjerg, N., Moestrup, Ø. & Calado, A.J. 2021. Fine-structural characterization and phylogeny of *Sphaerodinium* (Suessiales, Dinophyceae), with the description of an unusual type of freshwater dinoflagellate cyst. *European Journal of Protistology* 78: 125770 (DOI: 10.1016/j.ejop.2021.125770) – Chapter 3

Pandeirada, M.S., Craveiro, S.C., Daugbjerg, N., Moestrup, Ø. & Calado, A.J. 2022. Cell fine structure and phylogeny of *Parvodinium*: towards an ultrastructural characterization of the Peridiniopsidaceae (Dinophyceae). *European Journal of Phycology*, published online (DOI: 10.1080/09670262.2022.2091798) – Chapter 4

Pandeirada, M.S., Craveiro, S.C., Daugbjerg, N., Moestrup, Ø. & Calado, A.J. 2022. Ultrastructure and phylogeny of *Parvodinium cunningtonii* comb. nov. (syn. *Peridiniopsis cunningtonii*) and description of *P. cunningtonii* var. *inerme* var. nov. (Peridiniopsidaceae, Dinophyceae). *European Journal of Protistology*, published online (DOI: 10.1016/j.ejop.2022.125930) – Chapter 5

TABLE OF CONTENTS

CHAPTER 4

CELL FINE STRUCTURE AND PHYLOGENY OF *PARVODINIUM*: TOWARDS AN ULTRASTRUCTURAL CHARACTERIZATION OF THE PERIDINIOPSIDACEAE (DINOPHYCEAE)

CHAPTER 5

ULTRASTRUCTURE AND PHYLOGENY OF *PARVODINIUM CUNNINGTONII* COMB. NOV. (SYN. *PERIDINIOPSIS CUNNINGTONII*) AND DESCRIPTION OF *P. CUNNINGTONII* VAR. *INERME* VAR. NOV. (PERIDINIOPSIDACEAE, DINOPHYCEAE)

CHAPTER 6

LIST OF ABBREVIATIONS

ab/ac, accumulation body

acs, accessory sulcal plate

ALP, apical line of narrow plates

apc, apical pore complex

as, anterior sulcal plate

Astx, astaxanthin

AVE-A-T-n, register number (n) of a new taxon type deposited at the University of Aveiro Herbarium

BA, Bayesian analysis

BB, basal bodies

BS, bootstrap support

bp, base pairs

c, cingulum

Ch/ch, chloroplast lobe

Cc, collecting chamber

cp, cover plate

cob, mitochondrial cytochrome b

cox1, mitochondrial cytochrome c oxidase 1

E/e, eyespot

EAV, elongate narrow vesicle

DNA, deoxyribonucleic acid

GPP complex, Gymnodiniales-Peridiniales-Prorocentrales clade

HgCl₂, mercuric chloride

HPLC-MS and HPLC-MS/MS, high-pressure liquid chromatography combined with mass spectrometry analyses

ICN, international nomenclature code

ITS, internal transcribed spacers of ribosomal operon

LB, longitudinal basal body

LC, layered connective

LF, longitudinal flagellum

LFC, longitudinal flagellar canal

LM, light microscopy

LMR/r1, longitudinal microtubular root

LMR-TBc, connective between LMR and TB

LMR-TBc, connective between LMR and TB

LMR-LSCc, connective between LMR and LSC

LMR-TSCc, connective between LMR and TSC

ls, left sulcal plate

LSC, longitudinal striated collar

LSU rDNA, nuclear DNA sequence that codes for large subunit ribosomal RNA

LSU rRNA, large subunit ribossomal RNA (the 28S strand)

MB, microtubular basket

ML, maximum likelihood

ms, middle sulcal plate

MSP, microtubular strand of the peduncle

MSP1, culture line number 1 defined by Mariana Sofia Pandeirada

N/n, nucleus; **N** also for nitrogen

nd, no detection

nu, nucleolus

O/o, oil droplets or globules

OsO$_4$, osmium tetroxide

P, phosphate or central compound pyrenoid

Pal, pallium

pc, pusule canal

PCR, polymerase chain reaction

PEV, pair of elongated amphiesmal vesicles

Po/po/pp, pore plate

PP, posterior probability

ps, posterior sulcal plate

PSC, peduncle striated collar

pu, pusular tubes

PuN, pusular network

PuS, pusular sheet

Py/py, central pyrenoid complex

RB1, RB2, replicated basal bodies

rDNA, nuclear DNA sequence that codes for ribosomal RNA subunits

rRNA, ribosomal RNA

rs, right sulcal plate

s, sulcus

S, **st**, starch grains

sbc, striated basal body connective

SEM, scanning electron microscopy

SMR/r2, single-stranded microtubular root

SP, sac pusule

sp, sulcal plate

SRC, striated root connective

SSU rDNA, nuclear DNA sequence that codes for small subunit ribosomal RNA

SSU rRNA, small subunit ribosomal RNA (the 18S strand)

Std. dev., standard deviation

sxtA, saxitoxin

TB, transverse basal body

T, transitional plate

t, trichocyst

TEM, transmission electron microscopy

TF, transverse flagellum

TFC, transverse flagellar canal

TMR/r3, transverse microtubular root

TMRE/r3E, transverse microtubular root extension

TSC, transverse striated collar

TSR(M)/r4, transverse striated root and associated microtubule

Tu, (hollow feeding) tube

Vest, vestigial

VF, ventral fibre

vr, ventral ridge

x, canal plate

LIST OF FIGURES

CHAPTER 1

CHAPTER 2

CHAPTER 3

CHAPTER 4

flagellar canal and extending from the ventral area to the centre of the cell. (B) Detail of pusular tube with the enveloping vesicle, showing fenestrations. (C, D) Pusular flattened tubes ramify. (E) Detail of ramified portion of the pusular tube with dotted contents. (F) Tangential section through a pusular tube with dotted content that penetrates the pyrenoid. (G) Pusular vesicle with vesicle including a granulated body, associated to the longitudinal flagellar canal (LFC). …………………………………193

CHAPTER 6

LIST OF TABLES

CHAPTER 1

INTRODUCTION

GENERAL CHARACTERIZATION OF DINOFLAGELLATES

Dinoflagellates are protists primarily unicellular, found widespread across the aquatic systems of earth. They are currently classified in the Alveolata together with the ciliates and apicomplexans, sharing with them the presence of alveoli (or vesicles) underlying the outer membrane of their cell cover (or cell amphiesma). The two heteromorphic flagella (see below) and nuclear traits such as chromosomes permanently condensed, distinguish the dinoflagellates from other Alveolata, and also from most known Eukarya (Fig. 1) (Baldauf 2008; Moestrup & Calado 2018; Adl et al. 2019).

About 4500 species, including extant and fossil, are known so far in the dinoflagellates. About 80% of the species are marine or estuarine and the remaining 20% live in fresh water (Moestrup & Daugbjerg 2007; Hoppenrath 2017; Moestrup & Calado 2018). Most species known are planktonic, while others are benthic or commute between the plankton and the benthos in diel vertical migrations (Hoppenrath et al. 2014). About half of the known species is phototrophic; the others are exclusively heterotrophic or can combine phototrophy and heterotrophy, a condition called mixotrophy. Dinoflagellates include, thus, primary producers and consumers, but also parasites in e.g., ciliates, copepods or other dinoflagellates, or symbionts in e.g., corals (Moestrup & Daugbjerg 2007; Moestrup & Calado 2018). Moreover, dinoflagellates are among the main sources of harmful algal blooms (HABs; e.g., red tides) occurring mainly, but not only, in the marine environment where the HAB species often release potent toxins that can reach humans by being accumulated in the food web (Hoppenrath et al. 2014; Figueroa et al. 2018).

Dinoflagellate motile cells typically have two heteromorphic flagella: the transverse flagellum (TF) is usually located in a transverse groove (the cingulum) that divides the cell in an anterior (or epicone) and a posterior part (or hypocone); and the longitudinal flagellum (LF), extending along a ventral-antapical groove (the sulcus) (Figs 1, 2). Exceptionally, in the Desmomastigales and Prorocentrales, both flagella are apical and there are no grooves (Popovský & Pfiester 1990; Moestrup & Calado 2018).

The cell amphiesma of a dinoflagellate includes vesicles located underneath the plasmalemma, which are either devoid of solid material or enclose plates of variable thickness of a cellulosic or similar polysaccharidic nature. The plates may be thick enough

to be observed in light microscopy (LM), in dinoflagellates called armoured or thecate (Fig. 2a, b), in opposition to so-called naked dinoflagellates, without plates observable in
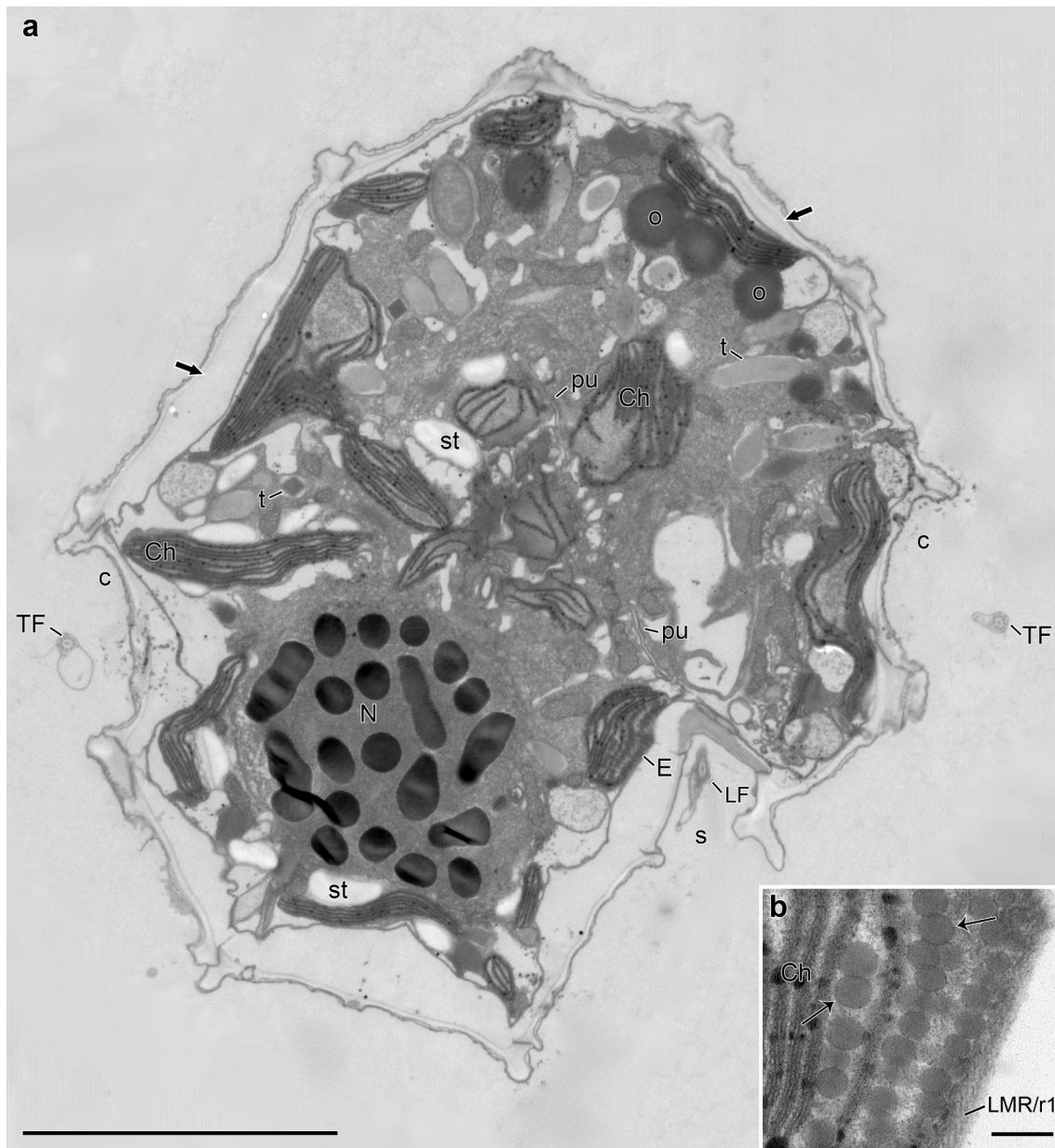
Fig. 1. Ultrastructure of *Parvodinium elpatiewskyi* (Ostenfeld) Kretschmann, Žerdoner Čalasan & Gottschling, a thecate dinoflagellate, TEM. (a) Longitudinal section of the cell seen from the right-ventral side showing some of the typical features of dinoflagellates: transverse (TF) and longitudinal flagella (LF) extending along the cingulum (c) and sulcus (s) respectively; thick thecal plates (arrows) inside the amphiesmal vesicles; eyespot (E) in the sulcal area; chloroplast lobes (Ch), nucleus (N), pusular vesicles (pu), trichocysts (t), oil globules (o) and starch (st). (b) Higher magnification of eyespot with oil globules (arrows) located inside a chloroplast lobe (ch) that underlies the microtubules of the longitudinal microtubular root (LMR/r1). Scale bars: 5 μm in (a); 200 nm in (b). Original.

LM. Alternatively, thin plates in the amphiesmal vesicles may suggest a thin wall-like structure covering the cell in dinoflagellates known as thin-covered (Fig. 2c–e); these individual plates often become visible only after special staining or in scanning electron microscopy (SEM) (Wołoszyńska 1917; Moestrup & Calado 2018).
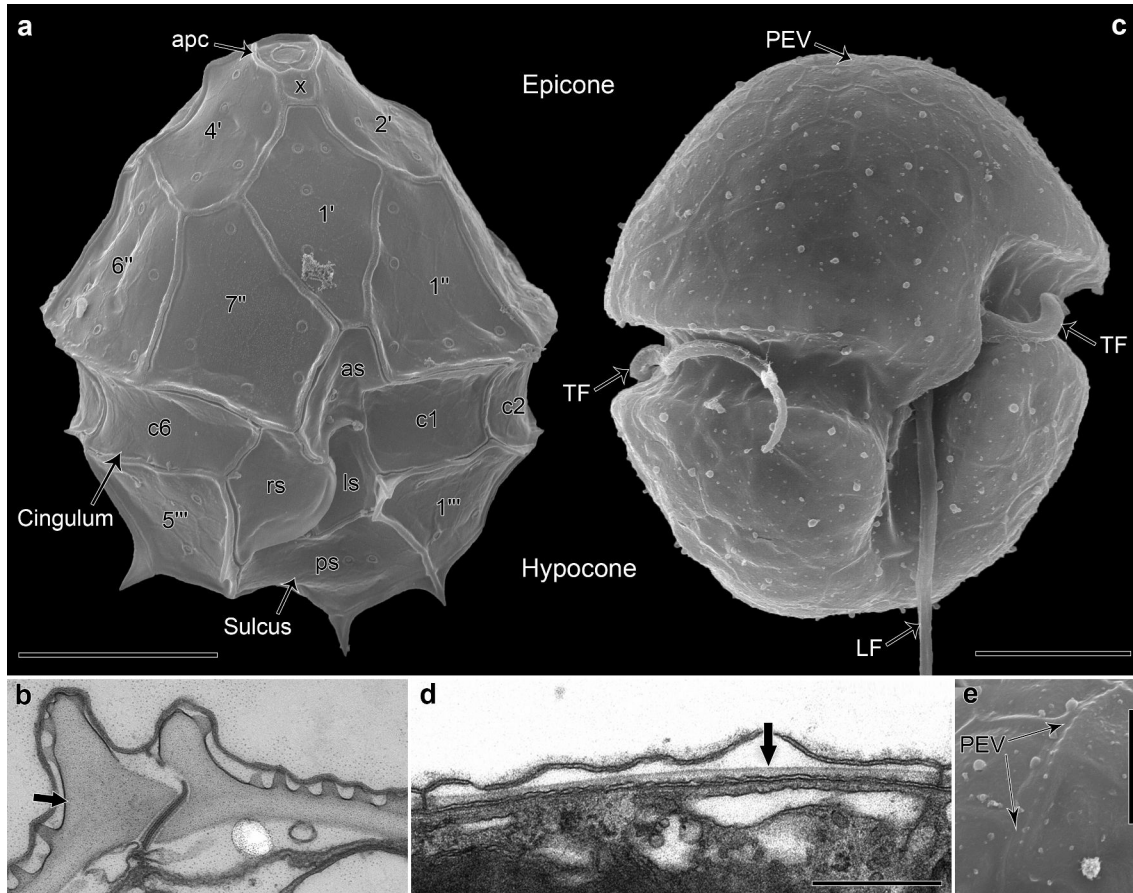
Fig. 2. Thecate and thin-covered dinoflagellates. (a) External morphology of the thecate *Parvodinium* cf. *umbonatum*, SEM. The cingulum divides the cell into an anterior part (epicone) longer than a posterior part (hypocone). Plate labelling based on Kofoidian system, including the cingular and sulcal plates, plus the small canal plate (labeled x) associated to the apical pore complex (apc). (b) Thick thecal plates (arrow) inside amphiesmal vesicles of the thecate *Parvodinium elpatiewskyi,* TEM. (c) External morphology of the thin-covered woloszynskioid *Borghiella andersenii* Daugbjerg, Andreasen, Happel, Pandeirada, Hansen, Craveiro, Calado & Moestrup, SEM. The transverse flagellum (TF) surrounds the cell insde the cingulum, and the longitudinal flagellum (LF) extends posteriorly in front of the sulcus. A pair of elongated amphiesmal vesicles (PEV) is marked in the cell apex. (d) Thin thecal plate (arrow) in an amphiesmal vesicle of *B. andersenii*, TEM. (e) Higher magnification of PEV seen in (c). Scale bars: 5 μm in (a); (b), same scale as (d); 2 μm in (c); 500 nm in (d), (e). All images are original except for (d), which was adapted from Daugbjerg et al. (2014).

The arrangement of plates in armoured dinoflagellates has been the basis of species identification since the late 1800s and is termed plate tabulation or plate formula. The term has been extended to mean the arrangement of amphiesmal vesicles on the cell surface, since there is a continuum between dinoflagellates with 'empty' vesicles and dinoflagellates with more or less thick plates inside the amphiesmal vesicles (Fensome et al. 1993). Among the different tabulation systems proposed so far, it was the one proposed by Kofoid (1907, 1909) that gained universal acceptance, and it has been expanded to include cingular and sulcal plates, plus the smaller plates at the cell apex, in addition to the larger plates covering the cell in transverse rings (or latitudinal series) originally included in Kofoid's system (Fensome et al. 1993; Moestrup & Calado 2018). An example of plate numbering according to the Kofoidian system is given in Fig. 3 for *Theleodinium calcisporum* Craveiro, Pandeirada, Daugbjerg, Moestrup & Calado.

TRADITIONAL DINOFLAGELLATE CLASSIFICATION BASED ON EXTERNAL MORPHOLOGY

In the earliest identifiable accounts of freshwater dinoflagellates, authored by the Dane Otto Friedrich Müller in the 1700s (1773, 1786), several species were treated as animals and assigned to such genera as *Bursaria* and *Vorticella*. The species *Bursaria hirundinella* was reassigned by Schrank (1793) to the genus *Ceratium* Schrank, the oldest generic name of dinoflagellates still in use. Many of the common species and genera of dinoflagellates were described in a series of works published from about 1828, by the celebrated German microscopist Christian Gottfried Ehrenberg. In his most influential work *Die Infusionsthierchen als vollkommene Organismen*, Ehrenberg (1838) assembled the dinoflagellates into the family Peridineae, whose name was based on the genus *Peridinium*, which he had described earlier (Ehrenberg 1830).

Both armoured and naked species were assigned to *Peridinium* by Ehrenberg (1830, 1838). Later, the naked ones were reassigned to the genus *Gymnodinium* by F. Stein (1878), who described numerous new species and genera of dinoflagellates (Stein 1878, 1883). The taxonomic work published up to the 1930s on both marine and freshwater dinoflagellates was extensively compiled in Joseph Schiller's (1933, 1937) contributions to the series *Kryptogamen-flora von Deutschland, Österreich und der Schweiz.*

Throughout this period, most taxa were defined according to their external morphology, including the nature and arrangement of amphiesmal components.
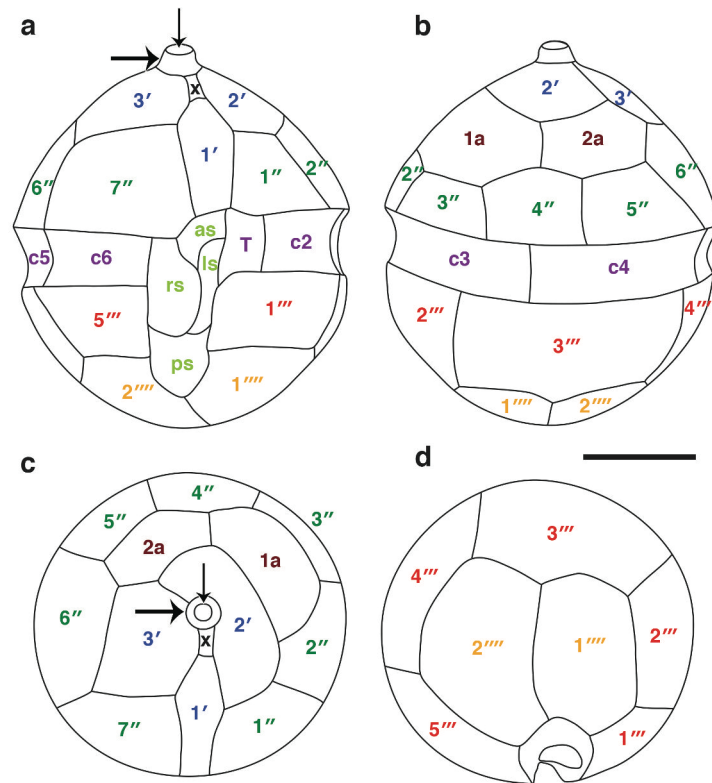
Fig. 3. *Theleodinium calcisporum*, schematic drawings showing morphology and plate arrangement. Kofoidian system used for plate labelling but extended to include the cingular and sulcal plates, plus smaller plates at the cell apex. (a)–(d) Ventral, dorsal, apical and antapical views, respectively. Apical (1′–3′), precingular (1″–7″) and anterior intercalary (1a, 2a) plate series on the epicone. Postcingular (1‴–5‴) and antapical series of plates (1⁗, 2⁗) on the hypocone. The cingulum has six plates: the first is short and invades the sulcus (termed transitional plate, labelled T), and five larger plates (c2–c6). The sulcus has five plates: anterior (as), right (rs), left (ls) and posterior sulcal plates (ps). The thin arrow points to the cover plate (cp) and the thick arrow to the pore plate (pp); x marks the canal plate. Scale bar = 5 μm. Adapted from Craveiro et al. (2013).

The flora of freshwater dinoflagellates by Popovský & Pfiester's (1990) still used the cell external morphology as a determinant criterium and the taxonomic treatment and identification keys of thecate dinoflagellates were based mainly on the number, shape, and arrangement of thecal plates.

In their book *A Classification of Living and Fossil Dinoflagellates*, Fensome et al. (1993) incorporated both extant and fossil species and used a systematic organization still founded mainly on the external morphology. The class Dinophyceae was divided into

subclasses based on the tabulation type and the general morphology of cells or cysts. Fensome et al. (1993) recognized six types of tabulation that were defined as: gymnodiniod type, when many amphiesmal vesicles appeared distributed randomly or in more than 10 latitudinal series, as found in naked species of e.g., *Gymnodinum* F. Stein; suessioid type, when the amphiesmal vesicles enclosed plates and were distributed in more than six but less than eleven latitudinal series, as found in e.g., *Symbiodinium* Gert Hansen & Daugbjerg; gonyaulacoid-peridinioid type, when the amphiesmal vesicles enclosing plates were arranged in five latitudinal series, plus the cingular and longitudinal sulcal series, as in *Peridinium* Ehrenberg, *Peridiniopsis* Lemmermann, *Protoperidinium* Bergh and *Gonyaulax* Diesing; dinophysioid type, as found in species of *Dinophysis* Ehrenberg and *Ornithocercus* F. Stein, with a theca formed by two lateral valves separated by a serrated sagittal suture, and a sulcus and cingulum in a markedly asymmetric position; prorocentroid type, as known mainly from *Prorocentrum* species, in which both cingulum and sulcus were absent and the cell was divided into two large plates and an apical insertion area for the flagella with several platelets; and nannoceratopsioid type, known only for a fossil genus in which the cingulum divided the cell into a dinophysioid hypotheca and a gonyaulacoid-peridinioid epitheca.

MODERN TOOLS FOR DINOFLAGELLATE CLASSIFICATION: A 'TAXONOMIC REVOLUTION'

Molecular phylogenetics

Molecular studies in the dinoflagellates have developed impressively over the last 20–25 years, mainly due to the build-up of phylogenies based on nuclear DNA sequences coding for the ribosomal RNA subunits (rDNA) and intervening spacers (Logares 2007; Kretschmann et al. 2018, 2019). The rDNA sequences are advantageous as they are widespread in eukaryotes with ribosomes, and correspond to the 18S (small subunit, SSU), the 28S (large subunit, LSU) and the 5.8S, plus two internal transcribed spacers (ITS1 and ITS2), located in a single pre-rRNA transcription unit; and to the 5S sequence found in other genome regions. The ITS spacers are less conservative and may offer a different level of discrimination. Also advantageous is the presence of many rDNA copies in the genome of dinoflagellates, to serve as template for genetic amplification (Taylor 2004; Craveiro 2010).

Mitochondrial cytochrome b (cob), mitochondrial cytochrome c oxidase 1 (cox1), saxitoxin (sxtA), HSP90, actin, alpha- and beta-tubulin gene sequences constitute examples of other phylogenetic markers used (Leander & Keeling 2004; Lin et al. 2002; Saldarriaga et al. 2004; Zhang et al. 2005; Orr et al. 2012). Phylogenies based on the alignment of multiple proteins, called phylotranscriptomics, have also been constructed for inferences of dinoflagellate phylogeny (Janouškovec et al. 2017).

Molecular studies have caused a deep change in our understanding of dinoflagellate phylogeny, from the origin of the group and its relationship to other protists, up to the dinoflagellate in-group relationships. All this information was reflected in dinoflagellate classification. The first gene sequence determined for a dinoflagellate, notably the 5S rDNA for *Crypthecodinium cohnii* (Seligo) Javornický (Hinnebusch et al. 1981) led to the abandonment of the Mesocaryota hypothesis that the dinoflagellates were the most primitive eukaryotes based mainly on the lack of histones in their chromosomes (Dodge 1966). Dinoflagellates formed a monophyletic group with apicomplexans and ciliates in later phylogenetic studies (Gajadhar et al. 1991; Van de Peer et al. 1996); the three groups were collectively named Alveolata by Cavalier-Smith (1991). Later, dinoflagellates were found to be more closely related to the apicomplexans than to the ciliates (Van de Peer & De Watcher 1997; Fast et al. 2002).

Phylogenies based on rDNA and on multiprotein gene sequences (e.g., Saunders et al. 1997; Saldarriaga et al. 2001, 2003, 2004) accounted for turning around 'Max' Taylor's (1980) phylogenetic tree, in which most heterotrophic dinoflagellate genera were at the top of the tree and photosynthetic species mainly occupied the basal branches. The inversion placed exclusively heterotrophic species, some free living (e.g., *Noctiluca scintillans* (Macartney) Kofoid) and some parasitic (e.g., the Syndiniales genus *Amoebophrya* Koeppen), at the base of the tree; and resolved the marine *Oxyrrhis marina* Dujardin, also heterotrophic, as a sister taxon to dinoflagellates (Moestrup & Daugbjerg 2007). The placement of *Noctiluca* was, however, not stable in Saldarriaga et al. (2004) rDNA-based phylogenies, either based on SSU, LSU or concatenation of the two. In fact, *Noctiluca*, with trophonts lacking permanently condensed chromosomes, has been resolved at the base but also deeply inside the dinoflagellate group in some phylogenetic trees (e.g., Orr et al. 2012; Janouškovec et al. 2017).

In rDNA-based phylogenies by Saldarriaga et al. (2004) there was a suggestion that the thecate Peridiniales was a paraphyletic group giving rise to important part of thecate but also non-thecate taxa (by repetitive thecal plate losses), which were almost all assembled in a large Gymnodiniales-Peridiniales-Prorocentrales clade, the so-called GPP complex (see also Saunders et al. 1997). With an opposite view, morphological evidence made Taylor (2004) hypothesize that thecate dinoflagellates may have evolved from athecate ones (and the Peridiniales would not be a paraphyletic group), which ended up receiving molecular support in more recent phylogenies that appeared with more support than the ones from Saldarriaga et al. (2004). These more recent phylogenies were enriched in number of taxa and markers analysed (nuclear or mitochondrial DNA, or multiple protein sequences) and it was suggested that the Gymnodiniales were paraphyletic and that a single event of acquisition of thecal plates occurred at the basis of the thecate dinoflagellates (Orr et al. 2012; Janouškovec et al. 2017; Gottschling et al. 2019).

A significant part of the articles published over the last 15 years involving dinoflagellate molecular phylogeny were focused on dinoflagellate subgroups. These works commonly incorporated data from cell ultrastructure (observed in electron microscopy – EM, see below), resulting into a series of descriptions and redefinitions of genera, first in the athecate dinoflagellates but later extending to the thecate forms. A major example of this was the description of the new genera *Akashiwo* Gert Hansen & Moestrup, *Karenia* Gert Hansen & Moestrup and *Karlodinium* J. Larsen, and the redefinition of the genus *Gymnodinium* based on information obtained from LSU rDNA partial sequences and cell ultrastructure (Daugbjerg et al. 2000). The freshwater genus *Woloszynskia* R.H. Thompson, established with thin-covered species earlier classified in *Gymnodinium*, has been extensively revised on the basis of LSU rDNA and ultrastructural data. New genera (e.g., *Tovellia* Moestrup, K. Lindberg & Daugbjerg, *Biecheleria* Moestrup, K. Lindberg & Daugbjerg) and the families Tovelliaceae and Borghiellaceae have been described to include species previously classified in *Woloszynskia* or in closely related taxa, the so-called woloszynskioids (Lindberg et al. 2005; Moestrup et al. 2008, 2009a, b).

In the Peridiniales, or, in a more general sense, peridinioids, the description of new genera and the new family Peridiniopsidaceae have also been the result of phylogenetic analyses using the several parts of the ribosomal operon, either concatenated or in

isolation, and analyses of ultrastructural features of freshwater species of previously placed in *Peridinium* and *Peridiniopsis* (e.g., Calado et al. 2009; Craveiro et al. 2009, 2011, 2016; Gottschling et al. 2017). Systematic positions within the new family Peridiniopsidaceae are, however, in need of further molecular and ultrastructural examination in view of the marked divergences in the external morphology of its members, which combine different plate arrangements with the presence or absence of an apical pore (Gottschling et al. 2017).

The freshwater genus *Sphaerodinium* Wołoszyńska, a peridinioid-looking organism in external morphology, was also the target of LSU rDNA-based phylogenetic study and ultrastructural examination (Craveiro et al. 2010). Surprisingly, the genus was found to be more closely related to the woloszynskioids classified in the order Suessiales (especially species of *Borghiella* Moestrup, Gert Hansen & Daugbjerg, of the family Borghiellaceae) than to peridinioids, appearing as an early diverging branch of the suessialean clade (Craveiro et al. 2010). The genus was placed into the separate family Sphaerodiniaceae, which was assigned to the order Suessiales (Moestrup & Calado 2018).

Scanning and transmission electron microscopy (SEM and TEM)

From the 1960s on, the study of the cell external morphology has been facilitated by the use of the SEM for the observation of small amphiesmal structures that were difficult to observe in LM. In thecate dinoflagellates, the arrangement of plates in the apical pore region, the plate overlap and ornamentation, plus the number of cingular or sulcal plates of several species were unveiled or determined more completely in SEM. This complementary information accounted for many taxa being reassessed and for many new taxa being described with more detail. In the athecate dinoflagellates, SEM observations allowed for an easier separation of thin-covered forms from naked forms. In addition, the amphiesmal organization and the presence of particular types of apical groove or furrow in both thin-covered and naked forms were recognized as relevant taxonomic characters (Daugbjerg et al. 2000; Moestrup et al. 2009b).

Earlier observations in transmission electron microscopy (TEM) date back to the 1950s, and were made on the theca, flagella and on the chromosomes, highlighting the peculiarity of the features of the group and the need for further observations (Pitelka & Schooley 1955; Fott & Ludvík 1956; Grell & Wohlfarth-Bottermann 1957). Reviews on

the general fine-structure of dinoflagellates and on particular features (e.g., chloroplasts, pyrenoids, food reserves and pusules) were published in the 1970s and 1980s (Dodge & Crawford 1971; Dodge 1971, 1972, 1975; Spector 1984; Taylor 1987).

Early descriptions of the flagellar apparatus, including the basal bodies and microtubular roots plus associated fibrous material, were published in the 1960s and 1970s, and were followed by increasingly detailed descriptions in the 1980s. In particular, three-dimensional reconstructions of this complex cell region based on TEM studies of serial sections of cells of e.g., *Oxyrrhis marina*, *Woloszynskia* sp. and *Ceratium furcoides* (Levander) Langhans (Roberts 1985; Roberts & Roberts 1991; Roberts et al. 1992). The flagellar apparatus and other cytoskeleton features were tentatively mapped onto a phylogenetic framework by Roberts (1991).

The general fine-structure of the type species of *Peridinium*, *P. cinctum* (O.F. Müller) Ehrenberg, and *Peridiniopsis*, *P. borgei* Lemmermann, were published by Calado et al. (1999) and Calado & Moestrup (2002) and constitute major comparison points for ultrastructural results that, usually combined with molecular data, have been the foundation of several taxonomic changes in the peridinioids (e.g., Calado et al. 2009; Craveiro et al. 2009, 2016).

In parallel, Daugbjerg et al. (2000) and Lindberg et al. (2005) examined the fine-structure of the naked and thinly thecate dinoflagellates, and combined the information with rDNA-based phylogenies to make taxonomic changes that have served as a basis for posterior studies of these dinoflagellates (e.g., Moestrup et al. 2006, 2008; Hoppenrath et al. 2012; Takano et al. 2014).

Some particular fine-structural features appear to be reliable phylogenetic markers: e.g., eyespot, flagellar apparatus, organization of the cell apex and the ventral microtubular strands that may associate with a peduncle or pallium. Notably, different types of organization of these features have been found in different dinoflagellate taxa, including different genera, families and even orders (Craveiro et al. 2010; Moestrup et al. 2009a, b; Hoppenrath 2017; Moestrup & Calado, 2018).

CELL ULTRASTRUCTURE OF PERIDINIOIDS, WOLOSZYNSKIOIDS AND *SPHAERODINIUM*

Historical notes

A general comparison of peridinioids, woloszynskioids and *Sphaerodinium* is given below, based on known morphological and ultrastructural features. Reviews of these features may be found in Moestrup & Daugbjerg (2007), Hoppenrath (2017), Moestrup & Calado (2018) and Craveiro (2010).

Peridinioids are thecate dinoflagellates with five latitudinal series of plates (including those in the cingulum but excluding incomplete series of intercalary plates) plus plates in the sulcus (in the sense of Taylor 2004). There is often an apical pore, two antapical plates, subequal and relatively large, and a single posterior sulcal plate in the hypotheca. Peridinioids tend to be bilaterally symmetric. This term peridinioids includes organisms classified in the order Peridiniales and Thoracosphaerales (Moestrup & Calado 2018). Taylor (1980) proposed the separation of the gonyaulacoids from the Peridiniales, into the order Gonyaulacales, based primarily on symmetry, but also on sulcal plate organization. This separation has been commonly followed and has received support in several molecular phylogenies (Fensome et al. 1993; Saunders et al. 1997; Janouškovec et al. 2017).

Peridinium and *Peridiniopsis* (as defined in classical floras as Popovský & Pfiester 1990) are the most common peridinioid genera in fresh water, whereas in marine and brackish waters *Heterocapsa* F. Stein, *Scrippsiella* Balech, *Protoperidinium* and *Diplopsalis* Bergh are the common genera. The two latter genera have a peridinioid tabulation but the cingular plates are reduced to three (or four, if a small plate at the cingulum-sulcus is taken as cingular); in addition, *Diplopsalis* (and several closely related genera) may have a single antapical plate and therefore lack a mid-antapical suture (Taylor 2004).

Different combinations in number of cingular plates and the presence or absence of an apical pore also occurred in the freshwater *Peridinium* and *Peridiniopsis* that composed the family Peridiniaceae in e.g., Popovský & Pfiester (1990). In more recent studies, re-examination of species with different combinations of the presence (or absence) of an apical pore and three, five or six cingular plates supported the reclassification of a considerable number of peridinioids at genus and sometimes even at family level. All these species had, notably, a different combination from that of five

cingular plates and no apical pore found in *Peridinium cinctum*, type species of *Peridinium* (and therefore of the family Peridiniaceae).

Former *Peridinium* and *Peridiniopsis* species with an apical pore and six cingular plates proved rather heterogeneous when examined in detail, and several were transferred to other genera, some of them newly described. Examples are: *Tyrannodinium* Calado, Craveiro, Daugbjerg & Moestrup – typified by *Peridinium berolinense* Lemmermann, now *Tyrannodinium edax* (A.J. Schilling) Calado; *Chimonodinium* Craveiro, Calado, Daugbjerg, Gert Hansen & Moestrup – based on *Peridinium lomnickii* Wołoszyńska; and *Apocalathium* Craveiro, Daugbjerg, Moestrup & Calado – typified by *Peridinium aciculiferum* Lemmermann. These new genera were found to be closely related to species of the mainly marine family Thoracosphaeraceae, together with well-known peridinoid taxa like *Scrippsiella* and *Pfiesteria* Steidinger & J.M. Burkholder (Calado et al. 2009; Craveiro et al. 2011, 2016). This combination of cell features is also present in *Theleodinium calcisporum* and in *Naiadinium polonicum* (Wołoszyńska) Carty, two recently established freshwater genera of Thoracosphaeraceae, for which both rDNA-based phylogenetic analyses and information on internal fine structure are available (Craveiro et al. 2013, 2015; Carty 2014).

Another group of species with an apical pore and six plates in the cingulum was segregated from *Peridinium* based on epithecal tabulation: the genus *Parvodinium* Carty, typified by *P. umbonatum* F. Stein, a species notably difficult to separate from several other species in the group, especially *P. inconspicuum* Lemmermann (Carty 2008). Recent phylogenetic analyses including rDNA sequences from members of the *P. umbonatum/inconspicuum* complex have placed *Parvodinium* in a distinct family, the recently described Peridiniopsidaceae (Gottschling et al. 2017; Kretschmann et al. 2018, 2019). As currently conceived, the Peridiniopsidaceae include the genera *Peridiniopsis*, *Parvodinium* and, somewhat surprisingly, the genus *Palatinus* Craveiro, Calado, Daugbjerg & Moestrup, which differs from its family relatives by lacking an apical pore (Calado & Moestrup 2002; Craveiro et al. 2009; Gottschling et al. 2017). Fine-structural information is available for the type species of both *Peridiniopsis* and *Palatinus*, respectively *P. borgei* and *P. apiculatus* (Ehrenberg) Craveiro, Calado, Daugbjerg & Moestrup, making a detailed analysis of the internal organization of *Parvodinium* species necessary if features common to this evolutionary line are to be found. Current

ultrastructural information on *Parvodinium* species does not present enough detail to elucidate relationships (e.g., Seo & Fritz 2002; Zhang et al. 2011).

The woloszynskioids are typically characterized by being covered with numerous thin plates, pentagonal or hexagonal, sometimes forming latitudinal series in a number too high to be described under the Kofoidian system of plate tabulation (Moestrup et al. 2009a, b). These organisms were assembled into the Gymnodiniales and Suessiales by Fensome et al. (1993). In more recent works the woloszynskioids were shown to be polyphyletic. Their consequent reclassification led to the description of several genera assigned to different families: *Tovellia*, *Jadwigia* Moestrup, K. Lindberg & Daugbjerg and *Opisthoaulax* were added to *Bernardinium* Chodat in the family Tovelliaceae (Lindberg et al. 2005; Calado et al. 2006, as *Esoptrodinium* Javornický; Calado 2011; Fawcett & Parrow 2012); *Borghiella* and *Baldinia* Gert Hansen & Daugbjerg were placed in the family Borghiellaceae (Hansen et al. 2007; Moestrup et al. 2008, 2009a); *Prosoaulax* Calado & Moestrup, *Biecheleria*, *Biecheleriopsis* Moestrup, K. Lindberg & Daugbjerg, *Asulcocephalium* Kazuya Takahashi, Moestrup & Iwataki and *Leiocephalium* Kazuya Takahashi, Moestrup & Iwataki were added to the family Suessiaceae (Calado & Moestrup 2005; Moestrup et al. 2009a, b; Takahashi et al. 2015). These extensive taxonomic changes were in great part supported by information obtained from rDNA sequences, and the eyespot and cell apex organization. The families Borghiellaceae and Suessiaceae are currently classified in the Suessiales and appear to be closely related to *Sphaerodinium*, a genus with a peridinioid-looking theca (Craveiro et al. 2010; Moestrup & Calado 2018).

Sphaerodinium includes freshwater, thecate dinoflagellates that correspond to Taylor's (2004) concept of peridinioids, both in bilateral symmetry and plate apparent tabulation. However, *Sphaerodinium* shows more plates in the epi- and hypotheca than the peridinioids, making it morphologically somewhat closer to the woloszynskioids; the outer features of the genus appear intermediate between peridinioids (Craveiro et al. 2010; Moestrup & Calado 2018). However, *Sphaerodinium cracoviense* Wołoszyńska revealed unique ultrastructural features (apical complex, eyespot type, flagellar apparatus) suggesting a relatively isolated evolutionary position of *Sphaerodinium*, although with affinities to peridinioids and woloszynskioids (Craveiro et al. 2010).

Whether the unusual features described from *S. cracoviense* are present in other species described in the genus (which has a confused taxonomy) needs further examination.

Cell apex structure

A characteristic common to many dinoflagellates is the presence of a differentiated structure at the cell apex, which has been found to be phylogenetically significant. In thecate taxa, an apical pore (or apical pore complex) is typically present. It is usually composed of a small, round or elongate 'cover plate' that covers the pore; the ring-shaped 'pore plate', surrounding the cover plate; and the usually rectangular 'canal plate', which contacts the ventral edge of the pore plate (as termed by Dodge & Hermes 1981, based on SEM studies on marine dinoflagellates). Four types of apical pore structure, further divided into sub-types, were distinguished in the past based on the presence or absence of a rim around the pore, the number of sections of the 'apical collar' (i.e., the raised margins of the plates encircling the apical pore) and how far the canal plate extends into the pore plate (Toriumi & Dodge 1993). Fine-structural studies have shown that the cytoplasm near the apical pore generally contains sets of oriented fibers and elongated vesicles (Roberts et al. 1987; Calado & Moestrup 2002; Craveiro et al. 2011, 2013, 2015).

Possession of an apical pore is the most common situation in peridinioids: *Peridinium* subg. *Poroperidinium*, *Parvodinium*, *Protoperidinium*, *Peridiniopsis*, *Tyrannodinium*, *Chimonodinium*, *Theleodinium*, *Naiadinium*, *Scrippsiella*, *Apocalathium*, etc. all have apical pores (Carty 2008, 2014; Calado et al. 2009; Craveiro et al. 2011, 2013, 2015, 2016; Moestrup & Calado 2018). However, an apical pore is absent in *Palatinus* (Craveiro et al. 2009) and in *Peridinium* 'subg. *Cleistoperidinium*' (currently with 8 species, including the type, *P. cinctum*; Moestrup & Calado 2018). In *Naiadinium*, the pore plate is unusual in having an elongate rather than round pore (Craveiro et al. 2015).

An apical furrow is typical of naked and thinly thecate dinoflagellates and its arrangement and structure are considerably variable in these groups. This variation has been found to be phylogenetically relevant: different taxonomic groups (at the ranks of family or order) show different types of apical furrow organization (Daugbjerg et al. 2000; Lindberg et al. 2005; Moestrup & Calado 2018). The apical furrow, more easily observed in SEM but first studied in LM after special staining (Wołoszyńska 1917), has been also called 'acrobase' or 'apical groove' (Biecheler 1952; Takayama 1985).

The families described for the woloszynskioids show divergence in the type of apical furrow organization. In the Tovelliaceae (order Tovelliales), species of *Tovellia* and *Jadwigia* have an apical line of narrow plates (the so-called ALP) that are ornamented with small thickenings (Lindberg et al. 2005; Moestrup et al. 2006; Pandeirada et al. 2014, 2017). In the Borghiellaceae, species of *Borghiella* have a pair of elongated vesicles (PEV), one of which has an axial row of knobs (Fig. 2b, d); however, an apical furrow is absent in *Baldinia* (Hansen et al. 2007; Moestrup et al. 2008; Daugbjerg et al. 2014). The Suessiaceae include species of e.g., *Biecheleria* and *Biecheleriopsis* that show a single, elongate, narrow amphiesmal vesicle (EAV) surrounded by one to several other narrow vesicles; however, species of *Asulcocephalium* and *Leiocephalium* lack an apical furrow (Moestrup et al. 2009a, b; Takahashi et al. 2015).

The apical structure in *Sphaerodinium*, as studied in *S. cracoviense*, suggests a unique organization with links to both peridinioids and woloszynskioids. It contains three small plates (or platelets) surrounded by four apical plates reminiscent of those surrounding the typical apical pore of peridinioids. The middle one of the three platelets is linear and has a furrow with a row of knobs possibly homologous of that of *Biecheleria* and *Biecheleriopsis* (Craveiro et al. 2010).

Chloroplasts and pyrenoids

Eight types of chloroplasts were distinguished in the dinoflagellates by Moestrup & Daugbjerg (2007), each interpreted as being the result of a different endosymbiotic event. Currently, new types of chloroplasts, or variants of the previous eight types (regarding e.g., the shape and distribution in the cell) continue being reported, rendering the dinoflagellates exceptionally diverse among protists in terms of chloroplast diversity (Moestrup & Calado 2018). The typical dinoflagellate chloroplast is believed to have derived from the red algal chloroplast; it has chlorophylls *a* and *c*, and peridinin as the major xanthophyll, conferring it a yellowish-brown or yellowish-green colour. This chloroplast, designated Type 1 in Moestrup & Daugbjerg (2007) or peridinin type Moestrup & Calado (2018), is bounded by three membranes and contains thylakoids mainly in groups of three (Dodge 1975; Keeling 2004). Unusual stacks of disk-shaped portions of thylakoids reminiscent of grana or pseudograna have been found in a few dinoflagellate species apparently unrelated phylogenetically, like the gonyaulacoid

Gonyaulax spinifera (Claparède & J. Lachmann) Diesing and the peridinioid *Theleodinium calcisporum* (Thoracosphaeraceae) (Dodge 1975; Hansen et al. 1996; Craveiro et al. 2013; Takahashi et al. 2015, 2017). The stability of such grana- or pseudograna-like stacks in dinoflagellate species is currently unknown. The finding in the newly described *Kirithra asteri* Boutrup, Tillmann, Daugbjerg & Moestrup (marine, thinly thecate species of Ceratoperidiniaceae) of a strain with up to 45-thylakoid stacks in the chloroplast, which was 100% identical in the LSU rDNA analysed to another strain with only three-thylakoid lamellae, suggests a limited taxonomic value for this feature (Boutrup et al. 2017).

Three different arrangements of chloroplasts were observed in the dinoflagellate groups addressed here:

1) numerous chloroplast lobes found at the cell periphery, lacking well-defined pyrenoids but often with thylakoid-free areas, as in some peridinioids (e.g., *Peridinium cinctum*), Tovelliaceae (e.g., *Jadwigia applanata* Moestrup, K. Lindberg & Daugbjerg), Borghiellaceae (e.g., *Borghiella dodgei* Moestrup, Gert Hansen & Daugbjerg, *B. andersenii* Daugbjerg, Andreasen, Happel, Pandeirada, Gert Hansen, Craveiro, Calado & Moestrup) and *Sphaerodinium cracoviense* (Calado et al. 1999; Lindberg et al. 2005; Moestrup et al. 2008; Craveiro et al. 2010; Daugbjerg et al. 2014);

2) numerous chloroplast lobes radiating from a central area with a pyrenoid complex, as in gonyaulacoids and some Tovelliaceae (e.g., *Tovellia sanguinea* Moestrup, Gert Hansen, Daugbjerg, Flaim & D'Andrea*, T. aveirensis* Pandeirada, Craveiro, Daugbjerg, Moestrup & Calado) and Borghiellaceae (e.g., *Baldinia anauniensis* Gert Hansen & Daugbjerg) (Hansen & Moestrup 1998; Moestrup et al 2006; Hansen et al. 2007; Pandeirada et al. 2014);

3) chloroplasts with well-defined, sometimes stalked, pyrenoids (one or more) that in several cases are lined by starch sheaths, as in the Peridiniopsidaceae (e.g., *Peridiniopsis borgei*, *Palatinus apiculatus, Parvodinium inconspicuum*), in species of *Heterocapsa* and Thoracosphaeraceae (e.g., *Scrippsiella* spp.*, Theleodinium calcisporum, Naiadinium polonicum*), and in Symbiodiniaceae and Suessiaceae (e.g., *Symbiodinium natans* Gert Hansen & Daugbjerg and *Biecheleria* spp.) (Gao & Dodge 1991; Seo & Fritz 2002; Calado & Moestrup 2002; Iwataki et al. 2003; Hansen & Daugbjerg 2009; Moestrup et al. 2009a; Craveiro et al. 2009, 2013, 2015).

Among other chloroplast types occurring in dinoflagellates, some well-known examples are the cryptomonad type (or Type 6) and the fucoxanthin type (or Type 7) (Moestrup & Daugbjerg 2007; Moestrup & Calado 2018). The former type represents a little-modified cryptomonad chloroplast, often characteristically blue; it is found in the widespread gymnodinioid genus *Nusuttodinium* Y. Takano & T. Horiguchi, which includes, among others, the freshwater *Gymnodinium aeruginosum* F. Stein. This chloroplast type has been found to be a so-called kleptochloroplast, and is acquired by engulfment of usually blue cryptomonads, commonly of the genera *Chroomonas* Hansgirg or *Komma* D.R.A. Hill. Its functionality in the dinoflagellate cell is, however, limited to a certain period (from about a week to over a month) before being digested, so that the dinoflagellate needs to take up new cryptomonad cells for replacing the plastids (Takano et al. 2014; Moestrup & Calado 2018).

The *fucoxanthin* type is a diatom-derived chloroplast relatively little modified, containing the yellow or brown carotenoid fucoxanthin. Its presence characterizes the peridinealean family Kryptoperidiniaceae, which includes freshwater species in the genera *Unruhdinium* Gottschling and *Durinskia* Carty & El.R. Cox (McEwan & Keeling 2004; Takano et al. 2008; Moestrup & Calado 2018).

Storage products and non-photosynthetic pigments

The main storage product of dinoflagellates is starch that may accumulate in large amounts in the cytoplasm, especially if cells grow in intense light. Lipid globules are also common, and some may be sufficiently large to be mistaken for eyespots, especially if tinged with carotenoid pigments (Moestrup & Calado 2018). A rare pigment is the carotenoid astaxanthin, known to occur in the genus *Tovellia*, notably in the red species *T. sanguinea* and *T. diexiensis* Qi Zhang & G.X. Liu, which are capable of forming blooms that may tinge the water red (Moestrup et al. 2006; Zhang et al. 2016). These species clustered together in LSU rDNA-based phylogenies, with *T. coronata* (Wołoszyńska) Moestrup, K. Lindberg & Daugbjerg as sister taxon; *Tovellia coronata* is also known to develop a red colour but the responsible pigment has not been identified (Lindberg et al. 2005; Zhang et al. 2016). Numerous 'carotenoid droplets' or 'red-pigmented bodies' were observed by LM in these three *Tovellia* species, and indicated as the cause of the unusual colour by masking the colour of the chloroplasts. The 'red-

pigmented bodies' in *T. sanguinea* were linked to cell aggregates and smaller bodies observed in TEM (Moestrup et al. 2006). These resembled the lipid bodies that have been interpreted as the location of accumulated astaxanthin-related compounds in green algal species that cause the phenomenon of red snow (Remias et al. 2016), and in industrially relevant species of *Chlorella* Beijerinck and *Haematoccocus* Flotow (Santos & Mesquita 1984; Mulders et al. 2015).

Eyespot

An eyespot has been found in several freshwater and marine dinoflagellates, typically located underneath the sulcal area, in association with the longitudinal microtubular root (LMR = root 1) of the flagellar apparatus (Moestrup et al. 2008; Moestrup & Calado 2018). This cell organelle is typically seen as red or orange in LM, and is assumed to play a similar role in cell phototaxis as the one demonstrated for other algal groups (Colley & Nilsson 2016; Moestrup & Calado 2018). Dinoflagellates lacking an eyespot are e.g., gonyaulacoids, heterotrophic peridinioids (*Tyrannodinium edax*), *Heterocapsa pygmaea* A.R. Loeblich, R.J. Schmidt & Sherley and species of *Apocalathium* (Wedemayer & Wilcox 1984; Bullman & Roberts 1986; Craveiro et al. 2016).

The eyespot structure is phylogenetically significant in dinoflagellates. Five different morphological types were distinguished by Moestrup & Daugbjerg (2007) and labelled Types A–E. A sixth type was added by Craveiro et al. (2010, Type F). This represents a marked contrast to the algal groups, in which a single eyespot type is usually shared by all members of a class or even phylum (Moestrup et al. 2008).

The least unusual eyespot type in dinoflagellates, the Type A, resembles the eyespot of many algal groups in being composed of osmiophilic globules located inside a chloroplast lobe, near the cell surface (visible in a chloroplast lobe facing the sulcus in Fig. 1). This type is common in the Peridiniales and Thoracosphaerales (Calado et al. 1999; Craveiro et al. 2009, 2011, 2015). Type B is similar but overlain by a layer of vesicles with brick-like material on the sulcus side. It occurs in several species of the family Borghiellaceae, and is also found in *Peridiniopsis borgei* (Calado & Moestrup 2002; Hansen et al. 2007; Moestrup et al. 2008). Type C is also composed of osmiophilic globules but these are extraplastidial and not surrounded by membranes. It is exclusive of the Tovelliaceae (Lindberg et al. 2005; Calado 2011; Pandeirada et al. 2014). Type D

only occurs in the peridinialean family Kryptoperidiniaceae, in e.g., *Kryptoperidinium foliaceum* (J. Stein) Er. Lindemann and *Durinskia baltica* (Levander) Carty & El.R. Cox, and is interpreted as a transformed chloroplast of red algal origin, from which thylakoids have been lost and only osmiophilic globules remain; the functional chloroplasts in these species originate from diatoms (Horiguchi & Pienaar 1994; Horiguchi 2003, 2004). Type E is, like type C, extraplastidial but lacks osmiophilic globules, being composed of several layers of crystal-like (or brick-like) units lined by membranes; it is exclusive of the Suessiaceae and Symbiodiniaceae (Moestrup et al. 2009a, b; Takahashi et al. 2015). Type F was found in *Sphaerodinium*, is also extraplastidial and not surrounded by membranes, and consists of a single layer of crystal-like units overlying more or less fused oil globules (Craveiro et al. 2010).

Pusule

This is an organelle so far confined to the dinoflagellates, originally named by Schütt (1895). In LM, it may look like a vesicle, sometimes quite voluminous. In TEM, it often appears a complex system of vesicles, tubes or canals lined by three membranes resulting from a vesicle wrapped around a more or less extensive invagination of a flagellar canal (Craveiro et al. 2016; Moestrup & Calado 2018).

The pusular organization has also been found to vary extensively in dinoflagellates, with seven types distinguished in an early review by Dodge (1972). Other variations have been reported more recently, and others perhaps remain to be uncovered as the detailed description of the components and locations in the cell of pusular elements is notoriously difficult (Moestrup & Calado 2018). The phylogenetic significance of the pusule has been difficult to resolve, in part perhaps as a result of an inadequate systematization of the pusular components and their distribution in cells. In some cases there seems to be a demonstrable regularity in the pusular description of all members of a dinoflagellate group. An example is seen in the Tovelliaceae, in which a well-defined, cylindrical, convoluted tube with roundish diverticula is internally lined by electron-opaque, elongate bodies along part of its length (e.g., Lindberg et al. 2005; Calado 2011; Pandeirada et al. 2014). In contrast, the elongated duct extending from a flagellar canal to an internal collecting chamber with numerous pusular tubes that was found in *Naiadinium polonicum* (Thoracosphaerales) seems unlikely to be homologous with an apparently similar one

found in *Sphaerodinium cracoviense* (Suessiales) (Craveiro et al. 2011, 2015). The pusules found in other Thoracosphaerales, as in *Chimonodinium*, *Theleodinium* or *Apocalathium*, showed common points in their organization and lacked large vesicles (so-called sac pusules) connected to the flagellar canals as in other peridinioids (Calado et al. 1999; Calado & Moestrup 2002; Craveiro et al. 2010, 2011, 2013, 2016).

Flagellar apparatus

A large number of components form the flagellar apparatus of dinoflagellates (Fig. 4 is a schematic representation of the flagellar apparatus of *Theleodinium calcisporum*, as an example of a peridinioid type of organization). Several components are present in most taxa, whereas others vary in different species.

All dinoflagellates have two basal bodies (transverse, TB, and longitudinal, LB) with a variable angle of insertion. In the peridinioids the angle is often 80–90°, as in *Peridiniopsis borgei* and *T. calcisporum*; however, it is much smaller, ca. 20°, in *Heterocapsa pygmaea*, and it is 60–65° in both *Peridinium cinctum* and *Naiadinium polonicum* (Thoracosphaerales) (Bullman & Roberts 1986; Calado et al. 1999; Calado & Moestrup 2002; Craveiro et al. 2013, 2015). In the Tovelliaceae, Borghiellaceae and Suessiaceae the angle is larger than 90°, and in gonyaulacoids it varies from 90° to over 145° (Hansen et al. 1996; Calado et al. 2006; Hansen & Daugbjerg 2009; Daugbjerg et al. 2014). Angles reaching almost 180° were found in several naked dinoflagellates, as in *Gymnodinium cryophilum* (G.J. Wedemayer, L.W. Wilcox & L.E. Graham) Gert Hansen & Moestrup and *Amphidinium rhynchocephalum* Anisimova (Wilcox et al. 1982; Farmer & Roberts 1989).

Three flagellar apparatus microtubular roots are widespread in dinoflagellates: the longitudinal microtubular root (LMR, r1 in Moestrup 2000), the transverse microtubular root (TMR, r3 in Moestrup 2000), and the transverse striated root and associated microtubule (TSRM, r4 in Moestrup 2000).

The LMR/r1 is a strand of a variable number of microtubules (typically more than 15 in peridinioids) that extends from the proximal-left side of the LB toward the posterior side of the cell, along the ventral surface, and eventually lining the amphiesmal vesicles underneath the sulcus. The TMR/r3 is composed of a single microtubule that associates with the anterior-proximal side of the TB, extending from a parallel orientation relative

to the basal body to a roughly anterior-dorsal orientation in the cell. The TMR/r3 usually nucleates one or several rows of 12–35 microtubules (forming the transverse microtubular root extension, TMRE/r3E) that generally project to the dorsal side of the cell.

Several aspects of the TMRE/r3E have been found to differ among peridinioids, even among taxa that appear closely related in molecular phylogenies. For example, part of the TMRE/r3E associates with a fibre and adopts a cylindrical configuration in *Peridiniopsis borgei*, a feature not detected in other Peridiniopsidaceae. Unexpectedly, a less complete association with fibrous material was found associated with the TMRE/r3E in the thoracosphaeracean *Chimonodinium lomnickii* (Calado & Moestrup 2002; Craveiro et al. 2009, 2011). The elaborated TMRE of *Peridinium cinctum*, formed by at least five rows of microtubules nucleated by a TMR looping around the flagellar canal and sac pusule, has not been found in other peridinioids (Calado et al. 1999); whether this feature is present in close relatives of this species is unknow and calls for further detailed observations in the group. Variants of this root extension outside the peridinioids include the several undulating rows that follow a pusule canal in *Sphaerodinium* (Craveiro et al. 2010), and the association with the nuclear fibrous connective, extending from the dorsal face of the LMR/r1 to the ventral surface of the nucleus, found in the gymnodinioid genus *Lepidodinium* M.M. Watanabe, S. Suda, I. Inouye, T. Sawaguchi & Chihara (Hansen & Moestrup 2005).

The third widespread component of the flagellar apparatus, the TSR, is normally associated with the dorsal-posterior surface of the TB and extends nearly parallel to the TB toward the striated collar that limits the external opening of the TFC. A single microtubule (TSRM) commonly accompanies the TSR, diverging from it proximally (Roberts et al. 1995; Calado & Moestrup 2002; Hansen & Daugbjerg 2009).

A single-stranded microtubular root (SMR, r2 in Moestrup 2000) may be present on the right side of the LB, oriented nearly parallel to the proximal part of the LMR/r1. It has been found in most peridinioids studied in detail and in several gonyaulacoids, but not in *Peridiniella catenata* (Levander) Balech (Hansen & Moestrup 1998). Outside peridinioids and gonyaulacoids, the SMR was reported in *Baldinia anauniensis* (Hansen et al. 2007).

Fig. 4. Schematic reconstruction of the flagellar base area of *Theleodinium calcisporum*, seen from the cell's left. The transverse and longitudinal striated collars, encircling the exits points of the flagella, are transparent to allow observation of underlying structures. LMR-TBc, fibrous connective between the longitudinal microtubular root (root 1) and the transverse basal body. Adapted from Craveiro et al. (2013).

The basal bodies in several dinoflagellate groups may connect with each other by means of fibrous structures. In peridinioids, a fibrous layered connective (LC) typically links the posterior-proximal side of the TB with the proximal end of the LB, and connects

the two roots LMR/r1 and TSR near their proximal ends (e.g., Calado et al. 1999; Calado & Moestrup 2002; Craveiro et al. 2009, 2013, 2016). The LC has not been found in other dinoflagellate groups. Most other dinoflagellates studied in detail, including *Sphaerodinium cracoviense*, display a fibrous connective (the striated root connective, SRC or r1–r4 connective) linking the TSR and the LMR/r1 (e.g., Calado et al. 1998, 2006; Craveiro et al. 2010; Calado 2011; Daugbjerg et al. 2014). The SRC is absent in peridinioids except for *Heterocapsa pygmaea* that revealed both a 'bilayered connective' resembling an LC and an SRC (Bullman & Roberts 1986).

In addition, the basal bodies may contact the LMR/r1 through more or less simple connectives, which vary between groups. Connectives between the LB and the ventral side of the LMR/r1 are unknown in both peridinioids and gonyaulacoids (except for *Ceratium furcoides*; Roberts 1989) but are common in woloszynskioids, e.g., *Bernardinium bernardinense* Chodat, *Baldinia anauniensis* and *Symbiodinium natans*, and are also present in *Sphaerodinium cracoviense*; most of these connectives are very thin and link individual triplets of the LB to several microtubules of the LMR (Calado et al., 2006; Hansen et al. 2007; Hansen & Daugbjerg 2009; Craveiro et al. 2010). One or more connectives can link the TB and the dorsal side of the LMR (TB-LMRc), as in some peridinioids and gonyaulacoids, e.g., *Peridiniopsis borgei* and *Protoceratium reticulatum* (Claparède & J. Lachmann) Buetschli, and in Borghiellaceae, e.g., *Borghiella dodgei* and *Baldinia anauniensis*. These so-called bi- or three-armed connectives are unknown in the Tovelliaceae and Suessiaceae (Hansen et al. 1997, 2007; Calado & Moestrup 2002; Moestrup et al. 2008). A 'ventral fibre' is present in the *Sphaerodinium cracoviense*, *Baldinia anauniensis* and *Dactylodinium pterobelotum* Kazuya Takahashi, Moestrup & Iwataki, extending ventrally from the right-anterior side of the LB. Both *S. cracoviense* and *B. anauniensis* have quite distinctive, conspicuous membranous bodies with hexagonal units in a honeycomb pattern (also named lamellar bodies) in the flagellar base area, perhaps with a function in phototaxis (Hansen et al. 2007; Craveiro et al. 2010; Takahashi et al. 2017).

The flagellar canals are commonly bordered by striated, complete or incomplete collars near the area where each flagellum exits the cell, designated transverse and longitudinal striated collars (TSC and LSC). In gonyaulacoids and some peridinioids the collars are linked by one or more fibrous connectives (Hansen et al. 1997; Calado &

Moestrup 2002; Craveiro et al. 2009, 2016). Moreover, the collars of several woloszynskioids, e.g., *Borghiella dodgei* and *Jadwigia applanata*, and of *Sphaerodinium cracoviense*, associate with a fibrous structure supporting a ventral ridge (Roberts et al. 1995; Moestrup et al. 2008; Craveiro et al. 2010).

Feeding apparatus and homologous structures

Many of the dinoflagellates studied in detail displayed one or several microtubular strands in the ventral area, near the flagellar apparatus but without connection to any flagellar roots. In the heterotrophic pfiesteriaceans, e.g., *Pfiesteria piscicida* Steidinger & J.M. Burkholder and *Tyrannodinium edax*, a feeding tube is supported by several such rows of microtubules (16 rows in *P. piscicida* and over 20 in *T. edax*), which overlap at the edges and are accompanied by elongated electron-opaque vesicles, forming the 'microtubular basket' (MB; Calado & Moestrup 1997; Litaker et al. 2002). A MB and sometimes a small peduncle have been found in several Thoracosphaerales with chloroplasts, e.g., *Chimonodinium lomnickii*, *Theleodinium calcisporum* and *Naiadinium polonicum*, although direct evidence of feeding activity (and so, of mixotrophy) in these species is still lacking (Craveiro et al. 2011, 2013, 2015; Moestrup & Calado 2018). In contrast, no MB or any other peduncle-related microtubular strands (see below) were found in *Scrippsiella trochoidea*, *Apocalathium aciculiferum* (Lemmermann) Craveiro, Daugbjerg, Moestrup & Calado and *A. malmogiense* (G. Sjöstedt) Craveiro, Daugbjerg, Moestrup & Calado. This was interpreted as a possible loss of this character in a group of species with MB-containing ancestors (Craveiro et al. 2016).

Alternatively to the MB, many species contain a single row of microtubules, which are sometimes accompanied by electron-opaque vesicles – the microtubular strand of the peduncle (MSP). The vesicles with electron-opaque contents have been interpreted as containing digestive enzymes to be added to a forming food vacuole, or to an accumulation body. A MSP was documented in Tovelliaceae (*Tovellia* species and *Esoptrodinium*), Symbiodiniaceae (*Symbiodinium natans*) and Borghiellaceae (*Baldinia anauniensis*) (Lindberg et al. 2005; Calado et al. 2006; Hansen et al. 2007; Hansen & Daugbjerg 2009). A particular type of MSP was found in *Peridiniopsis borgei*, comprising a single strand of 75–80 microtubules on the ventral side (located near elongated electron-opaque vesicles), which divided into two and then into four

progressively smaller strands along its long path inside the cell; the four groups of microtubules (totaling a similar number as the MSP in the ventral area) ended in a mid-dorsal region of the cell, between the pyrenoid and the large sac pusule connected with the LFC (Calado & Moestrup 2002). In many other dinoflagellates, the MSP is not accompanied by electron-opaque vesicles, although it is presumed homologous to other MSPs for which an association with a feeding peduncle was demonstrated (Hansen et al. 1996. These presumably non-functional MSPs (at least not functional for feeding) have been found in several distantly related dinoflagellate groups, as in the gonyaulacoids *Gonyaulax spinifera* and *Protoceratium reticulatum*, in the peridinioid *Palatinus apiculatus*, and in *Sphaerodinium cracoviense* (Hansen et al. 1996, 1997; Craveiro et al. 2009, 2010). In these cases, no protruded peduncle was found.

Direct engulfment of prey cells may also occur in some dinoflagellates, with or without participation of microtubular strands and peduncles. Moreover, digestion in situ of preys by a thin cytoplasmic layer extruded from the ventral area (the so-called pallium) is known in the family Protoperidiniaceae (Moestrup & Calado 2018).

OBJECTIVES OF THE WORK

The combination of detailed cell ultrastructure with DNA sequence-based phylogenies has led to major changes to dinoflagellate classification over the past two decades. The application of this combined approach to the peridinioids has induced significant changes in our understanding of phylogenies, some of them quite unexpected. The present Ph.D. work is primarily focused on species with phylogenetic affinities in need of further clarification, especially those currently classified in the peridinioid genera *Parvodinium* and *Peridiniopsis*.

As in other dinoflagellate groups, some characters are found to be present in some peridinioids and are absent in others in a pattern which is not easily fitted to any current view on the phylogenetic relationships of the species involved. Distinguishing what constitutes multiple losses of characters and what represents independent acquisition of characters is strongly dependent on (1) the set of characters present in the ancestor of the group and (2) the stability of each character. The detailed examination of a thecate species of the unusual genus *Sphaerodinium* and of a species of the thin-covered genus *Tovellia* provide the opportunity of evaluating the stability of fine-structural characters in species

that belong to groups, which are thought to share a 'recent' (in terms of the origin of the group) common ancestor with the peridinioids (Tovelliales and Suessiales); it is intended to shed light on both aspects (1) and (2) above, i.e. what features were present in the ancestor to the peridinioids and how stable are the features we find in these groups. Several of the potentially relevant features are found in the morphologically complex area surrounding the flagellar bases. Identifying which fine-structural features are stable (i.e. phylogenetically informative) and adding these key features to phylogenetic scenarios is expected to contribute to stabilize dinoflagellate taxonomy, and to help define the boundaries among taxa of peridinioid dinoflagellates.

Objectives of the work:

- Improving the knowledge on dinoflagellate ultrastructure through SEM and TEM analyses of peridinioids and their potential sister groups;
- Increasing the database of comparable gene sequences obtained from reliably identified dinoflagellates, by means of an extended sequencing of the ribosomal operon, including SSU, LSU and ITS rDNA;
- Inferring the phylogenetic affinities of peridinioid dinoflagellates from morphological, ultrastructural and molecular data;
- Identifying potential phylogenetic markers of distinct groups of peridinoid dinoflagellates by mapping key fine-structural features onto rDNA phylogenies;
- Effecting taxonomic and nomenclatural changes where needed.

REFERENCES

Adl S.M., Bass D., Lane C.E., Lukeš J., Schoch C.L., Smirnov A., Agatha S., Berney C., Brown M.W., Burki F. et al. 2019. Revisions to the classification, nomenclature, and diversity of eukaryotes. *Journal of Eukaryotic Microbiology* 66: 4–119.

Baldauf S.L. 2008. An overview of the phylogeny and diversity of eukaryotes. *Journal of Systematics and Evolution* 46: 263–273.

Biecheler B. 1952. Recherches sur les Péridiniens. *Bulletin Biologique de la France et de la Belgique, Suppl.* 36: VI + 149 pp.

Boutrup P.V., Moestrup Ø., Tillmann U. & Daugbjerg N. 2017. Ultrastructure and phylogeny of *Kirithra asteri* gen. et sp. nov. (Ceratoperidiniaceae, Dinophyceae) — a free-living, thin-walled marine photosynthetic dinoflagellate from Argentina. *Protist* 168: 586–611.

Bullman V. & Roberts K.R. 1986. Structure of the flagellar apparatus in *Heterocapsa pygmaea* (Pyrrophyta). *Phycologia* 25: 558–571.

Calado A.J. 2011. On the identity of the freshwater dinoflagellate *Glenodinium edax*, with a discussion on the genera *Tyrannodinium* and *Katodinium*, and the description of *Opisthoaulax* gen. nov. *Phycologia* 50: 641–649.

Calado A.J. & Moestrup Ø. 1997. Feeding in *Peridiniopsis berolinensis* (Dinophyceae): new observations on tube feeding by an omnivorous, heterotrophic dinoflagellate. *Phycologia* 36: 47–59.

Calado A.J. & Moestrup Ø. 2002. Ultrastructural study of the type species of *Peridiniopsis*, *Peridiniopsis borgei* (Dinophyceae), with special reference to the peduncle and flagellar apparatus. *Phycologia* 41: 567–584.

Calado A.J. & Moestrup Ø. 2005. On the freshwater dinoflagellates presently included in the genus *Amphidinium*, with a description of *Prosoaulax* gen. nov. *Phycologia* 44: 112–119.

Calado A.J., Craveiro S.C. & Moestrup Ø. 1998. Taxonomy and ultrastructure of a freshwater, heterotrophic *Amphidinium* (Dinophyceae) that feeds on unicellular protists. *Journal of Phycology* 34: 536–554.

Calado A.J., Hansen G. & Moestrup Ø. 1999. Architecture of the flagellar apparatus and related structures in the type species of *Peridinium*, *P. cinctum* (Dinophyceae). *European Journal of Phycology* 34: 179–191.

Calado A.J., Craveiro S.C., Daugbjerg N. & Moestrup Ø. 2006. Ultrastructure and LSU rDNA-based phylogeny of *Esoptrodinium gemma* (Dinophyceae), with notes on feeding behavior and the description of the flagellar base area of a planozygote. *Journal of Phycology* 42: 434–452.

Calado A.J., Craveiro S.C., Daugbjerg N. & Moestrup Ø. 2009. Description of *Tyrannodinium* gen. nov., a freshwater dinoflagellate closely related to the marine Pfiesteria-like species. *Journal of Phycology* 45: 1195–1205.

Colley N.J. & Nilsson D. 2016. Photoreception in phytoplankton. *Integrative and Comparative Biology* 56: 764–775.

Carty S. 2008. *Parvodinium* gen. nov. for the Umbonatum group of *Peridinium* (Dinophyceae). *Ohio Journal of Science* 108: 103–107.

Carty S. 2014. *Freshwater dinoflagellates of North America*. Cornell University Press, Ithaca & London, 260 pp.

Craveiro S.C. 2010. *Ultrastructure and phylogeny of peridinioid dinoflagellates*. PhD thesis, Aveiro University, Portugal, 204 pp.

Craveiro S.C., Calado A.J., Daugbjerg N. & Moestrup Ø. 2009. Ultrastructure and LSU rDNA-based revision of *Peridinium* group palatinum (Dinophyceae) with the description of *Palatinus* gen. nov. *Journal of Phycology* 45: 1175–1194.

Craveiro S.C., Moestrup Ø., Daugbjerg N. & Calado A.J. 2010. Ultrastructure and large subunit rDNA-based phylogeny of *Sphaerodinium cracoviense*, an unusual freshwater dinoflagellate with a novel type of eyespot. *Journal of Eukaryotic Microbiology* 57: 568–585.

Craveiro S.C., Calado A.J., Daugbjerg N., Hansen G. & Moestrup Ø. 2011. Ultrastructure and LSU rDNA-based phylogeny of *Peridinium lomnickii* and description of *Chimonodinium* gen. nov. (Dinophyceae). *Protist* 162: 590–615.

Craveiro S.C., Pandeirada M.S., Daugbjerg N., Moestrup Ø. & Calado A.J. 2013. Ultrastructure and phylogeny of *Theleodinium calcisporum* gen. et sp. nov., a freshwater dinoflagellate that produces calcareous cysts. *Phycologia* 52: 488–507.

Craveiro S.C., Daugbjerg N., Moestrup Ø. & Calado A.J. 2015. Fine-structural characterization and phylogeny of *Peridinium polonicum*, type species of the recently described genus *Naiadinium* (Dinophyceae). *European Journal of Protistology* 51: 259–279.

Craveiro S.C., Daugbjerg N., Moestrup Ø. & Calado A.J. 2016. Studies on *Peridinium aciculiferum* and *Peridinium malmogiense* (=*Scrippsiella hangoei*): comparison with *Chimonodinium lomnickii* and description of *Apocalathium* gen. nov. (Dinophyceae). *Phycologia* 56: 21–35.

Daugbjerg N., Hansen G., Larsen J. & Moestrup Ø. 2000. Phylogeny of some of the major genera of dinoflagellates based on ultrastructure and partial LSU rDNA sequence data, including the erection of three new genera of unarmoured dinoflagellates. *Phycologia* 39: 302–317.

Daugbjerg N., Andreasen T., Happel E., Pandeirada M.S., Hansen G., Craveiro S.C., Calado A.J. & Moestrup Ø. 2014. Studies on woloszynskioid dinoflagellates VII: description of

Borghiella andersenii sp. nov.: light and electron microscopy and phylogeny based on LSU rDNA. *European Journal of Phycology* 49: 436–449.

Dodge J.D. 1966. The Dinophyceae. In: *The chromosomes of the algae* (Ed. by M.B.E Godward), Edward Arnold, London, pp. 96–115.

Dodge J.D. 1971. Fine structure of the Pyrrophyta. *Botanical Review* 37: 481–508.

Dodge J.D. 1972. The ultrastructure of the dinoflagellate pusule: A unique osmo-regulatory organelle. *Protoplasma* 75: 285–302.

Dodge J.D. 1975. A survey of chloroplast ultrastructure in the Dinophyceae. *Phycologia* 14: 253–263.

Dodge J.D. & Crawford, R.M. 1970. The morphology and fine structure of *Ceratium hirundinella*. *Journal of Phycology* 6: 137–149.

Dodge J.D. & Crawford R.M. 1971. A fine-structural survey of dinoflagellate pyrenoids and food-reserves. *Botanical Journal of the Linnean Society* 64: 105–115.

Dodge J.D. & Hermes H.B. 1981. A scanning electron microscopical sudy of the apical pores of marine dinoflagellates (Dinophyceae). *Phycologia* 20: 424–430.

Ehrenberg C.G. 1830. Beiträge zur Kenntniss der Organisation der Infusorien und ihrer geographischen Verbreitung, besonders in Sibiren. *Abhandlungen der Königlichen Akademie der Wissenschaften zu Berlin, Physikalische-Mathematische Klasse* 1830: 1–88, pls 1–8. (The journal issue was published in 1832, but was preceded by a separatum released in 1830).

Ehrenberg C.G. 1838. *Die Infusionsthierchen als volkommene Organismen. Ein Blick in das tiefere organische Leben der Natur.* Leopold Voss, Leipzig, Germany, 547 pp., 64 pls.

Farmer M.A. & Roberts K.R. 1989. Comparative analyses of the dinoflagellate flagellar apparatus. III. Freeze substitution of *Amphidinium rhynchocephalum*. *Journal of Phycology* 25: 280–292.

Fast N.M., Xue L., Bingham S. & Keeling P.J. 2002. Re-examining alveolate evolution using multiple protein molecular phylogenies. *Journal of Eukaryotic Microbiology* 49: 30–37.

Fawcett R.C. & Parrow M.W. 2012. Cytological and phylogenetic diversity in freshwater *Esoptrodinium/Bernardinium* species (Dinophyceae). *Journal of Phycology* 48: 793–807.

Fensome R.A., Taylor F.J.R., Norris G., Sarjeant W.A.S., Wharton D.I. & Williams G.L. 1993. A classification of living and fossil dinoflagellates. *Micropaleontology, Special Publication* 7: 1–351.

Figueroa R.I., Estrada M. & Garcés E. 2018. Life histories of microalgal species causing harmful blooms: Haploids, diploids and the relevance of benthic stages. *Harmful Algae* 73: 44–57.

Fott B. & Ludvík J. 1956. Über den submikroskopischen Bau des Panzers von *Ceratium hirundinella*. *Preslia* 28: 278–280, pls 16–17.

Gajadhar A.A., Marquardt W.C., Hall R., Gunderson J., Ariztia-Carmona E.V. & Sogin M.L. 1991. Ribosomal RNA sequences of *Sarcocystis muris*, *Theileria annulata* and *Crypthecodinium cohnii* reveal evolutionary relationships among apicomplexans, dinoflagellates, and ciliates. *Molecular and Biochemical Parasitology* 45: 147–154.

Gao X. & Dodge J.D. 1991. The taxonomy and ultrastructure of a marine dinoflagellate, *Scrippsiella minima* sp. nov. *British Phycological Journal* 26: 21–31.

Gottschling M., Kretschmann J. & Žerdoner Čalasan A. 2017. Description of Peridiniopsidaceae, fam. nov (Peridiniales, Dinophyceae). *Phytotaxa* 299: 293–296.

Gottschling M., Chacón J., Žerdoner Čalasan A., Neuhaus S., Kretschmann J., Stibor H. & John U. 2019. Phylogenetic placement of environmental sequences using taxonomically reliable databases helps to rigorously assess dinophyte biodiversity in Bavarian lakes (Germany). *Freshwater Biology* 65: 193–208.

Grell K.G. & Wohlfarth-Bottermann K.E. 1957. Licht- und elektronenmikroskopische Untersuchungen an dem Dinoflagellaten *Amphidinium* elegans n. sp. *Zeitschrift fur Zellforschung und mikroskopische Anatomie* 47: 7–17.

Hansen G. & Moestrup Ø. 1998. Fine-structural characterization of *Alexandrium catenella* (Dinophyceae) with special emphasis on the flagellar apparatus. *European Journal of Phycology* 33: 281–91.

Hansen G. & Moestrup Ø. 2005. Flagellar apparatus and nuclear chambers of the green dinoflagellate *Gymnodinium chlorophorum*. *Phycological Research* 53: 169–181.

Hansen G. & Daugbjerg N. 2009. *Symbiodinium natans* sp. nov.: a 'free-living' dinoflagellate from Tenerife (Northeast-Atlantic Ocean). *Journal of Phycology* 45: 251–263.

Hansen G., Moestrup Ø. & Roberts K.R. 1996. Fine structural observations on *Gonyaulax spinifera* (Dinophyceae), with special emphasis on the flagellar apparatus. *Phycologia* 35: 354–366.

Hansen G., Moestrup Ø. & Roberts K.R. 1997. Light and electron microscopical observations on *Protoceratium reticulatum* (Dinophyceae). *Archiv für Protistenkunde* 147: 381–391.

Hansen G., Daugbjerg N. & Henriksen P. 2007. *Baldinia anauniensis* gen. et sp. nov.: a 'new' dinoflagellate from Lake Tovel, N. Italy. *Phycologia* 46: 86–108.

Hoppenrath M. 2017. Dinoflagellate taxonomy - a review and proposal of a revised classification. *Marine Biodiversity* 47: 381–403.

Hoppenrath M., Murray S., Sparmann S.F. & Leander B.S. 2012. Morphology and molecular phylogeny of *Ankistrodinium* gen. nov. (Dinophyceae), a new genus of marine sand-dwelling dinoflagel- lates formerly classified within *Amphidinium*. *Journal of Phycology* 48: 1143–1152

Hoppenrath M., Murray S.A., Chomérat N. & Horiguchi T. 2014. *Marine benthic dinoflagellates – unveiling their worldwide biodiversity*. Kleine Senckenberg-Reihe 54, Schweizerbart Science, Stuttgart, 276 pp.

Horiguchi T. 2003. *Diversity and phylogeny of dinoflagellates with a diatom endosymbiont and molecular phylogenetics of the genus Protoperidinium.* Seventh International Conference on Modern and Fossil Dinoflagellates, Nagasaki 2003. Program, Abstracts & Participants, p. 53.

Horiguchi T. 2004. Origin and evolution of dinoflagellates with a diatom endosymbiont. In: *Neo-Science of Natural History: Integration of Geoscience and Biodiversity Studies* (Ed. by S.F. Mawatari & H. Okada), Graduate School of Science, Hokkaido University, Sapporo, pp. 53–59. (Proceedings of International Symposium on 'Dawn of a New Natural History – Integration of Geoscience and Biodiversity Studies').

Horiguchi T. & Pienaar R.N. 1994. Ultrastructure of a new marine, sand-dwelling dinoflagellate, *Gymnodinium quadrilobum* sp. nov. (Dinophyceae) with special reference to its endosymbiotic alga. *European Journal of Phycology* 29: 237–245.

Hinnebusch A.G., Klotz L.C., Blanken R.L. & Loeblich III A.R. 1981. An evaluation of the phylogenetic position of the dinoflagellate *Crypthecodinium cohnii* based on 5S rRNA characterization. *Journal of Molecular Evolution* 17: 334–347.

Iwataki M., Botes L., Sawaguchi T., Sekiguchi K. & Fukuyo Y. 2003. Cellular and body scale structure of *Heterocapsa ovata* sp. nov. and *Heterocapsa orientalis* sp. nov. (Peridiniales, Dinophyceae). *Phycologia* 42: 629–637.

Janouškovec J., Gavelis G.S., Burki F., Dinh D., Bachvaroff T.R., Gornik S.G., Bright K.J., Imanian B., Strom S.L., Delwiche C.F. et al. 2017. Major transitions in dinoflagellate evolution unveiled by phylotranscriptomics. *PNAS* 114: E171-E180.

Keeling P.J. 2004. Diversity and evolutionary history of plastids and their hosts. *American Journal of Botany* 91: 1481–1493.

Kofoid C.A. 1907. The plates of *Ceratium* with a note on the unity of the genus. *Zoologischer Anzeiger* 32: 177–183.

Kofoid C.A. 1909. On *Peridinium steinii* Jörgensen, with a note on the nomenclature of the skeleton of the Peridinidae. *Archiv für Protistenkunde* 16: 25–47.

Kretschmann J., Owsianny P.M., Žerdoner Čalasan A.. & Gottschling M. 2018. The hot spot in a cold environment: puzzling *Parvodinium* (Peridiniopsidaceae, Peridiniales) from the Polish Tatra Mountains. *Protist* 169: 206–230.

Kretschmann J., Žerdoner Čalasan A., Meyer B. & Gottschling M. 2019 ('2020'). Zero intercalary plates in *Parvodinium* (Peridiniopsidaceae, Peridiniales) and phylogenetics of *P. elpatiewskyi*, comb. nov. *Protist* 171: Article 125700.

Leander B.S. & Keeling P.J. 2004. Early evolutionary history of dinoflagellates and apicomplexans (Alveolata) as inferred from HSP90 and actin phylogenies. *Journal of Phycology* 40: 341–350.

Lin S., Zhang H., Spencer D., Norman J. & Gray M. 2002. Widespread and extensive editing of mitochondrial mRNAs in dinoflagellates. *Journal of Molecular Biology* 320: 727–739.

Lindberg K., Moestrup Ø. & Daugbjerg N. 2005. Studies on woloszynskioid dinoflagellates I: *Woloszynskia coronata* re-examined using light and electron microscopy and partial LSU rDNA sequences, with description of *Tovellia* gen. nov. and *Jadwigia* gen. nov. (Tovelliaceae fam. nov.). *Phycologia* 44: 416–440.

Litaker R.W., Vandersea M.W., Kibler S.R., Madden V.J., Noga E.J. & Tester P.A. 2002 Life cycle of the heterotrophic dinoflagellate *Pfiesteria piscicida* (Dinophyceae). *Journal of Phycology* 38: 442–463.

Logares R. 2007. *Microbial evolution: patterns of diversity in aquatic protists*. PhD thesis, Lund University, Sweden. 160 pp.

McEwan M.L. & Keeling P.J. 2004. HSP90, tubulin and actin are retained in the tertiary endosymbiont genome of *KryptoPeridinium foliaceum*. Journal of Eukaryotic Microbiology 51: 651–659.

Moestrup Ø. 2000. The flagellate cytoskeleton. Introduction of a general terminology for microtubular flagellar roots in protists. In: *The flagellates. Unity, diversity and evolution* (Ed. by B.S.C. Leadbeater & J.C. Green), Taylor & Francis, New York, pp. 69–94. (Systematics Association Special Volume No. 59).

Moestrup Ø. & Calado A.J. 2018. Dinophyceae. In: *Süßwasserflora von Mitteleuropa — Freshwater Flora of Central Europe*, vol. 6, ed. 2 (Ed. by B. Büdel, G. Gärtner, L. Krienitz & M. Schagerl), Springer-Verlag, Berlin, 560 pp.

Moestrup Ø. & Daugbjerg N. 2007. On dinoflagellate phylogeny and classification. In: *Unravelling the algae: the past, present, and future of algal systematics* (Ed. by J. Brodie & J. Lewis), CRC Press, Boca Raton, pp. 215–230. (Systematics Association Special Volume No. 75).

Moestrup Ø., Hansen G., Daugbjerg N., Flaim G. & D'Andrea M. 2006. Studies on woloszynskioid dinoflagellates II: On *Tovellia sanguinea* sp. nov., the dinoflagellate responsible for the reddening of Lake Tovel, N. Italy. *European Journal of Phycology* 41: 47–65.

Moestrup Ø., Hansen G. & Daugbjerg N. 2008. Studies on woloszynskioid dinoflagellates III: the ultrastructure and phylogeny of *Borghiella dodgei* gen. et sp. nov., a cold-water species from Lake Tovel, N. Italy, and on *B. tenuissima* comb. nov. (syn. *Woloszynskia tenuissima*). *Phycologia* 47: 54–78.

Moestrup Ø., Lindberg K. & Daugbjerg N. 2009a. Studies on woloszynskioid dinoflagellates IV: The genus *Biecheleria* gen. nov. *Phycological Research* 57: 203–220.

Moestrup Ø., Lindberg K. & Daugbjerg N. 2009b. Studies on woloszynskioid dinoflagellates V: Ultrastructure of *Biecheleriopsis* gen. nov., with description of *Biecheleriopsis adriatica* sp. nov. *Phycological Research* 57: 221–237.

Müller O.F. 1773. *Vermium terrestrium et fluviatilium, seu animalium Infusoriorium, Helminthicorum et Testaceorum, non marinorum, succincta historia.*, vol. 1, Martini Hallager, Hauniae et Lipsiae. Preface, bibliography and a synopsis of classification (30 unnumbered pages), 135 pp.

Müller O.F. 1786. *Animalcula Infusoria fluviatilia et marina, quae detexit, systematice descripsit et ad vivum delineari curavit Otho Fridericus Müller, Regi Daniae quondam a consiliis conferentiae, pluriumque academiarum et societatum scientiarum sodalist, sistit opus hoc posthumum quod cum tabulis aeneis L. in lucem tradit vidua ejus nobilissima, cura Othonis Fabricci.* Nicolai Mölleri, Hauniae. LVI, 367 pp., 50 pls (With a 4-page foreword by Otho Fabricius).

Mulders K.J.M., Weesepoel Y., Bodenes P., Lamers P.P., Vincken J., Martens D.E., Gruppen H. & Wijffels R.H. 2015. Nitrogen-depleted *Chlorella zofingiensis* produces astaxanthin, ketolutein and their fatty acid esters: a carotenoid metabolism study. *Journal of Applied Phycology* 27: 125–140.

Orr R.J.S, Murray S.A, Stüken A., Rhodes L. & Jakobsen K.S. 2012. When naked became armored: an eight-gene phylogeny reveals monophyletic origin of theca in dinoflagellates. *PLOS One* 7: Article e50004.

Pandeirada M.S., Craveiro S.C., Daugbjerg N., Moestrup Ø. & Calado A.J. 2014. Studies on woloszynskioid dinoflagellates VI: description of *Tovellia aveirensis* sp. nov. (Dinophyceae), a new species of Tovelliaceae with spiny cysts. *European Journal of Phycology* 49: 230–243.

Pandeirada M.S., Craveiro S.C., Daugbjerg N., Moestrup Ø. & Calado A.J. 2017. Studies on woloszynskioid dinoflagellates VIII: life cycle, resting cyst morphology and phylogeny of *Tovellia rinoi* sp. nov. (Dinophyceae). *Phycologia* 56: 533–548.

Pitelka D.R. & Schooley C.N. 1955. Comparative morphology of some protistan flagella. *University of California Publications in Zoology* 61: 79–128.

Popovský J. & Pfiester L.A. 1990. Dinophyceae (Dinoflagellida). In: *Süßwasserflora von Mitteleuropa*, vol. 6 (Ed. by H. Ettl, J. Gerloff, H. Heynig & D. Mollenhauer), Gustav Fischer, Jena, 272 pp.

Remias D., Pichrtová M., Pangratz M., Lütz C. & Holzinger A. 2016. Ecophysiology, secondary pigments and ultrastructure of *Chlainomonas* sp. (Chlorophyta) from the European Alps compared with *Chlamydomonas nivalis* forming red snow. *FEMS Microbiology Ecology* 92:1–11.

Roberts K.R. 1985. The flagellar apparatus of *Oxyrrhis marina* (Pyrrophyta). *Journal of Phycology* 21: 641– 655.

Roberts K.R. 1989. Comparative analyses of the dinoflagellate flagellar apparatus. II. *Ceratium hirundinella*. *Journal of Phycology* 25: 270–280.

Roberts K.R. 1991. The flagellar apparatus and cytoskeleton of dinoflagellates: organization and use in systematics. In: *The Biology of Free-living Heterotrophic Flagellates* (Ed. by D.J. Patterson & J. Larsen), Clarendon Press, Oxford, pp. 285–302. (Systematics Association special volume 45).

Roberts K.R. & Roberts J.E. 1991. The flagellar apparatus and cytoskeleton of the dinoflagellates. A comparative overview. *Protoplasma* 164: 105–122.

Roberts K.R., Timpano P. & Montegut A.E. 1987. The apical pore fibrous complex: a new cytological feature of some dinoflagellates. *Protoplasma* 137: 65–69.

Roberts K.R., Roberts J.E. & Cormier S.A. 1992. The dinoflagellate cytoskeleton. In: *The cytoskeleton of the algae* (Ed. by D. Menzel), CRC Press, London, pp. 19–38.

Roberts K.R., Hansen G. & Taylor F.J.R. 1995. General ultrastructure and flagellar apparatus architecture of *Woloszynskia limnetica* (Dinophyceae). *Journal of Phycology* 31: 948–957.

Schütt F. 1895. Die Peridineen der Plankton-Expedition. I. Theil. Studien über die Zellen der Peridineen. In: *Ergebnisse der Plankton-Expedition der Humboldt-Stiftung*, vol. 4, MaA (Ed. by V.A.C. Hensen), Lipsius & Tischer, Kiel, Leipzig, pp. 1–170, pls 1–27.

Saldarriaga J.F., Taylor F.J.R., Keeling P.J. & Cavalier-Smith T. 2001. Dinoflagellate nuclear SSU rRNA phylogeny suggests multiple plastid losses and replacements. *Journal of Molecular Evolution* 53: 204–213.

Saldarriaga, J.F., McEwan, M.L., Fast, N.M., Taylor, F.J.R. & Keeling, P.J. 2003. Multiple protein phylogenies show that *Oxyrrhis marina* and *Perkinsus marinus* are early branches of the dinoflagellate lineage. *International Journal of Systematic and Evolutionary Microbiology* 53: 355–365.

Saldarriaga J.F., Taylor F.J.R., Cavalier-Smith T., Menden-Deuer S. & Keeling P.J. 2004. Molecular data and the evolutionary history of dinoflagellates. *European Journal of Protistology* 40: 85–111.

Santos M.F. & Mesquita J.F. 1984. Ultrastructural study of *Haematococcus lacustris* (Girod.) Rostafinksi (Volvocales) I. Some aspects of carotenogenesis. *Cytologia* 49: 215–228.

Saunders G.W., Hill D.R.A., Sexton J. & Andersen R.A. 1997. Small-subunit ribosomal RNA sequences from selected dinoflagellates: testing classical evolutionary hypotheses with

molecular systematic methods. In: *Origins of algae and their plastids* (Ed. by D. Bhattacharya), Springer, New York, pp. 237–259.

Schrank F.v.P. 1793. Mikroskopische Wahrnehmungen. *Der Naturforscher (Halle)* 27: 26–37, pl. 3, figs 10–23.

Schiller J. 1933. Dinoflagellatae (Peridineae) in monographischer Behandlung. In: *Rabenhorst's Kryptogamen-flora von Deutschland, Österreich und der Schweiz*, vol. 10, ed. 2, Part 1 (Ed. by R. Kolkwitz), Akademische Verlagsgesellschaft, Leipzig, 617 pp.

Schiller J. 1937. Dinoflagellatae (Peridineae) in monographischer Behandlung. In: *Rabenhorst's Kryptogamen-flora von Deutschland, Österreich und der Schweiz*, vol. 10, ed. 2, Part 2. (Ed. by R. Kolkwitz), Akademische Verlagsgesellschaft, Leipzig, 589 pp.

Seo K.S. & Fritz L. 2002. Diel changes in pyrenoid and starch reserves in dinoflagellates. *Phycologia* 41: 22–28.

Spector D.L. [Ed.] 1984. *Dinoflagellates*. Academic Press, Orlando, Florida, USA. 545 pp.

Stein F. 1878. *Der Organismus der Infusionsthiere nach eigenen Forschungen in systematischer Reihenfolge bearbeitet. III. Abtheilung. Die Naturgeschichte der Flagellaten oder Geisselinfusorien. I. Hälfte. Den noch nicht Abgeschlossenen allgemeinen Theil nebst Erklärung der sämmtlichen Abbildungen enthaltend.* Wilhelm Engelmann, Leipzig, 154 pp., 24 pls.

Stein F. 1883. *Der Organismus der Infusionsthiere… III. Abtheilung. II. Hälfte. Die Naturgeschichte der arthrodelen Flagellaten. Einleitung und Erklärung der Abbildungen.* Wilhelm Engelmann, Leipzig, 30 pp., 25 pls.

Takahashi K. Moestrup Ø., Jordan R.W. & Iwataki M. 2015. Two new freshwater woloszynskioids *Asulcocephalium miricentonis* gen. et sp. nov. and *Leiocephalium pseudosanguineum* gen. et sp. nov. (Suessiaceae, Dinophyceae) lacking an apical furrow apparatus. *Protist* 166: 638–658.

Takahashi K., Moestrup Ø., Wada M. et al. 2017. *Dactylodinium pterobelotum* gen. et sp. nov., a new marine woloszynskioid dinoflagellate positioned between the two families Borghiellaceae and Suessiaceae. *Journal of Phycology* 53: 1223–1240.

Takano Y., Hansen G., Fujita D. & Horiguchi T. 2008. Serial replacement of diatom endosymbionts in two freshwater dinoflagellates, *Peridiniopsis* spp. (Peridiniales, Dinophyceae). *Phycologia* 47: 41–53.

Takano Y., Yamaguchi H., Inouye I., Moestrup Ø. & Horiguchi T. 2014. Phylogeny of five species of *Nusuttodinium* gen. nov. (Dinophyceae), a genus of unarmoured kleptoplastidic dinoflagellates. *Protist* 165: 759–778.

Takayama H. 1985. Apical grooves of unarmored dinoflagellates. *Bulletin of the Plankton Society of Japan* 32: 129– 40.

Taylor F.J.R. 1980. On dinoflagellate evolution. *ByoSystem* 13: 65–108.

Taylor F.J.R. 1987. General group characteristics; special features of interest; short history of dinoflagellate study. In: *The biology of dinoflagellates* (Ed. by F.J.R. Taylor), Blackwell Scientific Publibications, Oxford, pp. 1–23 (Botanical Monographs, vol. 21).

Taylor F.J.R. 2004. Illumination or confusion? Dinoflagellate molecular phylogenetic data viewed from a primarily morphological standpoint. *Phycological Research* 52: 308–324.

Toriumi S. & Dodge J.D. 1993. Thecal apex structure in the Peridiniaceae (Dinophyceae). *European Journal of Phycology* 28: 39–45.

Van de Peer Y. & De Wachter R. 1997. Evolutionary relationships among the eukaryotic crown taxa taking into account site-to-site rate variation in 18S rRNA. *Journal of Molecular Evolution* 45: 619–630.

Van de Peer Y., Van der Auwera G. & De Wachter R. 1996. The evolution of Stramenopiles and Alveolates as derived by 'substitution rate calibration' of small ribosomal subunit RNA. *Journal of Molecular Evolution* 42: 201–210.

Wedemayer G.J. & Wilcox L.W. 1984. The ultrastructure of the freshwater colorless dinoflagellate *Peridiniopsis berolinense* (Lemm.) Bourrelly. *Journal of Protozoology* 31: 444–453.

Wilcox L.W., Wedemayer G.J. & Graham L.E. 1982. *Amphidinium cryophilum* sp. nov. (Dinophyceae), a new freshwater dinoflagellate. II. Ultrastructure. *Journal of Phycology* 18: 18–30.

Wołoszyńska J. 1917. Nowe gatunki Peridineów, tudzież spostrzeżenia nad budową okrywy u Gymnodiniów i Glenodiniów. — Neue Peridineen-Arten, nebst Bemerkungen über den Bau der Hülle bei *Gymno-* und *Glenodinium*. *Bulletin International de l'Academie des Sciences de Cracovie, Classe des Sciences Mathématiques et Naturelles, Sér B, Sciences Naturelles* 1917: 114–122, pls 11–13.

Zhang H., Bhattacharya D. & Lin S. 2005. Phylogeny of dinoflagellates based on mitochondrial cytochrome *b* and nuclear small subunit rDNA sequence comparisons. *Journal of Phycology* 41: 411–420.

Zhang Q., Liu G-X. & Hu Z-Y. 2011. Morphological observation of a freshwater *Peridinium* strain and phylogenetic analysis of *Peridinium*. *Plant Science Journal* 29: 1–10.

Zhang Q., Zhu H., Hu Z. & Liu G. 2016. Blooms of the woloszynskioid dinoflagellate *Tovellia diexiensis* sp. nov. (Dinophyceae) in Baishihai Lake at the eastern edge of Tibetan Plateau. *Algae* 31: 205–217.

CHAPTER 2

STUDIES ON WOLOSZYNSKIOID DINOFLAGELLATES X: ULTRASTRUCTURE, PHYLOGENY AND COLOUR VARIATION IN *TOVELLIA RUBESCENS* N. SP. (DINOPHYCEAE)

Pandeirada, M.S., Craveiro, S.C., Daugbjerg, N., Moestrup, Ø., Domingues, P. & Calado, A.J. 2019. Studies on woloszynskioid dinoflagellates X: ultrastructure, phylogeny and colour variation in *Tovellia rubescens* n. sp. (Dinophyceae). *Journal of Eukaryotic Microbiology* 66: 937–953 (DOI: 10.1111/jeu.12745)

ABSTRACT

The external morphology and internal cell fine structure of a new species of Tovelliaceae, *Tovellia rubescens* n. sp., is described. Phylogenetic analyses based on partial LSU rDNA sequences place the new species in a clade containing *Tovellia* species that accumulate red pigments and identify *T. aveirensis* as its closest known relative. Cells of *T. rubescens* n. sp. were mostly round and had the cingulum located near the middle, with its ends displaced about one cingular width. Small numbers of distinctly flat cells appeared in culture batches; their significance could not be determined. Cells of the new species in culture batches progressively changed from a yellowish-green, mainly due to chloroplast colour, to a reddish-brown colour that appeared associated with lipid bodies. The switch to a reddish colour happened earlier in batches grown in medium lacking sources of N or P. Pigment analyses by HPLC-MS/MS revealed the presence of astaxanthin and astaxanthin-related metabolites in the new species, but also in *T. aveirensis*, in which a reddish colour was never observed. The chloroplast arrangement of *T. rubescens* n. sp. resembled that of *T. aveirensis*, with lobes radiating from a central pyrenoid complex. The flagellar apparatus and pusular system fell within the general features described from other Tovelliaceae. A row of microtubules interpretable as a microtubular strand of the peduncle was present. Spiny resting cysts with red contents and an ITS sequence identical to that of cultured material of the new species were found in the original locality.

Key words: astaxanthin, central pyrenoid complex, flagellar apparatus, ITS1-5.8S-ITS2 rDNA, LSU rDNA, Tovelliaceae

INTRODUCTION

The dinoflagellates commonly designated 'woloszynskioids' are artificially linked by the presence of an amphiesma with fewer vesicles than typical gymnodinioids, but with amphiesmal vesicles more numerous and containing thinner plate-like material than typical peridinioid or gonyaulacoid species (Lindberg et al. 2005). The name of this artificial assemblage stems from the generic name *Woloszynskia* R.H. Thompson, originally proposed to accommodate species previously classified as *Gymnodinium* F.

Stein in which a thin theca had been demonstrated (Thompson 1951, p. 286). The genus was found to be polyphyletic, as initially suggested by Stosch (1973), who pointed out the presence of different cyst and eyespot types within the group of species assigned to *Woloszynskia* (Lindberg et al. 2005). Most species of woloszynskioids are currently recognized as members of different dinoflagellate groups, which are partly characterized by one or a few distinct eyespot types. Species with an eyespot made of more or less fused, carotenoid-rich oil globules not surrounded by membranes are currently grouped in their own family and order, respectively named Tovelliaceae and Tovelliales (Moestrup and Calado 2018). Species of Tovelliaceae studied ultrastructurally have been shown to share several distinctive features of their flagellar and pusular apparatuses (Calado 2011) and provide useful comparison points.

The genus *Tovellia* Moestrup, K. Lindberg and Daugbjerg currently includes about a dozen species that bear peridinin-containing, yellowish-green or brownish-green chloroplasts (Pandeirada et al. 2017; Zhang et al. 2016). However, in a group of species that appear to be phylogenetically related the cells often show a distinct reddish colour, and blooms of these species may result in a spectacular blood-red coloration of the water (Moestrup et al. 2006; Zhang et al. 2016). In two of these species, *T. sanguinea* Moestrup, Gert Hansen, Daugbjerg, Flaim and d'Andrea and *T. diexiensis* Qi Zhang and G. X. Liu, the red carotenoid astaxanthin was shown to be abundant in the cells (Frassanito et al. 2006; Zhang et al. 2016). A new species of *Tovellia* with cell colour varying from yellowish-green to reddish-brown is described herein on the basis of light, scanning electron and transmission electron microscopy, and placed by partial LSU rDNA-based phylogenetic analysis within the clade that includes the red-coloured species. Pigment analysis by HPLC-MS revealed the presence of astaxanthin and related metabolites. The new species is the third species of *Tovellia* to be reported from continental Portugal (Pandeirada et al. 2013, 2014, 2017).

MATERIAL AND METHODS

Biological material

The species described herein was found in the plankton of a shallow, freshwater pond in Gafanha da Boavista, Ílhavo, Portugal (40°35'44.70"N, 8°41'49.66"W), sampled 28 October 2010. A culture was started from the isolation of a single cell from this sample

into quadruple concentration L16 medium (Lindström 1991) supplemented with vitamins according to Popovský and Pfiester (1990) — 4×L16 + vit. A second isolate from the same pond, collected 18 August 2011, proved identical in morphology and LSU rDNA sequence and was also used for observations and experiments. Maintenance of cultures and all experiments were conducted in a chamber at 18 ºC with 12h:12h light:dark photoperiod and photon flux density about 25 μmol/m/s. Resting cysts were isolated from the same pond into the same conditions, but failed to produce viable cultures; the cysts were similar to one another in morphology and the ITS1-5.8S-ITS2 rDNA sequence established from one of them was 100% identical to that obtained from the culture started in October 2010. Attempts to induce sexual reproduction included isolation of about 20 cells into 250 μL of either full medium, or the same medium with sources of nitrogen excluded, or the same medium without phosphate; alternatively, about 20 cells of each culture line were mixed into 250 µL of full or either nitrogen- or phosphate-deficient medium. These experiments were conducted in 96-well cell culture plates (Sarstedt, Numbrecht, Germany). For the experimental induction of production of astaxanthin-related compounds, see below.

Light microscopy (LM)

Light micrographs of swimming cells, dividing cells, and resting stages were taken with a Zeiss Axioplan 2 imaging light microscope (Carl Zeiss, Oberkochen, Germany), using DP70 and ColorView IIIu Olympus cameras (Olympus Corp., Tokyo, Japan). Cells emerging from division cysts were recorded with a JVC TK-C1481BEG color video camera (Norbain SD Ltd, Reading, U.K.), coupled to a Leitz Labovert FS inverted light microscope (Leica Microsystems, Wetzlar, Germany).

Scanning electron microscopy (SEM)

Swimming cells were fixed by mixing equal portions of cell suspension and a fixative containing a 1:5 proportion of saturated $HgCl_2$ solution and 2% OsO_4 for 15 min, and further processed as detailed in Daugbjerg et al. (2014) for the Portuguese material of *Borghiella andersenii* Daugbjerg, Andreasen, Happel, Pandeirada, Gert Hansen, Craveiro, Calado and Moestrup. The material was critical-point-dried in a Baltec CPD-030 (Balzers, Liechtenstein), mounted on stubs, sputter-coated with gold-palladium and

observed in a Hitachi S-4100 scanning electron microscope (Hitachi High-Technologies Corp., Tokyo, Japan).

Transmission electron microscopy (TEM)

Vegetative cells with reddish-brown colour were prepared for TEM as in Pandeirada et al. (2014). Serial sections of one cell were observed with a JEM 1010 electron microscope (JEOL Ltd., Tokyo, Japan) and images recorded with a Gatan Orius digital camera (Gatan, Inc., Pleasanton, CA).

HPLC-MS and HPLC-MS/MS characterization of pigment extract

The pigment composition of cultures of the new species grown in full and N-deficient medium was compared to that of cultures of *Tovellia aveirensis* Pandeirada, Craveiro, Daugbjerg, Moestrup and Calado grown in similar conditions. For the sake of clarity, the new species, which is formally described at the end of the text, is hereafter referred by its proposed name, *T. rubescens* n. sp. Pigments were separated on a HPLC system (Waters Alliance 2690, Mildford, MA) coupled to a linear ion trap mass spectrometer LXQ (ThermoFinnigan, San Jose, CA). Cultures of *T. rubescens* n. sp. and *T. aveirensis* were grown for about 20 d in 50-ml tissue culture flasks (Sarstedt) with 4×L16 + vit or the equivalent N-deficient medium. To compensate for the reduced growth supported by the N-deficient medium, the contents of two flasks were pooled, thereby increasing cell numbers for pigment extraction. The number of cells filtered for pigment extraction was, for *T. aveirensis*, about 68,900 cells grown in N-deficient medium, and some 133,800 in the full medium. For *T. rubescens* n. sp., about 108,000 cells were collected from each growth condition. The cells were harvested with nylon filters (Pall membrane filters, Nylaflo membrane, diam. 25 mm, pore size 0.45 μm) and the pigments were extracted through the following steps: 1) 2 ml of acetone for about 3 min, followed by 2 ml of methanol; 2) another 2 ml of acetone immediately followed by 2 ml of methanol. The extract was then dried under a controlled stream of nitrogen, and dissolved in 100 μL of 50% methanol in water. A volume of 5 μL of this solution was introduced into a Supelco Bio Wide Pore C5 column (15 cm × 0.5 mm, 5 μm; Supelco, Bellefonte, PA). The mobile phase A consisted of 95% water and 5% acetonitrile with 0.1% of formic acid. The mobile phase B consisted of 100% methanol. The mobile phase gradient was programmed as

follows: the initial conditions were 50% of B for 2 min; 2–42 min linear gradient to 100% of B; 42 –50 min isocratic at 100% of B, and the flow rate was 10 µL/min, obtained using a house-made splitter. To obtain the product-ion spectra of the major components during LC experiments, cycles consisting of one full scan mass spectrum in the m/z range from 70 to 1,000, and three data-dependent MS/MS scans were repeated continuously throughout the experiments with the following dynamic exclusion settings: repeat count 3; repeat duration 15 s; exclusion duration 45 s. The LXQ was operated in positive mode (electrospray voltage +5 kV), with a capillary temperature of 275 ºC and a sheath gas flow of 8 AU (arbitrary units). Normalized collision energy™ (CE) was set to 35 AU for MS/MS experiments. Data acquisition was carried out on an Xcalibur data system (V2.0).

Single-cell polymerase chain reaction (PCR)

Cells of both culture lines were used for PCR amplification of ca. 1,500 base pairs (bp) of the LSU rDNA. Cells of the culture line started in October 2010 and resting cysts from field samples were used for amplification of ca. 600 bp of ITS1-5.8S-ITS2 rDNA. In all cases, single swimming cells or single cysts were transferred to 0.2-ml PCR tubes and immediately frozen at –8 ºC for 4 d, before PCR reactions. LSU rDNA amplification involved the use of the terminal primers D1R (Scholin et al. 1994) and 28-1483R (Daugbjerg et al. 2000). PCR amplifications were based on the illustra™ puReTaq Ready-To-Go PCR Beads kit (GE Healthcare, UK Ltd., Buckinghamshire, U.K.), and used the thermocycler Biometra-Tprofessional (Biometra GmbH, Göttingen, Germany). The thermal profile was as outlined in Pandeirada et al. (2014). The same thermocycler was used for ITS amplifications, which were carried out according to Takano and Horiguchi (2005), with one modification: the external primer LSU R2 used in the first round of amplification was replaced by the primer 28-1483R mentioned above. PCR products from all amplifications were loaded on a 1% agarose gel, run for 20 min at 90 V and viewed on a UV light table (Molecular imager chemiDoc XRS System, Bio-Rad Laboratories, Inc., Hercules, CA). To increase the amount of LSU rDNA products, a nested-PCR was performed using 1 µL from the first PCR products in two PCR reactions with two combinations of primers: D1R-D3B and D3A-28-1483. The thermal profile can be found in Pandeirada et al. (2017). The PCR products were purified using the QIAquick PCR Purification Kit (Qiagen), following the manufacturer's recommendations, and sent

to Macrogen Europe (Amsterdam, The Netherlands) for sequence determination. The sequencing primers for LSU rDNA were the same as in Pandeirada et al. (2014), while those for ITS were those listed in Takano and Horiguchi (2005).

Alignment and phylogenetic analyses

Two alignments (alignment 1 and 2) were performed for this study. In alignment 1 the LSU rDNA sequence of *Tovellia rubescens* n. sp. was added to the alignment recently used to infer the phylogeny of the congener *T. rinoi* Pandeirada, Craveiro, Daugbjerg, Moestrup and Calado (see details in Pandeirada et al. 2017). Alignment 1 included 1,151 base pairs (domain D2 was deleted due to possible alignment ambiguities when including a systematic broad range of dinoflagellates and outgroup taxa). To examine the phylogenetic position of the recently described *T. diexiensis*, a red *Tovellia* species that could not be included in alignment 1 because the known part of its LSU rDNA sequence was too short, a second alignment was prepared. In alignment 2 only dinoflagellates in the Tovelliaceae were included. This allowed inclusion of domain D2, and the alignment included 714 base pairs (from 27 upstream domain D1 to 7 base pairs downstream domain D2 following the secondary structure model by Lenaers et al. 1989). Both alignment 1 and 2 were used to infer the phylogeny using Bayesian (MrBayes, ver. 3.2.2 x64, Ronquist and Huelsenbeck 2003) and maximum likelihood analyses (PhyML, ver. 3.0, Guindon and Gascuel 2003). Bayesian analyses were run on a local computer with 5 million generations, and trees were sampled every 1,000th generation. The burn-in was evaluated by plotting the LnL values as a function of generations. Burn-in occurred after 501.000 generations (conservative number) resulting in the removal of 501 trees in both Bayesian analyses (alignment 1 and 2). This left 4,500 trees as input for 50% majority-rule consensus trees in PAUP* (Swofford 2003). jModelTest (ver. 2.1.7, Darriba et al. 2012) was used to find the best fit model for the data matrices and the model chosen was GTR+I+G (i.e. general time-reversible with the proportion of invariable sites and gamma distribution). The Montpellier bioinformatics platform at http://www.atgc-montpellier.fr/phyml was used to run PhyML analyses, and the robustness of clades was evaluated with 1,000 bootstrap replications. Values (≥50%) were plotted on Bayesian trees when identical topologies were suggested.

Outgroup taxa

In alignment 1 the diverse assemblage of dinoflagellates (78 taxa) was rooted with three ciliates, four apicomplexan and one perkinsozoan species. Based on the tree topology from alignment 1 *Jadwigia applanata* Moestrup, K. Lindberg and Daugbjerg was used to root *Bernardinium bernardinense* Chodat and *Tovellia* spp. in alignment 2.

RESULTS

General morphology (LM and SEM)

Vegetative cells of *Tovellia rubescens* n. sp. are illustrated by LM and SEM in Fig. 1A–2H and 3A–E, respectively. Epi- and hypocone were similar in size, the epicone nearly hemispherical and the hypocone hemispherical to rounded-conical, sometimes with a pointed antapex (Fig. 1A–2D, 3A–C). The epicone was usually slightly projected near the apex, at the level of the apical line of plates (ALP, see below) (Fig. 1B, E). The cingulum was displaced about one cingulum width (Fig. 1A–D, 2A–D, 3A–C). Cells were slightly compressed dorsoventrally, with the hypocone somewhat obliquely flattened in lateral view (Fig. 1F). Cells were 18.5–43 μm long, 12.5–33 μm wide (n = 54 for both measurements) and 11.5–28 μm thick (n = 37). Chloroplasts were yellowish-green with lobes radiating from the centre (Fig. 1B, D, E). A large, bright-red eyespot was located across the anterior to middle part of the sulcus; its length was mostly 4–8 μm, and it appeared independent of chloroplast lobes (Fig. 1A, C, E, F). The nucleus was usually transversely elongated along the dorsal side of the hypocone (Fig. 1B, F, 2E); in a few smaller cells, it was ellipsoid and extended to the middle of the cell (Fig. 2D). The amphiesma lining swimming cells was usually undetectable, but revealed the presence of thin amphiesmal plates when shed (Fig. 2E).

Colour variation of vegetative cells

Yellowish-green cells of *T. rubescens* n. sp. usually displayed two types of cytoplasmic inclusions: brownish-yellow accumulation bodies in the epicone (Fig. 1F), and reddish granules with an eyespot-like colour in the hypocone (Fig. 1B, D, E). Old, dense cultures grown in full medium, and ca. 10-d old batches grown in medium without nitrogen or phosphorus, often showed darker cells with a more distinctly reddish-brown

colour. These cells accumulated red to brown granules, usually first in the hypocone (Fig. 1E, 2A, B), but eventually over the entire cell, masking the colour of chloroplasts (Fig. 2C–H). Reddish-brown cells were usually of similar shape to the yellowish-green cells of less dense batches (Fig. 2C–E). However, morphologically distinct cells were regularly found in low numbers in red-coloured batches; these cells were nearly circular in ventral view, were strongly flattened dorsoventrally, and often had a wavy or denticulate outline, especially on the hypocone (Fig. 2F–H).
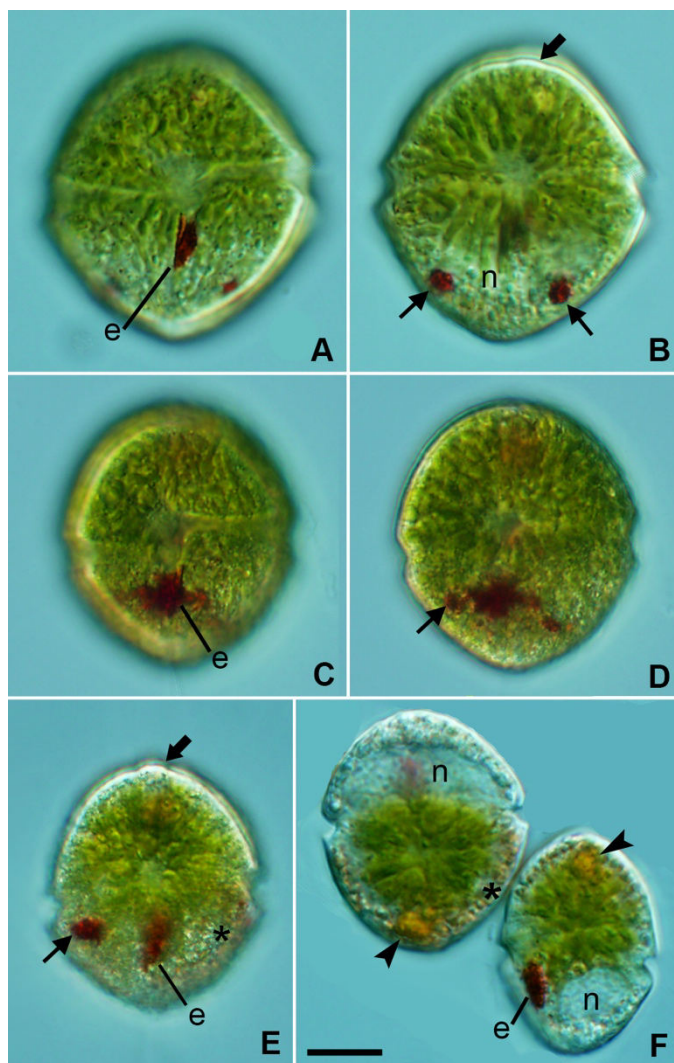
Fig. 1. *Tovellia rubescens* n. sp., swimming cells, LM. **A-E**. Surface focus and optical sections of ventral views showing the cingulum displaced about one cingulum width and reddish bodies in the hypocone (thin arrows). The eyespot (e) is visible along the anterior part of the sulcus. The radiating arrangement of chloroplasts is discernible in B and D. The slight apical protrusion is visible in B and E (thick arrows). **F**. Dorsal (left) and lateral (right) views showing accumulation bodies in the epicone (arrowheads) and the transversely elongated nucleus (n) in the hypocone. Brownish granules are visible near the cell surface (asterisk). Scale bar = 10 μm. All to the same scale.
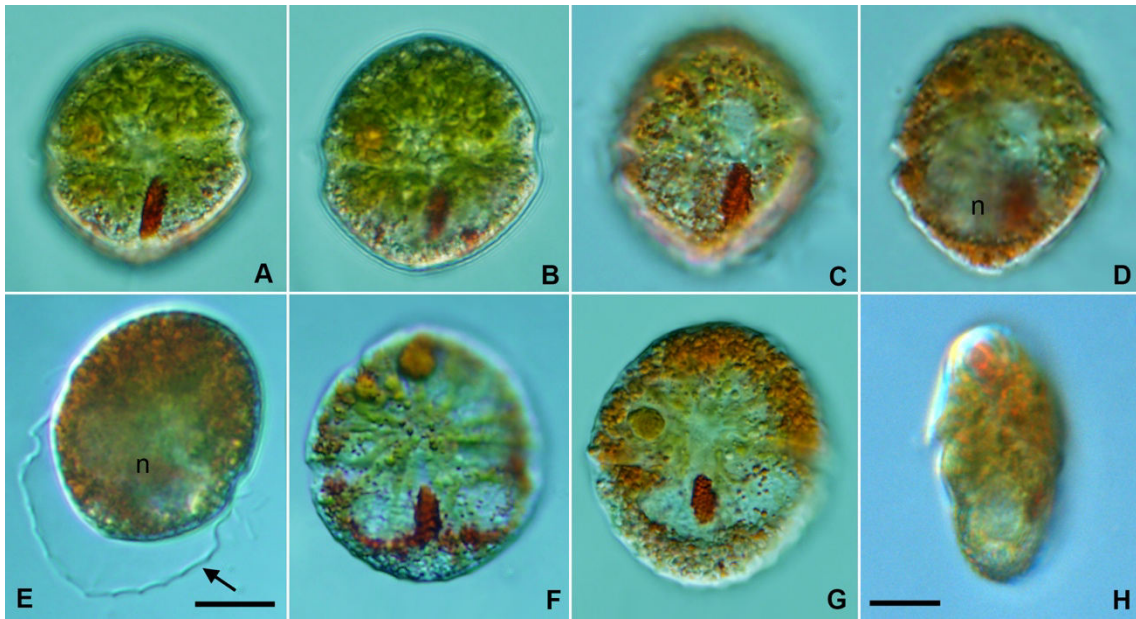
Fig. 2. *Tovellia rubescens* n. sp., swimming cells in several stages of reddening, LM. **A**, **B**. Surface focus and optical section of a cell with reddish-brown granules in the hypocone. **C**, **D**. Surface focus and optical section of a cell with more numerous reddish-brown granules that mask the greenish colour of chloroplasts. In D, note the nucleus (n) extending to the cell centre and the cell surface somewhat wavy. **E**. Reddish-brown cell shedding the amphiesma through the anterior half, with the lower part somewhat denticulate (arrow). **F-H**. Ventral (F, G) and lateral (H) views of cells strongly compressed dorsoventrally, showing a round outline in ventral view and different amounts of reddish-brown granules in the cytoplasm. Scale bars = 10 μm. A to D, same scale as E; F and G, same scale as H.

Structure of the amphiesma

The epi- and hypocone were covered by numerous pentagonal or hexagonal plates arranged in roughly six latitudinal series on the epicone and four or five on the hypocone (Fig. 3A–C, E). The cingulum was lined by two series of amphiesmal vesicles, the anterior one with rectangular or pentagonal plates abutting the sharply defined anterior edge, and the posterior one with roughly hexagonal plates that extended onto the hypocone, over the rounded posterior cingulum edge (Fig. 3A–C). A line of narrow amphiesmal vesicles (apical line of plates–ALP) extended from the ventral side, nearly above the sulcus, over the apex, and ended on the dorsal side; one plate usually separated the ventral end of the ALP from the proximal end of the cingulum, and there were two (seldom three) plates between ALP and cingulum on the dorsal side (Fig. 3A–D). The ALP amphiesmal vesicles were 0.2–0.4 μm wide (n = 22), and usually displayed one or several axial knobs (Fig. 3D). The length of ALP vesicles was difficult to determine with

the available SEM images; it ranged roughly from twice to at least five times the width (Fig. 3D). About nine elongated plates bordered both sides of the ALP; they were four- or five-sided, 1.5–5.0 μm long and 0.5–1.5 μm wide (n = 38). The sulcal area contained four or five plates, arranged linearly (Fig. 3B). A ventral ridge (vr) was observed in the upper part of the sulcus, between the ends of the cingulum, partly covering the flagellar pores (Fig. 3A, B). Sutures between amphiesmal plates were sometimes raised on the hypocone, giving rise to a wavy or denticulate outline (Fig. 3B) reminiscent of the one seen in LM in some reddish cells (see above). Antapical plates did not differ significantly from other plates on the hypocone (Fig. 3E).

Cell ultrastructure (TEM)

General ultrastructural features are shown in Fig. 4A–6C. An approximately longitudinal section shows a postcingular, transversely elongated nucleus and chloroplast lobes radiating from a central pyrenoid to the cell surface (Fig. 4A, B). The chloroplast lobes were surrounded by three membranes and contained thylakoids in groups of three (Fig. 4D). The central pyrenoid extended irregularly into the chloroplast lobes and contained scattered thylakoid lamellae (Fig. 4B). In the epicone, the space between chloroplast lobes was mainly filled with oil droplets, whereas starch grains were the main storage material in the hypocone (Fig. 4A, B). Many vesicles bounded by a single membrane and containing numerous electron-opaque granules 20−50 nm in diameter were present between the central pyrenoid complex and the peripheral oil droplets, especially in the epicone (Fig. 4A–D). Scattered trichocysts were observed near the periphery and accumulation bodies were present near the pyrenoid (Fig. 4A, B). The pusular system is shown in Fig. 5A as a convoluted tube extending for about 10 μm from the flagellar insertion area. The tube was about 300 nm wide and was limited in stretches by a single membrane in direct contact with the cytoplasm (arrowheads in Fig. 5A, C), whereas in other zones it formed numerous diverticula closely enveloped by a surrounding vesicle, in a typical pusular configuration (arrows in Fig. 5A, B). The cell examined had accumulated a large number of oil droplets in the ventral area surrounding the sulcus, which made delimitation of the eyespot uncertain (not shown).

The flagellar base area of *T. rubescens* n. sp. is shown in serial sections in Fig. 6A–J, as seen from the ventral-right side and progressing away from the observer. A row of

microtubules, accompanied by numerous electron-opaque vesicles, extended toward the protruding, electron-opaque structure called ventral ridge (vr), just anterior to the insertion position of the basal bodies (Fig. 6A, B). No connection was seen between any of the flagellar roots and this row of microtubules, which is interpreted as the microtubular strand of the peduncle (MSP), although an extended peduncle was not detected in any cell. Each flagellum was inserted in the cytoplasm within a depression lined by a single membrane; the opening to the exterior of these so-called flagellar canals was surrounded by a fibrous ring, known as the transverse and the longitudinal striated collars (TSC and LSC, respectively) (Fig. 6E, F). The basal bodies were roughly 400 nm apart and formed an angle of about 120°, as estimated from serial-section observations. The longitudinal basal body (LB) associated on its proximal-left side with a strand of microtubules, the so-called longitudinal microtubular root or root 1 (LMR/r1). The proximal end of the LMR/r1 extended past the LB toward the ventral side for almost 1 μm (Fig. 6C–F). The proximal end of the transverse basal body (TB) was associated with two roots. The so-called transverse microtubular root, or root 3, (TMR/r3) started as a single microtubule closely following the anterior surface of the TB for some 300 nm before diverging gradually toward the anterior-left until it reached the surface of the flagellar canal; the TMR/r3 then sharply turned towards the cell apex, along a row of collared pits, and nucleated a series of about a dozen microtubules (Fig. 6F–J). The second microtubular root associated with the proximal end of the TB was a single microtubule closely connected to a striated fibre known as the transverse striated root (TSR; Fig. 6E–J); the microtubule is interpreted as root 4 (TSRM/r4). The TSR extended from the posterior surface of the TB toward the cell surface and ended near the TSC (Fig. 6I, J); on its proximal end, the TSR continued to the right, beyond the base of the TB, for over 500 nm (Fig. 6F). A distinctly striated fibrous component, the so-called striated root connective (SRC), linked the dorsal-anterior face of the LMR/r1 to the posterior side of the TSR (Fig. 6D–F).
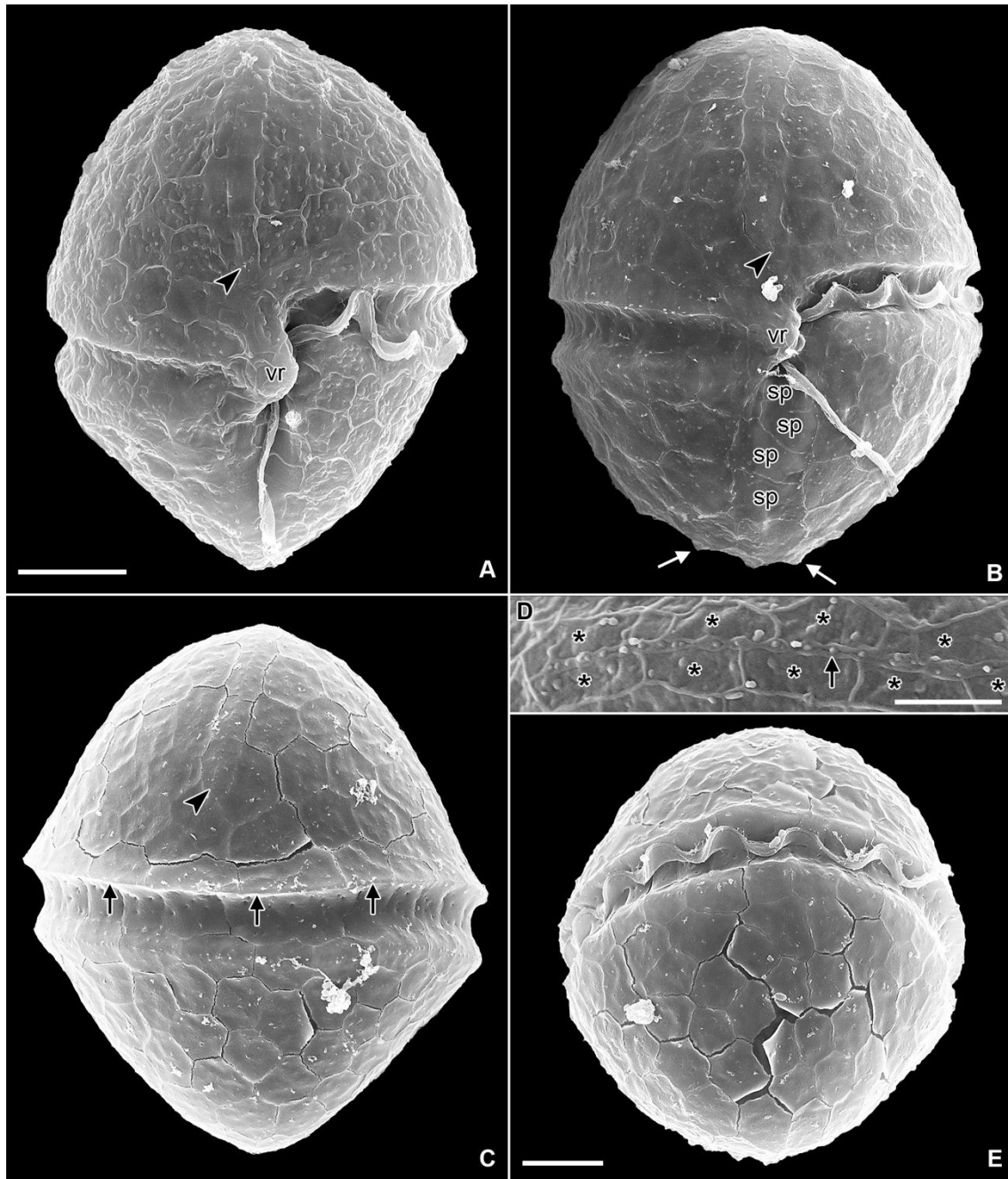
Fig. 3. *Tovellia rubescens* n. sp., SEM. **A**, **B**. Ventral views, cell in **A** with smooth surface and conical hypocone, cell in **B** ellipsoid, with the hypocone somewhat denticulate in outline caused by a slight projection of the sutures (arrows). Four plates (sp) are disposed almost linearly along the sulcus. The arrowheads indicate the proximal end of the apical line of narrow plates (ALP). **C**. Dorsal view showing the distal end of the ALP (arrowhead) and the sharply delineated anterior border of the cingulum (arrows). **D**. Detail of the ALP composed by a row of very narrow plates with an axial row of knobs (arrow) and bordered by two rows of elongated plates (asterisks). **E**. Dorso-antapical view, showing the antapex. vr, ventral ridge. Scale bars: A = 5 µm; D = 2 µm; E = 5 µm. B and C, same scale as A.
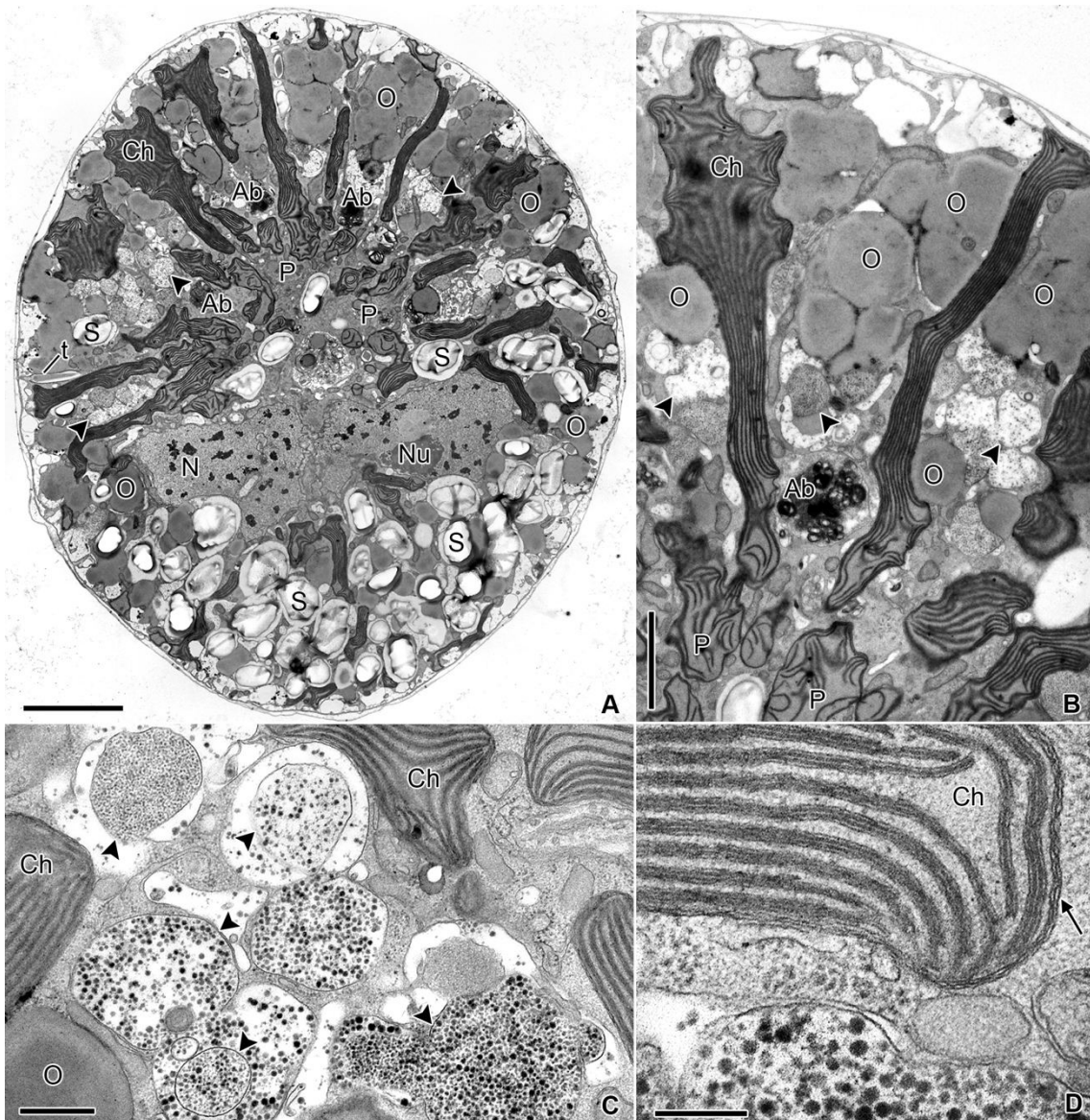
Fig. 4. *Tovellia rubescens* n. sp., general ultrastructure, TEM. **A**. Longitudinal section of a cell seen from the ventral-right side showing the position of the nucleus (N) and the chloroplast lobes (Ch) radiating from a central compound pyrenoid (P). Numerous oil droplets (O) are visible in the epicone and starch grains (S) in the hypocone. Vesicles with numerous, small, electron-opaque granules are marked with arrowheads. **B**. Chloroplast lobes (Ch) intercalated with oil droplets and vesicles with electron-opaque granules (arrowheads). **C**. Vesicles with electron-opaque granules (arrowheads). **D**. Detail of a chloroplast lobe surrounded by three membranes (arrow) and part of a vesicle containing electron-opaque granules. Ab, accumulation body; nu, nucleolus; t, trichocyst. Scale bars: A = 5 µm; B = 2 µm; C = 500 nm; D = 200 nm.
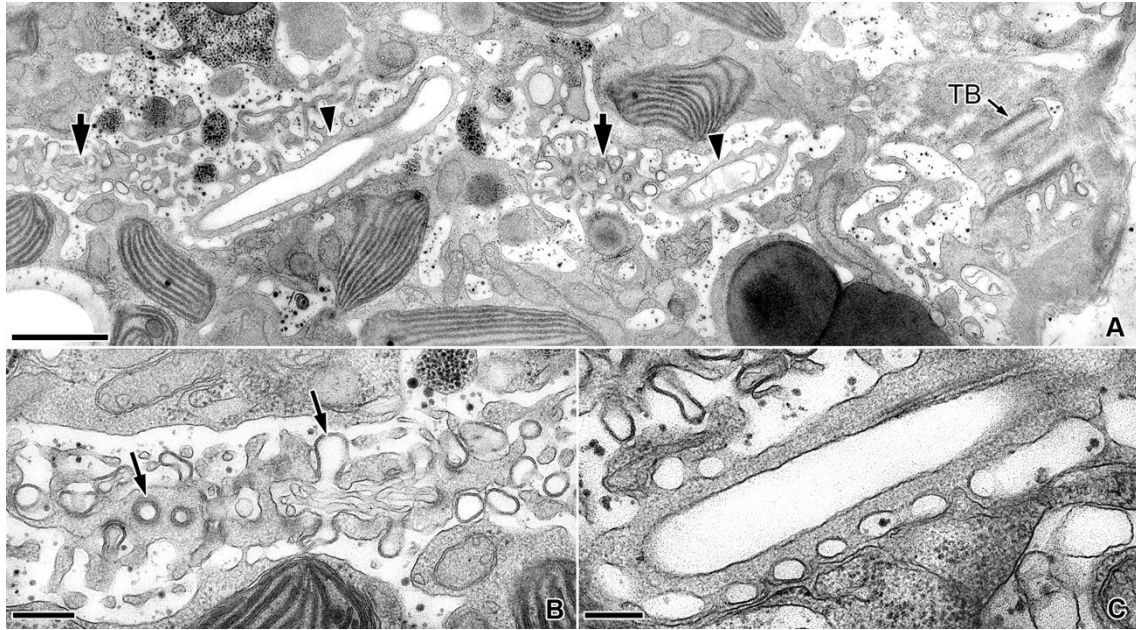
Fig. 5. *Tovellia rubescens* n. sp., pusular system, TEM. **A**. Sections through the pusular tube, some showing diverticula (short arrows) and others showing the tube lined by a single membrane (arrowheads). The flagellar base area is marked on the right side of the image by the transverse basal body (TB). **B**. Transverse and longitudinal sections through diverticula of the pusular tube (arrows). **C**. Portion of pusular tube lined by a single membrane. Scale bars: A = 1 μm; B = 300 nm; C = 200 nm.

Notes on the life cycle

Cells of *T. rubescens* n. sp. divided into two or four in the immobile stage (Fig. 7A–H). Before division, cells stopped, lost both flagella and rounded up, revealing a separate, outer layer. The nucleus of these division cysts then migrated towards the cell centre, where mitosis took place (Fig. 7A, B). Cytokinesis into two cells closely followed mitosis through the development of a cleavage furrow across the middle of the cell (Fig. 7B). Cytokinesis into four cells seemed to be a one-step process in which cleavage furrows extended inward from the periphery, separating four cells in a tetrahedral arrangement (Fig. 7C–E). Offspring cells slowly emerged from the division cyst following the rupture of its surface layer and started swimming, usually within a few minutes (Fig. 7F–H); the flagella, especially the longitudinal, were sometimes noted already inside the cyst. After being released from division cysts most cells grew for several days until they eventually divided again.

Attempts to induce sexual reproduction were generally unsuccessful. A minority of small cells eventually appeared in all batches, whether in single culture lines grown in

full growth medium, or in single or mixed culture lines grown in full, N-deficient or P-deficient medium. However, groups of small cells swimming around one another (the "dancing groups" of Stosch 1973) were never observed and the origin of pairs of connected cells that appeared in the batches is uncertain. Cells in these pairs were connected by the epicones (Fig. 8A) or by their dorso-lateral sides (Fig. 8B). Repeated observations of such paired cells isolated into separate culture-plate wells showed progressive fusion, suggesting they were in fact fusing gametes. However, the putative fusion was never observed to yield regular planozygotes; instead, cells kept an abnormal aspect, with the longitudinal flagella emerging from different, sometimes distant positions in the cell (not shown). To confuse matters further, similar cells were seen exiting from immobile stages reminiscent of division cysts. Whatever their origin, these "double-cell" forms swam for several days and eventually died, leaving their significance uncertain. Ellipsoid or ovoid brownish-red cells without flagella and with a smooth wall-like cover appeared in low numbers in old batches and in cultures grown in N-deficient and P-deficient medium (Fig. 8C). These cyst-like cells were repeatedly observed on the bottom of culture wells and their contents were seen to degrade soon, rendering further observations unfeasible. Fully formed resistance cells were never found in the cultures. Resting cysts resembling these cyst-like cells in general shape and contents were collected several times from the pond where the original strain of *T. rubescens* n. sp. originated. However, contrary to the smooth surface of walled cells formed in culture, cysts collected from the field had 2.5–5.0-µm long spines with pointed or sometimes branched tips (Fig. 8D–F). On the basis of ITS sequences determined from field-collected cysts with the described morphology, these resting cells were interpreted as belonging to *T. rubescens* n. sp. Field-collected cysts isolated into full medium germinated after 4–6 d, giving rise to swimming cells with *T. rubescens* n. sp. morphology, also with reddish bodies in the hypocone. However, these cells divided, at most, a few times and did not produce viable cultures.
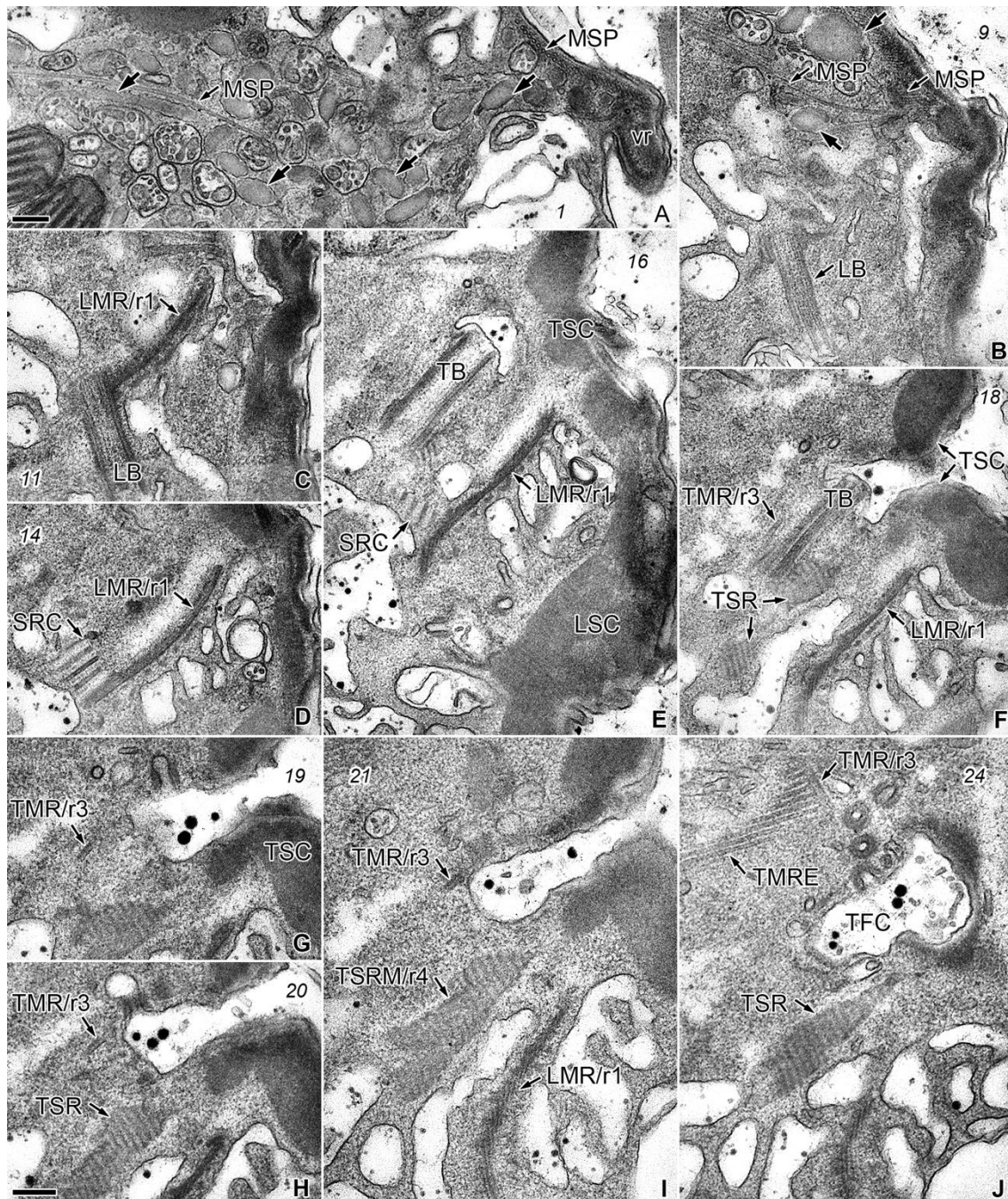
Fig. 6. *Tovellia rubescens* n. sp., flagellar apparatus, TEM. Non-adjacent serial sections viewed approximately from the ventral-right side of the cell and progressing away from the observer. Small slanted numbers represent section number. **A**, **B**. The microtubular strand of the peduncle (MSP) and accompanying electron-opaque vesicles (arrows) converge to the ventral area, near the ventral ridge (vr). **C-F**. The relatively long and straight proximal part of the longitudinal microtubular root (LMR/r1) contacts the longitudinal basal body (LB) in C, and the striated root connective (SRC) in D. In E, the SRC reaches the transverse striated root (TSR). The transverse microtubular root (TMR/r3) is marked in F, near the anterior surface of the TB. **G-J**. The TMR/r3 extends towards a row of collared pits at the surface of the transverse flagellar canal (TFC), turns upward and nucleates a row of microtubules (transverse microtubular root extension, TMRE; marked in J). The TSR and its associated microtubule (TSRM/r4) extend towards the cell surface, near the transverse striated collar (TSC). LSC, longitudinal striated collar. Scale bars = 200 nm. B-E, same scale as A. F, G, I and J, same scale as H.
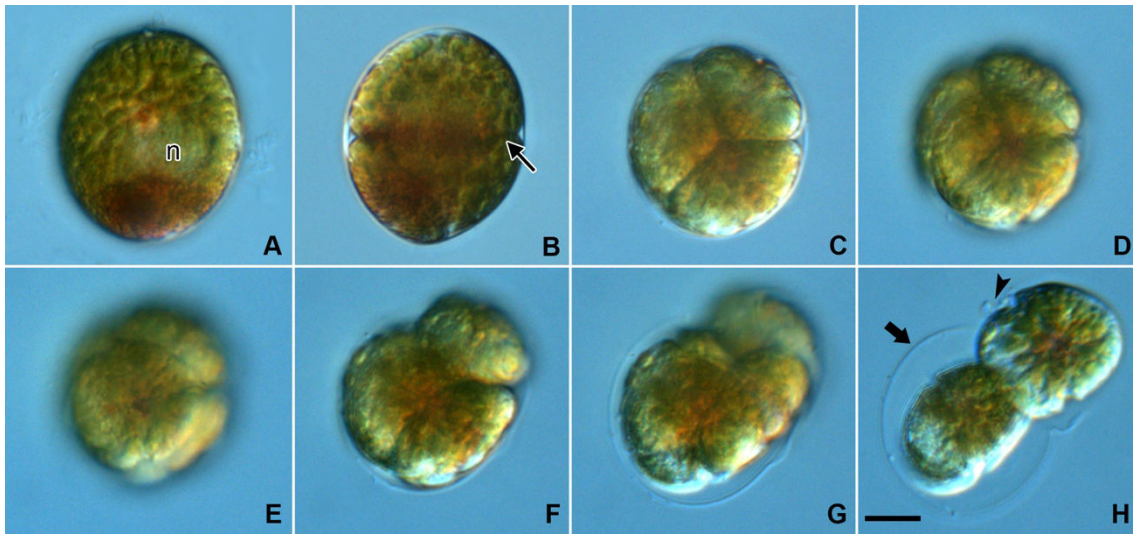
Fig. 7. *Tovellia rubescens* n. sp., asexual reproduction, LM. **A**, **B**. Stages during division into two cells. The cell lost mobility and the nucleus (n) migrated to the cell centre (A). Cytokinesis occurs through the formation of a cleavage furrow (thin arrow in B). **C-E**. Division cyst with four cells in tetrahedral arrangement (different focal levels). **F-H**. Release of daughter cells following the rupture of the enveloping layers of the cyst (thick arrow). The transverse flagellum of one cell is perceptible (arrowhead in H). Scale bar = 10 μm. All to the same scale.
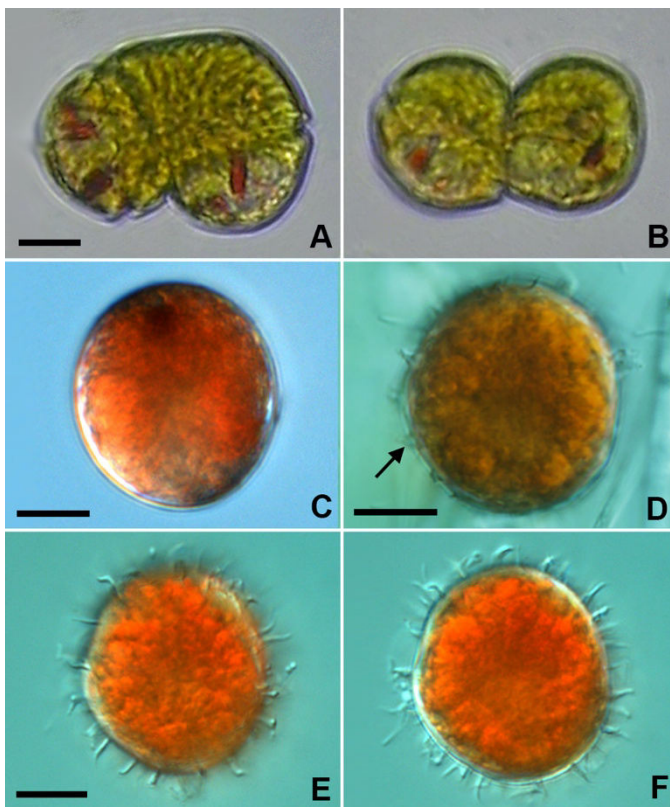
Fig. 8. *Tovellia rubescens* n. sp., paired cells of uncertain significance, and resting stages, LM. **A**, **B**. Cells connected by the epicones and by their dorsal-lateral sides, respectively. **C**. A non-motile, brownish-red cell from culture. **D-F**. Field-collected cysts with ornamented walls. Scale bars = 10 μm. A and B, same scale. E and F, same scale.

Colour changes and pigment analyses

The acquisition of a reddish tinge occurred gradually in cells as batches grown in full medium approached the lag phase. Although distinct at the cell level, colouration of batches was very slight, manifesting mostly in reddish-brown deposits on the bottom of culture bottles. In N-deficient and P-deficient media, the reddening developed sooner and was visible in most cells of 10-d old batches. The final cell densities obtained in incomplete media, quite lower than in full medium, along with the shorter exponential growth phase, made direct comparisons of pigment concentrations unreliable. In addition, differences in cell size, which tended to be more irregular, but generally smaller in incomplete media, precludes any attempt to normalize results based on the number of cells extracted. The pigments detected in extracts from batches of *T. rubescens* n. sp. grown in full and in N-deficient medium, and of *T. aveirensis* grown in similar conditions are shown in Table 1. The results in Table 1 are not quantitative, both in the sense that concentrations cannot be inferred from these data and in that direct comparisons across columns are not valid. However, the relative values associated with the detection intensities are a rough indication of proportions between pigments detected in a particular batch. Also, only the more abundant species were identified by MS/MS, while less abundant species were only identified by their molecular weight. The photosynthetic apparatus pigments identified were standard for peridinin-containing dinoflagellates. Astaxanthin and several compounds related to astaxanthin metabolism (adonirubin, astacene, astaxanthin monoesters) were unequivocally identified in *T. rubescens* n. sp., both in full- medium and in N-deficient-medium grown batches. Astaxanthin, two of its monoesters and astacene were also present in *T. aveirensis*, although neither the cells nor the extract showed a red tinge.

Phylogeny of *Tovellia rubescens* n. sp.

The *Tovellia* species included in alignment 1, based on partial LSU rDNA sequences, formed a single clade with maximum statistical support (Fig. 9). *Tovellia rubescens* n. sp. formed a highly supported sister taxon to *T. aveirensis* and *T.* cf. *aveirensis* (posterior probability = 1, bootstrap support = 100%). *Tovellia sanguinea* and *T. coronata* (Wołoszyńska) Moestrup, K. Lindberg and Daugbjerg (both species with red cells) appear in the Bayesian tree (Fig. 9) as the nearest relatives to *T. rubescens* n. sp. and *T. aveirensis*

with lower statistical support. *Tovellia rinoi* formed the earliest divergent lineage among the *Tovellia* species included in alignment 1 (Fig. 9). The analysis did not clarify the closest relative to the Tovelliaceae because the deep branches formed a polytomy (Fig. 9).

The analysis of alignment 2, including only the Tovelliaceae present in alignment 1 with the addition of *Tovellia diexiensis*, again displays *T. rubescens* n. sp. as a sister taxon to *T. aveirensis* and *T.* cf. *aveirensis* with the highest statistical support (Fig. 10). *Tovellia diexiensis* and *T. sanguinea* form a clade with high posterior probability (pp = 1), but poor bootstrap support (bs = 75%). *Tovellia coronata*, the *T. sanguinea*/*T. diexiensis* clade and the *T. rubescens* n. sp./*T. aveirensis* clade formed a polytomy (i.e. no statistical support for the tree topology) (Fig. 10).

DISCUSSION

Taxonomic affinities of *Tovellia rubescens* n. sp.

Motile cells of *T. rubescens* n. sp. showed a combination of morphological features typical of Tovelliaceae, including a tubular pusule with diverticula (see Calado 2011; Calado et al. 2006), an extraplastidial eyespot of type C (Moestrup and Daugbjerg 2007), an amphiesma made of numerous vesicles with thin plates roughly arranged in latitudinal series, and the general arrangement of basal bodies and flagellar roots (see below). The presence of an ALP sensu Lindberg et al. (2005) surrounded by two rows of narrow apical plates places the new species in *Tovellia*. The taxonomic affinity with other *Tovellia* species is also unequivocally supported by LSU rDNA-based analyses, which mark *T. aveirensis* as the closest known relative of *T. rubescens* n. sp.

Morphological comparisons between described species of *Tovellia* have been summarized in Pandeirada et al. (2014), Li et al. (2015) and Zhang et al. (2016); a further species, *T. rinoi*, was described after the publication of these articles (Pandeirada et al. 2017). *Tovellia rubescens* n. sp. cells showed a wide range of sizes, which reduces the value of cell dimensions as a feature for distinction from other species. In contrast, plate arrangement, with 12–15 latitudinal series of plates (including two series in the cingulum) separates *T. rubescens* n. sp. from *T. coronata*, *T. diexiensis*, *T. glabra* (Wołoszyńska) Moestrup, K. Lindberg and Daugbjerg, *T. nygaardii* Moestrup, K. Lindberg and Daugbjerg, *T. paldangensis* Zhun Li, M. S. Han and H. H. Shin, *T. rinoi* and *T. sanguinea*,

Table 1. Pigments identified by HPLC–MS/MS in extracts from *Tovellia rubescens* n. sp. and *Tovellia aveirensis* culture batches grown with and without a nitrogen (N) source.

Pigment	m/z ([M+H]+)	*T. rubescens*[a]		*T. aveirensis*[a]	
		with N	without N	with N	without N
Adonirubin	581.4	1.3×10^4	2×10^4	nd	nd
Astaxanthin	597.4	1.4×10^5	3.2×10^4	3.8×10^5	1.5×10^4
Astx monoester 14:0	807.6	8.4×10^4	7.8×10^4	vest	vest
Astx monoester 16:0	835.6	1.5×10^5	1.3×10^5	1.7×10^4	nd
Astx monoester 16:4	829.6	9.3×10^3	3.3×10^4	4.0×10^4	nd
Astx monoester 18:0	863.7	3.1×10^4	4.0×10^4	nd	nd
Astx monoester 18:1	861.6	1.0×10^4	3.8×10^3	nd	nd
Astacene	593.4	4.0×10^4	1.7×10^4	1.8×10^4	nd
Canthaxanthin	565.4	3.2×10^4	nd	nd	nd
Chlorophyll a	893.5	5.1×10^3	nd	nd	nd
Chlorophyll c2	609.2	1.7×10^4	nd	nd	nd
Diadinoxanthin	583.4	2.0×10^5	8.0×10^4	4.6×10^4	5.3×10^4
Dinoxanthin	643.4	3.4×10^4	9.4×10^3	7.0×10^4	2.5×10^4
Peridinin	631.4	2.7×10^4	2.7×10^4	1.0×10^4	8.4×10^3
β-Carotene	537.4	2.0×10^4	5.6×10^3	nd	nd

[a] Relative abundance of the molecular ion of the pigment, in counts, from cells grown with and without a source of nitrogen (N). nd, no detection; vest, vestigial.

The approximate number of cells used for pigment extraction was: 108.000 for both growth conditions of *T. rubescens* n. sp.; 68.900 cells of *T. aveirensis* grown in N-deficient medium, and 133.800 grown in full medium.

none of which exceed 10 latitudinal series; and from *Tovellia stoschii* (Shyam and Sarma) Moestrup, K. Lindberg and Daugbjerg, which has about 17 latitudinal series of relatively small plates (Christen 1958; Li et al. 2015; Lindberg et al. 2005; Moestrup et al. 2006; Shyam and Sarma 1976; Wołoszyńska 1917; Zhang et al. 2016). *Tovellia apiculata* (Stosch) Moestrup, K. Lindberg and Daugbjerg, *T. aveirensis* and *T. leopoliensis* (Wołoszyńska) Moestrup, K. Lindberg and Daugbjerg have numbers of latitudinal plate series similar to *T. rubescens* n. sp., but show other differences. Motile cells of *T. leopoliensis* are strongly flattened dorsoventrally, making it very distinctive within the genus (Moestrup and Calado 2018; Wołoszyńska 1917). Vegetative cells of *T. aveirensis* are more smoothly rounded than *T. rubescens* n. sp., especially on the hypocone, which rarely is slightly pointed; the ALP of *T. aveirensis* is shorter on the dorsal side (Pandeirada et al. 2014), with up to five plates separating its dorsal end from the cingulum, versus two (rarely three) plates in *T. rubescens* n. sp. The cell shape of *T. rubescens* n. sp. resembles that of *T. apiculata*, except for the antapical "apiculus," made by three to four plates, that justifies the latter species' name (Stosch 1973). The cyst described for *T. apiculata* also showed a sharp antapical projection and was of the *T. coronata* type, that is, somewhat projected along the axis and with two latitudinal rings of protuberances, one anterior and one posterior to an equatorial con- striction (Stosch 1973). In contrast, the field-collected red cysts with an ITS rDNA sequence identical to motile cells of *T. rubescens* n. sp. did not show a marked paracingulum and were covered by evenly distributed spines. This general morphology appears closer to the cysts of *T. aveirensis*, which, however, showed a marked paracingulum and spines twice as long when mature; and, to some extent, to cysts of *T. paldangensis*, which had much fewer and shorter spines (Moestrup and Calado 2018; Pandeirada et al. 2014). The presence of a cyst of the same general type was the justification for the recent transfer of *T. dodgei* (Sarma and Shyam) K. N. Mertens and H. Gu from the genus *Gymnodinium* (Luo et al. 2016; Sarma and Shyam 1974). The cysts of *T. dodgei* were also red, but the motile cells were more elongate and the sulcus invaded the epicone, creating a distinct plough-shaped depression. The chloroplasts of *T. dodgei* were described as discoid, whereas radiating chloroplast lobes were visible in *T. rubescens* n. sp., even in LM. The organization of the amphiesmal plates of *T. dodgei* was not described (Moestrup and Calado 2018; Sarma and Shyam 1974). A sequence divergence was estimated to evaluate the molecular support for a species delineation

between the closely related *T. rubescens* n. sp. and *T. aveirensis*. Using the Kimura-2-parameter model and 1,344 aligned base pairs of the LSU rDNA (including domain D2) the divergence estimate was 3.9%. Despite some overlap in morphology, this divergence indicates two distinct species.

Cell ultrastructure

The arrangement of flagellar bases and roots observed in one cell of *T. rubescens* n. sp. closely matched what has been described from other members of the Tovelliaceae, particularly the relative positioning of the basal bodies, with the nearly 400-nm distance between their proximal ends highlighted by the large SRC and its connection to the proximal part of the TSR (see summary of tovelliacean characters in Calado 2011). The nearly straight proximal part of the LMR/r1 that projects ventrally past the LB is another feature in common with species of Tovelliaceae for which the disposition of flagellar roots is known in enough detail (Calado 2011; Calado et al. 2006; Roberts and Timpano 1989; Roberts et al. 1995). The arrangement of roots and connectives near the flagellar bases is consistently different in species of Peridiniales, in which the SRC is replaced by a much wider layered connective, which spans a rather shorter distance between the TSR and a fibrous layer on the dorsal face of the LMR/r1 (Calado et al. 1999; Craveiro et al. 2009, 2013, 2015). Where known, species of Gonyaulacales and Suessiales have the dorsal side of the LMR/r1 linked to a more distal area of the TSR by a narrow SRC and, like the Peridiniales, have a curved proximal end of LMR/r1 barely projecting beyond the LB (Craveiro et al. 2010; Hansen and Moestrup 1998; Jeong et al. 2014; Roberts 1989).

$\longrightarrow$

Fig. 9. Phylogeny of *Tovellia rubescens* n. sp. based on nuclear-encoded LSU rDNA (1151 base pairs) and analysed with Bayesian inference. The ingroup of dinoflagellates was polarized using ciliates (3 species), apicomplexan (4 species) and a perkinsozoan. Numbers to the left of slashes at internal nodes are posterior probabilities ($\geq$ 0.5) from Bayesian analysis followed by bootstrap values ($\geq$ 50%) from maximum likelihood with 1000 replications. Bootstrap values <50% are indicated by a '-'. Filled circles replace numbers when statistical support was the highest possible for both Bayesian and maximum likelihood analyses (1.0 and 100%, respectively). GenBank accession numbers are added in parentheses. Dinoflagellates with type C eyespot sensu Moestrup and Daugbjerg (2007), corresponding to the family Tovelliaceae, are marked by a rectangle. Branch lengths are proportional to the number of character changes.

The radial chloroplast lobes associated with a central pyrenoid complex observed in *T. rubescens* n. sp. match the chloroplast arrangement of the closely related *T. sanguinea* and *T. aveirensis* (Moestrup et al. 2006; Pandeirada et al. 2014). In contrast, *T. coronata* did not display a central pyrenoid complex (Lindberg et al. 2005). The recently described *T. diexiensis*, which appears as a close relative of *T. sanguinea* in LSU rDNA-based

phylogenies, was reported to have small, parietal chloroplasts that were often difficult to discern due to the presence of numerous red bodies (Zhang et al. 2016). The reported absence of a central pyrenoid complex in *T. diexiensis* suggests an unexpected lability in the plastidome of this group of species. The observation by LM of the radial arrangement of chloroplast lobes can be remarkably difficult even in cells larger than *T. diexiensis* (Craveiro et al. 2009); whether a central pyrenoid complex may have passed undetected during epifluorescence observations is, however, unclear.
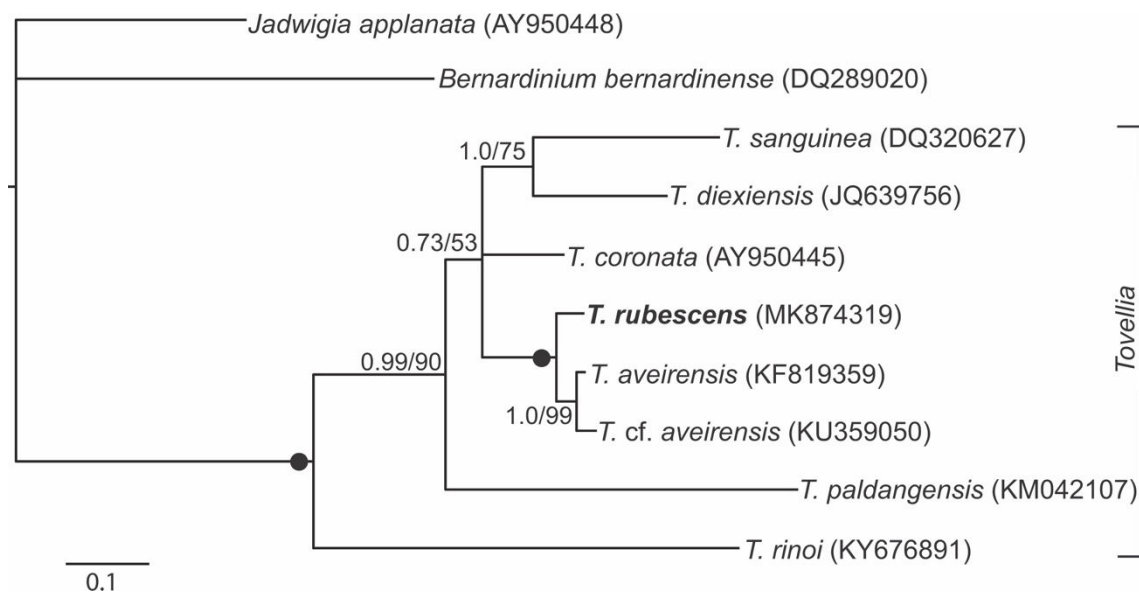
Fig. 10. Phylogeny of *Tovellia rubescens* n. sp. and 6 other well circumscribed species of *Tovellia* based on 714 base pairs (including domain D1-D2) and analysed with Bayesian inference. *Jadwigia* formed the outgroup taxon. Numbers to the left of slashes at internal nodes are posterior probabilities (≥ 0.5) from Bayesian analysis followed by bootstrap values (≥ 50%) from maximum likelihood with 1000 replications. Filled circles represent maximum support. GenBank accession numbers are written in parentheses and branch lengths are proportional to the number of character changes.

A row of microtubules accompanied by vesicles with electron-opaque contents, interpretable as an MSP, similar to the ones shown here for *T. rubescens* n. sp. and in Moestrup et al. (2006) for *T. sanguinea*, has been found in all species of *Tovellia* that have been examined by TEM (Moestrup et al. 2006, p. 59 concerning *T. coronata*; unpublished observations on *T. aveirensis*). Although observations on the MSP of species of *Tovellia* resemble what was demonstrated from predatory species with feeding mechanisms involving similar microtubular strands and vesicles (Calado et al. 1998, 2006), direct evidence of mixotrophy in the genus has not been reported.

The abundant oil droplets found between chloroplast lobes in a red cell of *T. rubescens* n. sp. are reminiscent of the oil bodies interpreted as the location of accumulated astaxanthin-related compounds in cells of green algae associated with red snow (Remias et al. 2016) and in species of the industrially important genera *Chlorella* Beijerinck and *Haematococcus* Flotow (Bar et al. 1995; Mulders et al. 2015; Santos and Mesquita 1984; Solovchenko 2015). Although apparently more localized in the cell, the pigment aggregates documented by TEM in *T. sanguinea* also displayed the roundish outline of lipid globules, suggesting the oil droplets of *T. rubescens* n. sp. as the likely structures where reddish pigments accumulate in this species (Moestrup et al. 2006). The significance of the numerous vesicles containing electron-opaque globules is unknown.

Life cycle

The mechanism of vegetative cell multiplication observed in *T. rubescens* n. sp. falls within the typical pattern established from other *Tovellia* species, in which 2–8 offspring cells are produced in a temporary, or division, cyst (Christen 1958; Pandeirada et al. 2014, 2017; Shyam and Sarma 1976; Stosch 1973; Wołoszyńska 1917; Zhang et al. 2016). However, contrary to what is known from other species of *Tovellia*, *T. dodgei* cells were reported to divide in the swimming stage (Sarma and Shyam 1974). Examination of *T. dodgei* by modern methods, including the clarification of amphiesmal features and molecular analysis, is necessary to establish its relationship with species of Tovelliaceae (Pandeirada et al. 2017).

The production of resting cysts as one of the possible outcomes of sexual reproduction is well established in the genus *Tovellia* (Pandeirada et al. 2017; Stosch 1973). The finding in the same pond of swimming cells of *T. rubescens* n. sp. and resting cysts with an identical ITS1-5.8S-ITS2 rDNA sequence suggests the occurrence of sexual reproduction in wild populations of the species. The lack of successful gamete fusion and viable resting cyst formation in culture batches maintained in the same conditions under which sexually reproducing strains of *T. aveirensis* and *T. rinoi* were observed may be explained by heterothally of the strains available (Pandeirada et al. 2014, 2017). Mixing the two available lines of *T. rubescens* n. sp. did not result in detectable sexual reproduction indicating sexual incompatibility. Likewise, no signs of sexual reproduction

were detected in experimental mixtures of *T. rubescens* n. sp. with available strains of *T. aveirensis*.

The occurrence in the culture batches of distinctly flattened cells that appeared strikingly different from the more common globose cells, with no intermediate morphologies, is noteworthy. The regular formation of small numbers of these cells in batches started by re-isolation of single cells of the cultures excluded the possibility that they originated from a contamination. We were not able to link the flat cells to any particular life cycle stage, nor to any particular function in the culture batches. A recent discussion on the significance of flattened cells appearing in cultures of *Protoceratium reticulatum* (Claparède and J. Lachmann) Buetschli and *Ceratocorys mariaovidiorum* P. Salgado, S. Fraga, F. Rodríguez, Riobó and I. Bravo suggests a link to a benthic stage of these species, arguably because flat cells would be better adapted to move in the interstitial environment of the sediment, or to attach to sediment particles (Salgado et al. 2018). Whether benthic flattened cells of *T. rubescens* n. sp. occur in the shallow ponds where the species was found is currently unknown.

Colour changes and pigment composition

The observed switch from a general yellowish-green colour of cells of *T. rubescens* n. sp. in culture batches during early exponential growth to a distinctly reddish-brown colour as batches approached the terminal lag phase suggests that the accumulation of red pigment is a response to stress. The more rapid induction of the reddish-brown colour in batches grown in N- or P-deficient medium points to nutrient deficiency as a trigger for the increase in red pigment concentration in the cells. Stress conditions, such as nutrient starvation or high light intensity, are among the standard methods for the induction of astaxanthin accumulation in mass cultures of industrially important producers of this antioxidant, green algae of the genera *Chlorella* and *Haematococcus* (Bar et al. 1995; Fábregas et al. 1998; Mulders et al. 2015).

Although astaxanthin has been reported from very few dinoflagellates, the abundance of astaxanthin and its esters in some red species of *Tovellia* is well documented (Frassanito et al. 2005; Zhang et al. 2016; see Frassanito et al. 2006 for earlier records of astaxanthin-related carotenoids in dinoflagellates). The finding of adonirubin and canthaxanthin in extracts of *T. rubescens* n. sp., and the absence of beta-cryptoxanthin,

zeanxanthin and adonixanthin suggest the pathway of astaxanthin biosynthesis that involves the enzyme beta-carotene ketolase (Han et al. 2013). The pigment analysis performed in the present work was expected to reveal the changes in pigment composition that determine the reddening of the cells of *T. rubescens* n. sp., namely through a marked increase in proportion of some of the red compounds relative to other pigments. However, the results of the analyses, summarized in Table 1, do not provide a clear explanation for the observed increase of the reddish-brown colour in cells of older or nutrient-depleted batches. It has been shown that the later stages of astaxanthin accumulation in *Haematococcus* and several other green algae mainly involve diesters of astaxanthin (Orosa et al. 2001) and astaxanthin diesters were identified in *T. sanguinea* and *T. diexiensis* (Frassanito et al. 2006; Zhang et al. 2016). However, the analyses reported herein for *T. rubescens* n. sp. were limited to a maximum range of m/z 1,000, leaving astaxanthin diesters out of range and rendering their participation in cell reddening in this species as speculative.

The inability of culture batches of *Tovellia aveirensis* to acquire a reddish colour, even when submitted to the same treatments that never failed to elicit the reddening of *T. rubescens* n. sp., was one of the earliest noted constant differences between the two species. Therefore, the detection of astaxanthin and astaxanthin monoesters in *T. aveirensis* came as a surprise. However, batches of *T. aveirensis* fared more poorly under nutrient stress than those of *T. rubescens* n. sp., and the overall amount of astaxanthin showed no signs of increasing, suggesting that a response to stress through activation of astaxanthin-related metabolic pathways is either reduced or absent in *T. aveirensis*. The presence of astaxanthin-related metabolism in *T. aveirensis* is coherent with its well-established phylogenetic relationship to a group of species in which reddish colouration has been linked to the accumulation of astaxanthin metabolites. In this context, the reported absence of astaxanthin in the phylogenetically related *T. coronata*, which also displays a red colour, is difficult to explain (Lindberg et al. 2005). Perhaps re-examination of the pigment composition of *T. coronata* using a combination of HPLC and mass spectroscopy would be justified to clarify the presence or absence of astaxanthin in this species.

TAXONOMIC SUMMARY

Meeting the requirements of the ICN 2018 (Turland et al. 2018).

Supergroup Alveolata [informal; based on Cavalier-Smith (1991), as infrakingdom]

Phylum Dinoflagellata Fensome et al. 1993

Class Dinophyceae F. E. Fritsch 1927

Order Tovelliales Moestrup and Calado 2018

Family Tovelliaceae Moestrup, K. Lindberg and Daugbjerg 2005

Genus Tovellia Moestrup, K. Lindberg and Daugbjerg 2005

Tovellia rubescens **Pandeirada, Craveiro, Daugbjerg, Moestrup and Calado n. sp.**

Description. Epicone nearly hemispherical and hypocone hemispherical to rounded conical, sometimes with a pointed antapex. Epicone occasionally projected at the level of the ALP. Cingulum descending, displaced about one cingulum width, epi- and hypocone of similar size. Most cells slightly compressed dorsoventrally, with hypocone somewhat flattened obliquely in lateral view, 18.5–43 μm long, 12.5–33 μm wide and 11.5–28 μm thick. Chloroplasts yellowish-green, with lobes radiating from a central pyrenoid complex. Eyespot red, extraplastidial, located along the sulcal area. Transversely elongated nucleus in the dorsal part of the hypocone. Accumulation bodies predominantly in the epicone, and small, rounded reddish-brown bodies in the hypocone. Vegetative cells changing from yellowish-green to reddish-brown in response to stress conditions. Some reddish-brown cells almost circular in ventral view and strongly compressed dorsoventrally. Amphiesma with numerous pentagonal or hexagonal vesicles containing thin plates, roughly disposed along six latitudinal series on the epicone and four or five series on the hypocone; cingulum with two series of plates, those of the anterior series rectangular or pentagonal and sharply defining the anterior edge of the cingulum, plates of the posterior series roughly hexagonal and extending onto the hypocone, over the rounded posterior cingulum edge. A line of narrow plates (ALP) extends over the apex of the cell, from nearly above the sulcus, about one plate away from the proximal end of the cingulum, to the dorsal side, two or three rows of plates from the anterior cingulum edge. Astaxanthin and metabolically related pigments present. Asexual division into two or four cells, by means of division cysts. Ellipsoid to ovoid brownish-red cysts without a marked

paracingulum, with the wall provided with evenly distributed 2.5–5 μm long spines with pointed or branched tips.

<u>Holotype</u>. SEM stub with critical point-dried cells from MSP1 culture line deposited at the University of Aveiro Herbarium, registered as AVE-A-T-8. Fig. 3A–E show cells from this stub.

<u>Type locality</u>. Freshwater lake in Gafanha da Boavista, Íhavo, Portugal (40°35′44.70″N, 8°41′49.66″W), sampled on 28 October 2010.

<u>Etymology</u>. Epithet from Latin *rubescens*, turning red, reddening.

<u>Gene sequence</u>. LSU rDNA sequence for *T. rubescens* deposited in GenBank with the accession number MK874319; the ITS1-5.8S-ITS2 rDNA sequence has the accession number MK874823.

<u>Zoobank registration number</u>. urn:lsid:zoobank.org: act:165E6F44-1A0E-44DE-91C9-0D662833FA00.

ACKNOWLEDGEMENTS

REFERENCES

Bar, E., Rise, M., Vishkautsan, M. & Arada, S. M. 1995. Pigment and structural changes in *Chlorella zofingiensis* upon light and nitrogen stress. *J. Plant Physiol.*, 146: 527–534.

Calado, A. J. 2011. On the identity of the freshwater dinoflagellate *Glenodinium edax*, with a discussion on the genera *Tyrannodinium* and *Katodinium*, and the description of *Opisthoaulax* gen. nov. *Phycologia*, 50: 641–649.

Calado, A. J., Craveiro, S. C., Daugbjerg, N. & Moestrup, Ø. 2006. Ultrastructure and LSU rDNA-based phylogeny of *Esoptrodinium gemma* (Dinophyceae), with notes on feeding behavior and the description of the flagellar base area of a planozygote. *J. Phycol.*, 42: 434–452.

Calado, A. J., Craveiro, S. C. & Moestrup, Ø. 1998. Taxonomy and ultrastructure of a freshwater, heterotrophic *Amphidinium* (Dinophyceae) that feeds on unicellular protists. *J. Phycol.*, 34: 536–554.

Calado, A. J., Hansen, G. & Moestrup, Ø. 1999. Architecture of the flagellar apparatus and related structures in the type species of *Peridinium*, *P. cinctum* (Dinophyceae). *Eur. J. Phycol.*, 34: 179–191.

Cavalier-Smith, T. 1991. Cell diversification in heterotrophic flagellates. *In*: Patterson, D. J. & Larsen, J. (ed.), The Biology of Free-living Heterotrophic Flagellates. Clarendon Press, Oxford. p. 113–131.

Christen, H. R. 1958. *Gymnodinium nygaardi* sp. nov. Ber. Schweiz. Bot. Ges., 68: 44–49.

Craveiro, S. C., Calado, A. J., Daugbjerg, N. & Moestrup, Ø. 2009. Ultrastructure and LSU rDNA-based revision of *Peridinium* group palatinum (Dinophyceae) with the description of *Palatinus* gen. nov. *J. Phycol.*, 45: 1175–1194.

Craveiro, S. C., Daugbjerg, N., Moestrup, Ø. & Calado, A. J. 2015. Fine-structural characterization and phylogeny of *Peridinium polonicum*, type species of the recently described genus *Naiadinium* (Dinophyceae). *Eur. J. Protistol.*, 51: 259–279.

Craveiro, S. C., Moestrup, Ø., Daugbjerg, N. & Calado, A. J. 2010. Ultrastructure and large subunit rDNA-based phylogeny of *Sphaerodinium cracoviense*, an unusual freshwater dinoflagellate with a novel type of eyespot. J. *Eukaryot. Microbiol.*, 57: 568–585.

Craveiro, S. C., Pandeirada, M. S., Daugbjerg, N., Moestrup, Ø. & Calado, A. J. 2013. Ultrastructure and phylogeny of *Theleodinium calcisporum* gen. et sp. nov., a freshwater dinoflagellate that produces calcareous cysts. *Phycologia*, 52: 488–507.

Darriba, D., Taboada, G. L., Doallo, R. & Posada, D. 2012. jModelTest 2: more models, new heuristics and parallel computing. *Nat. Methods*, 9: 772.

Daugbjerg, N., Andreasen, T., Happel, E., Pandeirada, M. S., Hansen, G., Craveiro, S. C., Calado, A. J. & Moestrup, Ø. 2014. Studies on woloszynskioid dinoflagellates VII: description of *Borghiella andersenii* sp. nov.: light and electron microscopy and phylogeny based on LSU rDNA. *Eur. J. Phycol.*, 49: 436–449.

Daugbjerg, N., Hansen, G., Larsen, J. & Moestrup, Ø. 2000. Phylogeny of some of the major genera of dinoflagellates based on ultrastructure and partial LSU rDNA sequence data, including the erection of three new genera of unarmoured dinoflagellates. *Phycologia*, 39:302–317.

Fábregas, J., Domínguez, A., Álvarez, D. G., Lamela, T. & Otero, A. 1998. Induction of astaxanthin accumulation by nitrogen and magnesium deficiencies in *Haematococcus pluvialis*. *Biotechnol. Lett.*, 20: 623–626.

Frassanito, R., Cantonati, M., Tardìo, M., Mancini, I. & Guella, G. 2005. On-line identification of secondary metabolites in freshwater microalgae and cyanobacteria by combined liquid chromatography-photodiode array detection-mass spectrometric techniques. *J. Chromatogr. A*, 1082: 33–42.

Frassanito, R., Flaim, G., Mancini, I. & Guella, G. 2006. High production of unexpected carotenoids in Dinophyceae. Astaxanthin esters from the freshwater dinoflagellate *Tovellia sanguinea*. *Biochem. Syst. Ecol.*, 34: 843–853.

Guindon, S. & Gascuel, O. 2003. A simple, fast, and accurate algorithm to estimate large phylogenies by maximum likelihood. *Syst. Biol.*, 52: 694–704.

Han, D., Li, Y. & Hu, Q. 2013. Astaxanthin in microalgae: pathways, functions and biotechnological implications. *Algae*, 28: 131–147.

Hansen, G. & Moestrup, Ø. 1998. Fine-structural characterization of *Alexandrium catenella* (Dinophyceae) with special emphasis on the flagellar apparatus. *Eur. J. Phycol.*, 33: 281–291.

Jeong, H. J., Jang, S. H., Moestrup, Ø., Kang, N. S., Lee, S. Y., Potvin, É. & Noh, J. H. 2014. *Ansanella granifera* gen. et sp. nov. (Dinophyceae), a new dinoflagellate from the coastal waters of Korea. *Algae*, 29: 75–99.

Lenaers, G., Maroteaux, L., Michot, B. & Herzog, M. 1989. Dinoflagellates in evolution. A molecular phylogenetic analysis of large subunit ribosomal RNA. *J. Mol. Evol.*, 29: 40–51.

Li, Z., Shin, H. H. & Han, M. 2015. Morphology and phylogeny of a new woloszynskioid dinoflagellate *Tovellia paldangensis* sp. nov. (Dinophyceae). *Phycologia*, 54: 67–77.

Lindberg, K., Moestrup, Ø. & Daugbjerg, N. 2005. Studies on woloszynskioid dinoflagellates I: *Woloszynskia coronata* re-examined using light and electron microscopy and partial LSU rDNA sequences, with description of *Tovellia* gen. nov. and *Jadwigia* gen. nov. (Tovelliaceae fam. nov.). *Phycologia*, 44: 416–440.

Lindström, K. 1991. Nutrient requirements of the dinoflagellate *Peridinium gatunense*. *J. Phycol.*, 27: 207–219.

Luo, Z., You, X., Mertens, K. N. & Gu, H. 2016. Morphological and molecular characterization of *Tovellia* cf. *aveirensis* (Dinophyceae) from Jiulong River, China. *Nova Hedwigia*, 103: 79–94.

Moestrup, Ø. & Calado, A. J. 2018. Dinophyceae. *In*: Büdel, B., Gärtner, G., Krienitz, L. & Schagerl, M. (ed.), Süsswasserflora von Mitteleuropa — Freshwater Flora of Central Europe, vol. 6, 2nd ed., Springer-Verlag, Berlin. XII + 561 pp.

Moestrup, Ø. & Daugbjerg, N. 2007. On dinoflagellate phylogeny and classification. *In*: Brodie, J. & Lewis, J. (ed.), Unravelling the Algae. The Past, Present, and Future of Algal Systematics. CRC Press, Boca Raton, FL. Systematics Association Special Volume No. 75: 215–230.

Moestrup, Ø., Hansen, G., Daugbjerg, N., Flaim, G. & D'Andrea, M. 2006. Studies on woloszynskioid dinoflagellates II: on *Tovellia sanguinea* sp. nov., the

dinoflagellate responsible for the reddening of Lake Tovel, N. Italy. *Eur. J. Phycol.*, 41: 47–65.

Mulders, K. J. M., Weesepoel, Y., Bodenes, P., Lamers, P. P., Vincken, J., Martens, D. E., Gruppen, H. & Wijffels, R. H. 2015. Nitrogen-depleted *Chlorella zofingiensis* produces astaxanthin, ketolutein and their fatty acid esters: a carotenoid metabolism study. *J. Appl. Phycol.*, 27: 125–140.

Orosa, M., Valero, J. F., Herrero, C. & Abalde, J. 2001. Comparison of the accumulation of astaxanthin in *Haematococcus pluvialis* and other green microalgae under N-starvation and high light conditions. *Biotechnol. Lett.*, 23: 1079–1085.

Pandeirada, M. S., Craveiro, S. C. & Calado, A. J. 2013. Freshwater dinoflagellates in Portugal (W Iberia): a critical checklist and new observations. *Nova Hedwigia*, 97: 321–348.

Pandeirada, M. S., Craveiro, S. C., Daugbjerg, N., Moestrup, Ø. & Calado, A. J. 2014. Studies on woloszynskioid dinoflagellates VI: description of *Tovellia aveirensis* sp. nov. (Dinophyceae), a new species of Tovelliaceae with spiny cysts. *Eur. J. Phycol.*, 49: 230–243.

Pandeirada, M. S., Craveiro, S. C., Daugbjerg, N., Moestrup, Ø. & Calado, A. J. 2017. Studies on woloszynskioid dinoflagellates VIII: life cycle, resting cyst morphology and phylogeny of *Tovellia rinoi* sp. nov. (Dinophyceae). *Phycologia*, 56: 533–548.

Popovský, J. & Pfiester, L. A. 1990. Dinophyceae (Dinoflagellida). *In*: Ettl, H., Gerloff, J., Heynig, H. & Mollenhauer, D. (ed.), Süsswasserflora von Mitteleuropa, Vol. 6. G. Fischer, Jena. p. 272.

Remias, D., Pichrtová, M., Pangratz, M., Lütz, C. & Holzinger, A. 2016. Ecophysiology, secondary pigments and ultrastructure of *Chlainomonas* sp. (Chlorophyta) from the European Alps compared with *Chlamydomonas nivalis* forming red snow. *FEMS Microbiol. Ecol.*, 92: 1–11.

Roberts, K. R. 1989. Comparative analyses of the dinoflagellate flagellar apparatus. II. *Ceratium hirundinella*. *J. Phycol.*, 25: 270–280.

Roberts, K. R., Hansen, G. & Taylor, F. J. R. 1995. General ultrastructure and flagellar apparatus architecture of *Woloszynskia limnetica* (Dinophyceae). *J. Phycol.*, 31: 948–957.

Roberts, K. R. & Timpano, P. 1989. Comparative analyses of the dinoflagellate flagellar apparatus. I. *Woloszynskia* sp. *J. Phycol.*, 25: 26–36.

Ronquist, F. & Huelsenbeck, J. P. 2003. MrBayes 3: Bayesian phylogenetic inference under mixed models. *Bioinformatics*, 19: 1572–1574.

Salgado, P., Fraga, S., Rodríguez, F. & Bravo, I. 2018. Benthic flattened cells of the phylogenetically related marine dinoflagellates *Protoceratium reticulatum* and *Ceratocorys mariaovidiorum* (Gonyaulacales): a new type of cyst? *J. Phycol.*, 54: 138–149.

Santos, M. F. & Mesquita, J. F. 1984. Ultrastructural study of *Haematococcus lacustris* (Girod.) Rostafinksi (Volvocales) I. Some aspects of carotenogenesis. *Cytologia*, 49: 215–228.

Sarma, Y. S. R. K. & Shyam, R. 1974. On the morphology, reproduction and cytology of two freshwater dinoflagellates from India. *Brit. Phycol. J.*, 9: 21–29.

Scholin, C. A., Herzog, M., Sogin, M. & Anderson, D. M. 1994. Identification of group- and strain-specific genetic markers for globally distributed *Alexandrium* (Dinophyceae). II. Sequence analysis of a fragment of the LSU rRNA gene. *J. Phycol.*, 30: 999–1011.

Shyam, R. & Sarma, Y. S. R. K. 1976 ('1975'). *Woloszynskia stoschii* and *Gymnodinium indicum*, two new freshwater dinoflagellates from India: morphology, reproduction and cytology. *Plant Syst. Evol.*, 124: 205–212.

Solovchenko, A. E. 2015. Recent breakthroughs in the biology of astaxanthin accumulation by microalgal cell. *Photosynth. Res.*, 125: 437–449.

Stosch, H. A. 1973. Observations on vegetative reproduction and sexual life cycles of two freshwater dinoflagellates. *Gymnodinium pseudopalustre* Schiller and *Woloszynskia apiculata* sp. nov. *Brit. Phycol. J.*, 8: 105–134.

Swofford, D. L. 2003. PAUP*: phylogenetic analysis using parsimony (*and other Methods), Version 4. Sinauer Associates, Sunderland, MA.

Takano, Y. & Horiguchi, T. 2005. Acquiring scanning electron microscopical, light microscopical and multiple gene sequence data from a single dinoflagellate cell. *J. Phycol.*, 42: 251–256.

Thompson, R. H. 1951 ('1950'). A new genus and new records of freshwater Pyrrophyta in the Desmokontae and Dinophyceae. *Lloydia*, 13: 277–299.

Turland, N. J., Wiersema, J. H., Barrie, F. R., Greuter, W., Hawks- worth, D. L., Herendeen, P. S., Knapp, S., Kusber, W.-H., Li, D.-Z., Marhold, K., May, T. W., McNeill, J., Monro, A. M., Prado, J., Price, M. J. & Smith, G. F. (ed.) 2018. International Code of Nomenclature for algae, fungi, and plants (Shenzhen Code) adopted by the Nineteenth International Botanical Congress Shenzhen, China, July 2017. Koeltz Botanical Books, Glashütten. XXXVIII + 254 pp. (Regnum Vegetabile vol. 159). https://doi.org/10.12705/code.2018

Wołoszyńska, J. 1917. Nowe gatunki Peridineów, tudzież spostrzeżenia nad budową okrywy u Gymnodiniów i Glenodiniów. — Neue Peridineen-Arten, nebst Bemerkungen über den Bau der Hülle bei *Gymno-* und *Glenodinium. Bull. Int. Acad. Sci. Cracovie, Cl. Sci. Math., Sér. B, Sci. Nat.*, 1917: 114–122, pls 11– 13.

Zhang, Q., Zhu, H., Hu, Z. & Liu, G. 2016. Blooms of the woloszynskioid dinoflagellate *Tovellia diexiensis* sp. nov. (Dinophyceae) in Baishihai Lake at the eastern edge of Tibetan Plateau. *Algae*, 31: 205–217.

CHAPTER 3

FINE-STRUCTURAL CHARACTERIZATION AND PHYLOGENY OF *SPHAERODINIUM* (SUESSIALES, DINOPHYCEAE), WITH THE DESCRIPTION OF AN UNUSUAL TYPE OF FRESHWATER DINOFLAGELLATE CYST

ABSTRACT

Two strains of *Sphaerodinium* were established from two mountain areas in Portugal and examined by light microscopy, scanning and transmission electron microscopy, and sequence analyses of nuclear-encoded SSU, ITS1–5.8S–ITS2 and LSU rDNA. Both strains were identified as *S. polonicum* var. *tatricum* on the basis of comparison with the original taxonomic descriptions within the genus. The two strains were nearly identical in morphology and ultrastructure, except for the presence of pseudograna-like thylakoid stacks within more rounded chloroplast lobes in one of them. Sexual reproduction occurred in culture batches and resting cysts with single or grouped processes with wide bases and distal platforms with slightly recurved margins were seen to develop by sudden retraction of planozygote cytoplasm. Morphological, fine-structural and molecular characters were compared with previously available information from *S. cracoviense*, allowing for a more robust characterization of the genus. Important characters include a type F eyespot, a pusule canal linking the transverse flagellar canal to a collecting chamber connected to regular pusular tubes, a ventral fibre extending from the proximal-right side of the longitudinal basal body, and a membranous, lamellar body with a honeycomb pattern near the flagellar base area. The latter two features are shared with *Baldinia anauniensis*.

Key words: dinoflagellates, flagellar apparatus, phylogeny, resting cyst, *Sphaerodinium*, ultrastructure

INTRODUCTION

The genus *Sphaerodinium* Wołoszyńska includes freshwater, thecate dinoflagellates with relatively large plates, which are comparable in size to those of peridinioid and gonyaulacoid species (Moestrup and Calado 2018; Schiller 1935; Starmach 1974; Wołoszyńska 1916). The plate disposition in six latitudinal series is, according to Taylor (2004), of the peridinioid type. It differs, however, from what is common in peridinioids in having four intercalary plates (instead of zero to three) and six postcingular plates, rather than the usual five. However, it is now known that there is no close evolutionary relationship between the Peridiniales and *Sphaerodinium* (Craveiro et al. 2010; Moestrup

and Calado 2018). With the exception of *S. fimbriatum* R.H. Thompson, all species in the genus were described by Wołoszyńska (1916, three species and one variety; 1930, one species; see also Schiller 1935). *Sphaerodinium fimbriatum* has fimbriate projections on sutures and plates of the hypocone, which make it quite distinct (Carty 2014; Couté and Iltis 1984; Thompson 1951). However, the significance of characters used by Wołoszyńska to distinguish taxa within *Sphaerodinium* has been the subject of divergent opinions and some monographic treatments of freshwater dinoflagellates lump her taxa into a single species with varieties (e.g. Huber-Pestalozzi 1950). Moestrup and Calado (2018) opted for presenting the original concepts of Wołoszyńska's *Sphaerodinium* taxa to allow their morphologies to be recognized in natural populations so that their taxonomic status may be established by further studies.

The detailed morpho-molecular study of a dinoflagellate population collected near Cracow, Poland, identified as *S. cracoviense* Wołoszyńska, suggested a phylogenetic affinity with the Borghiellaceae and Suessiaceae/Symbiodiniaceae sensu lato, placing *Sphaerodinium* in or near the order Suessiales; and serial section electron microscopy revealed several unusual features that may be useful for understanding character evolution in this group of species (Craveiro et al. 2010). However, determining which of these characters are variable among species and which are stable, and therefore relevant characters at the generic level, requires comparative analysis of several species within the genus. In the present account, we examined two strains started from material collected in two mountain areas in Portugal. Their morphology was almost mutually identical, but both showed consistent differences from *S. cracoviense*. Comparisons between nuclear-encoded ribosomal operon sequences of *S. cracoviense* and the new strains confirmed the existence of species-level diversity within *Sphaerodinium*. Ultrastructural analysis of this new material revealed a number of potentially stable features that may be suggested as features characterizing the genus *Sphaerodinium* and possibly the family Sphaerodiniaceae.

In addition, the morphology and formation process of resting cysts that were produced in batches of the two strains is described and compared with previously reported information about freshwater dinoflagellate cysts.

MATERIAL AND METHODS

Biological material

Two uni-algal cultures were used, both started from single cells isolated from plankton samples taken in two mountain sites in Portugal (both at 350–400 m alt.). Collection site 1 was a pond in Vila do Gerês, Peneda-Gerês National Park in Northern Portugal, sampled 1 September 2014 (41°43'49.97"N, 8°09'43.22"W). Collection site 2 was a water tank next to the Buçaco Palace Hotel, a 19th century royal retreat built in the Buçaco Forest, Central Portugal, sampled 7 July 2015 (40°22'33.74"N, 8°21'55.62"W). Cultures were grown in MBL culture medium (Nichols 1973) at 18 °C with 12:12 light:dark photoperiod and photon flux density of about 25 μmol m^{-2} s^{-1}. Cells of both strains closely agreed in general characteristics and cell cover plate arrangement with the original description of *Sphaerodinium polonicum* var. *tatricum* Wołoszyńska (Wołoszyńska 1916) and this name is used herein. See further consideration on the organisms' identity in Discussion.

Light microscopy (LM)

Swimming cells, stained cells, empty thecae and cysts were photographed with a DP70 Olympus camera (Olympus Corp., Tokyo, Japan) mounted on a Zeiss Axioplan 2 imaging light microscope (Carl Zeiss, Oberkochen, Germany). Encystment was recorded with a JVC TK-C1481BEG colour video camera (Norbain SD Ltd, Reading, United Kingdom) coupled to a Leitz Labovert FS inverted light microscope (Leica Microsystems, Wetzlar, Germany). Nuclei were stained with acetocarmine added to the edge of a preparation coverslip and briefly heated over a flame.

Scanning electron microscopy (SEM)

Different fixation protocols were used for the visualization of different aspects of vegetative cells: 1) good preservation of cell shape and flagella was obtained with a 1-h fixation of a 2:1 mixture of cell suspension and a fixative made of 2% aqueous OsO$_4$ and saturated aqueous HgCl$_2$ (3:1, v/v); 2) somewhat swollen cells showing more distinct surface knobs were obtained with a 1-h fixation of a 1:1 mixture of cell suspension and 50% ethanol. Cyst preservation was similar for both fixation protocols. Fixed cells and cysts were retained on Nuclepore polycarbonate filters with 5-μm pore size (Whatman,

GE Healthcare Life Sciences, Maidstone, United Kingdom). Filters from fixation 1 were washed with distilled water for 30–60 min. All material was dehydrated in a graded ethanol series (10–15 min in each concentration) and critical-point-dried in a Baltec CPD-030 (Balzers, Liechtenstein). Filters were glued onto stubs and sputter-coated with gold-palladium. Cells were observed with the scanning electron microscopes Hitachi S-4100 (Hitachi High-Technologies Corp., Tokyo, Japan) and JEOL JSM 6335F (Jeol Ltd, Tokyo, Japan).

Transmission electron microscopy (TEM)

The general steps for the preparation of cells of *Sphaerodinium polonicum* var. *tatricum* for TEM observations were similar to the ones used for *S. cracoviense* (Craveiro et al. 2010). In particular, swimming cells of both strains were picked up with a micropipette and immersed in full concentration fixative. Cells of both strains fixed for 20–30 min in a mixture of 1% glutaraldehyde and 0.5% OsO_4 (final concentrations) in phosphate buffer 0.1 M, pH 7.2, were examined. In addition, cells from the Buçaco isolate fixed for 1 h in 2% glutaraldehyde (final concentration) in the same buffer were also examined. Serial sections of two cells from Buçaco (both fixations) and one cell from Gerês were examined with a JEM 1010 electron microscope (JEOL Ltd., Tokyo, Japan), fitted with a Gatan Orius digital camera (Gatan, Inc., Pleasanton, California USA).

DNA extraction and PCR amplification

About 50–70 swimming cells from each strain of *Sphaerodinium polonicum* var. *tatricum* and *S. cracoviense* were pipette-washed in miliQ water before DNA extraction with QuickExtract[TM] FFPE DNA Extraction Kit (epicentre, Illumina company, San Diego, California USA), following instructions from the manufacturer. Two microliters of extracted DNA were used in each PCR amplification of SSU rDNA, ITS1-5.8S-ITS2 rDNA and LSU rDNA. Amplification of LSU rDNA followed Pandeirada et al. (2017) with two modifications: in the nested-PCR following the first PCR amplification the dinoflagellate specific Dino-ND primer was used instead of the terminal primer 28-1483R; and 2 µl of the first PCR product were added (instead of 1 µl) (see primer sequences in Hansen et al. 2007). Amplifications of SSU rDNA and ITS rDNA were based on Takano and Horiguchi (2005), skipping the first round of PCR amplification

and going directly to the second round. The products from all PCR amplifications were purified with the QIAquick PCR Purification Kit (Qiagen, Hilden, Germany), and sent to Macrogen Europe (Amsterdam, The Netherlands) for sequencing in both directions with the primers indicated in Hansen et al. (2007), Pandeirada et al. (2017) and Takano and Horiguchi (2005), except for 28-1483R, which was replaced by the Dino-ND.

To increase the number of taxa of Tovelliaceae for SSU rDNA and concatenated phylogenetic analyses we added previously unpublished SSU rDNA sequences of three species of *Tovellia* Moestrup, K. Lindberg & Daugbjerg. PCR amplification of SSU rDNA from *Tovellia aveirensis* Pandeirada, Craveiro, Daugbjerg, Moestrup & Calado, *T. rinoi* Pandeirada, Craveiro, Daugbjerg, Moestrup & Calado and *T. rubescens* Pandeirada, Craveiro, Daugbjerg, Moestrup & Calado was performed from groups of 2–10 swimming cells isolated from the original cultures to PCR tubes that were frozen for at least 24 h. After the addition of a bead of ilustra puReTak Ready-To-Go PCR (GE Healthcare, UK Ltd, Buckinghamshire, UK) in each tube, the procedure for PCR amplification was the same as in Takano and Horiguchi (2005) except for the use of the terminal primer 28-1483R instead of LSUR2 in the first PCR amplification round and using 1 μl (instead of 0.5 μl) from the first PCR product in the second PCR amplification round. Purification of PCR products was made with the same kit as for *Sphaerodinium polonicum* var. *tatricum*. Sequencing in both directions was made in Macrogen Europe (Amsterdam, The Netherlands) with the same primers used in the PCR amplification.

Phylogeny

Phylogeny based on LSU rDNA: partial sequences of the two *Sphaerodinium polonicum* var. *tatricum* strains were added to a data matrix previously compiled and used by Pandeirada et al. (2017). However, this data matrix was slightly modified prior to phylogenetic analyses as *Sphaerodinium cracoviense* (Craveiro et al. 2010) and *Dactylodinium pterobelotum* Kazuya Takahashi, Moestrup & Iwataki (Takahashi et al. 2017) were added and a few dinoflagellates of no importance to this study were deleted. The data matrix was edited in Jalview (ver. 14, Waterhouse et al. 2009) and sequences aligned with Mafft (default setting) as implemented in the software. A total of 48 genera and 71 species of dinoflagellates were considered and 1680 base pairs including introduced gaps were analyzed using Bayesian inference and maximum likelihood. Three

ciliates, four apicomplexans and *Perkinsus andrewsi* Coss, Robledo, Ruiz & Vasta formed the outgroup. For Bayesian analyses we used the program MrBayes (ver. 3.2.6 × 64, Ronquist and Huelsenbeck 2003) with 5×10^6 generations and a tree was sampled every 1000 generations. The burn-in was evaluated by plotting LnL scores as a function of generations and it was reached after 501,000 generations (conservative estimate). This left 4500 trees for construction of a 50% majority-rule consensus tree. jModeltest (ver. 2.1.7, Darriba et al. 2012) was used for selecting the best parameter settings for maximum likelihood among the 88 different models examined, and GTR + I+G was chosen as the best fit model (pinvar = 0.2 and shape = 0.61). The robustness of the tree topology in ML was evaluated with 1000 bootstrap replications using PhyML (Guindon et al. 2010) available at the Montpellier bioinformatics platform (http://www.atgc-montpellier.fr/phyml/).

Phylogeny based on SSU rDNA: nearly complete nuclear-encoded SSU rDNA sequences of *Sphaerodinium cracoviense* (1731 bp) and of both strains of *S. polonicum* var. *tatricum* (1736 bp of the Buçaco strain and 1747 bp of the Gerês strain) were added to a data matrix comparing 31 other dinoflagellate genera (68 strains). These included species assigned to Tovelliaceae (three genera, seven strains), Borghiellaceae (five genera, five strains) and Suessiaceae (10 genera and 32 strains). *Gymnodinium catenatum* H.W. Graham formed the outgroup taxon and was thus used to polarize the ingroup. The final data matrix comprised 1760 base pairs including introduced gaps and the sequences were manually edited in Jalview (ver. 14, Waterhouse et al. 2009) and aligned using Mafft with default settings as implemented in the software. Bayesian inference used 10 mill generations and a tree was sampled for each 1000's generation. A burn-in was evaluated to occur after 501,000 generations, thus leaving 9500 trees for construction of a majority-rule consensus tree. Maximum likelihood bootstrap analyses used the parameter settings suggested by jmodel test. The best fit model was GTR + I + G (proportion of invariable sites I = 0.48 and gamma shape G = 0.588).

Phylogeny based on concatenation of SSU and LSU rDNA: we included as many overlapping dinoflagellate taxa for which both LSU and SSU rDNA sequences were available. Thus, a concatenated data matrix comprising 24 genera (45 strains) was compiled. The alignment included 2854 bp including introduced gaps. The approach for alignment and phylogenetic analyses were similar to those described for analyses of SSU

rDNA except that in Bayesian analysis SSU and LSU rDNA sequences were divided into two partitions. This allowed each of these regions to evolve under different models of evolution using the 'unlink' option. The software jmodeltest suggested the GTR + I + G model as the best fit and the proportion of invariable sites (I = 0.373) and gamma shape (G = 0.518) were used for bootstrap analysis using PhyML. The aligned matrices are available upon request to n.daugbjerg@bio.ku.dk.

Sequence divergence

The sequences determined here (nuclear-encoded SSU and LSU rDNA and the internal transcribed spacers) were compared using PAUP* (ver. 4.0a build 161, Swofford 2002) and divergence estimates used both p-values and the Kimura-2- parameter model.

RESULTS

Morphology and plate pattern

The external morphology of cells from the two strains analyzed herein closely matched the original description of *Sphaerodinium polonicum* var. *tatricum*. The following description is primarily based on the strain from Gerês, in Northern Portugal, with reference here and there to slight variations observed in the strain from Buçaco, in Central Portugal. Vegetative, mobile cells are shown in Figs. 1 and 2. They were spherical to slightly oval, very little compressed dorsoventrally or not at all (Fig. 1A–C). Epi- and hypocone were of similar size. The slightly descending, transversely oriented cingulum was about 3 μm wide and had its distal end about 1–1.5 cingulum widths posterior to the proximal, left end (Fig. 1G, H; Fig. 2A). Cell length and width mostly fell within the range 22–32 μm (mean = 27.0 μm; std. dev. = 2.6) and 20–27 μm (mean = 23.7 μm; std. dev. = 2.1) (n = 43), respectively; exceptional cells, either small or large, extended the size limits to 19.5–47 μm × 16–31 μm. Abundant yellowish-brown chloroplast lobes ramified extensively from deep inside the cytoplasm to the periphery; a large, red eyespot, mostly up to 8 × 8 μm, typically with a concave anterior edge, was visible along the middle-anterior part of the sulcus; roundish bodies with an orange tinge, reminiscent of accumulation bodies were visible in the epicone (Fig. 1A–C). Immobile cells with the cingulum faintly marked were frequent on the bottom of wells, usually with a single prominent eyespot, sometimes with two (Fig. 1D). In most cells the nucleus was

concealed by the numerous peripheral chloroplast lobes and its shape and position were not readily perceptible in LM. Cells stained with acetocarmine showed an ellipsoid nucleus, positioned in the mid-dorsal cytoplasm with its longer axis along the cingulum (Fig. 1E). A few cells revealed presumably dividing, elongated nuclei (Fig. 1F).

The amphiesma of vegetative, motile cells was relatively thin and details were only visible in LM in empty thecae. The tabulation had a nearly symmetrical plate arrangement in the epitheca including, in Kofoidian notation, four apical plates centred around an apical complex and four intercalary plates (Figs. 1G, I, J, L; 2 A, C–E). The apical complex was roughly rectangular, with the long axis oriented from ventral-right to dorsal-left (Figs. 1I; 2 C), and displayed three platelets (Fig. 2D): a central, elongated platelet (marked 1), 1.3 μm long and 0.5 μm wide, with an axial row of small knobs; a larger platelet (marked 2) that surrounded the lateral and dorsal sides of the central platelet; and a smaller platelet (marked 3) that contacted platelets 1 and 2 on the ventral side. In the ventral area, a narrow rectangular plate, labelled Z in Figs. 1 and 2, separated the first apical plate from the sulcal plates (Figs. 1G; 2 A, C). Plate Z was 4–5 μm long and ca. 2 μm wide and contacted laterally precingular plates 1 and 7, thereby closing on the ventral side a ring of eight plates covering the epicone next to the cingulum. The number of cingular plates was difficult to ascertain, but a maximum of eight plates were counted in a few cells (Figs. 1M, N; 2 A, F); cingular plates appeared to have a similar length, except for the first two, which were slightly shorter. Empty thecae displayed two flap-like thickenings on the anterior-left part of the sulcus when viewed in LM (Fig. 1G, H, K; Fig. S1A). Six plates were identified in the sulcus (Figs. 1H, K; 2 A, B, F): four small plates (asterisks in Fig. 2A, B) occupied the anterior part of the sulcus below plate Z, filling the area between the proximal and distal ends of the cingulum and surrounding the flagellar pores; adjacent to the two lowermost of these four plates was a single, larger plate (middle sulcal, ms) that ranged the full width of the sulcus and separated a small, squarish to rhombic posterior sulcal plate (ps) from the upper part of the sulcus (Fig. 2A, B, F). The hypotheca had six postcingular plates, and two antapical plates of similar size (Figs. 1K–N; 2 A, B, F).

Plate sutures were generally ornamented by rows of knobs, which were visible in LM observations of empty thecae and in SEM observations (Fig. 1G–N; Fig. 2A, B).

Vegetative, motile cells of the Buçaco isolate matched the features described above except for the morphology of the chloroplast (Figs. S1 and S2). Chloroplast lobes of the strain from Buçaco were usually less numerous and more rounded, and appeared less profusely interconnected than in the strain from Gerês (Fig. 3A–C). However, a minority of cells from Buçaco displayed a chloroplast arrangement very similar to the one observed in cells from Gerês (Fig. 3D–F).
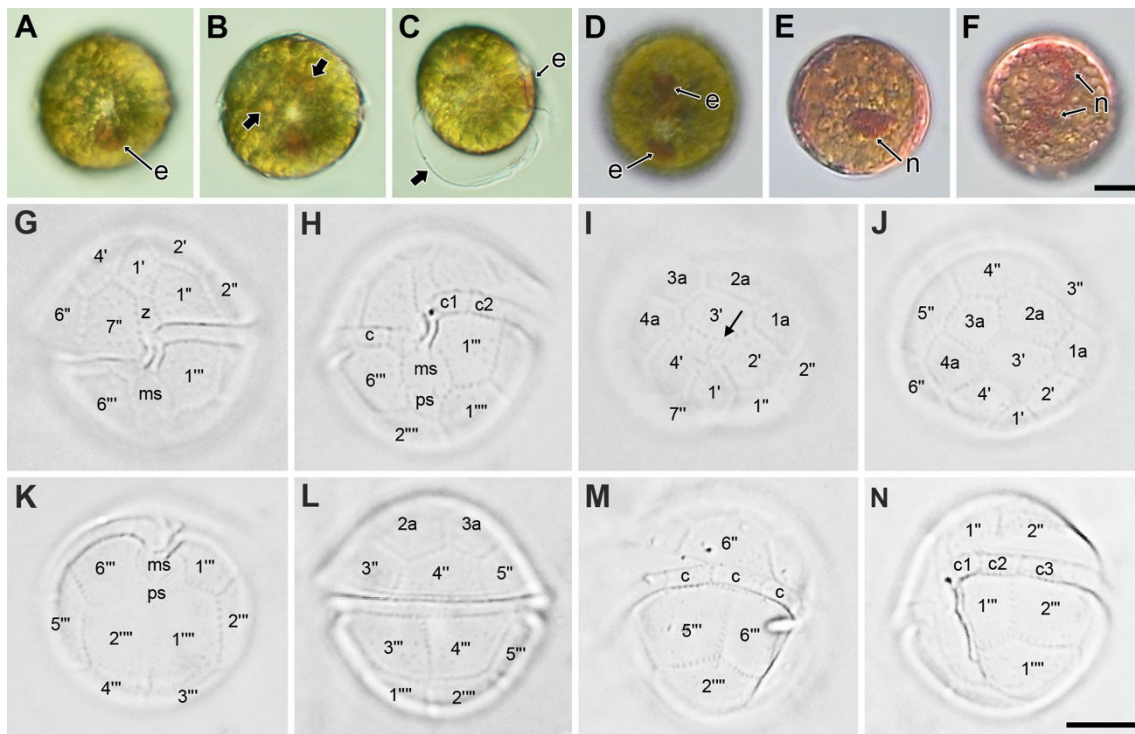
Fig. 1. *Sphaerodinium polonicum* var. *tatricum* from Gerês, LM. (**A, B**) Surface focus and optical section of vegetative cell in ventral view displaying dense arrangement of chloroplast lobes, the conspicuous eyespot (e) in the sulcal area, and roundish orange bodies, reminiscent of accumulation bodies, in the epicone and at cingulum level (arrows). (**C**) Lateral view of cell exiting the theca (arrow), which opened along the cingulum. (**D**) Cell with two eyespots (presumably dividing). (**E, F**) Cells stained with acetocarmine showing in (E) the ellipsoid nucleus (n), and in (F) an apparently dividing nucleus. (**G–N**) Empty thecae with plates labelled according to Kofoidian notation: ventral view (G, H); apical view (**I, J**) showing apical complex (arrow in I); antapical view (K); dorsal view (L); right view (M); left view (N). ms, middle sulcal plate; ps, posterior sulcal plate. (**A–F**) to the same scale. (**G–N**) to the same scale. Scale bars = 10 μm.
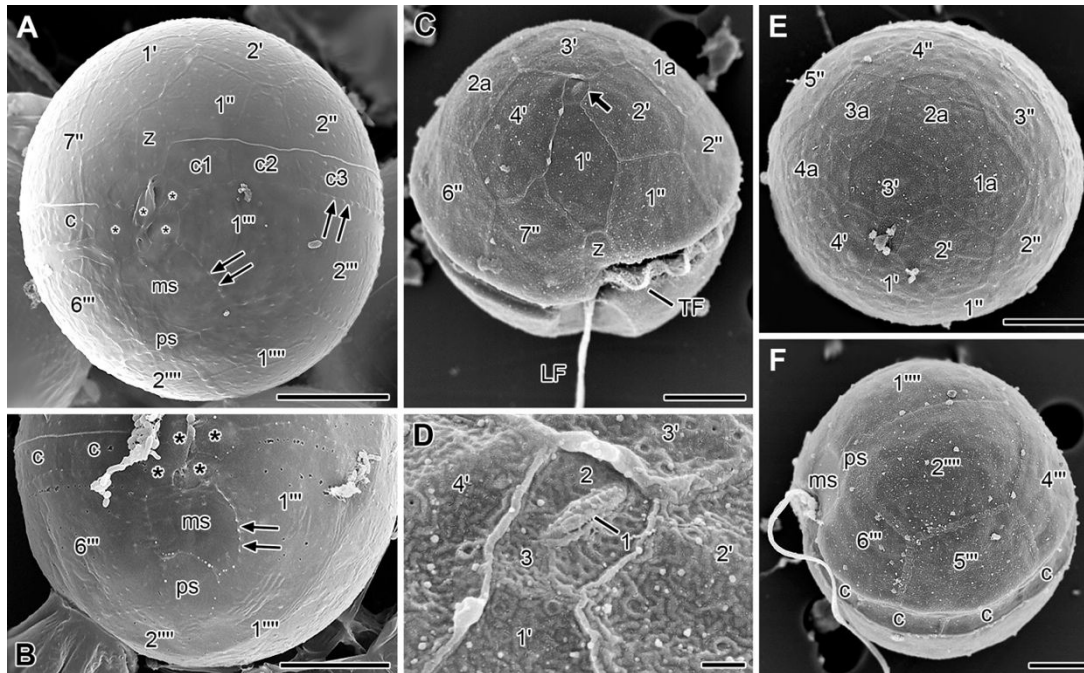
Fig. 2. *Sphaerodinium polonicum* var. *tatricum* from Gerês, SEM. Kofoidian notation. Swollen cells in A and B prepared with fixation schedule 2; cells with preserved furrows and flagella (C–F) prepared with fixation schedule 1. (**A, B**) Ventral view of whole, swollen cell (only hypotheca visible in B); arrows point to knobs over plate sutures. Sulcus with four small plates (asterisks) surrounding the flagellar pores, a middle (ms) and a posterior (ps) sulcal plates. (**C**) Apical-ventral view showing location of apical complex (arrow) and both the transverse (TF) and longitudinal flagellum (LF) in place. (**D**) Apical complex with elongated platelet (1) bearing a row of small knobs, surrounded by platelet 2 on the dorsal and lateral sides and by platelet 3 on the ventral side. (**E, F**) Apical and antapical views. Scale bars = 8 μm (A); 10 μm (B); 5 μm (C, E, F); 500 nm (D).
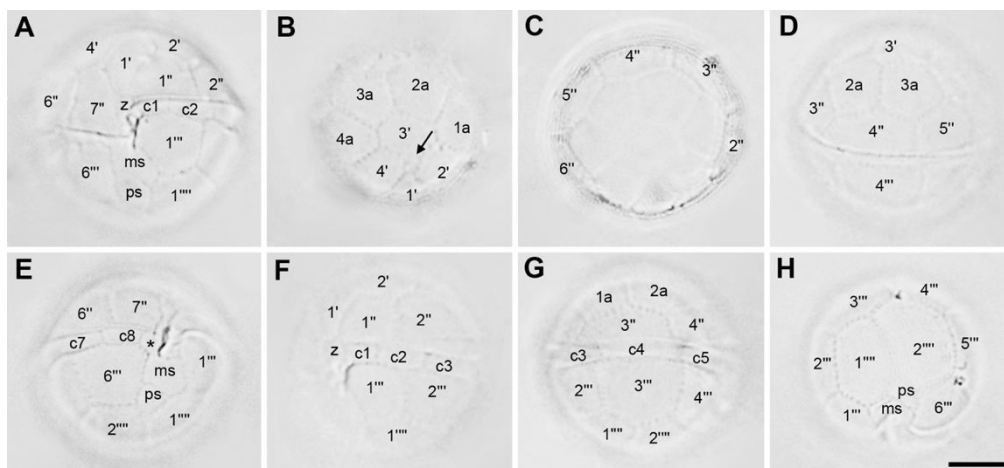
Fig. S1. *Sphaerodinium polonicum* var. *tatricum* from Buçaco, LM. (**A–H**) Empty thecae with plates labelled in Kofoidian notation: ventral view (A); apical view (B, C) with arrow indicating apical complex; dorsal view (D); ventral-posterior view (E); ventral-left view (F); dorsal-left view (G); antapical view (H). Anterior (asterisk), middle (ms) and posterior (ps) sulcal plates. All to the same scale. Scale bar = 10 μm.
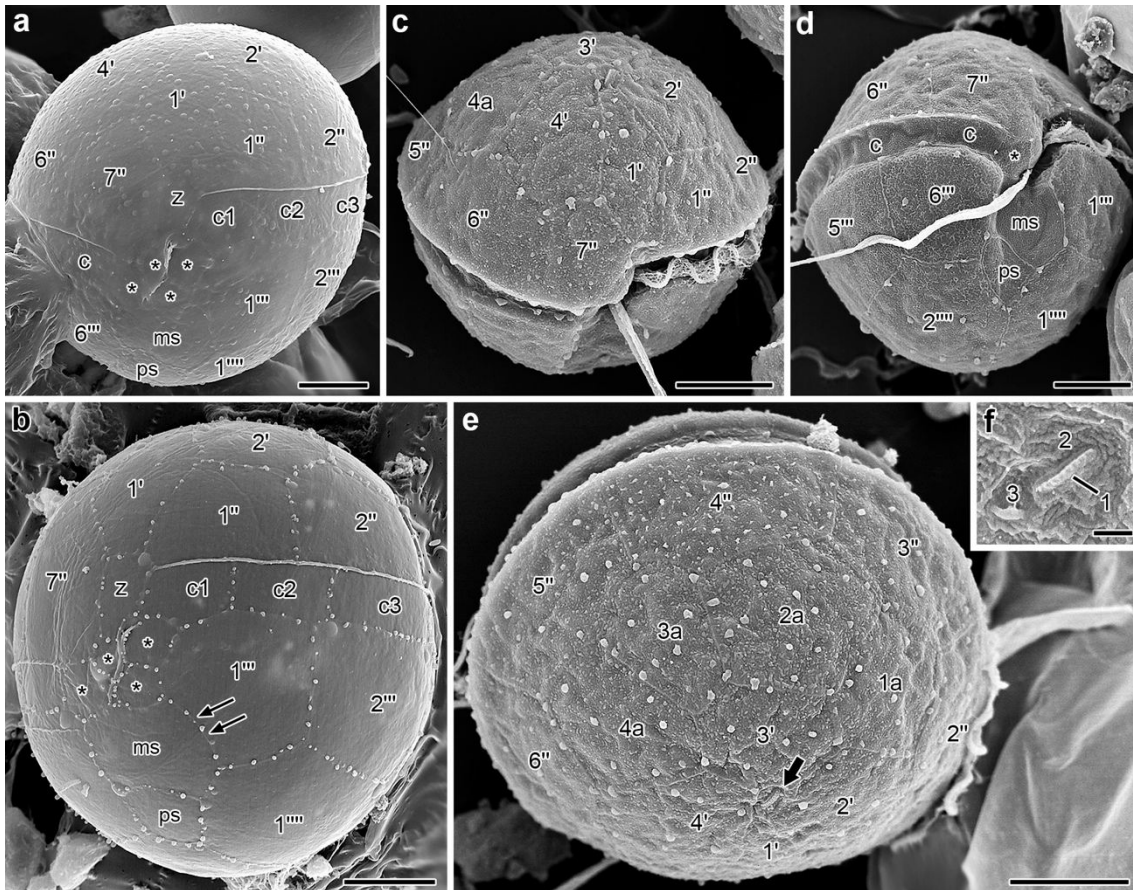
Fig. S2. *Sphaerodinium polonicum* var. *tatricum* from Buçaco, SEM. Kofoidian notation. Swollen cells in A and B prepared with fixation schedule 2; cells with preserved furrows and flagella (C–F) prepared with fixation schedule 1. (**A, B**) Ventral and ventral-left views; arrows point to knobs over plate sutures. Sulcus with four anterior (asterisk), one middle (ms) and one posterior (ps) plates. (**C, D**) Apical and ventral-posterior views. (**E**) Apical view with apical complex indicated by arrow. (**F**) Apical complex with three platelets. The central, elongated plate 1 has an axial row of knobs. Scale bars = 5 μm (A-E); 500 nm (F).

Cyst morphology and encystment

Cysts of both strains of *Sphaerodinium polonicum* var. *tatricum* were similar in appearance and size range: 34–46 μm long (mean = 39.8 μm; std. dev. = 3.5; n = 26) and 28–39 μm wide (mean = 33.0 μm; std. dev. = 3.0; n = 22), not including processes. Cyst contents varied from light yellowish-brown to darker orange-brown (Fig. 4A–F) and usually contained several round, orange to red bodies interpretable as accumulation bodies or perhaps lipid droplets (Fig. 4A, D). The eyespot was often visible in recently formed cysts (Fig. 4C). Cysts were subspherical with a more or less pronounced equatorial constriction (paracingulum) (Fig. 4H, J, thick arrow). Cysts were ornamented by simple or most often branched processes up to 10 μm long (n = 22). These wall

processes tapered from broad and somewhat flattened bases and widened abruptly near the tips, which were somewhat flattened and showed recurved margins (Fig. 4). Most bases of processes were nearly aligned and apparently marked the position of some of the plate limits of the cell that originated the cyst (Fig. 4H, J), although it was not clear if they reflected a paratabulation. Numerous small knobs were scattered over the cyst surface (Fig. 4G–J) and formed short alignments here and there, perhaps also in the location of former plate sutures (Fig. 4J, double arrows). Cysts were often surrounded by an envelope, which looked like a colourless periphragm sensu Ellegaard et al. (2003) (Figs. 4A, E, thick arrow; 4 K, L). Recognizable plate limits, visible in SEM, established a link between these cyst covers and the former amphiesma of the encysting cell (Fig. 4K, L, double arrows). As shown in Fig. 4, the cyst type appeared to be proximochorate to chorate. The cysts were not treated by acetolysis.
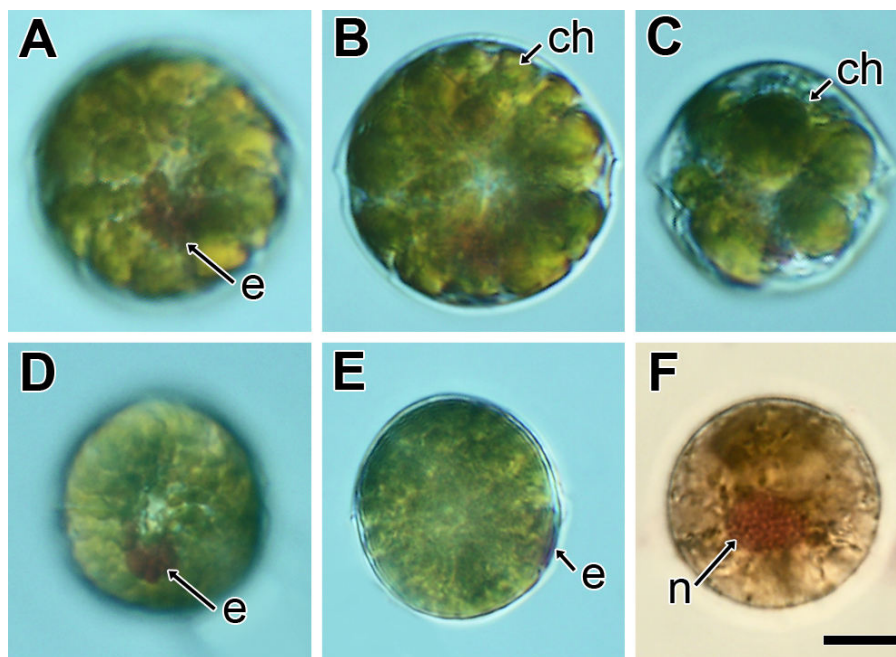
Fig. 3. *Sphaerodinium polonicum* var. *tatricum* from Buçaco, LM. (**A, B**) Surface focus and optical section of vegetative cell in ventral view, showing eyespot (e) and chloroplast lobes (ch). (**C**) Optical section of cell with markedly rounded and well-defined chloroplast lobes (ch). (**D, E**) Ventral and right-lateral views of cell showing a chloroplast arrangement similar to cells from Gerês. The eyespot (e) marks the position of the sulcus. (**F**) Cell stained with acetocarmine showing the nucleus (n). All to the same scale. Scale bar = 10 μm.
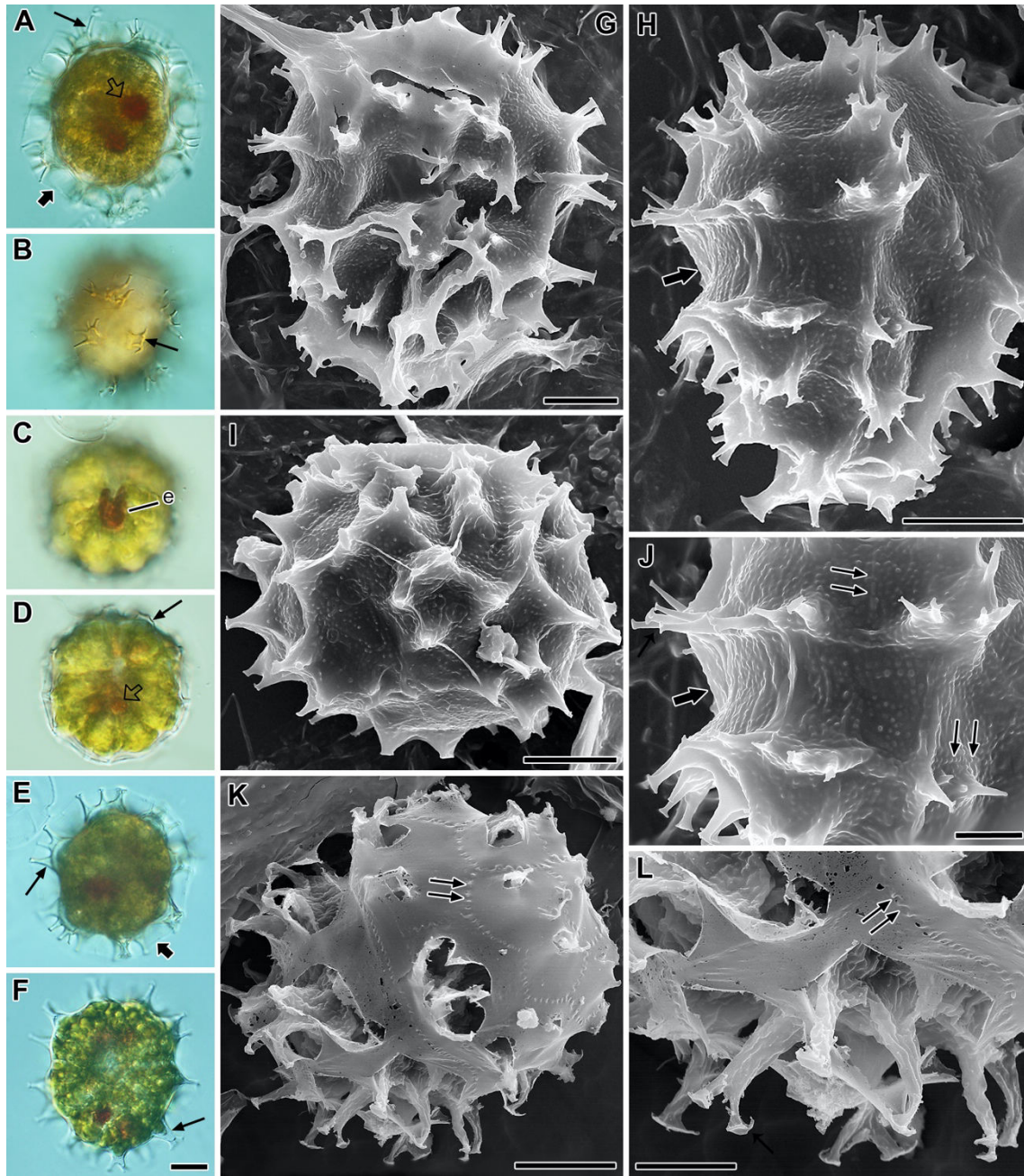
Fig. 4. Resting cysts of *Sphaerodinium polonicum* var. *tatricum*, LM and SEM. (**A–D, G–J**) Strain from Gerês and (**E, F, K, L**) from Buçaco. Cysts were subspherical, ornamented by processes with wide and somewhat flattened bases and variously branched (thin arrows in A, B, D, E, F). Reddish accumulation marked by open arrow in A, D. Eyespot (e) visible in early stage of cyst formation (C). Remnants of old cell cover visible in LM (thick arrow in A, E). Equatorial constriction marked by thick arrow in H, J. Amphiesmal plate limits visible on old cell cover in SEM in K, L (double arrows). Similar limits were also suggested on cyst surface by dashed lines or knobs in linear arrangement (double arrows in J). Scale bars = 10 μm (F, G–I, K); 5 μm (J, L). (A–F) to the same scale.

The encystment process was similar in both strains of *Sphaerodinium polonicum* var. *tatricum*. Most of the external morphological changes from motile cell to cyst occurred over the course of a few seconds following the transfer of the encysting cell to a new culture well or microscope slide. The process is outlined in Fig. 5. The encysting stages were large, dark cells with prominent accumulation bodies (Fig. 5A, wide arrows). Detailed observations of these cells were made difficult by their rapid transformation in response to being transferred to a slide and it was only possible to briefly observe two longitudinal flagella in few cases (Fig. 5B, arrows). Pairs of fusing cells that were occasionally seen swimming in the culture batches were the likely origin of planozygotes with paired longitudinal flagella matching the features of encysting cells. During the process of encystment the flagella were soon discarded after the cells stopped swimming (Fig. 5C) and the peripheral cytoplasm suddenly retracted from the amphiesma (Fig. 5D, E; see also Video S1 in Supplementary material). The retraction was not uniform and led to the formation of the process-bearing surface of the cyst, which remained surrounded by a colourless cover, presumably derived from the amphiesma of the encysting cell (Fig. 5G, H). This outer, delicate cover was eventually lost and was partially or totally absent in presumably older cysts from aged culture batches. The observation of empty cyst walls in culture wells indicated that germination took place in the cultures, but the germination process was never observed and the archeopyle type could not be determined.

General internal fine-structure

Cells of *Sphaerodinium polonicum* var. *tatricum* displayed features typical of dinoflagellates (Figs. 6 and 7). In sectioned cells, the ellipsoid nucleus was in a mid-dorsal position, approximately at cingulum level (Fig. 6A). The periphery of the cytoplasm was mainly occupied by chloroplast lobes, large ellipsoid vesicles with irregular contents, and trichocysts (respectively marked ch, short black arrows and t in Figs. 6A, 7 A). Starch grains and a few oil droplets were present in the inner portion of cytoplasm (Figs. 6A, 7 A, st, o). Two other kinds of vesicles were seen: small, mainly peripheral vesicles with electron-dense, spherical or ellipsoidal granules (Figs. 6B, 7 D arrows); and electron-translucent vesicles associated with electron-opaque microbodies with irregular shape, more common in the inner portion of the cytoplasm (Fig. 6A, D, short, white arrows). The eyespot, located along the sulcus, was extraplastidial and composed by two types of

elements: a row of variously developed brick-like or crystal-like elements apparently enclosed in a long, flat vesicle located underneath the longitudinal microtubular root (LMR, named r1 in Moestrup 2000) (Figs. 6C, 7 B, double arrow); and at least one layer of more or less fused oil globules underlying the brick-like elements (Figs. 6C, 7 B, o). The pusular system was found in the ventral area, between the sulcus and the nucleus. The most conspicuous part of the pusular system extended from the transverse flagellar canal in the format of a tube with an inner diameter of 230–290 nm, herein called pusule canal following Craveiro et al. (2010) (Fig. 6D–F, pc). The pusule canal was accompanied by a rather discrete layer of fibrous material, barely visible in Fig. 6E, F (arrowhead). About 5 μm into the cell, the pusule canal connected with a sac some 450 nm in diameter, the so-called collecting chamber, from which radiated 100-nm wide, typical pusular tubes (Fig. 6E, G).
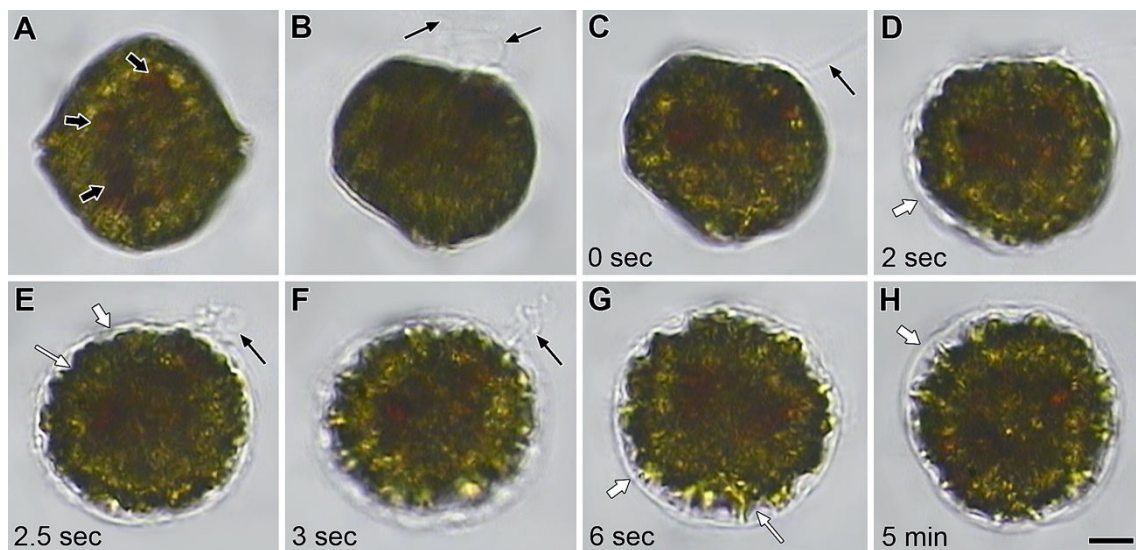
Fig. 5. Encystment in *Sphaerodinium polonicum* var. *tatricum* from Gerês. Images taken from video recording. Time elapsed from the moment the cell stopped is indicated. See also Video S1 in Supplementary material. (**A**) Encysting cell with dark contents and several accumulations bodies (wide black arrows). (**B**) Same cell as in A. Thin black arrows indicate two longitudinal flagella, which displayed distinct movement in the video recording. (**C–G**) The cell stopped, released the flagella (thin black arrows) and the cytoplasm retracted from the outer amphiesma (wide white arrows) originating a rough, then process-bearing surface (thin white arrows). (**H**) The same cell after 5 min. All to the same scale. Scale bar = 10 μm.
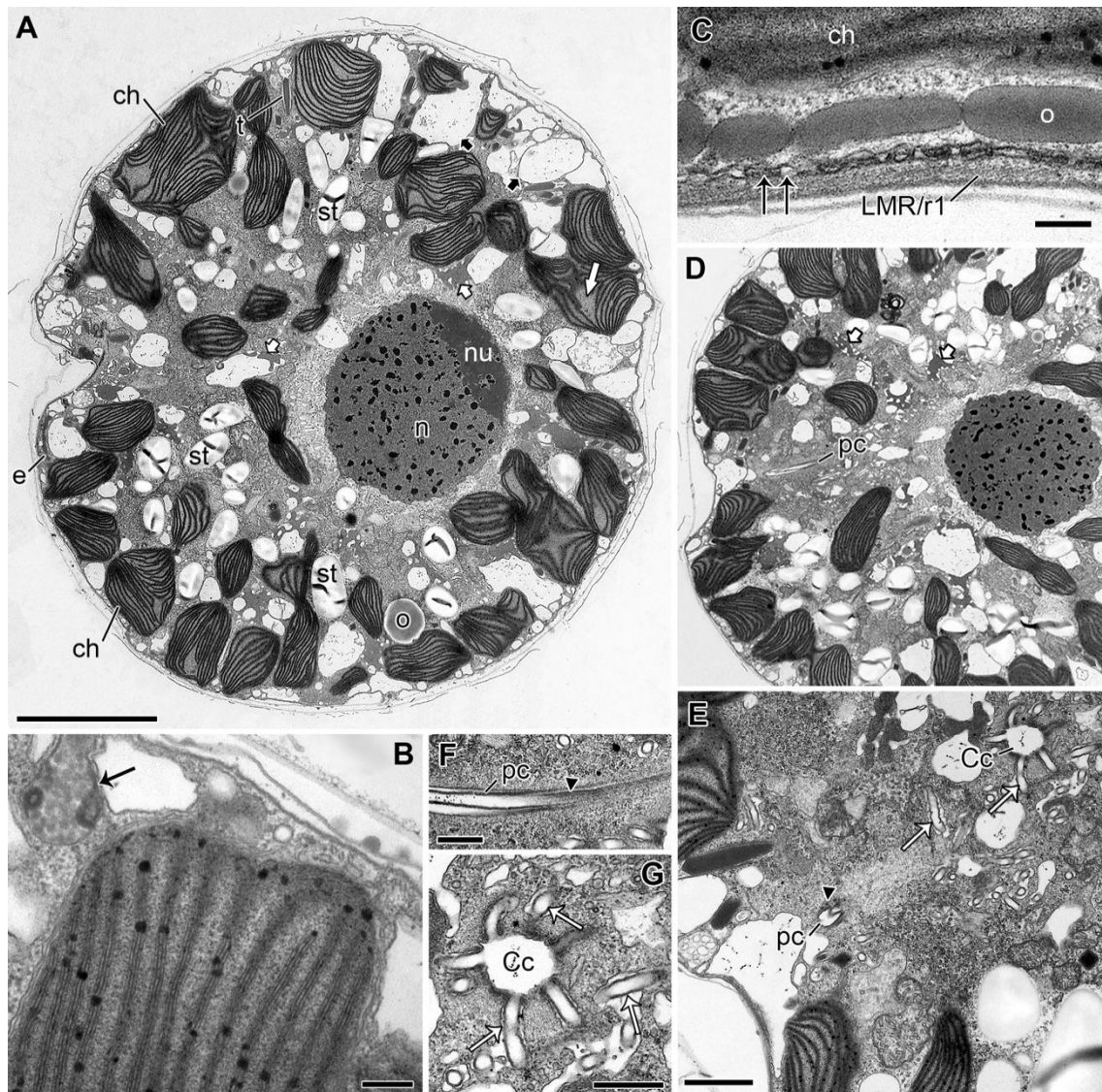
Fig. 6. *Sphaerodinium polonicum* var. *tatricum* from Gerês, TEM. (**A**) Longitudinal section of a cell seen from the left side, showing the eyespot (e) in the ventral area and the nucleus (n), on the dorsal side, at cingulum level. Small thylakoid-free areas (long white arrow) are visible in peripheral chloroplast lobes (ch). Large ellipsoid vesicles (short black arrows) are present between chloroplast lobes and vesicles associated with microbodies (short white arrows) are visible in the inner cytoplasm. (**B**) Chloroplast lobe and nearby vesicle with electron-opaque granules (arrow). (**C**) Detail of eyespot with brick-like elements (double arrow) included in a vesicle between the longitudinal microtubular root (LMR/r1) and a layer of oil globules (o). (**D–G**) Pusular system in longitudinal sections of the same cell as in A, showing location of pusule canal (pc), collecting chamber (Cc) and associated pusular tubes (white arrows). nu, nucleolus; o, oil globules; st, starch; t, trichocysts. (A, D) to the same scale. Scale bars = 5 μm (A); 200 nm (B, C); 1 μm (E); 500 nm (F, G).
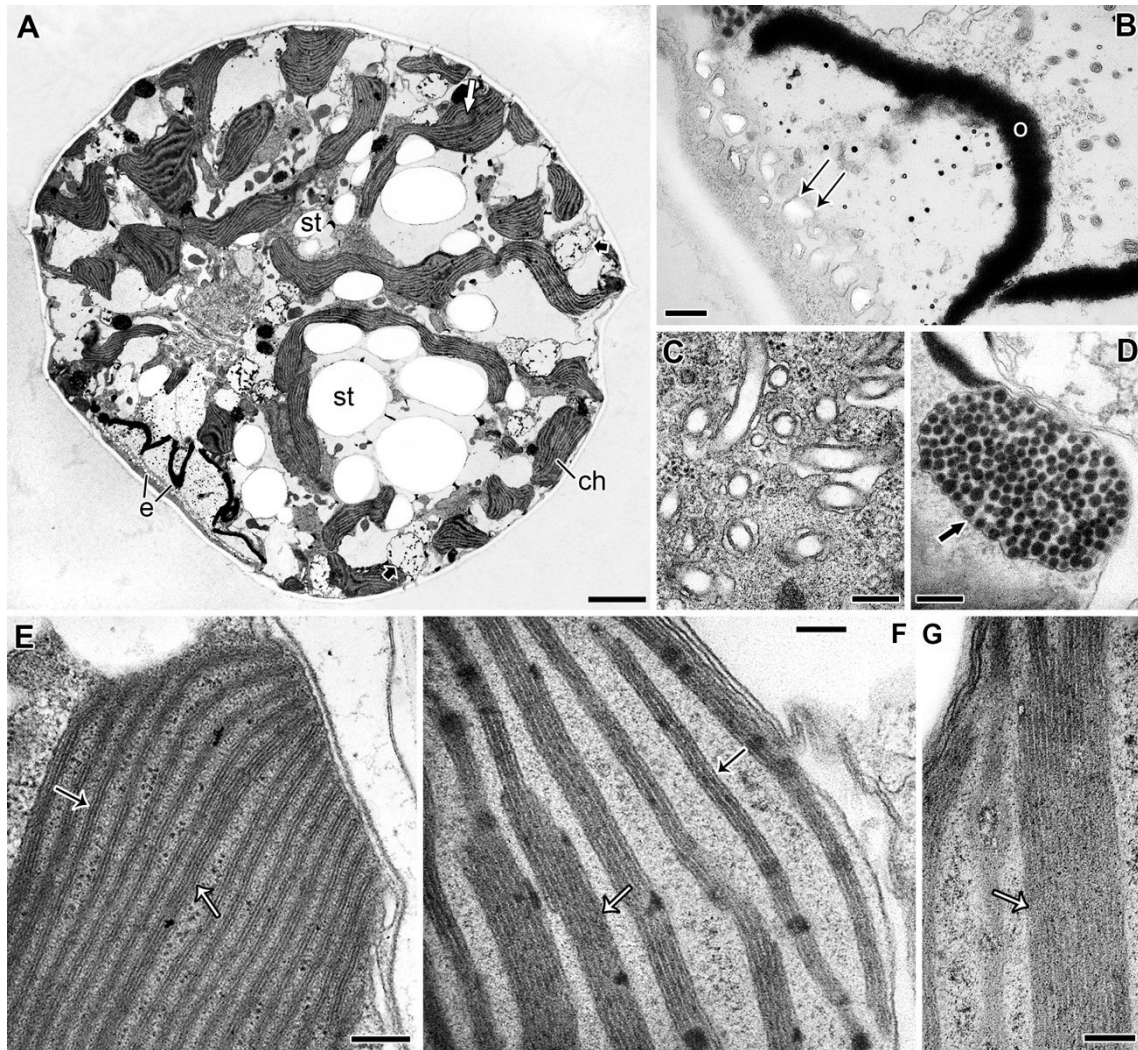
Fig. 7. *Sphaerodinium polonicum* var*. tatricum* from Buçaco, TEM. (**A**) Longitudinal section of a cell seen from left-ventral side. The eyespot (e) is visible in the somewhat retracted ventral region. Chloroplast lobes (ch) are visible intercalated with large starch grains (st). Some thylakoid-free areas are visible inside some chloroplast lobes (long white arrow). Large ellipsoid vesicles at the periphery, between chloroplast lobes (short black arrows). (**B**) Section oriented obliquely relative to the surface, giving an almost ventral view of some crystal-like elements of the eyespot (double arrow). The oil components (o) appear fused into continuous layers. (**C**) Pusular tubes near the collection chamber (not visible). (**D**) Peripheral vesicle with electron-opaque, spherical or ellipsoidal granules of unknown significance (arrow). (**E–G**) Chloroplast lobes with different thylakoid arrangements, including three-thylakoid lamellae (black arrows) and stacks of up to 14 thylakoids in a pseudograna-like arrangement (white arrows). Scale bars = 2 μm (A); 200 nm (B–E); 100 nm (F, G).

Chloroplast lobes in cells from both strains were prominent at the cytoplasm periphery and extended inward into numerous, ramifying lobes (Figs. 6A, D, 7 A). However, the thylakoid arrangement showed variation: regular, three-thylakoid lamellae

were visible in the chloroplasts of the strain isolated from Gerês (Fig. 6B), whereas in the strain from Buçaco thylakoid lamellae were more irregular, with stretches of 3–14 associated thylakoids, reminiscent of pseu-dograna (Fig. 7E–G). Small areas without thylakoids were found in chloroplasts of both strains (Figs. 6A, 7 A, long, white arrows).

Flagellar apparatus

The organization of the flagellar bases and associated structures was similar in cells from both strains. The general organization of the flagellar base area is shown as viewed from the left in a series of sections taken from a cell of the Gerês isolate (Fig. 8). Different viewpoints from two series of sections from cells of the Buçaco strain are given in Fig. 9. As estimated from serial sections, the basal bodies were inserted at an angle of about 120°. Each single-membrane bounded region where the flagella emerged from the cytoplasm was externally limited by a ring of fibrous material that showed striations in at least some views (Figs. 8I, 9 A–C); these striated collars were not connected by any prominent fibres, but some electron-opaque material was present along the cell surface in the area between the collars (not shown). Replicated basal bodies were seen in one cell, located side by side near the anterior end of the transverse basal body (TB); their orientation was not ascertained (Fig. 8C–E, RB1 and RB2). Functional basal bodies, i.e. those associated with emergent flagella, were associated with three microtubule-containing roots. A single, multistranded microtubular root was associated with the left side of the longitudinal basal body (LB) near its proximal end. The number of microtubules in this longitudinal microtubular root (LMR; labelled r1 in Moestrup 2000) varied from about 10 near the LB to some 30–40 further down along the sulcus (Figs. 8B–E; 9 A, C). Two thin fibres connected the LB to the ventral face of the LMR/r1 some 250 nm from its proximal end (Fig. 9A, white arrow). An electron-opaque fibre about 70 nm wide contacted the dorsal-anterior side of the LMR/r1, surrounded the dorsal side of the proximal end of the LB and progressed toward the ventral-posterior side of the cell (Figs. 8F–I; 9 A, C). As seen in Fig. 9C, this ventral fibre (VF) seemed to extend from electron-opaque material lining the dorsal face of the LMR/r1 near the point of attachment of a clearly striated connective (named striated root connective, SRC) linking this root with the proximal 500 nm or so of the main fibrous root of the TB, the transverse striated root (TSR). The TSR extended for about 1.5 μm from the dorsal-posterior side of TB

toward the left and ended near the left side of the transverse striated collar (TSC) (Fig. 9A–C). A microtubule ran along the TSR (Fig. 9C, short arrow), making up the microtubular component of the root (r4 in Moestrup 2000). The second root associated with the TB was a single microtubule that was seen parallel to one of the triplets of the anterior-dorsal side of the basal body (Fig. 8B). This transverse microtubular root (TMR/r3 in Moestrup 2000) continued around the transverse flagellar canal (TFC) and nucleated several rows of microtubules that extended dorsally, roughly along the right-hand side of the pusule canal (marked TMRE in Fig. 8A, which is about 1 μm to the right of Fig. 6D, F). At least two membranous bodies with a honeycomb pattern and an electron-opaque spot at the centre of the hexagonal units were visible near the flagellar bases (Fig. 8B–I). Approximately longitudinal sections along these membranous structures showed a lamellate appearance (Fig. 9A, D).

A row of some 15 microtubules, interpretable as a homologue of a microtubular strand of the peduncle (MSP) based on its location, was seen between the ventral surface and the TFC (Fig. 8A). The MSP extended near the anterior edge of the TSC (Fig. 9A) and continued past the pusule canal, curving in a dorsal direction, just anterior to the microtubular extensions of the TMR/r3 (not shown).

Phylogeny based on LSU rDNA

The tree topology from phylogenetic inferences based on nuclear-encoded LSU rDNA sequences is depicted in Fig. 10. The resolution of the deepest branches was not well supported as both posterior probabilities (pp) and bootstrap values were low (evolutionary lineages were not resolved). However, the clade with the genus *Sphaerodinium* received maximum support (pp = 1.0 and BS = 100%) and formed a sister taxon to a clade containing Borghiellaceae, Suessiaceae and Symbiodiniaceae s.s. The family Suessiaceae plus Symbiodiniaceae s.s. formed a well-supported clade (pp = 1.0 and BS = 91%) that grouped with *Baldinia* Gert Hansen & Daugbjerg and *Borghiella* spp. to form a statistically unsupported trichotomy (Fig. 10). *Dactylodinium* Kazuya Takahashi, Moestrup & Iwataki appeared as a sister group to the remaining Suessiaceae, although *D. pterobelotum* has a type-B eyespot.
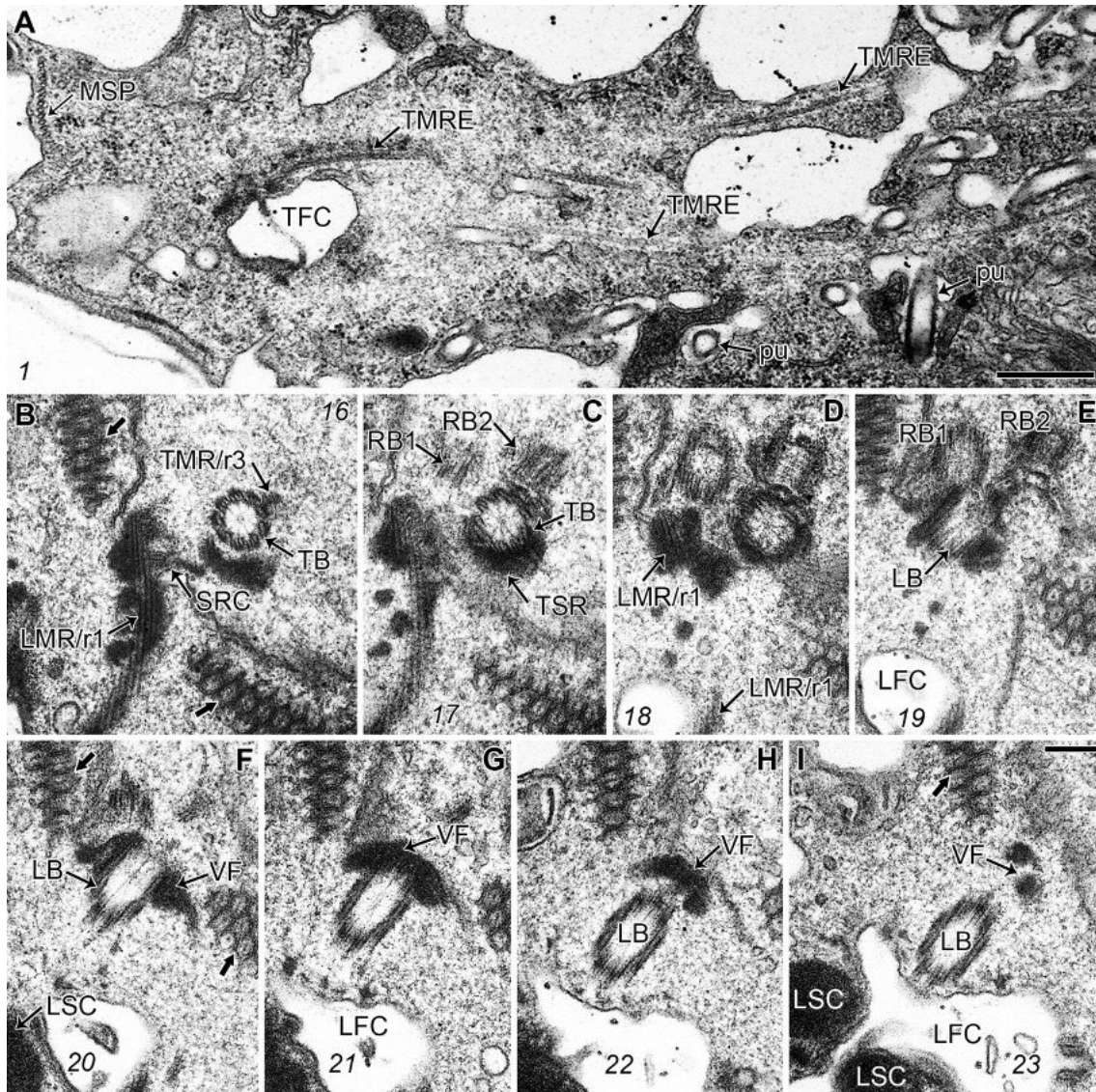
Fig. 8. *Sphaerodinium polonicum* var. *tatricum* from Gerês, TEM. Flagellar apparatus and microtubular strand of the peduncle (MSP) viewed from the left. Longitudinal sections, progressing from left to right. Slanted numbers refer to the section number. (**A**) Ventral area about 1.3 μm to the left of the proximal end of the basal bodies. Several rows of the transverse microtubular root extension (TMRE) extend from the vicinity of the transverse flagellar canal (TFC). Pusular tubes (pu) extend into this area. The MSP is visible near the ventral surface as a wavy row of some 15–20 microtubules. (**B–I**) Consecutive sections with the transverse (TB) and longitudinal basal bodies (LB), and associated roots and fibrous connectives: transverse microtubular root (TMR/r3), longitudinal microtubular root (LMR/r1), striated root connective (SRC), transverse striated root (TSR). On the bottom-left of the area shown is visible fibrous material of the longitudinal striated collar (LSC), which surrounds the exterior opening of the longitudinal flagellar canal (LFC). A ventral fibre (VF) is noted next to the right-anterior end of LB. Two membranous bodies with a honeycomb pattern are visible near the basal bodies (long black arrows in B, F and I). Two replicated basal bodies (RB1, RB2) are visible next to the anterior end of the functional basal bodies. Scale bars = 500 nm (A); 200 nm (B–I).
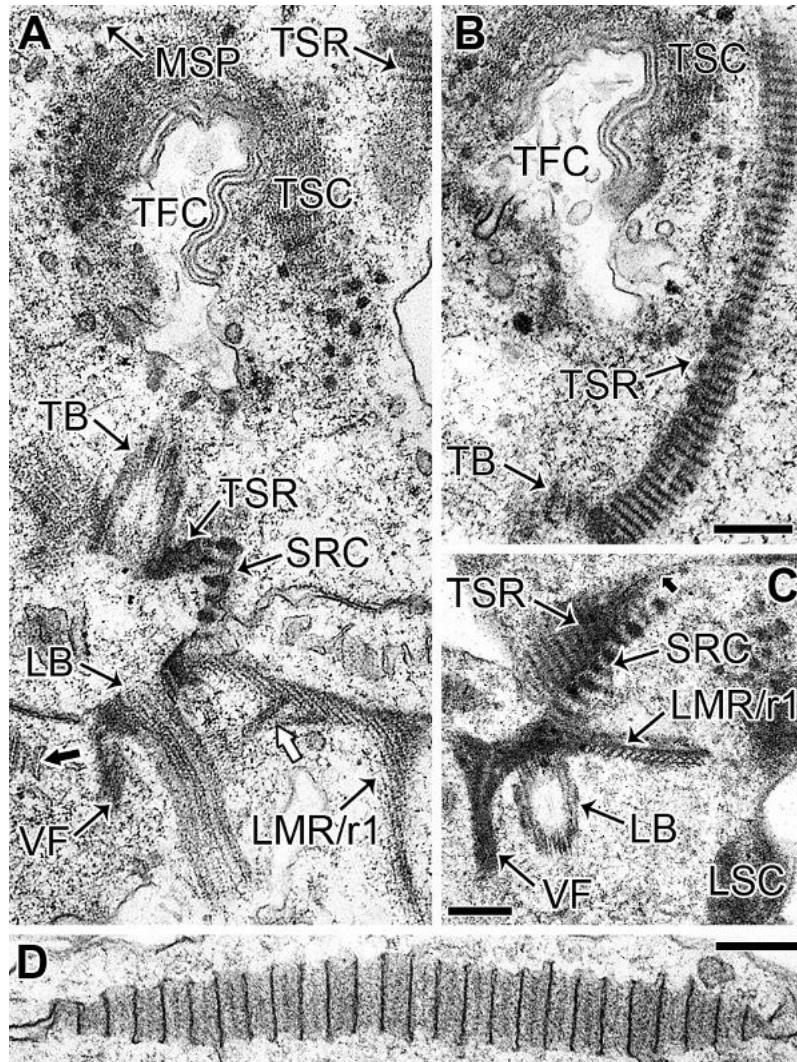
Fig. 9. *Sphaerodinium polonicum* var. *tatricum* from Buçaco, TEM. Details of flagellar apparatus, microtubular strand of the peduncle (MSP) and lamellar body. (**A, B**) Two almost consecutive sections (B is two sections to the dorsal-right of A and slightly rotated anticlockwise) showing basal bodies (TB and LB) and associated roots. Note two thin fibers linking the LMR/r1 to the LB (white arrow in A) and the striated root connective (SRC) extending from the dorsal side of the LMR/r1 to the proximal end of the TSR. The TSR extends from the proximal end of the TB to the transverse striated collar (TSC). (**C**) Flagellar base area of a different cell showing the ventral fibre (VF) extending to the ventral-right of the obliquely sectioned LB. The proximal part of the LMR/r1, TSR and SRC are visible at this level. Note the microtubule (TSRM/r4, short arrow) associated with TSR. (**D**) Longitudinal section through a lamellar body. Flagellar apparatus abbreviations as in Fig. 8. (A, B) to the same scale. Scale bars = 200 nm.
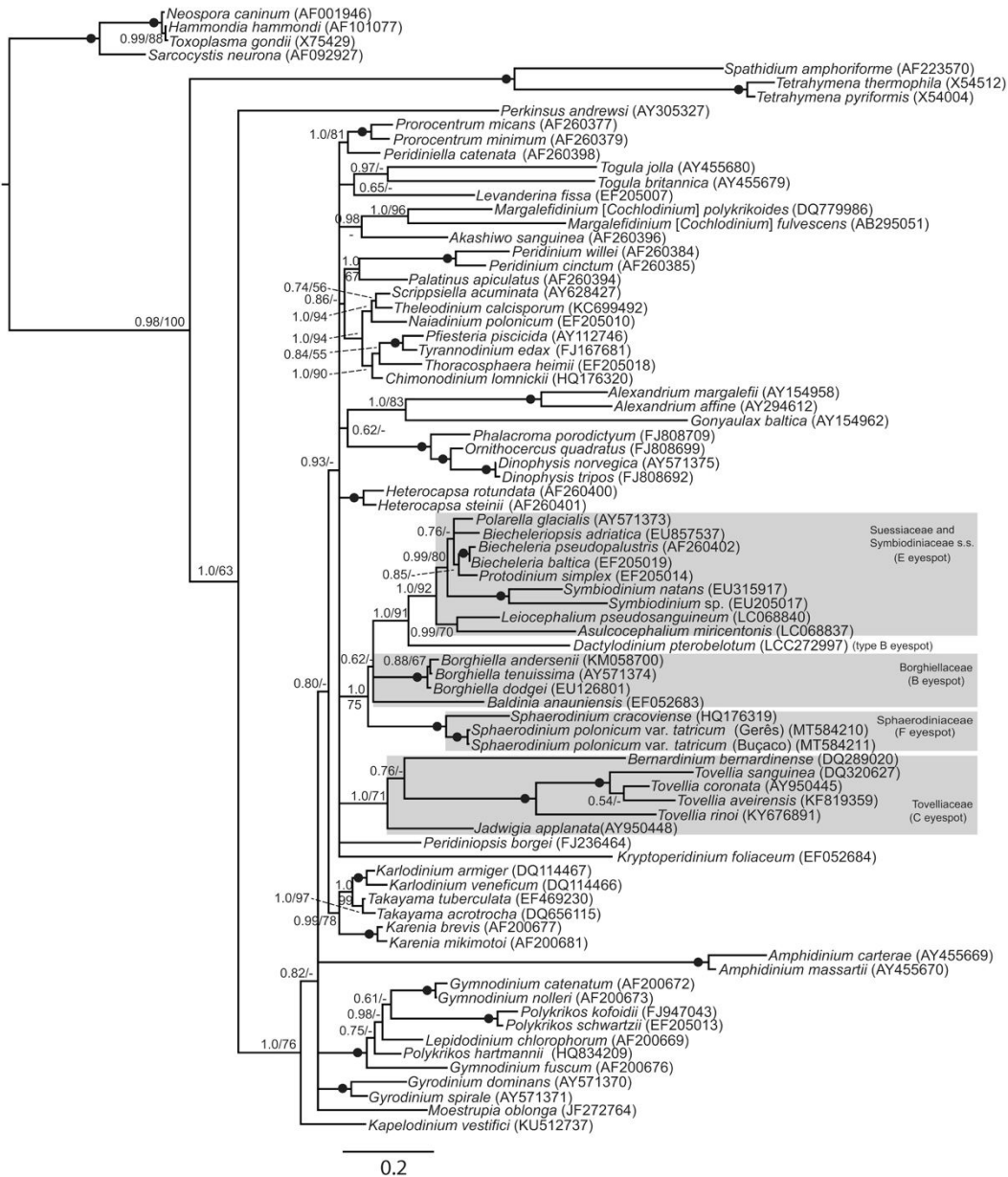
Fig. 10. Phylogeny of *Sphaerodinium polonicum* var. *tatricum* based on nuclear-encoded partial LSU rDNA sequences and inferred from Bayesian analysis (BA). The analysis was based on 1680 base pairs including introduced gaps and encompassed 48 genera and 71 species of dinoflagellates (i.e. the ingroup). The outgroup comprised 4 apicomplexans, 3 ciliates and *Perkinsus*. The robustness of the tree topology was evaluated by posterior probabilities (PP ≥0.5) from BA and 1000 bootstrap replications (BS ≥50%) in maximum likelihood (ML). These values were written at internodes. Filled circles were used to indicate the highest possible support in BA (1.0) and ML bootstrap (100%) whereas PP < 0.5 and BS <50% were indicated by a dash (–). GenBank accession numbers were provided in parentheses following the species names. The character distribution of eyespot types was indicated by grey boxes. Symbiodiniaceae s.s., used in the sense of LaJeunesse et al. (2018), are represented in the tree only by two species of *Symbiodinium*, which appear nested within the Suessiaceae. The branch lengths are proportional to the number of character changes and a scale bar was provided below.

Phylogeny based on SSU rDNA

The phylogenetic relationship between terminal lineages generally received high support in terms of posterior probabilities and bootstrap support values (Fig. 11). In contrast, the tree topology for many of the deepest branches was not well supported and the phylogeny of the monophyletic clade of Suessiaceae and Symbiodiniaceae s.s. was likewise unresolved. *Dactylodinium* formed a sister group, with maximum support, to a clade containing the Suessiaceae and Symbiodiniaceae s.s. The monophyletic *Sphaerodinium* (with two species, three strains) formed a sister group to a clade that grouped "*Glenodinium* sp.", *Baldinia* and the two coccoid forms *Cystodinium phaseolus* Pascher and *Phytodinium* sp.; and the *Sphaerodinium-Baldinia-Cystodinium* clade appeared as sister to a morphologically undefined species here labelled *Borghiella* sp., with moderate support (PP = 1.0 and BS = 75%). Hence, nuclear-encoded SSU rDNA did not support monophyly of the Borghiellaceae. Though the tree topology indicated a sister group relationship between Tovelliaceae and the clade with Sphaerodiniaceae-Borghiellaceae-Suessiaceae *s.l.* this branching had no statistical support (PP = 0.69, BS = <50%).

Phylogeny based on concatenation of SSU and LSU rDNA

The concatenated data matrix comprised fewer dinoflagellates as the complete ribosomal operon has not been determined for many of the taxa included in the single gene analyses. Sphaerodiniaceae and Suessiaceae each formed highly supported monophyletic clades (PP = 1.0, BS = 100%), whereas Borghiellaceae received less support (PP = 0.76, BS = 71%) (Fig. 12). A clade with both species of *Dactylodinium* appeared as a sister group to the Suessiaceae with maximum support. The clade comprising these three families was well supported (PP = 1.0, BS = 96%), but the relationship between them could not be established (PP = 0.59, BS = 75%). In this phylogenetic analysis the monophyletic Tovelliaceae formed a highly supported sister taxon to the three families mentioned above (PP = 1.0, BS = 94%). Similar to each of the single gene analyses, the deepest branches in the concatenated phylogeny received little or no support (Fig. 12) preventing a rewarding discussion of the evolutionary history of the dinoflagellates.
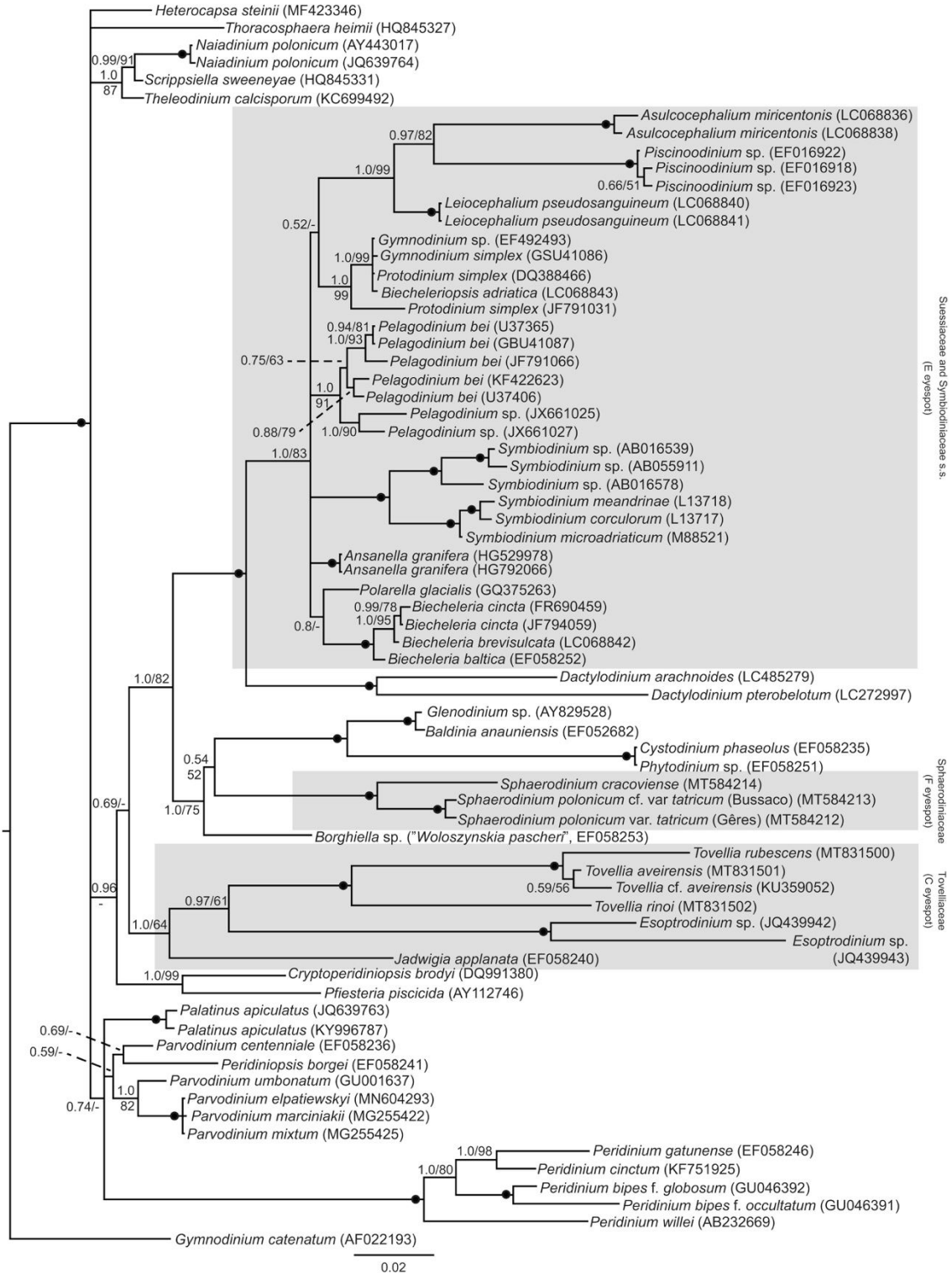
Sequence divergence

To further elucidate the relatedness of the two strains of *S. polonicum* var. *tatricum* we compared ITS1, 5.8S rDNA and ITS2 as single fragments and all of them combined (Table 1). Including all three fragments the divergence was 2.1%. For ITS1 and ITS2 fragments, the sequence divergence was 3.7 and 1.1%, respectively. Interestingly divergence values for 5.8S rDNA are marginally higher than ITS2 (1.3 versus 1.1%).

Table 1. Sequence divergence estimates in percent between *Sphaerodinium polonicum* var. *tatricum* (Gerês) and *S. polonicum* var. *tatricum* (Buçaco) based on ITS1, 5.8 S rDNA, ITS2 and all three fragments combined (in total 533 base pairs). Uncorrected distances (P-values) and distance values calculated using the Kimura-2-parameter model were estimated using PAUP* (ver. 4.0a build 161). Genbank accession numbers: MT584215 (Gerês); MT584216 (Buçaco).

	P-values (%)	Kimura-2-p (%)
ITS1	3.7	3.8
5.8 S rDNA	1.3	1.3
ITS2	1.1	1.1
All three fragments	2.1	2.1

←

Fig. 11. Phylogeny of *Sphaerodinium polonicum* var. *tatricum* based on nearly complete nuclear-encoded SSU rDNA sequences and inferred from Bayesian analysis (BA). The analysis was based on 1760 base pairs including introduced gaps and encompassed 31 genera (68 strains) of dinoflagellates including the outgroup (i.e. *Gymnodinium catenatum*). The robustness of the tree topology was evaluated by posterior probabilities (PP ≥ 0.5) from BA and 1000 bootstrap replications (BS ≥ 50%) in maximum likelihood (ML). These values were written at internodes. Filled circles were used to indicate the highest possible support in BA (1.0) and ML bootstrap (100%) whereas PP < 0.5 and BS < 50% were indicated by a dash (–). GenBank accession numbers are provided in parentheses following the species names. The families Sphaerodiniaceae, Suessiaceae and Symbiodiniaceae s.s., and Tovelliaceae are indicated on the phylogenetic tree together with their type of eyespot. Symbiodiniaceae s.s., used in the sense of LaJeunesse et al. (2018), are represented in the tree only by species of *Symbiodinium*, which appear nested within the Suessiaceae. The branch lengths are proportional to the number of character changes, see scale bar.
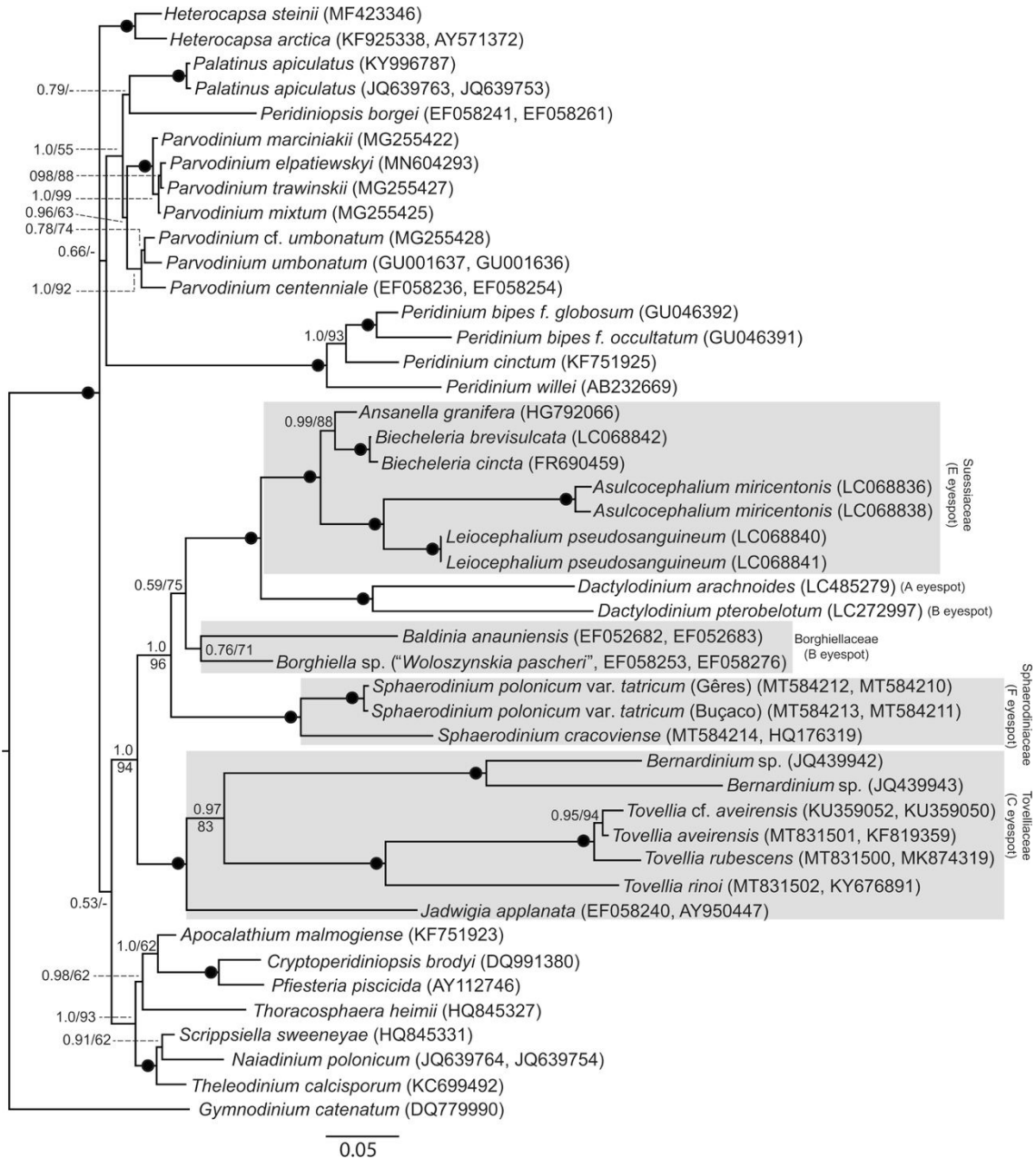
Fig. 12. Phylogeny of *Sphaerodinium polonicum* var. *tatricum* based on concatenation of 45 nuclear-encoded LSU and SSU rDNA sequences and including a total of 24 dinoflagellate genera. Bayesian analysis and maximum likelihood analyses were based on 2,854 base pairs including introduced gaps. Robustness of tree topologies were evaluated by posterior probabilities (PP ≥ 0.5) in BA and 1,000 bootstrap replications (BS ≥ 50%) in maximum likelihood (ML). Support values are written at internodes. Filled circles indicate the highest possible support in BA (PP = 1.0) and in ML bootstrap (BS = 100%). PP < 0.5 and BS < 50% are indicated by a dash (–). GenBank accession numbers are provided following all species names. The families Borghiellaceae, Sphaerodiniaceae, Suessiaceae and Tovelliaceae are indicated on the phylogenetic tree together with their type of eyespot. Branch lengths are proportional to the number of character changes, see scale bar.

DISCUSSION

Morphological comparisons and identity of the organisms

The genus *Sphaerodinium* is readily identified by the nearly symmetrical amphiesmal plate arrangement on the epicone, which includes four intercalary plates (Kofoidian notation), and the presence on the hypocone of six postcingular plates (Moestrup and Calado 2018). Comparison with the original descriptions of the five species and one variety described in *Sphaerodinium* shows a good match between our material and the original drawings of *S. polonicum* var. *tatricum*, both in general morphology and in plate arrangement (Wołoszyńska 1916). Of particular importance is the papillate appearance of plates, and especially of plate sutures, that is clearly shown in light micrographs of empty thecae of both strains herein reported on, which matches what Wołoszyńska described for both *S. polonicum* and its variety. The two flap-like thickenings on the left-anterior part of the sulcus, just below the proximal end of the cingulum, closely match Wołoszyńska's original illustrations of *S. polonicum* var. *tatricum* (Wołoszyńska 1916, 1952); and the absence of corresponding thickenings on the right edge of the sulcus sets our material apart from typical *S. polonicum* (Moestrup and Calado 2018; Wołoszyńska 1916). Another distinguishing feature mentioned in the original description of the variety was the deeper extension of the anterior part of the sulcus into the epicone, and its different shape from the anterior sulcal area of typical *S. polonicum*. It is clear from the original drawings that this anterior sulcal area corresponds to the plate directly aligned with plate 1′, although its position at the same level and with a similar appearance as epithecal plates renders its interpretation as part of the sulcus arguable (Wołoszyńska 1952, pl. IV, Fig.9). The plate is herein labelled Z to accommodate different interpretations without disrupting the Kofoidian notation of plates in the precingular series, as explained in Craveiro et al. (2010). In contrast, Luo et al. (2019) interpreted a similarly located plate in *Caladoa arcachonensis* Z. Luo, K.N. Mertens & H. Gu as an anterior sulcal plate. The plate composition of the furrows is often difficult to work out and sulcal plates were not usually described in detail, even by exceptional observers like Wołoszyńska. However, the shape of the sulcus of *S. polonicum* var. *tatricum* was described as wider near the posterior end and drawn as somewhat asymmetric (Wołoszyńska 1916, 1952). The slight deviation toward the right of the posterior sulcal

plate of both strains described herein creates an irregular, asymmetric shape that appears compatible with the original illustrations. As shown in both the Gerês and the Buçaco strains, the sulcal plate arrangement is unusual in having a middle plate (ms) contacting postcingular plates on both sides of the sulcus, thereby separating the posterior sulcal from a set of four smaller plates on the anterior part of the sulcus, near the flagellar pores. This is quite different from what was found in *S. cracoviense*, in which the posterior sulcal plate extended along the right side of the sulcus and reached the right sulcal plate at the level of the cingulum (Craveiro et al. 2010).

Perhaps less significant but worth noting is the slight asymmetry of apical plate 3, which constantly shared a shorter suture with plate 3a than with 2a; the irregularly hexagonal shape of this central apical plate very closely matched the apical view of *S. polonicum* var. *tatricum* in Wołoszyńska (1952) and was noted as a feature of the variety by Moestrup and Calado (2018). The apical complex of *S. polonicum* var. *tatricum* was marked by Wołoszyńska (1952) as a small rectangle with its long axis oriented from ventral-right to dorsal-left; a similar orientation was here shown for both strains. Although little detail was visible in the apical complex by LM, SEM revealed an organization similar to that found in *S. cracoviense* (Craveiro et al. 2010).

The nucleus of *S. polonicum* was described as horseshoe-shaped and drawn with its long axis parallel to the cingulum (Wołoszyńska 1916). In the shorter description of the variety the horseshoe shape of the nucleus is again mentioned, this time without illustration (Wołoszyńska 1916). In contrast, non-dividing nuclei in both strains reported herein appeared ellipsoid in acetocarmine-stained cells and in TEM sections. The significance of this discrepancy is not clear. In view of the overall agreement with the characters described above, and until a population with similar characters and a horseshoe-shaped nucleus is studied by modern methods, we opt to identify our material as *S. polonicum* var. *tatricum*.

The morphology of the larger cells that developed into resting cysts, as shown in Fig. 5A, deviated from the smoothly round shape of vegetative cells. The outline of these cells, presumed to be planozygotes, is more similar to typical *S. polonicum* than it is to *S. polonicum* var. *tatricum*. Wołoszyńska (1916) mentioned sexual reproduction in typical *S. polonicum* and the possibility that the two taxa are part of the same life cycle (and therefore represent a single taxon) comes to mind. However, due to the small number of

fusing cells in culture batches and the rapid transformation of planozygotes into cysts, we were unable to examine in detail the thecae of these larger cells, leaving this hypothesis unsupported.

Cysts and encystment

In the original description of several *Sphaerodinium* species, Wołoszyńska (1916) mentioned resting cysts ('Dauerzellen') for *S. cracoviense* only, describing them simply as spherical to ovoid. However, resting or resistance cells were not illustrated, and it is uncertain whether division cysts or temporarily immobile cells were misinterpreted by Wołoszyńska. Neither sexual reproduction nor resting cysts were reported in cultured strains of *S. cracoviense* (Craveiro et al. 2010). The resting cysts reported here for *S. polonicum* var. *tatricum* show a complex morphology that has no obvious match among reported resting cysts produced by freshwater dinoflagellates (reviewed by Mertens et al. 2012; see also Craveiro et al. 2013; Li et al. 2015; Pandeirada et al. 2014, 2017; 2019; Takahashi et al. 2015). The morphology of the cysts shown in Fig. 4 bears some superficial resemblance to cysts produced by marine species of the *Gonyaulax spinifera* (Claparède & J. Lachmann) Diesing complex (Ellegaard et al. 2003). However, the phylogenetic and ecological distance between *Sphaerodinium* and the Gonyaulacales suggests that cyst processes in the two groups may be the result of convergent evolution.

The encystment process reported herein appears unusual, both in the mechanism that leads to the formation of wall projections and in the speed with which it occurs. The sudden retraction of the cytoplasm of encysting cells of *S. polonicum* var. *tatricum* resulted in the processes being nearly formed within seconds, in contrast with the longer times involved in the commonly reported outward growth of processes from wall layers deposited on the cytoplasmic surface, under the more or less disrupted cell cover (Bravo and Figueroa 2014; Kokinos and Anderson 1995; Pandeirada et al. 2017; Stosch 1973). Cysts with a smooth surface often mature inside the cell cover (which presumably contains at least the outer part of the amphiesma), as observed in, e.g. *Tovellia apiculata* (Stosch) Moestrup, K. Lindberg & Daugbjerg, and in *Chimonodinium lomnickii* (Wołoszyńska) Craveiro, Calado, Daugbjerg, Gert Hansen & Moestrup, *Peridinium cinctum* (O.F. Müller) Ehrenberg and other peridinioids (Craveiro et al. 2011; Lefèvre 1932; Stosch 1973). However, when cyst processes are formed the cell cover is either

released before process growth is completed (e.g., in *Tovellia rinoi*), or it remains around the process-bearing surface as seen in *Biecheleria pseudopalustris* (J. Schiller) Moestrup, K. Lindberg & Daugbjerg and *Lingulodinium polyedra* (F. Stein) J.D. Dodge, swelling to accommodate the growth of processes (Kokinos and Anderson 1995; Pandeirada et al. 2017; Stosch 1973). Although the outer amphiesma was visible around many cysts of *S. polonicum* var. *tatricum* no more than a slight swelling was ever detected and the detachment of the outer cell cover from the forming cyst surface seemed to result essentially from the cytoplasm retraction.

Chloroplasts

In contrast with the general similarity between the morphological features of the strains from Gerês and Buçaco, cells from the Buçaco culture batches were usually distinct by their less numerous and more rounded chloroplast lobes. Whereas the chloroplasts of cells from Gerês displayed the predominant association of thylakoids in groups of three, as commonly found in the peridinin-containing chloroplast type, chloroplasts of the Buçaco strain had lamellae with 3–14 associated thylakoids along part of their length. Unusual thylakoid arrangements in grana- or pseudograna-like associations have been reported from a small number of apparently distantly related dinoflagellate species (Craveiro et al. 2013; Dodge 1975; Hansen et al. 1996; Jeong et al. 2014; Takahashi et al. 2015, 2017). However, the stability of peudograna-like thylakoid associations in dinoflagellate species is generally unknown. The recent finding in *Kirithra asteri* Boutrup, Tillmann, Daugbjerg & Moestrup of a strain with up to 45-thylakoid stacks in the chloroplast, which had 100% identical nuclear-encoded LSU rDNA (>1400 base pairs) to another strain with only three-thylakoid lamellae, suggests that this feature has limited taxonomic value (Boutrup et al. 2017). Neither the function nor the mechanisms leading to the formation of pseudograna-like structures in the Buçaco strain of *S. polonicum* var. *tatricum* are understood. The rounded chloroplast lobes seemed to be a stable, intrinsic (i.e. genetically determined) feature maintained through successive generations of cells of this strain, but they were not detected in the strain from Gerês, which was grown in the same medium and maintained in the same light and temperature conditions. However, in view of the general morphological similarity and the relatively

small divergence found between compared ITS1, 5.8S and ITS 2 sequences of the two strains we prefer to refer them to the same taxon.

Eyespot, pusule, MSP and flagellar apparatus

The voluminous eyespot of *S. polonicum* var. *tatricum* was slightly less conspicuous in LM than the eyespot of *S. cracoviense*, but both species showed a single layer of crystal-like units located between the LMR/r1 and one or more layers of more or less fused, elongated oil globules: a type F eyespot (Craveiro et al. 2010; Moestrup and Calado 2018). The presence reported herein of a canal connecting the TFC with a collecting chamber linked with numerous pusular tubes represents a somewhat less extensive but similar arrangement to what was found in *S. cracoviense* (Craveiro et al. 2010). Contrary to what was seen in *S. cracoviense*, no pusular vesicles were found attached to the LFC in *S. polonicum* var. *tatricum*; they were perhaps not developed, but it is also possible that sections containing this area, which was relatively small in *S. cracoviense*, may have been missed. A similarity has been noted between the pusular system of *Sphaerodinium* species and that described from *Naiadinium polonicum* (Wołoszyńska) Carty, namely the presence in this species of a pusule canal connected to an inner collecting chamber associated with long, regular pusular tubes (Craveiro et al. 2015). However, the pusule canal of *N. polonicum* opens on the ventral side into the LFC and differs structurally from that of *Sphaerodinium* by being partly enwrapped by a vesicle (Craveiro et al. 2015). It appears unlikely that the two structures are evolutionarily closely related.

In *S. polonicum* var. *tatricum*, as in *S. cracoviense*, a single row of microtubules was found in a position, and with an orientation, that makes it likely homologous with microtubular strands extending into peduncles, particularly those used for feeding (Craveiro et al. 2010; Hansen and Calado 1999). However, in both species of *Sphaerodinium* this MSP lacked a definite area of association with the cell surface, and it was not accompanied by vesicles with electron-opaque contents, which are regularly present when the MSP is involved in feeding (Calado et al. 1998, 2006). No function is known at present for the MSP of *Sphaerodinium*. On the ventral surface of *S. cracoviense*, between the two flagellar collars, a relatively small ventral ridge was demonstrated (Craveiro et al. 2010). A smaller amount of fibrous material in a similar location of *S. polonicum* var. *tatricum* (mentioned above but not shown) is here interpreted as an even

smaller ventral ridge. A well-developed ventral ridge is a common feature on the mid-ventral area of gymnodinioid and woloszynskioid dinoflagellate cell types (e.g., Calado et al. 1998; Lindberg et al. 2005) and the presence of a ventral ridge was among the features showing that the long tradition of classifying *Sphaerodinium* among peridinioids was unjustified.

A direct comparison of the flagellar apparatus of *S. polonicum* var. *tatricum* with that of *S. cracoviense* shows great similarity in the main features, although fibrous structures, such as collars and their extensions, appear less developed in the former. Of particular interest are the unusual structures previously found in *S. cracoviense*, of which those also found in the cultures described herein may stand as typical features of the genus. The presence of a distinct SRC linking electron-opaque material on the dorsal side of the LMR/r1 with the TSR near its connection with the TB is common to both species of *Sphaerodinium*, as is the absence in this area of any traces of the layered connective that is typical of peridinioids (Calado et al. 1999; Craveiro et al. 2016). The extension of the TMR/r3, which occurs as several rows of microtubules that extend along the pusule canal in both species, is unusual and is perhaps involved in the orientation of the pusular system (Craveiro et al. 2010). Thin fibres connecting the ventral surface of the LMR/r1 with LB triplets are uncommon in peridinioids but were reported in several species of Suessiales (Craveiro et al. 2010; Hansen et al. 2007; Hansen and Daugbjerg 2009; Jeong et al. 2014; Takahashi et al. 2017).

Some of the most striking features of the flagellar base area that are common to *S. cracoviense* and *S. polonicum* var. *tatricum* are the ventral fibre extending from the right-anterior side of the LB and the membranous bodies with hexagonal units in a honeycomb pattern, also referred to as lamellar bodies by Craveiro et al. (2010). The lamellar body was first described from *Baldinia anauniensis* Gert Hansen & Daugbjerg where membranous structures of this kind were found to fill a large area in sections near the base of the LB (Hansen et al. 2007). How these membranous structures interact with other components is unknown, but the repeating, patterned arrangement invites speculation about interaction with light and suggests a function in phototaxis (Craveiro et al. 2010; Hansen et al. 2007). The ventral fibre has been documented from *B. anauniensis* and *Dactylodinium pterobelotum*, two species with a type B eyespot (sensu Moestrup and Daugbjerg, 2007) suggesting affinity with the Borghiellaceae, but was found lacking in

Borghiella andersenii Daugbjerg, Andreasen, Happel, Pandeirada, Gert Hansen, Craveiro, Calado & Moestrup and *B. dodgei* Moestrup, Gert Hansen & Daugbjerg (Daugbjerg et al. 2014; Hansen et al. 2007; Moestrup et al. 2008; Takahashi et al. 2017). A lamellar body of the kind described above is currently known only from *Baldinia* and *Sphaerodinium*.

Phylogeny

The three phylogenetic trees, one based on LSU, another on SSU rDNA and the other on concatenated LSU and SSU rDNA, display the two species of *Sphaerodinium* as members of the same clade with maximum support, and identify their closest relatives as species with eyespot type B (Borghiellaceae) or E (Suessiaceae and Symbiodiniaceae s.s.), suggesting a common origin for the presence of crystal-like units in dinoflagellate eyespots (Takahashi et al. 2017). The presence of predominantly coccoid forms (*Cystodinium*, *Phytodinium*) among the sister groups to the *Sphaerodinium* clade in the SSU rDNA phylogeny highlights the need for further work on these predominantly immobile species, which were traditionally grouped in a separate order (Moestrup and Calado 2018). As noted by Craveiro et al. (2010), the *Sphaerodinium* clade appears to have no close relatives in the trees, suggesting its classification in a separate family. The position of the genus *Sphaerodinum* (Sphaerodiniaceae) as an early diverging branch of the Suessiales agrees with other DNA-based phylogenies (Knechtel et al. 2020; Takahashi et al. 2017) and is compatible with the presence in *Sphaerodinium* of some apparently peridinioid characteristics, such as the arrangement of amphiesmal plates. The distances calculated between the two strains of *S. polonicum* var. *tatricum* in the ITS1-5.8S rDNA-ITS2 portion of the ribosomal operon would perhaps justify the recognition of two different taxa. However, having only the difference in chloroplast morphology and thylakoid arrangement as distinctive features, which may be of little value (Boutrup et al. 2017), we prefer to treat them at present as two different strains of the same taxon.

In view of the shared unusual characteristics, particularly the ventral fibre and the lamellate body, and the species position in phylogenetic inferences, *Baldinia anauniensis* stands out as the closest known relative of *Sphaerodinium*. In our phylogenetic inferences, *Dactylodinium* appeared as closely related to the Suessiaceae and Symbiodiniaceae s.s., in agreement with Knechtel et al. (2020). Although a type B eyespot was found in *D.*

pterobelotum (Takahashi et al. 2017), no crystal-like units were observed in the eyespot of *D. arachnoides* W.M. Lum, Kazuya Takahashi, Takayama & Iwataki, which was therefore classified as a type A eyespot (Lum et al. 2019). The inclusion of *Dactylodinium* in the Borghiellaceae is therefore not supported. The presence in the flagellar apparatus of *D. pterobelotum* of a ventral fibre apparently homologous with that seen in *Sphaerodinium* also suggests a close evolutionary relationship. However, both *B. anauniensis* and *D. pterobelotum* show important structural differences from *Sphaerodinium*, both external and in cytoplasmic features, which appear compatible with their current classification outside the Sphaerodiniaceae.

Conclusions

On the basis of detailed examination of *S. cracoviense* and *S. polonicum* var. *tatricum* the following features can be listed as characteristic of *Sphaerodinium* in addition to the general arrangement of the main amphiesmal plates: apical complex with three platelets, the middle one linear and with an axial row of small knobs; eyespot of type F, i.e. an extraplastidial eyespot combining a single, ventral row of crystal-like units with at least one layer of more or less fused oil globules; pusular system including a pusule canal linking the transverse flagellar canal with a dilated portion in the central cytoplasm, from which radiate numerous regular, 100-nm wide pusular tubes; flagellar apparatus with three microtubular roots, LMR/r1, TMR/r3 and TSRM/r4, and a ventral fibre extending ventroposteriorly from the proximal-right side of the longitudinal basal body; TMRE/r3-extension made of several rows of microtubules oriented roughly parallel to the pusule canal; one or several lamellar bodies in the flagellar base area, consisting of membranous structures with a honeycomb pattern in cross section and an electron-opaque spot in the middle of each hexagonal honeycomb unit; resting cyst with an equatorial constriction, ornamented overall with processes, some of which are branched, rapidly formed by cytoplasmic retraction (seen only in *S. polonicum* var. *tatricum*); closest known relatives are the type B eyespot-bearing members of the Borghiellaceae, particularly *Baldinia anauniensis*, which shares with *Sphaerodinium* the ventral fibre and the lamellar body.

REFERENCES

Boutrup, P.V., Moestrup, Ø., Tillmann, U., Daugbjerg, N., 2017. Ultrastructure and phylogeny of *Kirithra asteri* gen. et sp. nov. (Ceratoperidiniaceae, Dinophyceae) — a free-living, thin-walled marine photosynthetic dinoflagellate from Argentina. Protist 168, 586–611.

Bravo, I., Figueroa, R., 2014. Towards an ecological understanding of dinoflagellate cyst functions. Microorganisms 2, 11–32.

Calado, A.J., Craveiro, S.C., Moestrup, Ø., 1998. Taxonomy and ultrastructure of a freshwater, heterotrophic *Amphidinium* (Dinophyceae) that feeds on unicellular protists. J. Phycol. 34, 536–554.

Calado, A.J., Hansen, G., Moestrup, Ø., 1999. Architecture of the flagellar apparatus and related structures in the type species of *Peridinium*, *P. cinctum* (Dinophyceae). Eur. J. Phycol. 34, 179–191.

Calado, A.J., Craveiro, S.C., Daugbjerg, N., Moestrup, Ø., 2006. Ultrastructure and LSU rDNA-based phylogeny of *Esoptrodinium gemma* (Dinophyceae), with notes on feeding behavior and the description of the flagellar base area of a planozygote. J. Phycol. 42, 434–452.

Carty, S., 2014. Freshwater Dinoflagellates of North America. Cornell University Press, Ithaca and London.

Couté, A., Iltis, A., 1984. Mise au point sur la flore péridiniale (Algae, Pyrrhophyta) d'eau douce de Côte d'Ivoire. Rev. Hydrobiol. Trop. 17, 53–64.

Craveiro, S.C., Moestrup, Ø., Daugbjerg, N., Calado, A.J., 2010. Ultrastructure and large subunit rDNA-based phylogeny of *Sphaerodinium cracoviense*, an unusual freshwater dinoflagellate with a novel type of eyespot. J. Eukar. Microbiol. 57, 568–585.

Craveiro, S.C., Calado, A.J., Daugbjerg, N., Hansen, G., Moestrup, Ø., 2011. Ultrastructure and LSU rDNA-based phylogeny of *Peridinium lomnickii* and description of *Chimonodinium* gen. nov. (Dinophyceae). Protist 162, 590–615.

Craveiro, S.C., Pandeirada, M.S., Daugbjerg, N., Moestrup, Ø., Calado, A.J., 2013. Ultrastructure and phylogeny of *Theleodinium calcisporum* gen. et sp. nov., a freshwater dinoflagellate that produces calcareous cysts. Phycologia 52, 488–507.

Craveiro, S.C., Daugbjerg, N., Moestrup, Ø., Calado, A.J., 2015. Fine-structural characterization and phylogeny of *Peridinium polonicum*, type species of the recently described genus *Naiadinium* (Dinophyceae). Eur. J. Protistol. 51, 259–279.

Craveiro, S.C., Daugbjerg, N., Moestrup, Ø., Calado, A.J., 2016. Studies on *Peridinium aciculiferum* and *Peridinium malmogiense* (=*Scrippsiella hangoei*): comparison with *Chimonodinium lomnickii* and description of *Apocalathium* gen. nov. (Dinophyceae). Phycologia 56, 21–35.

Darriba, D., Taboada, G.L., Doallo, R., Posada, D., 2012. jModelTest 2: more models, new heuristics and parallel computing. Nat. Method 98, 772.

Daugbjerg, N., Andreasen, T., Happel, E., Pandeirada, M.S., Hansen, G., Craveiro, S.C., Calado, A.J., Moestrup, Ø., 2014. Studies on woloszynskioid dinoflagellates VII. Description of *Borghiella andersenii* sp. nov.: light and electron microscopy and phylogeny based on LSU rDNA. Eur. J. Phycol. 49, 436–449.

Dodge, J.D., 1975. A survey of chloroplast ultrastructure in the Dinophyceae. Phycologia 14, 253–263.

Ellegaard, M., Daugbjerg, N., Rochon, A., Lewis, J., Harding, I., 2003. Morphological and LSU rDNA sequence variation within the *Gonyaulax spinifera–Spiniferites* group (Dinophyceae) and proposal of *G. elongata* comb. nov. and *G. membranacea* comb. nov. Phycologia 42, 151–164.

Guindon, S., Dufayard, J.F., Lefort, V., Anisimova, M., Hordijk, W., Gascuel, O., 2010. New algorithms and methods to estimate maximum-likelihood phylogenies: assessing the performance of PhyML 3.0. Syst. Biol. 59, 307–321.

Hansen, P.J., Calado, A.J., 1999. Phagotrophic mechanisms and prey selection in free-living dinoflagellates. J. Eukar. Microbiol. 46, 382–389.

Hansen, G., Daugbjerg, N., 2009. *Symbiodinium natans* sp. nov.: a "free-living" dinoflagellate from Tenerife (Northeast-Atlantic Ocean). J. Phycol. 45, 251–263.

Hansen, G., Moestrup, Ø., Roberts, K.R., 1996. Fine structural observations on *Gonyaulax spinifera* (Dinophyceae), with special emphasis on the flagellar apparatus. Phycologia 35, 354–366.

Hansen, G., Daugbjerg, N., Henriksen, P., 2007. *Baldinia anauniensis* gen. et sp. nov.: a "new" dinoflagellate from Lake Tovel, N. Italy. Phycologia 46, 86–108.

Huber-Pestalozzi, G., 1950. Das Phytoplankton des Süsswassers. Systematik und Biologie. 3. Teil. Cryptophyceen, Chloromonadinen, Peridineen. In: Thienemann, A. (Ed.), Die Binnengewässer… 16. E. Schweizerbart'sche Verlagsbuch-handlung, Stuttgart.

Jeong, H.J., Jang, S.H., Moestrup, Ø., Kang, N.S., Lee, S.Y., Potvin, É., Noh, J.H., 2014. *Ansanella granifera* gen. et sp. nov. (Dinophyceae), a new dinoflagellate from the coastal waters of Korea. Algae 29, 75–99.

Knechtel, J., Kretschmann, J., Chacón, J., Gottschling, M., 2020. *Dinastridium verrucosum* Baumeister from Bavaria (Germany) is a borghiellacean dinophyte (†Suessiales). Protist 171, 125741.

Kokinos, J.P., Anderson, D.M., 1995. Morphological development of resting cysts in cultures of the marine dinoflagellate *Lingulodinium polyedrum* (=*L. machaerophorum*). Palynology 19, 143–166.

LaJeunesse, T., Parkinson, J.E., Gabrielson, P.W., Jeong, H.J., Reimer, J.D., Voolstra, C.R., Santos, S.R., 2018. Systematic revision of Symbiodiniaceae highlights the antiquity and diversity of coral endosymbionts. Curr. Biol. 28, 2570–2580.

Lefèvre, M., 1932. Monographie des espèces d'eau douce du genre *Peridinium*. Arch. Bot. Mém. 2 (mémoire 5), 1–210.

Li, Z., Shin, H.H., Han, M.-S., 2015. Morphology and phylogeny of a new woloszynskioid dinoflagellate *Tovellia paldangensis* sp. nov. (Dinophyceae). Phycologia 54, 67–77.

Lindberg, K., Moestrup, Ø., Daugbjerg, N., 2005. Studies on woloszynskioid dinoflagellates I: *Woloszynskia coronata* re-examined using light and electron microscopy and partial LSU rDNA sequences, with description of *Tovellia* gen. nov. and *Jadwigia* gen. nov. (Tovelliaceae fam. nov.). Phycologia 44, 416–440.

Luo, Z., Mertens, K.N., Nézan, E., Gu, L., Pospelova, V., Thoha, H., Gu, H., 2019. Morphology, ultrastructure and molecular phylogeny of cyst-producing *Caladoa arcachonensis* gen. et sp. nov. (Peridiniales, Dinophyceae) from France and Indonesia. Eur. J. Phycol. 54, 235–248.

Lum, W.M., Takahashi, K., Benico, G., Takayama, H., Iwataki, M., 2019. *Dactylodinium arachnoides* sp. nov. (Borghiellaceae, Dinophyceae): a new marine dinoflagellate with a loop-shaped apical structure complex and tubular membranous extrusomes. Phycologia 58, 661–674.

Mertens, K.N., Rengefors, K., Moestrup, Ø., Ellegaard, M., 2012. A review of recent freshwater dinoflagellate cysts: taxonomy, phylogeny, ecology and paleoecology. Phycologia 51, 612–619.

Moestrup, Ø., 2000. The flagellate cytoskeleton. Introduction of a general terminology for microtubular flagellar roots in protists. In: Leadbeater, B.S.C., Green, J.C. (Eds.), The Flagellates. Unity, Diversity and Evolution. Taylor & Francis, New York, pp. 69–94 (Systematics Association Special Volume No. 59).

Moestrup, Ø., Calado, A.J., 2018. Dinophyceae. In: Büdel, B., Gärtner, G., Krienitz, L., Schagerl, M. (Eds.), Süßwasserflora von Mitteleuropa — Freshwater Flora of Central Europe, 6., 2nd ed. Springer-Verlag, Berlin.

Moestrup, Ø., Daugbjerg, N., 2007. On dinoflagellate phylogeny and classification. In: Brodie, J., Lewis, J. (Eds.), Unravelling the Algae: the Past, Present, and Future of Algal Systematics. CRC Press, Taylor & Francis Group, Abingdon, U.K, pp. 215–230 (Systematics Association Special Volumes, vol. 75).

Moestrup, Ø., Hansen, G., Daugbjerg, N., 2008. Studies on woloszynskioid dinoflagellates III: on the ultrastructure and phylogeny of *Borghiella dodgei* gen. et sp. nov., a cold-water species from Lake Tovel, N. Italy, and on *B. tenuissima* comb. nov. (syn. *Woloszynskia tenuissima*). Phycologia 47, 54–78.

Nichols, H.W., 1973. Growth media — freshwater. In: Stein, J.R. (Ed.), Handbook of Phycological Methods. Culture Methods & Growth Measurements. Cambridge University Press, Cambridge, pp. 7–24.

Pandeirada, M.S., Craveiro, S.C., Daugbjerg, N., Moestrup, Ø., Calado, A.J., 2014. Studies on woloszynskioid dinoflagellates VI: description of *Tovellia aveirensis* sp. nov. (Dinophyceae), a new species of Tovelliaceae with spiny cysts. Eur. J. Phycol. 49, 230–243.

Pandeirada, M.S., Craveiro, S.C., Daugbjerg, N., Moestrup, Ø., Calado, A.J., 2017. Studies on woloszynskioid dinoflagellates VIII: life cycle, resting cyst morphology and phylogeny of *Tovellia rinoi* sp. nov. (Dinophyceae). Phycologia 56, 533– 548.

Pandeirada, M.S., Craveiro, S.C., Daugbjerg, N., Moestrup, Ø., Domingues, P., Calado, A.J., 2019. Studies on woloszynskioid dinoflagellates X: ultrastructure, phylogeny and colour variation in *Tovellia rubescens* n. sp. (Dinophyceae). J. Eukar. Microbiol. 66, 937–953.

Ronquist, F., Huelsenbeck, J.P., 2003. MrBayes 3: Bayesian phylogenetic inference under mixed models. Bioinformatics 19, 1572–1574.

Schiller, J., 1935. Dinoflagellatae (Peridineae) in monographischer Behandlung. In: Kolkwitz, R. (Ed.), Rabenhorst's Kryptogamenflora von Deutschland, Österreich und der Schweiz, vol. 10 (3), 2nd ed, Part 2, issue 1. Akademische Verlagsgesellschaft, Leipzig.

Starmach, K., 1974. Cryptophyceae, Dinophyceae, Raphidophyceae. In: Starmach, K., Siemińska, J. (Eds.), Flora Słodkowodna Polski vol. 4. Państwowe Wydawnictwo Naukowe, Warszawa, Kraków.

Stosch, H.A., 1973. Observations on vegetative reproduction and sexual life cycles of two freshwater dinoflagellates, *Gymnodinium pseudopalustre* Schiller and *Woloszynskia apiculata* sp. nov. Br. Phycol. J. 8, 105–134.

Swofford, D.L., 2002. PAUP*: Phylogenetic analysis using parsimony. (*and other methods). Version 4. Sinauer Associates, Sunderland, Massachusetts.

Takahashi, K., Moestrup, Ø., Jordan, R.W., Iwataki, M., 2015. Two new freshwater woloszynskioids *Asulcocephalium miricentonis* gen. et sp. nov. and *Leiocephalium pseudosanguineum* gen. et sp. nov. (Suessiaceae, Dinophyceae) lacking an apical furrow apparatus. Protist 166, 638–658.

Takahashi, K., Moestrup, Ø., Wada, M., Ishimatsu, A., Nguyen, V.N., Fukuyo, Y., Iwataki, M., 2017. *Dactylodinium pterobelotum* gen. et sp. nov., a new marine woloszynskioid dinoflagellate positioned between the two families Borghiellaceae and Suessi- aceae. J. Phycol. 53, 1223–1240.

Takano, Y., Horiguchi, T., 2005. Acquiring scanning electron microscopical, light microscopical and multiple gene sequence data from a single dinoflagellate cell. J. Phycol. 42, 251– 256.

Taylor, F.J.R., 2004. Illumination or confusion? Dinoflagellate molecular phylogenetic data viewed from a primarily morphological standpoint. Phycol. Res. 52, 308–324.

Thompson, R.H., 1951. A new genus and new records of freshwater Pyrrophyta in the Desmokontae and Dinophyceae. Lloydia 13, 277–299.

Waterhouse, A.M., Procter, J.B., Martin, D.M.A., Clamp, M., Barton, G.J., 2009. Jalview Version 2 — a multiple sequence alignment editor and analysis workbench. Bioinformatics 25, 1189–1191.

Wołoszyńska, J., 1916. Polskie Peridineae słodkowodne. – Polnische Süßwasser-Peridineen. Bull. Int. Acad. Sci. Cracovie, Cl. Sci. Math., Sér. B, Sci. Nat. 1915, 260–285.

Wołoszyńska, J., 1930. Beitrag zur Kenntnis des Phytoplanktons tropischer Seen. Arch. Hydrobiol. Rybactwa 5, 159–169.

Wołoszyńska, J., 1952. Bruzdnice Tatr i Karpat Wschodnich. Peridineae montium Tatrensium et Carpathorum Orientalium. Acta Soc. Bot. Poloniae 21, 311–316.

CHAPTER 4

CELL FINE STRUCTURE AND PHYLOGENY OF *PARVODINIUM*: TOWARDS AN ULTRASTRUCTURAL CHARACTERIZATION OF THE PERIDINIOPSIDACEAE (DINOPHYCEAE)

Pandeirada, M.S., Craveiro, S.C., Daugbjerg, N., Moestrup, Ø. & Calado, A.J. 2022. Cell fine structure and phylogeny of *Parvodinium*: towards an ultrastructural characterization of the Peridiniopsidaceae (Dinophyceae). *European Journal of Phycology*, published online (DOI: 10.1080/09670262.2022.2091798)

ABSTRACT

Recent molecular phylogenies that include species of *Parvodinium* revealed as its closest relatives the genera *Peridiniopsis*, *Palatinus* and *Johsia*. The clade containing these taxa is currently recognized as a family, Peridiniopsidaceae. The affinity between the members of Peridiniopsidaceae cuts across traditional boundaries based on features of the amphiesma, most notably the presence or absence of an apical pore complex. Detailed descriptions of the fine structure of *Peridiniopsis* and *Palatinus* are available from TEM studies of their type species. Here we provide a description in comparable detail of a species of the *Parvodinium umbonatum–inconspicuum* complex, which includes the type of the genus. The cells had an apical fibrous complex essentially similar to those described from other peridinioids prepared with comparable fixations. The pusular system was extensive and included areas with different aspects: an area with a sheet-like vesicle along the mid-right side of the cell, a ventral portion with ramified and anastomosed tubes and a somewhat flattened tube attached to the transverse flagellar canal. The most remarkable feature was the microtubular strand that extended from a ventral, protruding peduncle to the anterior part of the epicone, around an accumulation body, and came around along a more dorsal position toward the ventral side. This long microtubular strand of the peduncle (MSP) was reminiscent of the one described from *Peridiniopsis borgei*, both by its extension and looping path, and by the breaking up of the strand of microtubules into smaller portions with a wavy appearance; and contrasted with the reduced MSP of *Palatinus apiculatus*. The fine-structural features currently known from Peridiniopsidaceae are summarized. Members of the family include a flagellar apparatus with four microtubule-containing roots associated, the basal bodies inserted close to each other, nearly at right angles and a three-armed fibrous connective between root 1 and the transverse basal body.

Highlights

Detailed fine structure of *Parvodinium* (of *P. umbonatum–P. inconspicuum* complex)

Comparative analysis of the ultrastructure of *Parvodinium* and other Peridiniopsidaceae

Summary of ultrastructural features of the family Peridiniopsidaceae

Key words

Dinoflagellates; Flagellar apparatus; (Microtubular Strand of the) Peduncle; Peridinioid; Peridiniopsidaceae; Phylogeny; Pusule; SSU-ITS-LSU rDNA; Ultrastructure

INTRODUCTION

Over the past decade, many freshwater dinoflagellates formerly classified in the family Peridiniaceae have been reassigned to the mainly marine family Thoracosphaeraceae (including the Pfiesteriaceae), based on similarity of plate pattern, intracellular organization and molecular data (Craveiro *et al*., 2011, 2015, 2016; Moestrup & Calado, 2018). More recently, the family Peridiniopsidaceae was established to segregate from the Peridiniaceae three freshwater genera that consistently formed a well-supported clade in phylogenetic analyses based on ribosomal DNA sequences: *Peridiniopsis* Lemmermann, *Parvodinium* Carty and *Palatinus* Craveiro, Calado, Daugbjerg & Moestrup (Gottschling *et al*., 2017). The new genus *Johsia* Z.Luo, Na Wang, K.N.Mertens & H.Gu, was subsequently described from marine sediments of the Gulf of Thailand and off Manado (Indonesia), and added to the Peridiniopsidaceae (Luo *et al*., 2020). Another marine peridinioid, described from tide pools, '*Scrippsiella*' *hexapraecingula* has been grouping in the phylogenetic trees with the Peridiniopsidaceae (Luo *et al*., 2020). Members of the family display morphological diversity in aspects traditionally considered phylogenetically significant, such as the presence or absence of an apical pore. The amphiesmal arrangement of six plates in the cingulum and up to two anterior intercalary plates were suggested to be unifying features of the family (Gottschling *et al*., 2017; Kretschmann *et al*., 2018, 2019; Luo *et al*., 2020). However, it is unclear which internal cell features may be considered characteristic of the group. Detailed fine-structural descriptions, including flagellar apparatus, pusular system and strands of microtubules related with a homologous of a feeding apparatus, are available for the type species of *Peridiniopsis* (Calado & Moestrup, 2002) and *Palatinus* (Craveiro *et al*., 2009) but only limited information has been published for *Parvodinium*, *Johsia* and '*Scrippsiella*' *hexapraecingula* (Seo & Fritz, 2002; Horiguchi *et al*., 1999; Luo *et al*., 2020). Ultrastructural analyses of species of these genera are needed for a more complete characterization of the

Peridiniopsidaceae. Ultrastructural studies of peridinioids (e.g. Calado *et al.*, 1999; Calado & Moestrup, 2002; Craveiro *et al.*, 2009) have shown that their flagellar apparatus usually includes two microtubular roots associated with the longitudinal basal body (LB): a strand of microtubules on the left side of the LB, the so-called longitudinal microtubular root (LMR or r1 in Moestrup, 2000) and a single microtubule, on the right side of the LB, the so-called single microtubular root (SMR or r2 in Moestrup, 2000). Associated with the transverse basal body (TB) there are two other roots: a single microtubule, the transverse microtubular root (TMR or r3 in Moestrup, 2000) that nucleates one or several rows of microtubules (TMRE, transverse microtubular root extension), and a fibre associated with a microtubule, the transverse striated root and transverse striated root microtubule (TSR+TSRM/r4 in Moestrup, 2000). Also characteristic of peridinioids is the presence of a layered connective (LC) that associates two of these roots (LMR/r1 and TSR+TSRM/r4), one associated to each of the basal bodies (e.g. Calado *et al.*, 1999; Craveiro *et al.*, 2015). In other groups of dinoflagellates, the LC is usually replaced by an elongated striated fibre (the striated root connective, SRC), which links the same two roots at a more distal position (e.g. Iwataki *et al.*, 2010; Pandeirada *et al.*, 2021).

The pusular system is often very complex and difficult to elucidate due to the variable extent, to which pusular elements collapse in response to different fixation schedules (e.g. Craveiro *et al.*, 2009). Despite these difficulties, the pusular system has shown enough regularity in some dinoflagellate groups to be considered characteristic of those groups. A typical example is the strict tubular organization of the pusules of species of Tovelliaceae, in which pusular tubes display a regular arrangement of diverticula along part of their length and electron-opaque structures associated with the inner membrane in other areas (Lindberg *et al.*, 2005; Calado, 2011).

Most of the photosynthetic peridinioids examined in detail with transmission electron microscopy (TEM) have either a single microtubular strand of the peduncle (MSP) or a more developed system, with up to eight partially overlapping rows of microtubules (microtubular basket, MB). The most extensive MBs are found in pfiesteriaceans, a group of predatory dinoflagellates that includes marine (e.g. *Paulsenella* and *Pfiesteria*; Schnepf *et al.*, 1985; Litaker *et al.*, 2002) and freshwater genera (*Tyrannodinium*; Calado & Moestrup, 1997), in which they play a role in food

uptake (Hansen & Calado, 1999). In some freshwater members of the photosynthetic 'calcareous' clade, the Thoracosphaeraceae (e.g. *Chimonodinium lomnickii* and *Naiadinium polonicum* (Wołoszyńska) Carty; Craveiro *et al.*, 2011, 2013), a conspicuous MB is present but there is no evidence yet of food uptake in these species. The MSP is a more generally distributed structure that has been found in Borghiellaceae (*Baldinia anauniensis* Gert Hansen & Daugbjerg; Hansen *et al.*, 2007), Tovelliaceae (e.g. *Tovellia rubescens* Pandeirada, Craveiro, Daugbjerg, Moestrup & Calado; Pandeirada *et al.*, 2019), Suessiaceae (e.g. *Prosoaulax lacustris* (F.Stein) Calado & Moestrup; Calado *et al.*, 1998) and also in the Peridiniopsidaceae (e.g. *Peridiniopsis borgei*; Calado & Moestrup, 1997).

The genus *Parvodinium* includes freshwater peridinioid species with the plate formula: po, x, 4′, 2a, 7″, 6c, 5(?)s, 5‴, 2⁗ (Moestrup & Calado, 2018). About 16 species are currently recognized in this genus, but species identification can be quite difficult due to the small size of the cells, the similarity between described species and the variations of plate tabulation within species (Elbrächter & Meyer, 2001; Carty, 2008; Moestrup & Calado, 2018; Kretschmann *et al.*, 2018, 2019; Luo *et al.*, 2020). In particular, the identity of the type species of *Parvodinium*, *P. umbonatum* (F.Stein) Carty (=*Peridinium umbonatum* F.Stein) has been difficult to ascertain. The concept of *P. umbonatum*, as given in one of the most influential monographs that includes this group of taxa (Lefèvre, 1932), depicts it as so closely related to the species *Parvodinium inconspicuum* (Lemmermann) Carty (=*Peridinium inconspicuum* Lemmermann) that the two species were considered synonyms by Popovský & Pfiester (1986, 1990). The existence of a number of infraspecific taxa described in both these species further complicates the matter. However, populations identifiable as members of the complex *P. umbonatum*–*P. inconspicuum* can be easily found in different environments and often display minor differences in size, tabulation, or the presence of spines. This variability among populations, which suggests the existence of several species, was the basis for keeping *P. inconspicuum* separate from *P. umbonatum* in the latest freshwater dinoflagellate flora (Moestrup & Calado, 2018). The recent description of taxa in this species complex demonstrated a higher species-level diversity than was previously recognized (Kretschmann *et al.*, 2018).

A dinoflagellate strain isolated from fresh water in the Buçaco mountain, Central Portugal, revealed features that place it in the *P. umbonatum–P. inconspicuum* complex; this was confirmed by phylogenetic analyses based on rDNA sequences. The fine structure of this strain was studied in detail and compared with the features of a Danish population with similar morphology.

MATERIAL AND METHODS

Sampling and establishment of cultures

The *Parvodinium* strain described here comes from a freshwater tank in the gardens of the Buçaco Palace Hotel (40°22'33.74"N, 8°21'55.62"W; ~ 380 m altitude), Buçaco mountain, Central Portugal. A swimming cell, from a net sample (mesh size 25 μm) collected on 7 July 2015, was isolated into a 96-well cell culture plate (Sarstdet, Numbrecht, Germany) with L16 medium (Lindström, 1991); and grew into a culture maintained at 18ºC with 12h:12h light:dark photoperiod and photon flux density ca. 25 μmol m^{-2} s^{-1}. Cells from this culture were transferred to DY-V medium (Andersen *et al.,* 1997) as they stopped growing in medium L16 and the culture was reestablished under the same temperature, photoperiod and light intensity.

Cells of the *Parvodinium umbonatum–P. inconspicuum* species complex were isolated from a net sample collected in Gribsø, Hillerød, Denmark, on 7 October 1996, and prepared for TEM (see below).

The phylogenetic analyses included a new sequence of *Parvodinium elpatiewskyi* (Ostenfeld) Kretschmann, Zerdoner & Gottschling, a species recently included in the Peridiniopsidaceae. The analysed strain was collected from a system of shallow, freshwater lakes in Gafanha da Boavista, Ílhavo, Aveiro (40°36'13.54"N, 8°41'49.17"W). A swimming cell of *P. elpatiewskyi* was isolated from a net sample collected on 29 September 2017 and originated a culture from which rDNA was extracted. Cells in the culture divided slowly in quadruple concentration L16 medium (Lindström, 1991) at the same temperature, photoperiod and light intensity as above. The strain was characterized morphologically (Supplementary figs S1–S4) before the culture was lost.

Light microscopy (LM)

Swimming cells and empty thecae from Portuguese *Parvodinium* cultures were photographed with a ColorView IIIu Olympus camera (Olympus, Tokyo, Japan) mounted on a Zeiss Axioplan 2 imaging light microscope (Zeiss, Oberkochen, Germany). Images showing the position of the nucleus in cells of *Parvodinium* from Buçaco that sunk to the bottom of culture wells were recorded with a JVC TK-C1481BEG color video camera (Norbain SD, Reading, UK) mounted on a Leitz Labovert FS inverted light microscope (Leica Microsystems, Wetzlar, Germany).

Scanning electron microscopy (SEM)

A volume of 600 μl from Buçaco culture was fixed for 1 h with 320 μl of a fixing mixture of 2% osmium tetroxide and saturated $HgCl_2$ (3:1, v/v). Fixed material was retained on Nuclepore polycarbonate filters with 5-μm pore size (Whatman, GE Healthcare Life Sciences, Maidstone, UK) that were washed with distilled water, dehydrated through a graded ethanol series and critical-point-dried in a Baltec CPD-030 (Balzers, Liechtenstein). The filters were glued onto stubs, sputter-coated with gold-palladium and examined with a JEOL JSM 6335F scanning electron microscope (Jeol, Tokyo, Japan) at University of Copenhagen.

Transmission electron microscopy (TEM)

Fixation of the *Parvodinium* strain from Buçaco followed two protocols, which differed only in the fixative mixture: (1) a mixture of 1% glutaraldehyde and 0.5% osmium tetroxide (final concentrations), both in phosphate buffer 0.1 M, pH 7.2; and (2) 2% glutaraldehyde in the same buffer. In both cases, swimming cells were transferred to a watch glass with the fixative. After ca. 1 h 20 min of fixation the cells were washed in phosphate buffer, incorporated into 1.5% agar blocks and postfixed for 2 h with 1% osmium tetroxide in phosphate buffer. The agar blocks with the cells were washed in phosphate buffer followed by distilled water, dehydrated through a graded ethanol series and propylene oxide, and embedded in Agar 100 low viscosity resin (Agar Scientific, Stansted, Essex, UK). Cells were sectioned with a diamond knife in a Leica EM UC6 ultramicrotome. Ribbons of serial sections (70 nm thickness) were picked up with slot grids and transferred to Formvar film. They were contrasted with uranyl

acetate and lead citrate. Serial sections of two cells were examined with a JEOL JEM 1010 electron microscope with a Gatan Orius digital camera (Gatan, Pleasanton, USA) at University of Copenhagen.

Swimming cells of *Parvodinium umbonatum–P. inconspicuum* complex were picked up from a sample collected in Gribsø, Denmark, and fixed for 20 min in 2% glutaraldehyde in sodium cacodylate buffer 0.1 M, pH 7.4. The rest of the procedure was similar to that described above, except for the use of sodium cacodylate buffer for washing and Spurr resin (TAAB, Aldermaston, England) for embedding.

DNA extraction and PCR amplifications of SSU, ITS and LSU rDNA

DNA of the Buçaco strain of *Parvodinium* was extracted from a pellet obtained from centrifuging 0.5 ml of culture at 200 rpm for 10 min, in a Universal 16 A centrifuge (Hettich Zentrifugen, Tuttlingen, Germany). The pellet was transferred to 100 µl of the extracting solution QuickExtract™ FFPE DNA Extraction Kit (epicentre, Illumina, San Diego, California) and the kit instructions were followed. Two microlitres of the extracted DNA were used in the first PCR amplification of LSU rDNA, and one microlitre of the amplified product was used in a nested-PCR; the primers and thermal profiles for both amplifications are the same as in Pandeirada *et al.* (2014, 2017). For SSU rDNA and ITS amplifications, 2 µl of extracted DNA were used with the same primers and thermal profile as in the second round of amplification described in Takano & Horiguchi (2005). The amplified rDNA was purified with the QIAquick PCR Purification Kit (Qiagen, Hilden, Germany) and sent to Macrogen Europe (Amsterdam, The Netherlands) for sequencing with the same primers used for PCR amplifications.

DNA was extracted from 50–70 swimming cells of *P. elpatiewskyi* culture and used in PCR amplifications of rDNA (SSU, ITS and LSU), following the steps described for species of *Sphaerodinium* in Pandeirada *et al.* (2021). The purified DNA was sent for sequencing at Macrogen Europe.

Alignment and phylogeny

The phylogenetic position of the Buçaco strain of *Parvodinium* was inferred from analyses of nuclear-encoded LSU rDNA gene sequences and concatenation of SSU rDNA, ITS1 and ITS2, 5.8 rDNA and LSU rDNA. The LSU rDNA data matrix (1667

bp including introduced gaps) comprised 54 genera of dinoflagellates and a total of 90 taxa. The LSU rDNA sequences of three ciliates, four Apicomplexa and *Perkinsus* were also included and formed the outgroup. This diverse assemblage of Alveolata was aligned using Muscle with default settings as implemented in JALVIEW (ver. 2.10.3b1, Waterhouse *et al.,* 2009). The aligned sequences were analysed using two methods: Bayesian inference and Maximum likelihood. For Bayesian inference we used MrBayes (ver. 3.2.5 x64, Ronquist & Huelsenbeck, 2003) and for Maximum likelihood PhyML (ver. 3, Guindon *et al.,* 2010). Bayesian analysis was conducted on a local computer with 5 million generations and a tree was sampled every 1000 generations. The burn-in value was evaluated by plotting the LnL values as a function of generations in a spreadsheet. It occurred after 501 generations (conservative number) and therefore 4500 trees were used for generating a 50% majority-rule consensus tree in PAUP* (ver. 4.0a build 169, Swofford, 2002). Maximum Likelihood with 1000 bootstrap replications used the general time-reversible (GTR) substitution model and the option 'free rates' as the model for rates across sites. PhyML was run through the online version available on the Montpellier bioinformatics platform.

Based on the phylogenetic tree from analyses of LSU rDNA sequences, a concatenated data matrix comprising lineages of closely related dinoflagellates were prepared. The concatenated matrix comprised 3923 bp including introduced gaps. The ingroup included 11 genera and 21 species (including the Buçaco strain of *Parvodinium* and *P. elpatiewskyi*) whereas *Heterocapsa* spp. formed the outgroup. Sequence alignment and phylogenetic inference followed the same approach as outlined above for LSU rDNA. However, attempting a more accurate model of sequence evolution the genetic markers (coding and non-coding) were divided into five data partitions (SSU rDNA, ITS1, 5.8S rDNA, ITS2 and LSU rDNA). Hence, each region could evolve under different models of evolution using the 'unlink' option in MrBayes.

RESULTS

Cell description from LM and SEM observations

Motile cells and empty thecae of the *Parvodinium* strain from Buçaco are shown in Figs 1–23. Cells were ovoid and slightly compressed dorsoventrally (Figs 1–3, 9–13,

15–19). The epicone was semi-elliptical to conical and larger than the hemispherical to trapezoidal hypocone (Figs 1, 2, 7–12, 15–18). The cingulum descended about half of its width, and the sulcus invaded slightly onto the epicone and widened markedly toward the antapex (Figs 9–11, 15, 16, 20, 21). The apical pore complex (apc) was visible in ventral or dorsal view, protruding slightly at the apex (Figs 1, 4, 9, 15–18). Cells were 17.4 ± 2 μm long (range 10.5–21 μm; $n = 68$), 12.2 ± 1.5 μm wide (range 6.5–15 μm; $n = 52$) and 10.4 ± 1.2 μm thick (range 7.5–12.5 μm; $n = 16$). Individual measurements are presented in Supplementary table S1. Larger cells had a more angular shape (Fig. 4), and the smallest were roughly circular to slightly elongated (Figs 5, 6). No cysts were observed in the cultures.

Chloroplast lobes were golden or yellowish-brown, densely arranged in the epicone and appeared radiating from a central area in some cells; no central pyrenoid was noted (Figs 1–6). The nucleus was roundish to transversely elongated and occupied the hypocone up to about the cingulum level (Figs 2, 3, 6). In some immobile cells lying at the bottom of culture wells the nucleus was seen to move towards the epicone in a process that took up to 5 hours (Figs 7, 8). A nearly rectangular eyespot, sometimes somewhat tilted, 2.5–3.5 μm long ($n = 10$), was seen in the sulcus (Figs 1, 3–5). In smaller cells, the eyespot overlapped a large portion of the sulcus (Fig. 5).

The tabulation observed was (Kofoidian notation): po, cp, x, 4′, 2a, 7″, 6c, 5s, 5‴, 2⁗. The epitheca included four apical and seven precingular plates, and two anterior intercalary plates (1a, 2a) on the dorsal side (Figs 9–19, 21). The anterior intercalary plates were, in most cases (64% of the cells; $n=50$), separated from each other, with the third apical plate sharing a suture with the fourth precingular plate: a 3′-4″–*conjunctum* arrangement (Figs 12, 13, 19). In fewer cases (36% of the cells; $n=50$), the intercalary plates were closer to each other and plates 3′ and 4″ barely touched: a 3′-4″–*contactum* arrangement (Figs 14, 17, 18). The apical pore complex (apc) consisted of three plates: a central cover plate (cp), encircled by the pore plate (po), which showed a closed suture on the ventral side where the nearly rectangular canal (marked x) plate abutted (Figs 13, 16, 19, 22).

On the hypotheca, the first antapical plate (1⁗) was smaller than the second (2⁗), and there were five postcingular plates, of which plates 1‴ and 5‴ were the smallest (Figs 15, 20, 21). The cingulum included six plates of similar size except for the first

that was somewhat shorter (Figs 9–12, 15–18). The sulcus included five plates: the anterior sulcal plate (as) slightly penetrated the epitheca; the posterior, and larger, sulcal plate (ps) extended to the antapex; the right sulcal plate (rs) extended into a flap that covered the exit pores of the flagella and the peduncle, and partly overlapped both the left sulcal (ls) and the smaller accessory (acs) plates (Figs 15, 16, 20, 21, 23). An extruded peduncle ca. 4 µm long and 1.5 µm wide was visible in SEM (Figs 21, 23).
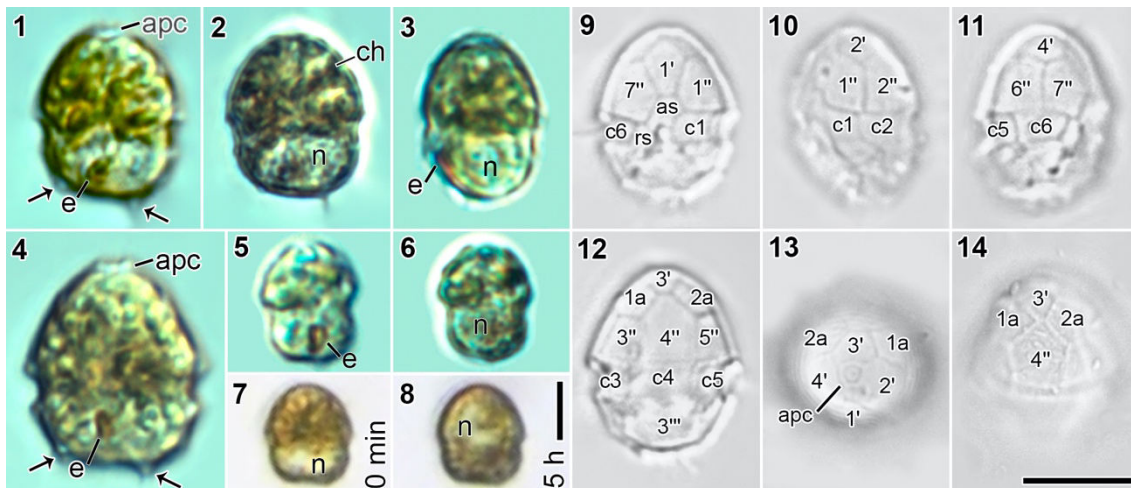
Figs 1–14. *Parvodinium* strain from Buçaco; LM of vegetative cells (Figs 1–8) and empty thecae (Figs 9–14). **Fig. 1**. Ventral view in surface focus showing the apical pore complex (apc), the eyespot (e) in the sulcus, and the position of two antapical spines (arrows). **Fig. 2**. Optical section of the same cell as in Fig. 1 with the nucleus (n) in the hypocone and the chloroplast lobes (ch) in the epicone. **Fig. 3**. Lateral view of a slightly dorsoventrally compressed cell. **Fig. 4**. Ventral view in surface focus of a larger cell with an angular outline. **Figs 5, 6**. Surface focus and optical section of a small, slightly elongated cell showing the eyespot (e) and the nucleus (n), respectively. **Figs 7, 8**. Still frames from a video recording made in an inverted microscope, of a small immobile cell, taken with 5 h interval, depicting the movement of the nucleus (n) towards the epicone. **Figs 9–11**. Empty thecae in ventral, left and right views showing Kofoidian notation of some plates. **Figs 12, 13**. Dorsal and apical views of two thecae with 3′-4″–*conjunctum* arrangement of plates. **Fig. 14**. Dorsal-anterior view with 3′-4″–*contactum* arrangement of plates. as and rs, anterior and right sulcal plates. Scale bars: Figs 1–6, 9–14 same scale as in Fig. 14, 10 µm; Figs 7, 8 to the same scale, 10 µm.

Three spines were regularly seen projecting from the edges of the antapical plates (Figs 1, 2, 4, 15, 16, 20, 21). The largest was 1.5–2.1 µm long and projected from plate 1‴′ near the corner with plates ps and 2‴′ (spine marked 1 in Figs 15, 16, 20, 21). A smaller spine, ca. 1 µm long, was usually present on plate 1‴′ where it contacted plates ps and 1‴ (marked 2 in Figs 15, 16, 20, 21); and another small spine projected from

plate 2⁗ near the corner abutting plates 4‴ and 5‴ (marked 3 in Figs 15, 16, 20, 21). Shorter spines were seen irregularly along antapical sutures (e.g. spine marked 4 in Fig. 21).
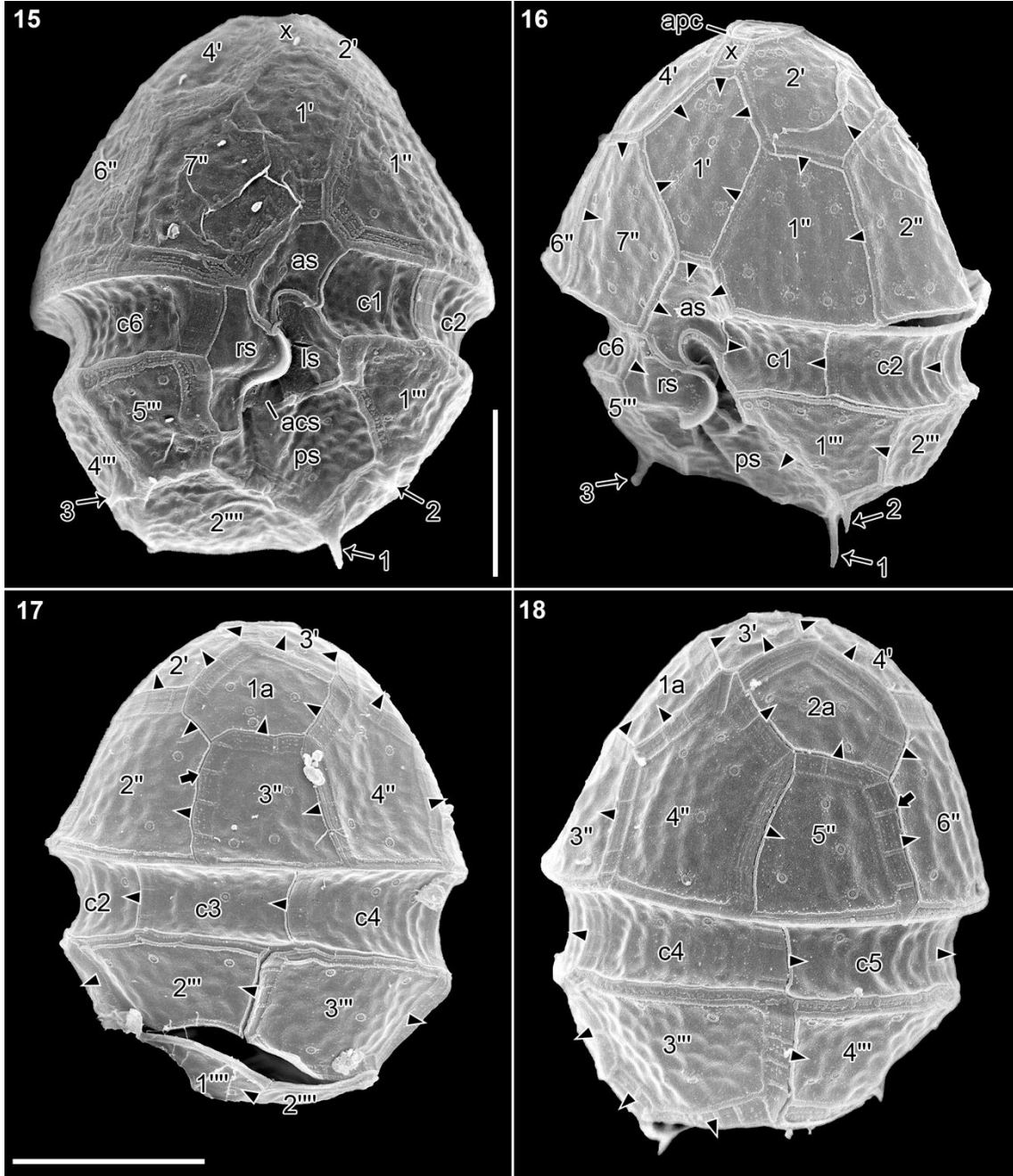
Figs 15–18. *Parvodinium* strain from Buçaco, SEM. Kofoidian notation. **Figs 15, 16.** Ventral and ventral-left views showing the five sulcal plates: anterior sulcal plate (as), right sulcal plate (rs), left sulcal plate (ls), posterior sulcal plate (ps) and the accessory sulcal plate (acs). The antapical spines are numbered 1 to 3. The apical pore complex (apc) is visible in Fig. 16. **Figs 17, 18.** Dorsal-left and dorsal-right views of thecae with wide striated sutures (arrows). Arrowheads in Figs 16–18 indicate the direction of plate overlap. Scale bars: Fig. 15, 5 μm; Figs 16–18 to the same scale, 5 μm.

Figs 19–23. *Parvodinium* strain from Buçaco, SEM. Kofoidian notation. **Fig. 19**. Apical view of a theca with wide striated sutures (arrows); apc, apical pore complex. **Fig. 20**. Antapical view showing two antapical plates of different size and five postcingular plates. The antapical spines are numbered 1 to 3. The sulcal plates are visible: anterior sulcal plate (as), right sulcal plate (rs), left sulcal plate (ls), posterior sulcal plate (ps) and the accessory sulcal plate (acs). All plates have a reticulated ornamentation (white arrows). **Fig. 21**. Ventral-antapical view of a cell with a peduncle protruding from the sulcus (large white arrow); the exit-pore of the transverse flagellum (large black arrow) is visible. An extra antapical spine is present (numbered 4). **Fig. 22**. Apical pore complex (apc), comprising pore plate (po), cover plate (cp) and canal plate (x). Trichocyst pores surrounded by small knobs (white arrow) and striation in the wide sutures are visible (short black arrows). **Fig. 23**. Detail of Fig. 21, showing the exit-pore of the transverse flagellum (black arrow) and the peduncle (white arrow). Scale bars: Figs 19–21, 5 μm; Fig. 22, 500 nm; Fig. 23, 1 μm.

The plate surface was generally smooth, with the appearance of a faint reticulation when seen in SEM (Fig. 20, white arrows). Trichocyst pores were present throughout the cell surface but were absent from sutures and were not seen in the apc nor in right

and left sulcal plates; each pore was surrounded by about a dozen small knobs, each about 40 nm in diameter (Figs 15–20, 22). Some, presumably older cells, showed wide sutures, up to over 1 μm, which were distinctly striated (Figs 17–19, 22, short black arrows). Plate overlap is indicated in Figs 16–18, marked with arrowheads. The tendential direction of overlapping was from dorsal to ventral side in the epitheca, cingulum and hypotheca. The plates that overlapped all the neighbour plates (keystone plates) were plate 4″ in the epitheca, plate 3‴ in the hypotheca and plate c4 in the cingulum.
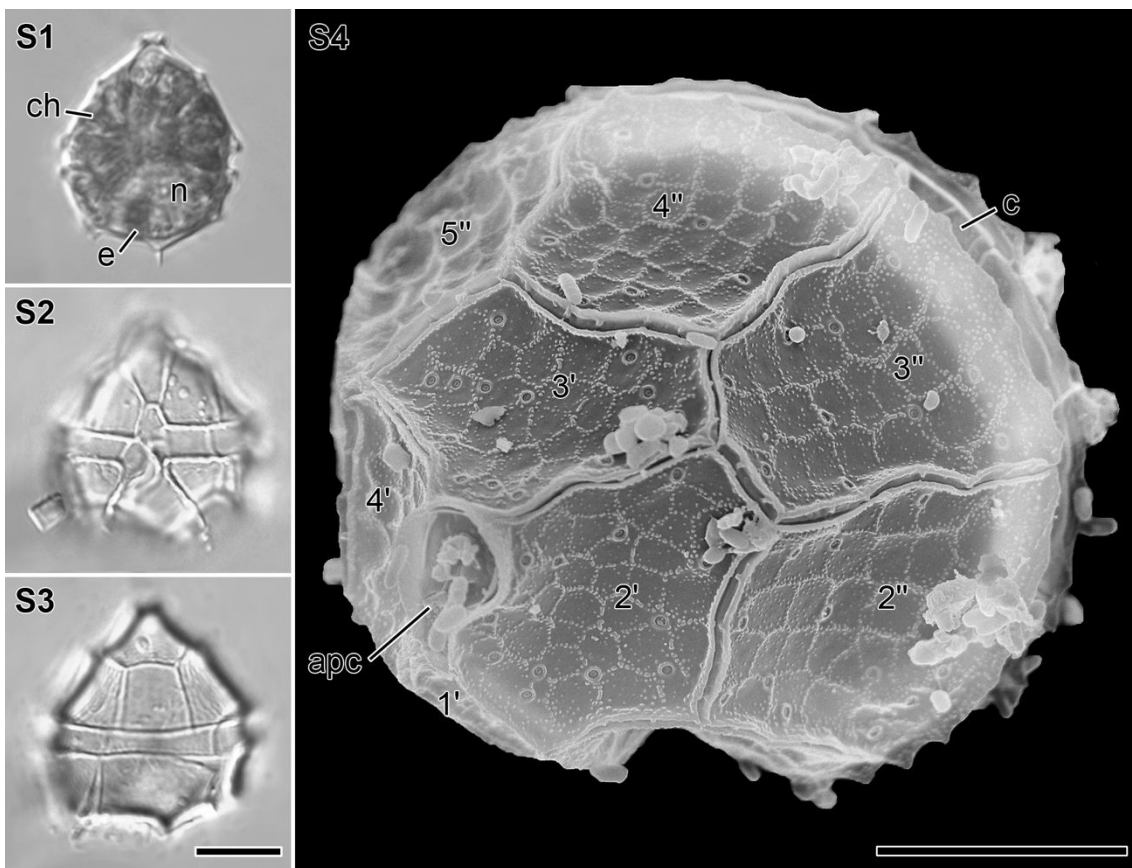
Supplementary figs S1–S4. LM and SEM of *Parvodinium elpatiewskyi* strain from Gafanha da Boavista, Ílhavo. **Fig. S1**. Ventral view of a living cell (LM). Nucleus (n), eyespot (e) and radiating chloroplast lobes (ch). **Figs S2, S3**. Superficial and deeper focus, from ventral to dorsal view, of an empty theca (LM). **Fig. S4**. Apical view of a cell showing the cingulum (c), the apical pore complex (apc) and plates marked in Kofoidean notation (SEM). Cells for SEM observation were fixed for 2 h 30 min in a mixture of 1:1 culture volume and 50% ethanol. Scale bars: Figs S1–S3, 10 μm; Fig. S4, 5 μm.

General cell ultrastructure (TEM)

The three cells analysed by TEM revealed similar fine-structural features (Supplementary figs S5–S19, Figs 24–44). General ultrastructural aspects are summarized in Supplementary figs S5, S12, S13, S17. Chloroplast lobes (ch) radiated from a central area near the base of the epicone and extended along the surface in the peripheral cytoplasm (Supplementary figs S5, S13, S17). Although some chloroplast lobes had thylakoid-free areas (Supplementary fig. S5, arrows), no pyrenoid complex was detected. Oil droplets (O), starch grains (st) and trichocysts (t) were seen at the cell periphery (Supplementary fig. S5). A distinct accumulation body (ab) was present on the anterior-left side of the epicone (Supplementary fig. S13). Pusular tubes and vesicles were visible along the longitudinal axis of the cell, but especially in the mid-ventral area (Supplementary fig. S5, pu). A cytoplasmic extension limited by a single membrane is shown outside the cell, near the sulcus, in Supplementary figs S5, S17. This so-called peduncle was supported by a microtubular strand (MSP) and contained round, electron-opaque bodies (Supplementary figs S5, S6, S17). An eyespot of type A (Moestrup & Daugbjerg, 2007) was located beneath the sulcus, and comprised numerous oil globules arranged in two rows inside a chloroplast lobe, underlying the microtubules of the longitudinal microtubular root (LMR/r1) (Supplementary figs S5, S7).

In oblique sections through the apical pore complex (apc) the apical cytoplasm appeared highly vesiculate (Supplementary fig. S12). Serial sections through the apc revealed both round and elongated vesicles underneath the pore, with some tubular vesicles extending through the apical-most cytoplasm toward the cover plate (Supplementary figs S8–S12). The cytoplasm inside the pore plate opening, underneath the cover plate, was lined with electron-opaque material, from which radiated several fibres that were striated in at least some views (Supplementary figs S8–S11).

Pusular system

The pusular system of the cells examined was rather extensive and complex. Three distinct portions are tentatively recognized based on the appearance and distribution in the cell of the pusular elements (Supplementary figs S5, S12–S19, Figs 24, 25, 28–36). The most extensive portion was mainly composed of a flat, sheet-like vesicle that extended for nearly 4 μm from the ventral area into the middle and right side of the cell.

138

It occurred in a vesicle-rich cytoplasmic region that also contained starch grains and oil droplets (Supplementary figs S13, S17, Fig. 24). This so-called pusular sheet (PuS) was a flat vesicle with a somewhat electron-opaque lumen mostly 40–50 nm thick (Fig. 24). It attained its largest development near the mid-ventral area and extended anteriorly toward the cell's right, where it progressively lost its nearly uninterrupted flat appearance and ramified into tubular portions and smaller vesicles with different profiles (Fig. 24). In its posterior part, the pusular sheet ramified extensively into more irregular vesicles that contained numerous, somewhat elongated, electron-opaque bodies about 100 × 400 nm (Supplementary figs S17, S19). Similar bodies occurred inside the more or less collapsed longitudinal flagellar canal (LFC), where some ramifications of the pusular sheet attached (not shown).

A different pusular arrangement accompanied the microtubular strand of the peduncle (MSP, described below), extending from the area of emergence of the peduncle (Supplementary figs S12–S16, Figs 24, 25, 28; PuN). This pusular area was mainly composed of 20–30 nm wide tubes, which ramified and anastomosed, forming a roughly cylindrical network. The lumen of the tubes of this part of the pusule was distinctly more electron-translucent than that of the PuS (Supplementary figs S14, S16, Figs 24, 25). The orientation of the PuN was approximately parallel to the PuS and the two systems were perhaps connected by narrow tubes (Fig. 24); however, we were unable to demonstrate a continuity between membranes of the tubes and the sheet, possibly because of the convoluted shape of the tubes in the area between the two pusular systems. No pusular elements were visible in the emergent part of the peduncle (Supplementary fig. S6).

The third pusular arrangement comprised a single, somewhat flattened tube about 100 × 250 nm in cross section, which opened into the anterior-dorsal side of the transverse flagellar canal (TFC) and extended into the left-dorsal side of the cell (Figs 31–36, white arrow). Parts of the tube membrane had a dotted appearance similar to that visible in the upper tube of Supplementary fig. S19. The tube descended for about 2 μm and turned toward the centre of the cell, where it apparently branched (not shown); the branches approached the other portions of the pusule making their distinction uncertain, although the dotted appearance of some tubes in the ventral area may indicate their continuity with this transverse pusular tube.
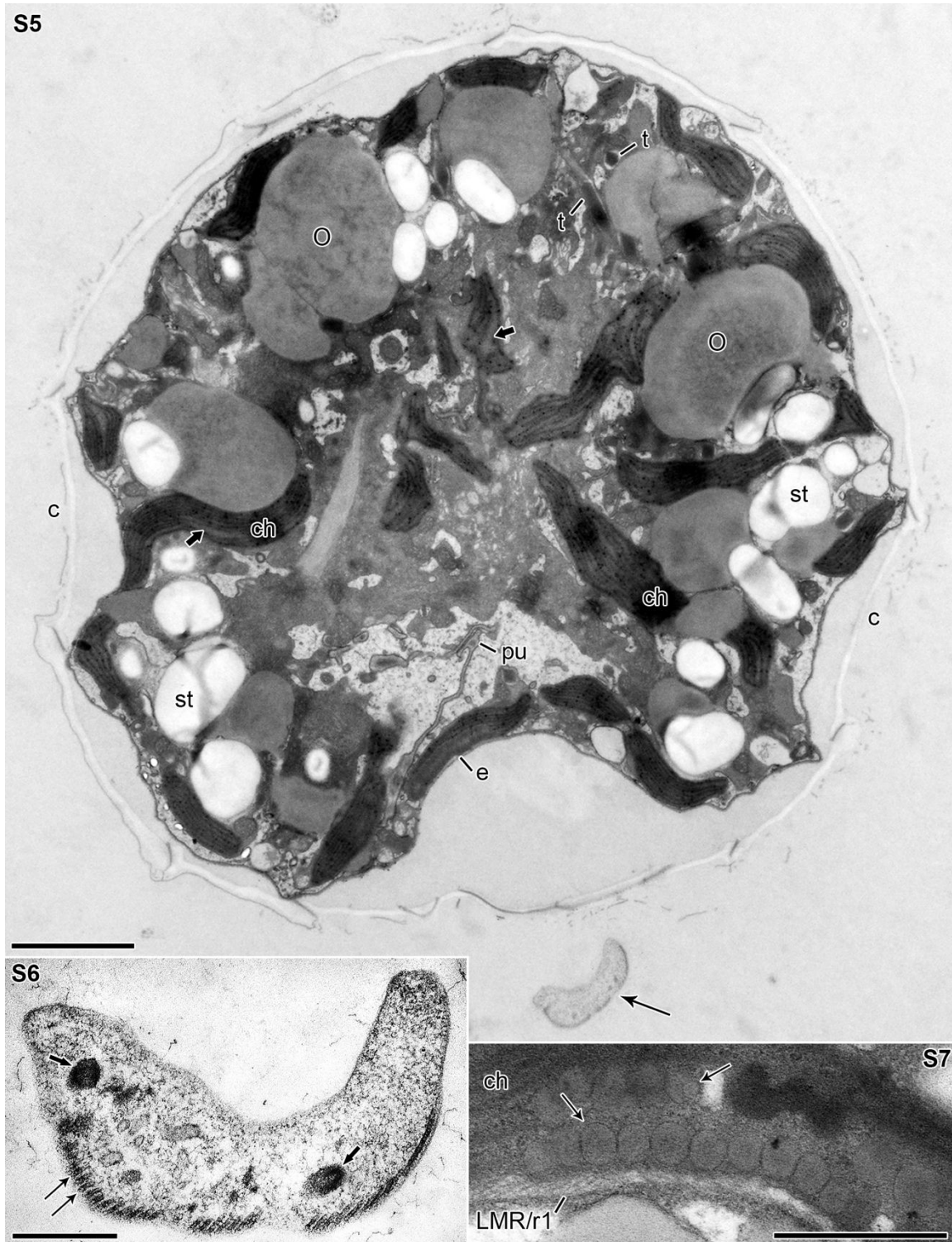
Supplementary figs S5–S7. *Parvodinium* strain from Buçaco, TEM. **Fig. S5**. Longitudinal section of a cell seen from the right-ventral side showing the chloroplast lobes (ch) with some thylakoid-free areas (short black arrows), oil droplets (O), starch grains (st) and trichocysts (t), scattered in the cell periphery. The eyespot (e) is visible in the sulcal region near pusular elements (pu). An almost transverse section of a peduncle (long black arrow) is present outside the cell. **Fig. S6**. Magnification of the peduncle displaying a strand of microtubules (thin arrows), and some electron-opaque vesicles (larger arrows). **Fig. S7**. Magnification of the eyespot-containing chloroplast lobe with two rows of globules (arrows) with the longitudinal microtubular root (LMR/r1) in the ventral side. Scale bars: Fig. S5, 2 μm; Figs S6, S7, 500 nm.
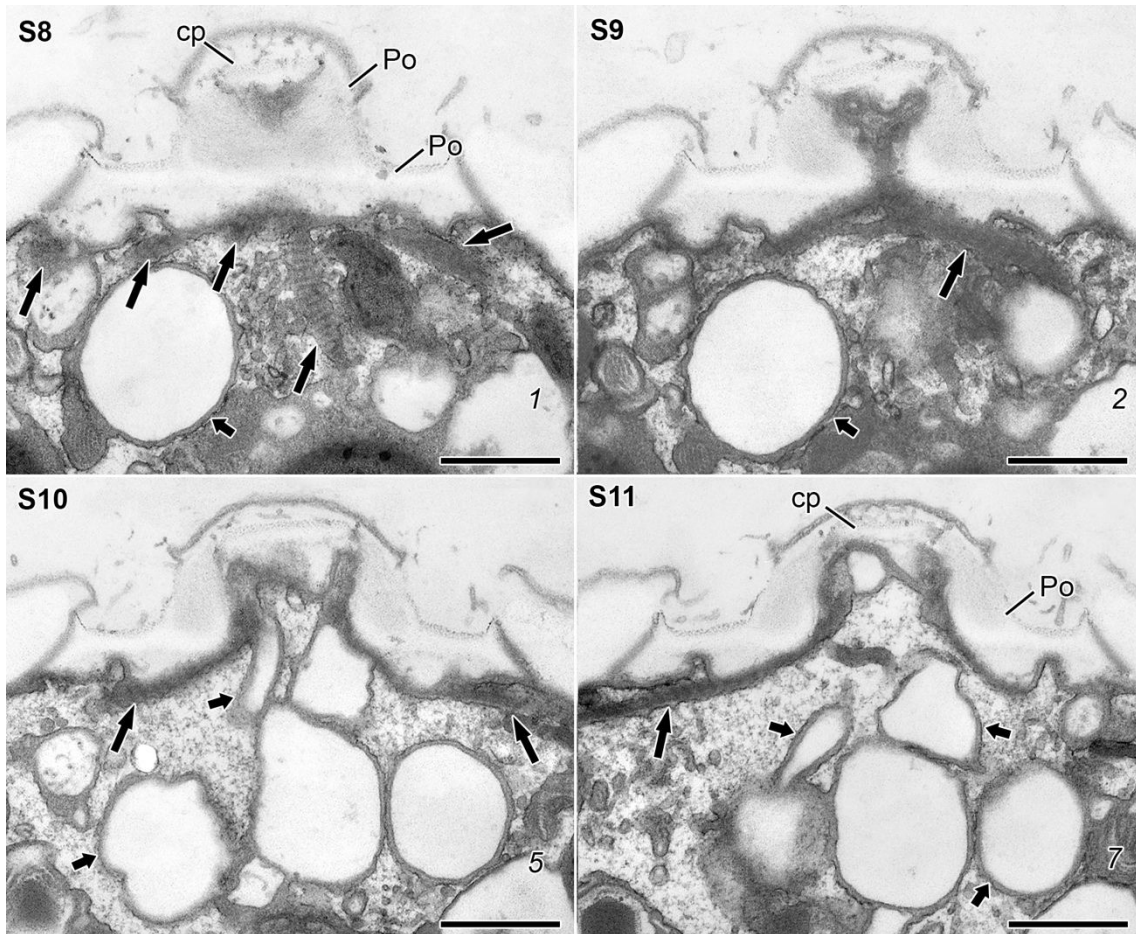
Supplementary figs S8–S11. *Parvodinium* strain from Buçaco, TEM. Longitudinal serial sections through the apical pore complex, viewed from the right-ventral side of the cell. Slanted numbers indicate the section number in the series. **Figs S8, S9**. Several striated fibres (long arrows) and a round vesicle (short arrow) are seen under the pore plate (Po). The cover plate (cp) is seen on top of the Po. **Figs S10, S11**. Several round and elongated vesicles (short arrows) extend under the Po and converge toward the cp. Scale bars: 500 nm.

Microtubular strand of the peduncle (MSP)

A single row of microtubules was found in the extruded portion of the peduncle and in the ventral area of the cell, near the basal bodies. This MSP extended into the cell, arching and breaking up into several groups of microtubules along its 15-µm path (Supplementary figs S12–S19, Figs 24–30). A schematic view of the whole path of the MSP is given in a left-ventral view in Fig. 26. The position of the MSP relative to the components of the flagellar apparatus is shown in left view in Fig. 27.

About 35 microtubules tightly arranged as a single row formed the MSP near the emergence area of the peduncle (Figs 25–27). A fibrous collar (striated collar of the
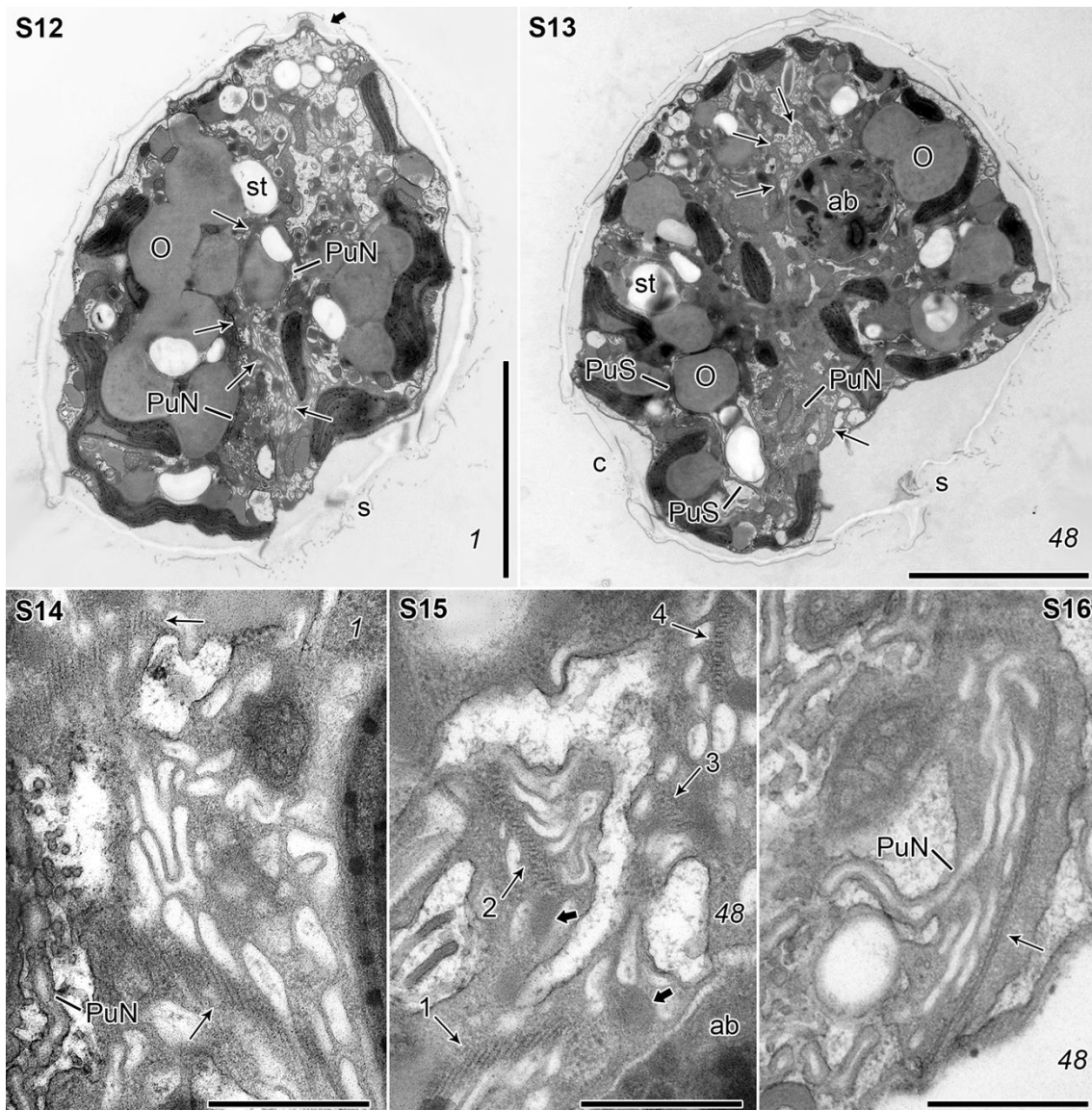
Supplementary figs S12–S16. *Parvodinium* strain from Buçaco, TEM. Pusular system and microtubular strand of the peduncle (MSP) in longitudinal serial sections proceeding toward the left-dorsal side, seen from the right-ventral side. Slanted numbers indicate the section number in the series. **Figs S12, S13**. The path of the MSP, breached up in several rows of microtubules and marked by arrows, is shown in two sections, the second one, 47 sections towards the left-dorsal side of the cell. In Fig. S12 the rows of microtubules are closer together and near the network of pusular tubes (PuN). The short arrow points to the apical pore. In Fig. S13 some rows are visible further up in the epicone, near an accumulation body (ab), while a single row of microtubules is present in the ventral area, near the PuN; the flat pusular vesicle (PuS) is visible on the right side of the cell. **Fig. S14**. Magnification of the microtubules and PuN from Fig. S12. **Figs S15, S16**. Magnification from Fig. S13, of four strands (marked 1–4) of microtubules visible near the ab (Fig. S15) and the microtubules in the ventral area (Fig. S16). Electron-opaque bodies are marked by short arrows (Fig. S15). c, cingulum; O, oil droplets; PuS, pusular sheet; s, sulcus; st, starch grains. Scale bars: Figs S12, S13, 5 μm; Figs S14–S16, 500 nm.

peduncle, PSC) surrounded the cytoplasm, including the MSP, that extended from the cell (Figs 25, 27). In the ventral area the MSP passed along the network of pusular tubes, PuN (Figs 24, 25) and extended on the ventral-right side of the basal bodies (Figs 26–30) toward an accumulation body (ab) on the anterior-left area of the epicone (Supplementary figs S12–S16, Fig. 26). The path of the MSP between the ventral area and the anterior edge of the ab was somewhat wavy (Supplementary figs S12, S14, Fig. 26), with a tendency for the microtubules to separate irregularly into several groups that appeared to re-associate further along (not shown). Electron-opaque bodies were visible near most of the ventral portion of the MSP (Supplementary figs S15, S18).

The MSP inflected to the left around the anterior-dorsal part of the ab and divided into two groups with slightly different routes (Supplementary figs S13, S15, S17, S18, Fig. 26). Both of these groups divided again creating a complex set of small microtubular strands, visible in sections through the mid-ventral part of the cell (Supplementary figs S15, S18, microtubular groups 1–4).
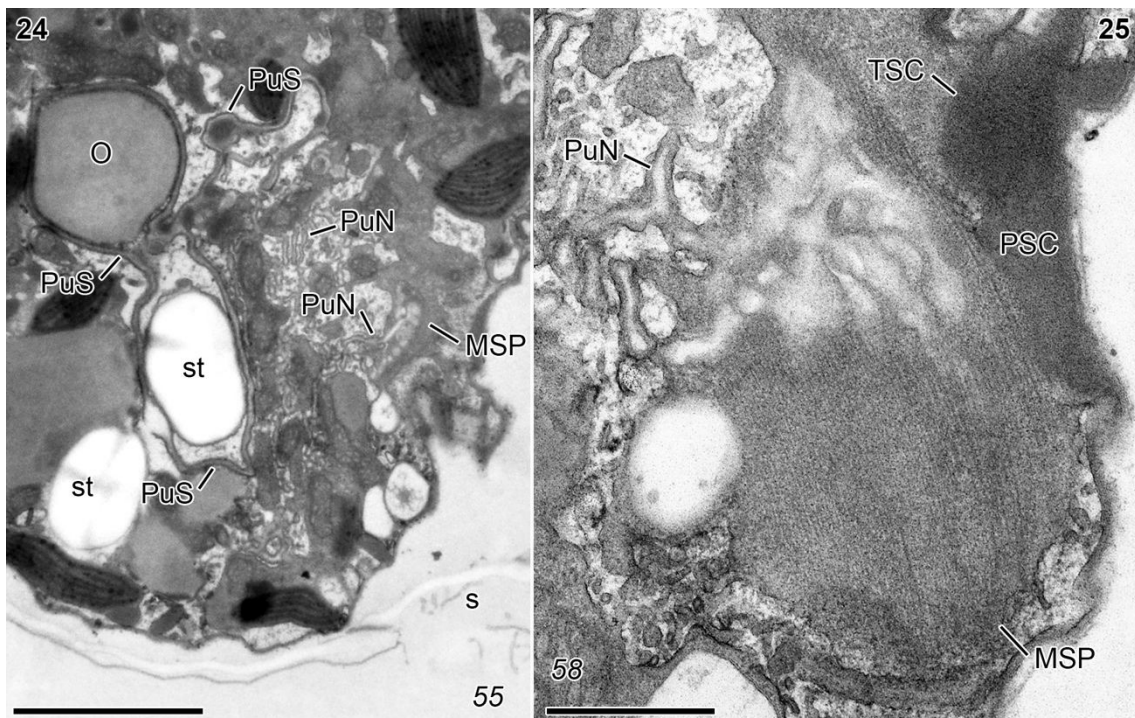
Figs 24, 25. *Parvodinium* strain from Buçaco, TEM. Ventral area with pusular system and microtubular strand of the peduncle (MSP); continuation of the series of sections shown in Figs S12–S16. Slanted numbers indicate the section number in the series. **Fig. 24**. The single row of microtubules from the microtubular strand of the peduncle and two pusular elements: the flat, sheet-like vesicle (PuS) and the network of pusular tubes (PuN). **Fig. 25**. Emergence area of the peduncle with the MSP extending along the PuN. The striated collar of the peduncle (PSC) contacts the transverse striated collar (TSC). O, oil droplets; s, sulcus; st, starch grains. Scale bars: Fig. 24, 2 μm; Fig. 25, 500 nm.
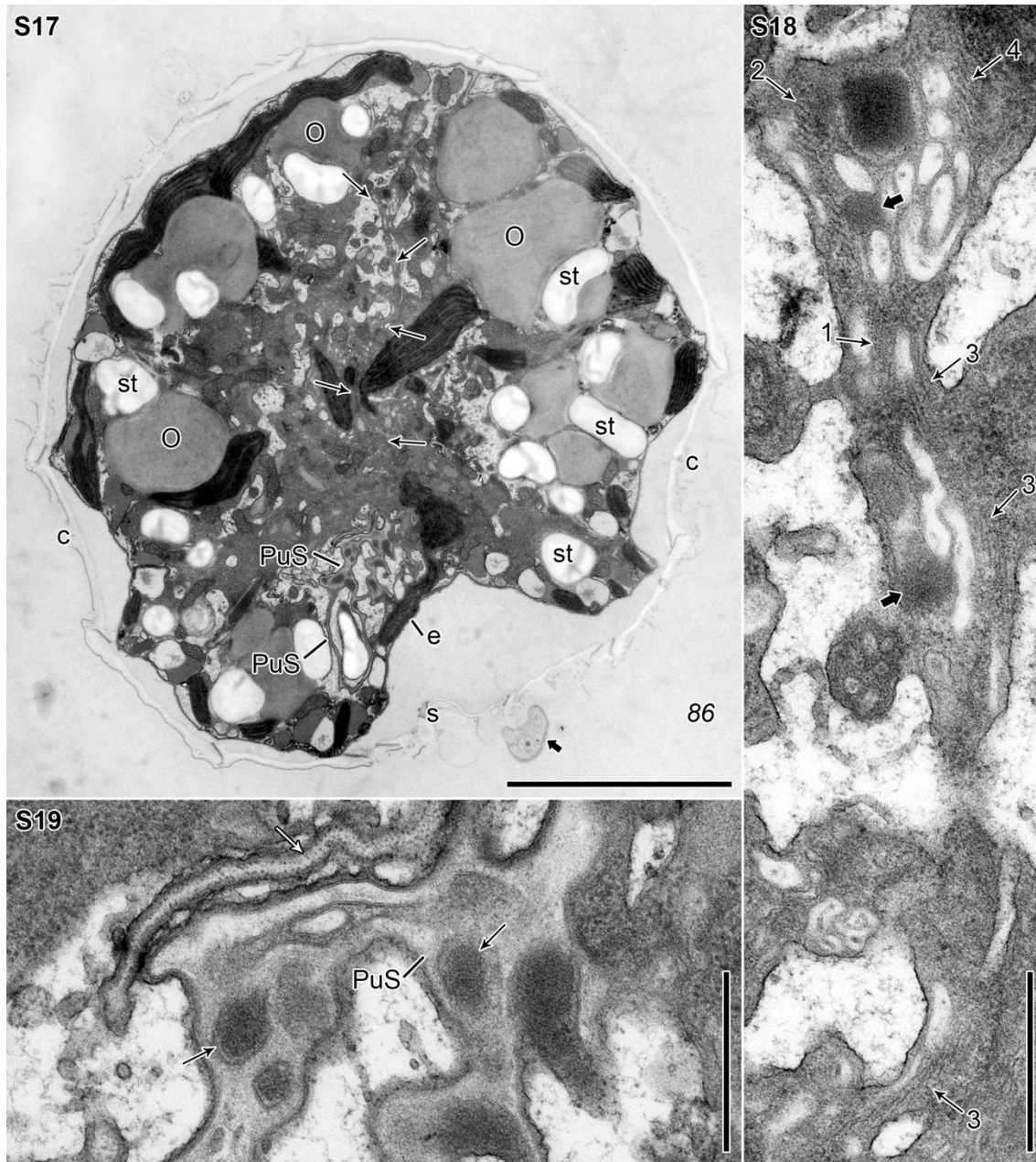
Supplementary figs S17–S19. *Parvodinium* strain from Buçaco, TEM. Pusular system and microtubular strand of the peduncle (MSP); continuation of the series of sections shown in Figs 24, 25. **Fig. S17.** General view showing the descending path of the microtubular strand of the peduncle after inflecting to the left side of the cell (thin arrows). The pusular network (PuN) and pusular sheet (PuS) are visible on the ventral-right side of the cell. A transverse section through a detached peduncle (short arrow) is visible outside the cell, on the ventral side, near the sulcus (s). **Fig. S18.** Magnification of Fig. S17 showing four rows of microtubules from the MSP and electron-opaque bodies (short arrows). **Fig. S19.** Magnification of the PuS from Fig. S17 containing electron-opaque bodies (black arrows) and a tubular portion with dot-like contents reminiscent of the pusular tube associated with the TFC (white arrow). c, cingulum; e, eyespot; O, oil droplets; s, sulcus; st, starch grains. Scale bars: Fig. S17, 5 μm; Figs S18, S19, 500 nm.
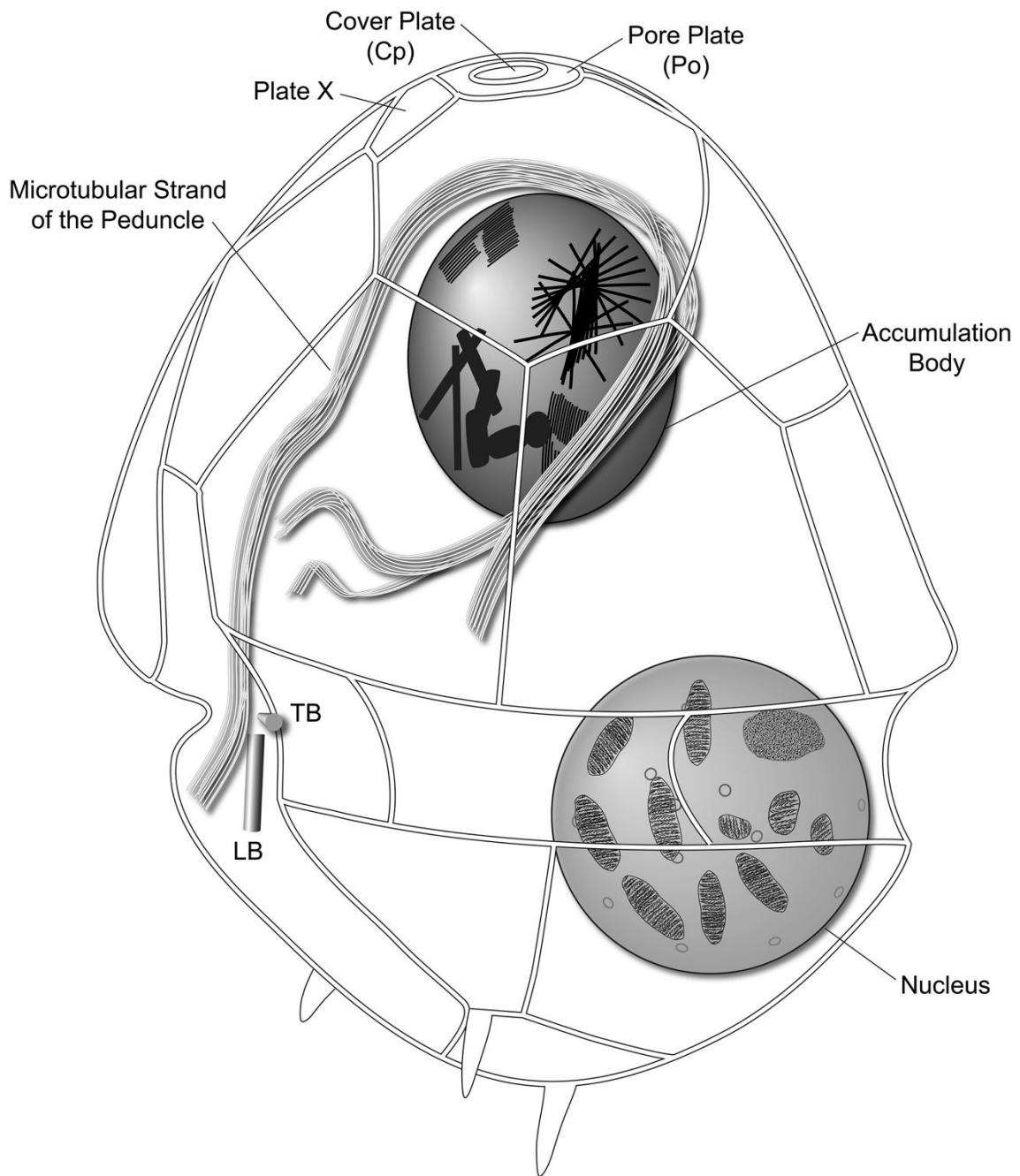
Fig. 26. Schematic representation of a cell's left-ventral view showing the plates and internally, the relative position of the nucleus, accumulation body, flagellar apparatus (represented by the basal bodies) and the path of the microtubular strand of the peduncle (MSP).

Flagellar apparatus

A schematic reconstruction of the flagellar apparatus as seen from the left of the cell is given in Fig. 27. Serial sections of the flagellar base area in an anterior-ventral-left point of view are shown in Figs 28–40; and from approximately left to right, with the cell slightly tilted toward the observer, in Figs 41–44. The basal bodies were inserted at an angle of ~90º, as estimated from serial sections (Figs 27, 31–44). Fibrous material was visible around the areas of emergence of each flagellum and the peduncle (marked as striated collars, TSC, LSC or PSC, in Figs 27–32, 34, 38–40, 43, 44). Two microtubular roots were associated with each basal body. A single microtubule, forming the transverse microtubular root (TMR/r3), attached to the proximal-anterior end of the TB, extended towards the upper side of the transverse flagellar canal (TFC) and nucleated a strand of about 11 microtubules (the transverse microtubular root extension, TMRE/r3 extension) that curved around the anterior margin of TFC and continued in a posterior-left direction (Figs 27–33). The transverse striated root and its associated microtubule (TSR and TSRM/r4) progressed from the proximal-dorsal side of the TB toward the transverse striated collar (TSC; Figs 27, 34–37, 41, 42). Both TSR and TB contacted the anterior part of a layered connective (LC) about 250 nm long and 70 nm thick (Figs 27, 38, 41, 42). A layer of electron-opaque material connected the posterior layer of the LC to the dorsal side of the longitudinal microtubular root (LMR/r1) (Figs 27, 38, 39, 41). Three short fibrous connectives extended from microtubular triplets of the TB to a layer of electron-opaque material on the dorsal face of the proximal end of the LMR/r1 (Figs 27, 41, 42, double white arrow). About 10 microtubules were present in this proximal end of the LMR/r1, but this number increased towards the sulcus (Figs 36–40). The right-hand side of the LMR/r1 contacted the proximal end of the LB (Figs 27, 36–44). The distal part of the LMR/r1 extended posteriorly on the left side of the longitudinal flagellar canal (LFC), passed next to the LSC and continued along the ventral side, adjacent to the amphiesmal vesicles lining the sulcus. A single-stranded microtubular root (SMR/r2) extended from the proximal-right side of the LB for about 650 nm, in a path nearly parallel to the LMR/r1 and ended near the surface of the LFC (Figs 27, 43, 44).
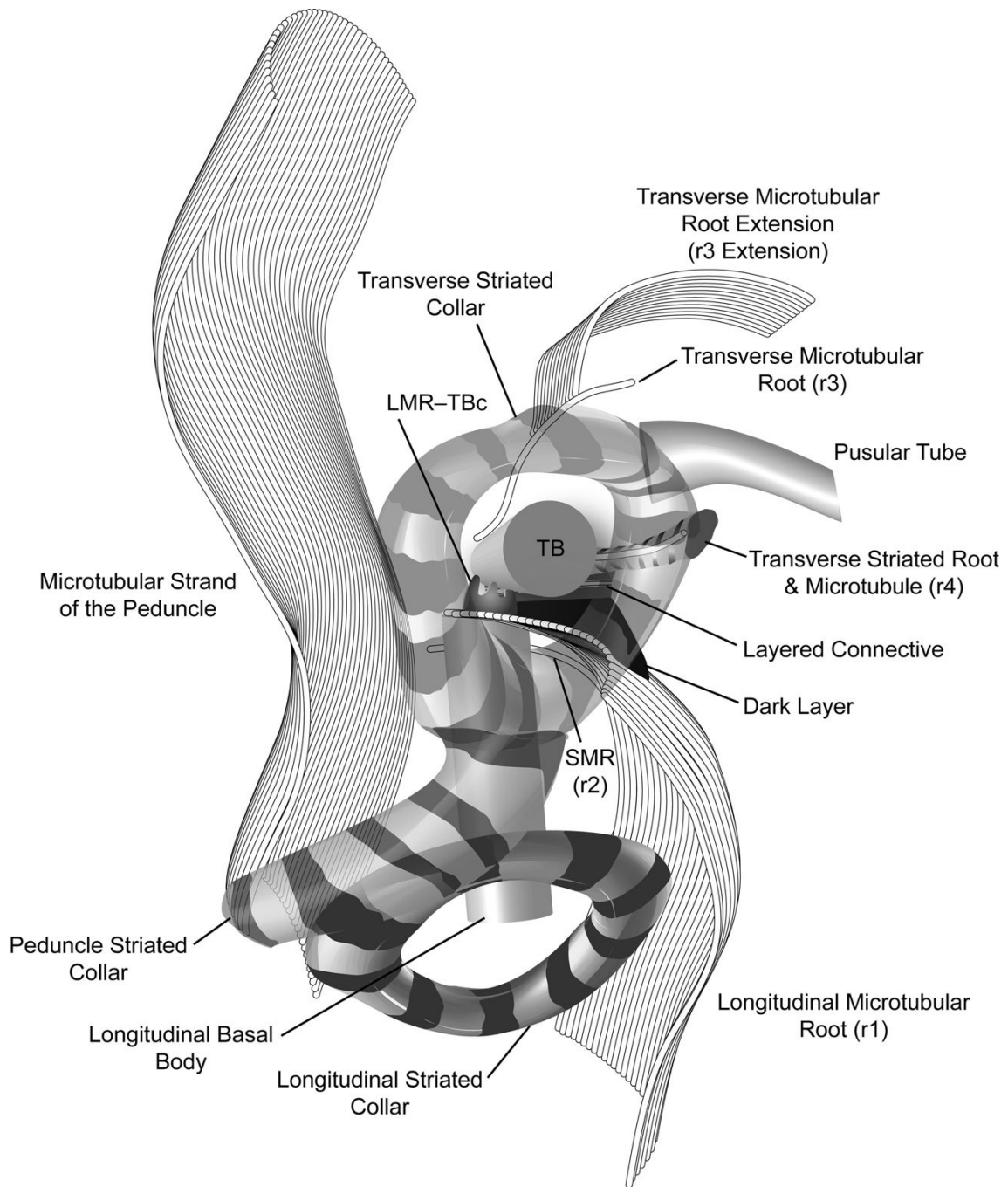
Fig. 27. Schematic representation of the flagellar base area of *Parvodinium*, viewed from the left side of the cell. The transverse and peduncle striated collars are made transparent to allow observation of underlying structures. SMR (r2), single-stranded microtubular root; LMR-TBc, three short fibrous connectives between the layer of electron-opaque material on the anterior-dorsal side of the LMR/r1 and microtubular triplets of the TB.
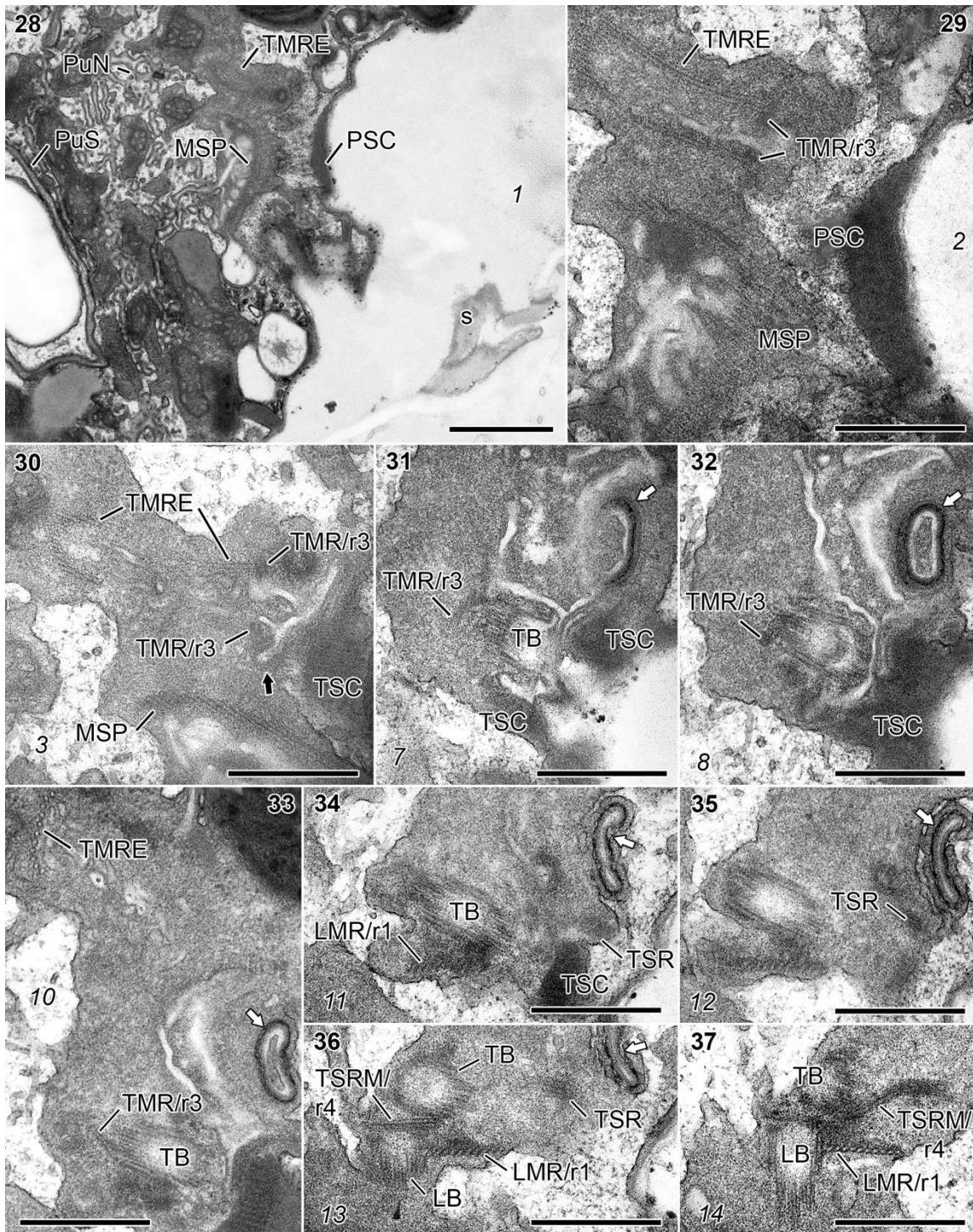
Figs 28–37. *Parvodinium* strain from Buçaco, flagellar apparatus, TEM. Non-adjacent serial sections progressing toward the left-dorsal side, seen from the right-ventral side. Slanted numbers indicate the section number in the series. **Fig. 28**. Ventral area of the cell, somewhat detached from the theca, with the pusular system (PuN and PuS), the microtubular strand of the peduncle (MSP) and the transverse microtubular root extension (TMRE). **Figs 29, 30**. The TMRE and the MSP are present near the peduncle striated collar (PSC) and the transverse striated collar (TSC). The TMRE is nucleated by the transverse microtubular root (TMR/r3), that runs near collared pits (black arrow). **Figs 31–33**. The proximal end of the TMR/r3 approaches the proximal end of the transverse basal body (TB). A flattened pusular tube (white arrow) opens into the anterior-dorsal side of the transverse flagellar canal. **Figs 34–37**. The proximal end of the longitudinal microtubular root (LMR/r1) is visible contacting the proximal end of the longitudinal basal body (LB). The transverse striated root (TSR) and its associated microtubule (TSRM/r4) extend from near the TSC to the proximal-dorsal side of the TB. Scale bars: Fig. 28, 1 μm; Figs 29–37, 500 nm.

148
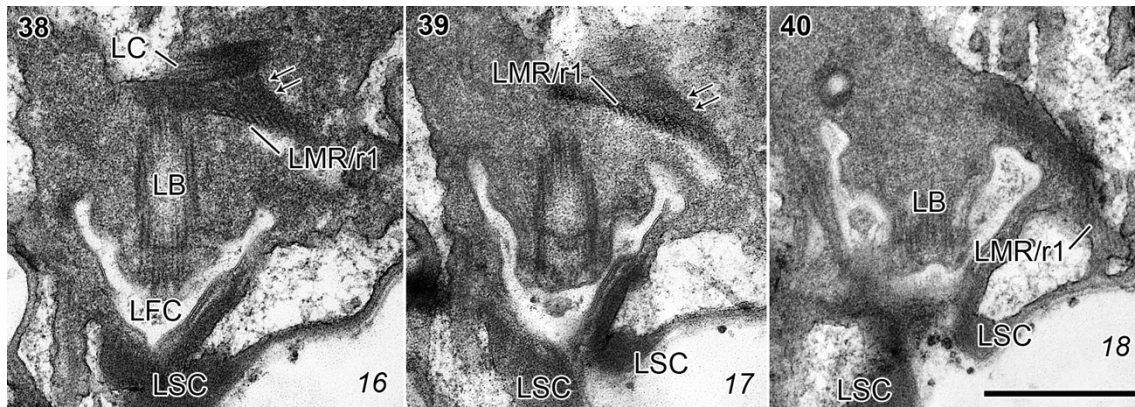
Figs 38–40. *Parvodinium* strain from Buçaco, flagellar apparatus, TEM. Continuation of the series of sections shown in Figs 28–37; adjacent serial sections. Slanted numbers indicate the section number in the series. The layered connective (LC) is linked, in its posterior side, to a layer of electron-opaque material (double arrows) that covers the dorsal side of the longitudinal microtubular root (LMR/r1). The longitudinal striated collar (LSC) surrounds, almost completely, the opening of the longitudinal flagellar canal (LFC). Scale bar: Figs 38–40 to the same scale, 500 nm.
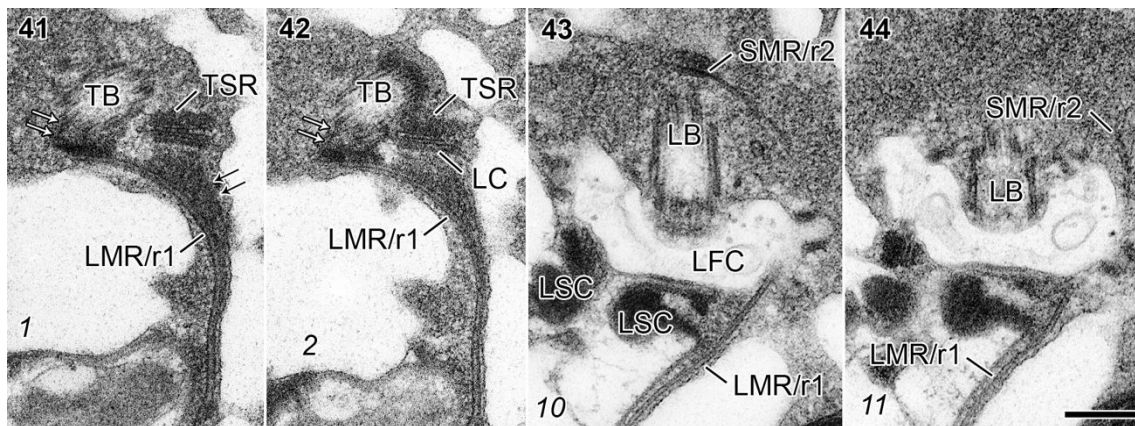
Figs 41–44. *Parvodinium* strain from Denmark, flagellar apparatus, TEM. Non-adjacent serial sections progressing toward the right-antapical side, seen from the left-apical side. Slanted numbers indicate the section number in the series. **Figs 41, 42**. Three short fibres (double white arrows) connect the transverse basal body (TB) to the dorsal side of the proximal end of the longitudinal microtubular root (LMR/r1). Note the layer of electron-opaque material (double black arrows) that covers the dorsal side of the LMR/r1. **Figs 43, 44**. The single-stranded microtubular root (SMR/r2) is visible on the right side of the longitudinal basal body (LB). LC, layered connective; LFC, longitudinal flagellar canal; LSC, longitudinal striated collar; TSR, transverse striated root. Scale bar: Figs 41–44 to the same scale, 200 nm.

Phylogeny

The position of *Parvodinium* within a large assemblage of dinoflagellates was examined by phylogenetic analyses based on nuclear-encoded partial LSU rDNA sequences (a single-gene tree). The resulting tree topology is shown in Fig. 45 and here *Parvodinium* formed a monophyletic group (marked as *Parvodinium* spp.). However, this only received little support from posterior probability (PP = 0.83) and Maximum likelihood bootstrap (BS = 59%). This clade containing species of *Parvodinium* was divided into two lineages, each fairly well supported. Hence, one clade comprised *Parvodinium mixtum* Kretschmann, Owsianny, Zerdoner & Gottschling, *P. parvulum* (Wołoszyńska) Na Wang, K.N.Mertens, H.Gu, *P. elpatiewskyi*, *Parvodinium* 'Buçaco', '*Peridinium inconspicuum*' strains CCAP 1140 and UTEX 2255 (PP = 0.97 and BS = 94%). The other clade contained '*Peridinium umbonatum* var. *inaequale*', *Parvodinium* cf. *centenniale*, *Parvodinium* cf. *umbonatum* strain GeoM*795 and *Peridinium centenniale* (Playfair) Carty (PP = 0.94 and BS = 79%). The clade, marked as *Parvodinium* spp., formed a sister group to *Johsia chumphonensis* Z.Luo, Na Wang, K.N.Mertens & H.Gu, *Peridiniopsis borgei* Lemmermann and *Palatinus* spp. However, this branching pattern received very little support from posterior probability (PP = 0.71) and no support from ML bootstrap (BS < 50%). The larger clade was part of a polytomy containing seven other lineages. The deepest lineages forming the backbone of the tree containing dinoflagellates were also unresolved (polytomy). However, most of these individual lineages received high branch support from posterior probabilities and bootstrap replicates.

$\longrightarrow$

Fig. 45. Phylogeny based on partial nuclear-encoded LSU rDNA sequences (1667 bp including introduced gaps) of 54 genera of dinoflagellates and inferred from Bayesian analysis. For this analysis three ciliates, four apicomplexans and *Perkinsus andrewsi* were used as outgroup taxa. Branch support was evaluated from posterior probabilities (PP ≥ 0.5) from Bayesian analyses and bootstrap (1000 replications, BS ≥ 50%) from maximum likelihood analyses, respectively. These support values are written to the left of internodes. A hyphen (-) indicates values below 0.5 for PP and 50% for bootstrap. GenBank accession numbers and, in some cases, strain numbers for *Parvodinium* spp. are written after the species epithet. The evolutionary lineage containing *Parvodinium* spp. is marked in grey, and the sequences determined in this study are in bold. The branch lengths are proportional to the number of character changes, see scale bar below the phylogenetic tree.
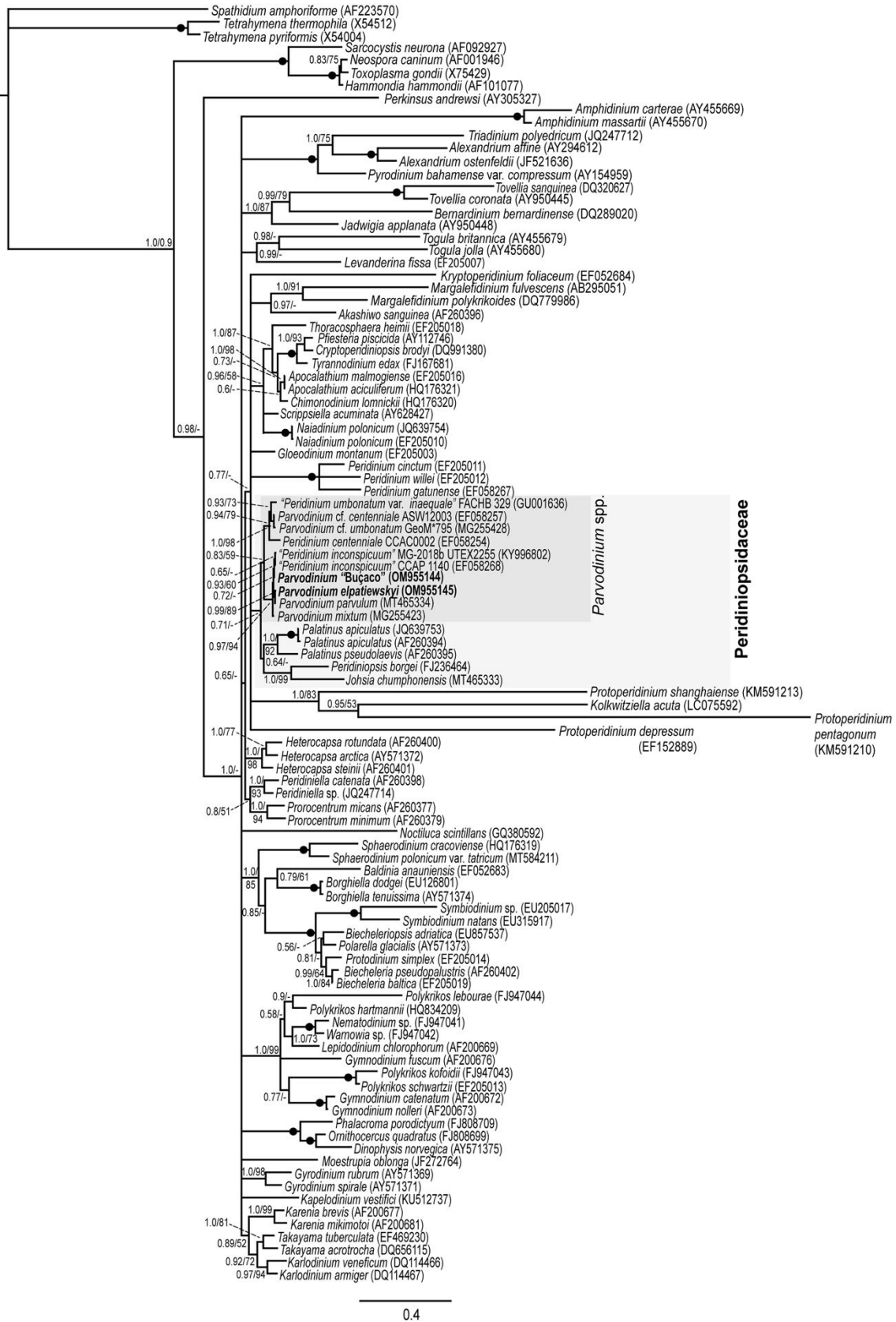
The phylogenetic inference based on the concatenated data matrix and containing species closely related to *Parvodinium* based on the analysis of LSU rDNA revealed

fairly good to moderate support for a monophyletic origin of *Parvodinium* from posterior probability and bootstrap, respectively (PP = 0.95 and BS = 70%) (Supplementary fig. S20). The seven species (nine strains) assigned to *Parvodinium*, and the clade comprising *Palatinus apiculatus* (Ehrenberg) Craveiro, Calado, Daugbjerg & Moestrup, *Peridiniopsis borgei* and *Johsia chumphonensis* formed a highly supported monophyletic clade (PP = 1.0 and BS = 98%). For the core group of *Parvodinium* species, a highly supported relationship was observed between the three strains of *P. mixtum* but also for the shared, and based on the short branch lengths, a relative recent
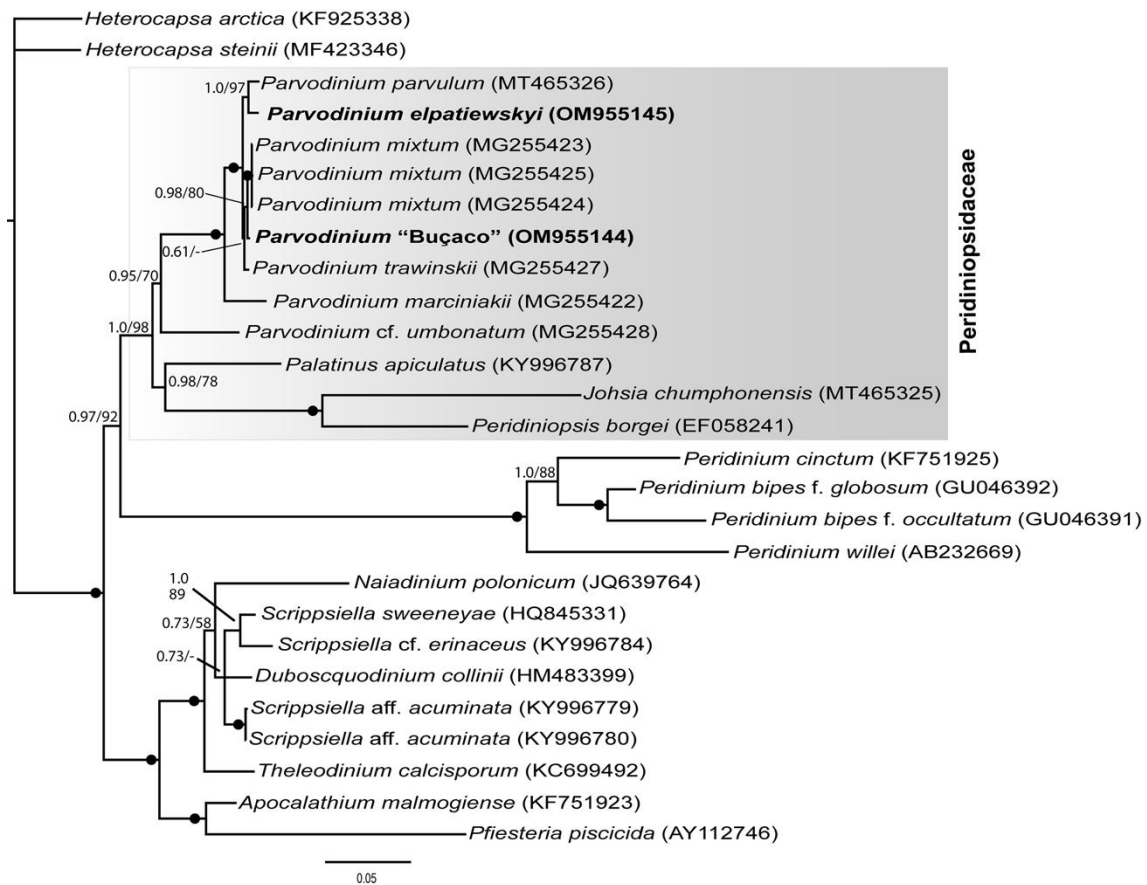
Supplementary fig. S20. Concatenated phylogeny based on 3923 base pairs of large subunit rDNA, internal transcribed spacers, 5.8S rDNA and small subunit rDNA of 12 genera of Dinophyceae (27 sequences) and inferred from Bayesian analysis. For this analysis *Heterocapsa* spp. were used as outgroup taxa. Branch support was evaluated from posterior probabilities (probabilities (PP ≥ 0.5) from Bayesian analyses and bootstrap (1000 replications, BS ≥ 50%) from maximum likelihood analyses, respectively. These support values are written at internodes. A hyphen (-) indicates values below 0.5 for PP and 50% for bootstrap. GenBank accession numbers are written after the species epithet. Sequences determined in this study were bold faced. The branch lengths are proportional to the number of character changes, see scale bar below the phylogenetic tree.

ancestry between *P. parvulum*, *P. elpatiewskyi*, *P. trawinskii* Kretschmann, Owsianny, Zerdoner & Gottschling, *Parvodinium* 'Buçaco' and *P. mixtum* (PP = 1.0 and BS = 100%). The other deep lineage of ingroup taxa formed a highly supported lineage comprising *Pfiesteria*, *Apocalathium*, *Scrippsiella* spp., *Naiadinium*, *Duboscquodinium* and *Theleodinium* (PP = 1.0, BS = 100%). Note that *Scrippsiella* did not form a monophyletic group due to the clustering of *Duboscquodinum collinii*.

DISCUSSION

Identity and phylogenetic affinities of the Buçaco strain

The cells of the culture strain examined showed the general features of the *P. umbonatum–P. inconspicuum* species complex. Relevant characters include the conspicuous apical pore complex located at the centre of the cell apex, the two similar-sized anterior intercalary plates symmetrically positioned on the dorsal side of the epitheca, the slightly descending cingulum, delimiting the longer anterior part of the cell from the shorter hypotheca, and the moderately compressed, ovoid to ellipsoid shape of the cell. Particularly significant is the shape of the sulcus, forming a trapezoid indentation in the epitheca and strongly widening toward the antapex. All the characters mentioned above are present in *P. mixtum*, *P. trawinskii* and *P. marciniakii* Kretschmann, Owsianny, Zerdoner & Gottschling (Kretschmann *et al.*, 2018), all of which appear in the same well-supported clade of the concatenated phylogenetic tree (Supplementary fig. S20) as *Parvodinium* 'Buçaco'. The other species in that clade, *P. elpatiewskyi*, lacks the intercalary plates but its sulcus shows the same general outline, slightly indenting the epitheca and widening toward the antapex (Moestrup & Calado, 2018; Kretschmann *et al.*, 2019). *Parvodinium* from Buçaco appears as a sister taxon to *Parvodinium mixtum* (Supplementary fig. S20), with which it shares the same pattern of plate overlap (Kretschmann *et al.*, 2018).

The original description of *Peridinium inconspicuum* Lemmermann was rather brief, did not include any details about the plates and was not accompanied by an illustration (Lemmermann, 1899). The earliest illustrations by Lemmermann show the oval outline of the cell, the slightly descending cingulum, the axial position of the apical pore and the presence of three spines aligned with the sutures of the antapical plates

(Lemmermann, 1905, 1910; figures reproduced in Moestrup & Calado, 2018). Although Lemmermann's (1910) figures lack precision, as seen in the representation of a similar-looking narrow plate at the apex in both ventral and dorsal views, the position of the three spines in a dorsal view of the cell (Lemmermann, 1910, p. 663, fig. 29), and the distinctly smaller size of antapical plate 1, suggest the arrangement we document for the Buçaco strain. Stein's (1883) original drawings of *Peridinium umbonatum* show details of the main plates in ventral and dorsal views, and include the complete tabulation of the epitheca in an apical view that shows a very slight dorsoventral compression. The cell outline appears distinctive in Stein's drawings, but the rather long, nearly truncated-cone-shaped ring of precingular plates has not been documented from other specimens. A description of *P. umbonatum* was included in Lemmermann (1910), who added to two of Stein's illustrations, in ventral and dorsal view, an apical and an antapical view by Schilling (1891), both of which showed a distinct dorsoventral compression. Lefèvre (1932) summarized the observations on *P. umbonatum*, *P. inconspicuum* and their infraspecific taxa, and established the concepts for these taxa that would influence the application of the names for the following decades (Schiller, 1935; Huber-Pestalozzi, 1950; Starmach, 1974). The overlap of features recognized by Lefèvre (1932) for the two species is quite extensive, with only size as a guide to identify populations of small cells (15–25 µm long) as *P. inconspicuum* and populations of cells longer than 30 µm as *P. umbonatum*, and leaving an uncomfortable overlap in the 25–30 µm range. In view of the natural variability in cell size found in many populations, and of the difficulty of selecting features that could reliably distinguish *P. inconspicuum* from *P. umbonatum*, the decision to treat the two names as synonyms was understandable (Popovský & Pfiester, 1986, 1990). However, the description of new taxa by the combined application of morphological and genetic analyses demonstrated more species-level diversity than previously recognized and highlighted the need for well-defined (morphologically and genetically) taxonomic and nomenclatural reference points in this group of species (Kretschmann *et al.*, 2018). The description of new taxa in this core group of *Parvodinium* species presupposes the establishment of a distinction between the newly described species and these older names. Several GenBank entries with the names *P. inconspicuum* and *P. umbonatum* are available and these names have been included in published phylogenetic trees (Logares *et al.*, 2007; Kretschmann *et al.*,

154

2018; Luo *et al*., 2019). However, the morphological characterization of the strains from which the DNA sequences were determined is scarce or non-existent and the topological location of strains with the same name in phylogenetic trees is often inconsistent (Saldarriaga *et al*., 2001; Stern *et al.*, 2012; Kretschmann *et al.*, 2018). Nomenclatural stability will eventually require that a strain be accepted as fixing the application of each name. While the choice of a reference strain for each of the species *P. umbonatum* and *P. inconspicuum* may have to be largely arbitrary, given the difficulty of defining characters and distinguishing the species morphologically, it is desirable that the selection of a reference strain be accompanied by a detailed morphological analysis and include the sequencing of, at least, major portions of the ribosomal operon, which are commonly used for phylogenetic inferences in dinoflagellates. A strain with small cells and a morphology compatible with early drawings of the species, similar to the Buçaco strain described herein, would appear eligible as a reference point fixing the application of the name *P. inconspicuum.* Ideally, the selected strain would come from one of the original locations for the taxon, namely two islands in Hawaii (Molokai and Oahu) and Chatham Islands, off the coast of New Zealand, some 7500 km south of Hawaii.

The selection of a morphologically and genetically characterized strain for fixing the application of the name *P. umbonatum* may have a larger impact on nomenclature because this is the type species of the genus. The use of the name in published phylogenetic trees may induce the tacit selection of one of the sequences available in GenBank as representing the phylogenetic position of *P. umbonatum*. However, the retrieval of two fairly well supported, separate lineages with *Parvodinium* species in the phylogenetic tree based on LSU rDNA (Fig. 45) recommends a closer look at the taxa in the clade containing *Parvodinium* cf. *umbonatum* GeoM*795, '*Peridinium umbonatum* var. *inaequale*' and *P. centenniale*. For example, EF058254 is currently labelled 'Dinophyceae sp. strain CCAC0002' in GenBank; it was submitted as '*Peridinium centenniale* CCAC0002' by Logares *et al.* (2007) and was referred as *Parvodinium centenniale* by Kretschmann *et al.* (2018). Both *Parvodinium* cf. *umbonatum* GeoM*795 and '*Peridinium umbonatum* var. *inaequale*' were illustrated, and they both show a broadly round epitheca that is wider than the hypotheca (Zhang *et al.*, 2011; Kretschmann *et al.*, 2018). A distinctly narrower hypotheca was the basis for

the original distinction of *Peridinium umbonatum* var. *inaequale* Lemmermann (1910, p. 669, 670), which, however, still showed the pronounced widening of the sulcus toward the antapex. In his monograph, Lefèvre (1932, p. 123, 124) adopted a broader concept of the variety and combined illustrations of cells with the typical widening sulcus and a symmetrical tabulation with others showing a smaller sulcus with a round posterior end, an off-axis apical pore and a somewhat asymmetrical arrangement of plates on the epitheca – a combination of characters reminiscent of *P. centenniale* as depicted by Playfair (1920) and Ling *et al.* (1989). The illustrations given for *Parvodinium* cf. *umbonatum* GeoM*795 show a narrower sulcus that closes posteriorly on the ventral side, and a slight asymmetry of outline and plate disposition, which suggest affinity with *P. centenniale* (Kretschmann *et al.*, 2018). Since the original illustrations of *P. umbonatum* show a symmetrical epithecal tabulation and the posteriorly widening sulcus, the effect of selecting a reference strain for the type of *Parvodinium* from this clade with apparent affinities with *P. centenniale* would be to change the application of the name relative to the one that prevailed for more than eight decades, viz. a species closely related to, and difficult to distinguish from, *P. inconspicuum*. Since no DNA sequence can be assigned at present to a strain unequivocally with the morphology of *P. umbonatum*, we suggest that stability and historical continuity of the application of species names in *Parvodinium* may be achieved by selecting as reference strain a population, or culture, with the general features of species in the clade of *P. inconspicuum*, *P. mixtum* and *P. trawinskii*, and an average cell length near or above 30 µm.

General ultrastructure and apical pore complex

Cells of the *Parvodinium* strain from Buçaco showed the fine-structural features typical of a photosynthetic dinoflagellate: a nucleus with condensed chromosomes, numerous chloroplast profiles, pusular system, trichocysts, and starch grains and oil droplets as reserves. No pyrenoids were observed; however, the chloroplast lobes had a radial disposition towards the centre of the cell compatible with what was observed by Seo & Fritz (2002) in '*Peridinium inconspicuum*' strain UTEX LB2255, which appears in our LSU rDNA-based phylogenetic tree in the same clade as *Parvodinium* from Buçaco (accession KY996802). The quantity of starch accumulated and the presence or

absence of a central pyrenoid (expressed as thylakoid-free areas of chloroplast lobes) were reported by Seo & Fritz (2002) to vary according to the light or dark phase in cultures of some dinoflagellates. This variability was not examined in our strain and, although it cannot be excluded that a central region rich in chloroplast lobes with thylakoid-free areas resembling a central compound pyrenoid may be formed in some conditions, no traces of a well-defined, central pyrenoid were found. The presence of a more or less complex central pyrenoid has been considered characteristic of other members of the Peridiniopsidaceae (Gottschling *et al.*, 2017). *Peridiniopsis* and *Johsia* have a single round pyrenoid surrounded by starch, whereas the central pyrenoid in *Palatinus* radiates into the associated chloroplast lobes (Calado & Moestrup, 2002; Craveiro *et al.*, 2009; Luo *et al.*, 2020). In contrast, typical Peridiniaceae, e.g. *Peridinium cinctum* (O.F.Müller) Ehrenberg and *P. gatunense* Nygaard, do not show this type of large, well-defined pyrenoid, only thylakoid-free areas in some chloroplast lobes (Messer & Ben-Shaul, 1969; Calado *et al.*, 1999).

An eyespot type A (Moestrup & Calado, 2018), consisting of one or more rows of lipid globules included in a chloroplast lobe, was observed in our strain and agrees with observations from Luo *et al.* (2020) for *Parvodinium parvulum.* An eyespot of type A is also present in *Palatinus* (Craveiro *et al.*, 2009) and '*Scrippsiella*' *hexapraecingula* (Horiguchi *et al.*, 1999), whereas an eyespot of type B, with a layer of crystal-containing vesicles overlying a lipid globule-containing chloroplast lobe, was found in *Peridiniopsis borgei* and in *Johsia chumphonensis* (Calado & Moestrup, 2002; Luo *et al.*, 2020). The eyespot type A is most common in the Peridiniales and Thoracosphaerales, while the eyespot type B has been mainly found in the family Borghiellaceae (Moestrup & Calado, 2018).

An apical pore complex is present in almost all peridinioids but is absent from species of *Peridinium* subg. *Cleistoperidinium* (Peridiniaceae) and from *Palatinus,* the only genus of the Peridiniopsidaceae without it. When present, the apical pore is usually underlain by fibres (apical fibrous complex) above a cytoplasm region rich in vesicles (e.g. Roberts *et al.*, 1987; Hansen *et al.*, 1996; Craveiro *et al.*, 2011). The appearance of the fibrous complex is somewhat influenced by the type of fixation (Calado & Moestrup, 2002), which complicates comparisons between different taxa. Our observations on the *Parvodinium* strain from Buçaco are compatible with what was

shown in cells of *Scrippsiella sweeneyae* Balech, *Peridiniopsis borgei*, *Chimonodinium lomnickii* (Wołoszyńska) Craveiro, Calado, Daugbjerg, Gert Hansen & Moestrup and *Theleodinium calcisporum* Craveiro, Pandeirada, Daugbjerg, Moestrup & Calado, all of which were fixed with a mixture of glutaraldehyde and osmium tetroxide: an uninterrupted fibrous layer lining the inner cylindrical raised area of the pore plate, which extends posteriorly along the cell surface as several independent fibres (Roberts *et al.*, 1987; Calado & Moestrup, 2002; Craveiro *et al.*, 2011, 2013).

Pusular system

The complex pusular system found in *Parvodinium*, with three distinct areas, has not been previously described from other dinoflagellates. The so-called pusular network (PuN) resembles, to some extent, the flattened and ramified pusular vesicles of *Scrippsiella trochoidea* (F.Stein) A.R.Loeblich (Thoracosphaeraceae)*,* which however, was restricted to a smaller region on the right mid-ventral side of the cell (Craveiro *et al.*, 2011). Pusular structure was described in detail in two other Peridiniopsidaceae, *Peridiniopsis borgei* and *Palatinus apiculatus*; both showed a large sac pusule connected to the LFC (Calado & Moestrup, 2002; Craveiro *et al.*, 2009). A sac pusule was not observed in the *Parvodinium* cells examined, either because the collapse of the ventral region may have concealed this feature, or because it is absent from this species. Both *Peridiniopsis borgei* and *Palatinus apiculatus* have flattened pusular vesicles scattered in the cell; in addition, two distinct pusular tubes connect to the TFC, and one to the LFC, of *P. apiculatus* (Calado & Moestrup, 2002; Craveiro *et al.*, 2009). A somewhat flattened pusular tube was also connected to the TFC in *Parvodinium*. Pusular tubes are some of the most common types of pusular structures in dinoflagellates, although they vary in number, width and in connecting to either the TFC or the LFC. The different pusular structures observed in *Parvodinium* contrast with the pusular organization of several other peridinioids, e.g. the genera *Chimnodinium* and *Apocalathium* (Thoracosphaeraceae), in which well-defined pusular tubes opening at the flagellar canals were the only pusular structures observed (Craveiro *et al.*, 2011, 2016).

Microtubular strand of the peduncle (MSP)

The MSP described herein for *Parvodinium* has a path inside the cell reminiscent of the one observed in *P. borgei* (Calado & Moestrup, 1997), although with a smaller number of microtubules (ca. 40 instead of ca. 80 in *P. borgei*). In both species the MSP extended from an extruded peduncle on the ventral area and was accompanied in this ventral region by electron-opaque bodies. The MSP continued toward the anterior-left side of the epicone in both *Parvodinium* and *P. borgei*, and in both cases the microtubular strand divided into several groups and was somewhat wavy in parts of its path (Calado & Moestrup, 1997). In contrast, *Palatinus* has a more simple strand of microtubules that lacks accompanying vesicles and does not extend into a peduncle; however, judging from its position and orientation it was considered homologous to the MSP (Craveiro *et al.*, 2009). The ultrastructure of the recently described marine genus *Johsia* was not examined in detail and no information concerning a MB or MSP is available (Luo *et al.*, 2020). '*Scrippsiella*' *hexapraecingula* was observed with an extruded peduncle similar to those known to be supported by an internal MSP or MB; this is compatible with its phylogenetic relationship to *P. borgei* (Horiguchi & Chihara, 1983; Luo *et al.*, 2020). As a contrast to what has been observed in members of the Peridiniopsidaceae, in the Peridiniaceae, as represented by the type species *Peridinium cinctum*, no type of microtubular system homologous to an MSP has been found (Calado *et al.*, 1999).

Flagellar apparatus

The general organization of the flagellar apparatus of peridinioids shows several variations concerning the presence or absence of small connectives linking its various components. One of these connectives, consisting of well-defined fibres associating the anterior-dorsal side of the LMR/r1 with two or three triplets of the TB (the LMR-TBc), was found in all members of the Peridiniopsidaceae for which detailed ultrastructural information is available: *Peridiniopsis borgei* (Calado & Moestrup, 1997), *Palatinus apiculatus* (Craveiro *et al.*, 2009) and *Parvodinium* (present work). In contrast to what was found in the Peridiniopsidaceae, the Thoracosphaeraceae revealed more variation, with some members also showing fibres attaching to two or three triplets of the TB (e.g. *Theleodinium calcisporum* and *Apocalathium aciculiferum* (Lemmermann) Craveiro,

Daugbjerg, Moestrup & Calado; Craveiro *et al.*, 2013, 2016), whereas others, like *Chimonodinium lomnickii,* have a single, wider band of thin fibres attaching to the TB (Craveiro *et al.*, 2011). A third variation was found in *Naiadinium polonicum,* in which the basal bodies were more widely separated and the only fibrous connection between LMR/r1 and TB was provided by the LC (Craveiro *et al.*, 2015). In *Peridinium cinctum* (Peridiniaceae) the LC was also the only structure found linking LMR/r1 and TB (Calado *et al.*, 1999).

Within peridinioids, variation was also found in the arrangement and number of microtubules that form the extension of the TMR/r3. In the Peridiniopsidaceae, three different types of TMR/r3 extension were observed until now, the simplest being the one described here for *Parvodinium* with a single strand of 11 microtubules. In *Palatinus apiculatus* the TMR/r3 looped around the transverse flagellar canal before nucleating one or two rows of 20 microtubules (Craveiro *et al.*, 2009). A more peculiar TMR/r3 extension was described from *Peridiniopsis borgei*; it was composed of ca. 35 microtubules, of which 23 gradually assumed a cylindrical arrangement surrounding a fibrous core and extended around a large, central vesicle (Calado & Moestrup, 2002). In the Thoracosphaeraceae, *Chimonodinium lomnickii* also showed a TMR/r3 extension with an association with fibrous material, although it did not develop into the association seen in *P. borgei* (Craveiro *et al.*, 2011). These variations on the type of TMR/r3 extension, which cross family borders, seem to devalue its potential to reflect phylogenetic relationships.

A description of the fine structure of the family Peridiniopsidaceae, based on current knowledge, may be (see also Supplementary table S2): cells with an extensive network of chloroplast lobes bounded by three membranes, with thylakoids predominantly associated in lamellae of three (peridinin chloroplast type); thylakoid-free areas usually present in some chloroplast lobes; a large, inner pyrenoid, extending into radial lobes (*Palatinus*), round and surrounded by starch (*Peridiniopsis*, *Johsia*, 'Scrippsiella' *hexapraecingula*), or pyrenoid absent (*Parvodinium*). Cytoplasmic channels sometimes penetrating the pyrenoid (*Palatinus*). Food reserves as starch grains and oil droplets, sometimes localized in different areas of the cell (*Peridiniopsis*). Eyespot present, of type A (*Parvodinium*, *Palatinus*, 'Scrippsiella' *hexapraecingula*) or B (*Peridiniopsis*, *Johsia*) with at least two (*Parvodinium*, *Palatinus*, *Johsia*,

'*Scrippsiella*' *hexapraecingula*) and up to six layers (*Peridiniopsis*; four layers in *Parvodinium parvulum*) of globules inside chloroplast lobe. Trichocysts present throughout the cell, of a single type. Apical pore complex present (*Peridiniopsis*, *Parvodinium*, *Johsia*, '*Scrippsiella*' *hexapraecingula*) underlain by apical fibrous complex (unknown in *Johsia* and '*Scrippsiella*' *hexapraecingula*), or absent (*Palatinus*). Mid-ventral area with extruded peduncle (*Peridiniopsis*, *Parvodinium*, '*Scrippsiella*' *hexapraecingula*) or peduncle absent (*Palatinus*; unknown in *Johsia*); microtubular strand homologous with MSP present (unknown in *Johsia*), reduced and without connection to the cell surface (*Palatinus*) or penetrating the peduncle and extending over the anterior area of the epicone and returning to the ventral area as separate rows of microtubules (*Peridiniopsis*, *Parvodinium*). Pusule (unknown in *Johsia* and '*Scrippsiella*' *hexapraecingula*) comprising flat vesicles and cylindroid tubes of variable diameter (*Palatinus*), a combination of rounded and flat vesicles (*Peridiniopsis*) or a very extensive assortment of ramifying flat and tubular vesicles with variable appearance (*Parvodinium*). Large sac pusule connected to the LFC (*Peridiniopsis*, *Palatinus*) or absent (*Parvodinium*). Flagellar apparatus (unknown in *Johsia* and '*Scrippsiella*' *hexapraecingula*) with basal bodies inserted about 100 nm apart and forming a 80–90º angle, each basal body associated with two microtubule-containing roots; LMR/r1 proximal end with 5–10 microtubules that do not extend beyond the LB, up to 30–40 microtubules distally; fibrous layer on dorsal face of LMR/r1 connecting to base of TB and TSR by an LC (striated root connective absent); proximal end of LMR/r1 linked by group of 2–3 fibres to 2–3 triplets of the TB; proximal ends of BBs linked by a striated fibre (*Palatinus*) or without direct connection (*Peridiniopsis*, *Parvodinium*); TMR/r3 extending around TFC (*Peridiniopsis*, *Palatinus*) or relatively short (*Parvodinium*), nucleating an extension of microtubules (TMRE) toward the dorsal side of the cell; TMRE with about 10–20 microtubules in a flat layer (*Palatinus*, *Parvodinium*) or about 35 proximately and arranged into a circle of 23 microtubules around a fibrous axis distally (*Peridiniopsis*). Distal part of flagellar canals (exit point of each flagellum) surrounded by conspicuous fibrous rings that are connected by one (*Peridiniopsis*, *Parvodinium*) or two fibrous extensions (*Palatinus*); when present, exit point of extended peduncle also surrounded by fibrous ring. Except for a short connective attaching the LMR/r1 of *Peridiniopsis* to the fibrous material that

limited the longitudinal flagellar canal, there are no fibres associated with the ventral face of this multistranded root; and there are no dorsal connectives linking the flagellar apparatus to other cytoplasmic structures.

REFERENCES

Andersen, R.A., Berges, J.A., Harrison, P.J. & Watanabe, M.M. (1997). Recipes for freshwater and seawater media. In *Algal culturing techniques* (Andersen, R.A., editor), 429–538. Elsevier Academic Press, Burlington.

Calado, A.J. (2011). On the identity of the freshwater dinoflagellate *Glenodinium edax*, with a discussion on the genera *Tyrannodinium* and *Katodinium*, and the description of *Opisthoaulax* gen. nov. *Phycologia*, **50**: 641–649.

Calado, A.J. & Moestrup, Ø. (1997). Feeding in *Peridiniopsis berolinensis* (Dinophyceae): new observations on tube feeding by an omnivorous, heterotrophic dinoflagellate. *Phycologia*, **36**: 47–59.

Calado, A.J. & Moestrup, Ø. (2002). Ultrastructural study of the type species of *Peridiniopsis*, *Peridiniopsis borgei* (Dinophyceae), with special reference to the peduncle and flagellar apparatus. *Phycologia*, **41**: 567–584.

Calado, A.J., Craveiro, S.C. & Moestrup, Ø. (1998). Taxonomy and ultrastructure of a

freshwater, heterotrophic *Amphidinium* (Dinophyceae) that feeds on unicellular protists. *Journal of Phycology*, **34**: 536–554.

Calado, A.J., Hansen, G. & Moestrup, Ø. (1999). Architecture of the flagellar apparatus and related structures in the type species of *Peridinium*, *P. cinctum* (Dinophyceae). *European Journal of Phycology*, **34**: 179–191.

Carty, S. (2008). *Parvodinium* gen. nov. for the Umbonatum group of *Peridinium* (Dinophyceae). *Ohio Journal of Science*, **108**: 103–107.

Craveiro, S.C., Calado, A.J., Daugbjerg, N. & Moestrup, Ø. (2009). Ultrastructure and LSU rDNA-based revision of *Peridinium* group palatinum (Dinophyceae) with the description of *Palatinus* gen. nov. *Journal of Phycology*, **45**: 1175–1194.

Craveiro, S.C., Calado, A.J., Daugbjerg, N., Hansen, G. & Moestrup, Ø. (2011). Ultrastructure and LSU rDNA-based phylogeny of *Peridinium lomnickii* and description of *Chimonodinium* gen. nov. (Dinophyceae). *Protist*, **162**: 590–615.

Craveiro, S.C., Pandeirada, M.S., Daugbjerg, N., Moestrup, Ø. & Calado, A.J. (2013). Ultrastructure and phylogeny of *Theleodinium calcisporum* gen. et sp. nov., a freshwater dinoflagellate that produces calcareous cysts. *Phycologia*, **52**: 488–507.

Craveiro, S.C., Daugbjerg, N., Moestrup, Ø. & Calado, A.J. (2015). Fine-structural characterization and phylogeny of *Peridinium polonicum*, type species of the recently described genus *Naiadinium* (Dinophyceae). *European Journal of Protistology*, **51**: 259–279.

Craveiro, S.C., Daugbjerg, N., Moestrup, Ø. & Calado, A.J. (2016). Studies on *Peridinium aciculiferum* and *Peridinium malmogiense* (=*Scrippsiella hangoei*): comparison with *Chimonodinium lomnickii* and description of *Apocalathium* gen. nov. (Dinophyceae). *Phycologia*, **56**: 21–35.

Elbrächter, M. & Meyer, B. (2001). Plate pattern variability and plate overlap in a clonal culture of the freshwater dinoflagellate *Peridinium umbonatum* Stein species complex (Dinophyceae). *Neues Jahrbuch für Geologie und Paläontologie/Abhandlungen*, **219**: 221–227.

Gottschling, M., Kretschmann, J. & Žerdoner Čalasan, A. (2017). Description of

Peridiniopsidaceae, fam. nov. (Peridiniales, Dinophyceae). *Phytotaxa*, **299**: 293–296.

Guindon, S., Dufayard, J.F., Lefort, V., Anisimova, M., Hordijk, W. & Gascuel, O. (2010). New algorithms and methods to estimate maximum-likelihood phylogenies: assessing the performance of PhyML 3.0. *Systematic Biology*, **59**: 307–321.

Hansen, P.J. & Calado, A.J. (1999). Phagotrophic mechanisms and prey selection in free-living dinoflagellates. *Journal of Eukaryotic Microbiology*, **46**: 382–389.

Hansen, G., Moestrup, Ø. & Roberts, K.R. (1996). Fine structural observations on *Gonyaulax spinifera* (Dinophyceae), with special emphasis on the flagellar apparatus. *Phycologia*, **35**: 354–366.

Hansen, G., Daugbjerg, N. & Henriksen, P. (2007). *Baldinia anauniensis* gen. et sp. nov.: a "new" dinoflagellate from Lake Tovel, N. Italy. *Phycologia*, **46**: 86–108.

Horiguchi, T. & Chihara, M. (1983). *Scrippsiella hexapraecingula* sp. nov. (Dinophyceae), a tide pool dinoflagellate from the Northwest Pacific. *The Botanical Magazine, Tokyo*, **96**: 351–358.

Horiguchi, T., Kawai, H., Kubota, M., Takahashi, T. & Watanabe, M. 1999. Phototactic responses of four marine dinoflagellates with different types of eyespot and chloroplast. *Phycological Research*, **47**: 101–107.

Huber-Pestalozzi, G. (1950). Das Phytoplankton des Süsswassers. Systematik und Biologie. 3. Teil. Cryptophyceen, Chloromonadinen, Peridineen. In *Die Binnengewässer...* (Thienemann, A., editor) vol. 16. E. Schweizerbart'sche Verlagsbuchhandlung, Stuttgart. IX + 310 pp.

Iwataki, M., Hansen, G., Moestrup, Ø. & Matsuoka, K. (2010). Ultrastructure of the harmful unarmored dinoflagellate *Cochlodinium polykrikoides* (Dinophyceae) with reference to the apical groove and flagellar apparatus. *The Journal of Eukaryotic Microbiology*, **57**: 308–321.

Kretschmann, J., Owsianny, P.M., Žerdoner Čalasan, A. & Gottschling, M. (2018). The hot spot in a cold environment: puzzling *Parvodinium* (Peridiniopsidaceae,

Peridiniales) from the polish Tatra mountains. *Protist*, **169**: 206–230.

Kretschmann, J., Žerdoner Čalasan, A., Meyer, B. & Gottschling, M. (2019). Zero intercalary plates in *Parvodinium* (Peridiniopsidaceae, Peridiniales) and phylogenetics of *P. elpatiewskyi*, comb. nov. *Protist*, **171**: Article 125700.

Lefèvre, M. (1932). Monographie des espèces d'eau douce du genre *Peridinium*. *Archives de Botanique*, **2** (Mémoire 5): 1–210.

Lemmermann, E. (1899). Ergebnisse einer Reise nach dem Pacific. H. Schauinsland 1896/97. *Abhandlungen herausgegeben vom Naturwissenschaftlichen Verein zu Bremen*, **16**: 313–398, pls I–III.

Lemmermann, E. (1905). Die Algenflora der Sandwich-Inseln. Ergebnisse einer Reise nach dem Pacific. H. Schauinsland 1896/97. *Botanische Jahrbücher fur Systematik Pflanzengeschichte und Pflanzengeographie*, **34**: 607–663, pls VII– VIII.

Lemmermann, E. (1910). *Algen I (Schizophyceen, Flagellaten, Peridineen). Kryptogamenflora der Mark Brandenburg, Bd. 3*. Gebrüder Borntraeger, Leipzig, 712 pp.

Lindberg, K., Moestrup, Ø. & Daugbjerg, N. (2005). Studies on woloszynskioid dinoflagellates I: *Woloszynskia coronata* re-examined using light and electron microscopy and partial LSU rDNA sequences, with description of *Tovellia* gen. nov. and *Jadwigia* gen. nov. (Tovelliaceae fam. nov.). *Phycologia,* **44**: 416– 440.

Lindström, K. (1991). Nutrient requirements of the dinoflagellate *Peridinium gatunense*. *Journal of Phycology*, **27**: 207–219.

Ling, H.U., Croome, R.L. & Tyler, P.A. (1989). Freshwater dinoflagellates of Tasmania, a survey of taxonomy and distribution. *British Phycological Journal*, **24**: 111–129.

Litaker, R.W., Vandersea, M.W., Kibler, S.R., Madden, V.J., Noga, E.J. & Tester, P.A. (2002). Life cycle of the heterotrophic dinoflagellate *Pfiesteria piscicida* (Dinophyceae). *Journal of Phycology*, **38**: 442–463.

Logares, R., Shalchian-Tabrizi, K., Boltovskoy, A. & Rengefors, K. (2007). Extensive

dinoflagellate phylogenies indicate infrequent marine-freshwater transitions. *Molecular Phylogenetics and Evolution*, **45**: 887–903.

Luo, Z., Mertens, K.N., Nézan, E., Gu, L., Pospelova, V., Thoha, H. & Gu, H. (2019). Morphology, ultrastructure and molecular phylogeny of cyst-producing *Caladoa arcachonensis* gen. *et* sp. nov. (Peridiniales, Dinophyceae) from France and Indonesia. *European Journal of Phycology*, **54**: 235–248.

Luo, Z., Mertens, K.N., Gu, H., Wang, N., Wu, Y., Uttayarnmanee, P., Pransilpa, M. & Roeroe, K.A. (2020). Morphology, ultrastructure and molecular phylogeny of *Johsia chumphonensis* gen. *et* sp. nov. and *Parvodinium parvulum* comb. nov. (Peridiniopsidaceae, Dinophyceae). *European Journal of Phycology*, **56**: 324–336.

Messer, G. & Ben-Shaul, Y. (1969). Fine structure of *Peridinium westii* Lemm., a freshwater dinoflagellate. *Journal of Protozoology*, **16**: 272–280.

Moestrup, Ø. (2000). The flagellate cytoskeleton. Introduction of a general terminology for microtubular flagellar roots in protists. In *The flagellates. Unity, diversity and evolution* (Leadbeater, B.S.C. & Green, J.C., editors), 69–94. Taylor & Francis, New York. (Systematics Association Special Volume No. 59).

Moestrup, Ø. & Daugbjerg, N. (2007). On dinoflagellate phylogeny and classification. In *Unravelling the Algae: the past, present, and future of algae systematics* (Brodie, J. & Lewis, J., editors), 215–230. CRC Press, Boca Raton. (Systematics Association Special Volume No. 75).

Moestrup, Ø. & Calado, A.J. (2018). Dinophyceae. In *Süßwasserflora von Mitteleuropa – Freshwater Flora of Central Europe* (Büdel, B., Gärtner, G., Krienitz, L. & Schagerl, M., editors), vol. 6, 2nd edition. Springer-Verlag, Berlin. XII + 561 pp.

Pandeirada, M.S., Craveiro, S.C., Daugbjerg, N., Moestrup, Ø. & Calado, A.J. (2014). Studies on woloszynskioid dinoflagellates VI: description of *Tovellia aveirensis* sp. nov. (Dinophyceae), a new species of Tovelliaceae with spiny cysts. *European Journal of Phycology*, **49**: 230–243.

Pandeirada, M.S., Craveiro, S.C., Daugbjerg, N., Moestrup, Ø. & Calado, A.J. (2017). Studies on woloszynskioid dinoflagellates VIII: life cycle, resting cyst

morphology and phylogeny of *Tovellia rinoi* sp. nov. (Dinophyceae). *Phycologia*, **56**: 533–548.

Pandeirada, M.S., Craveiro, S.C., Daugbjerg, N., Moestrup, Ø., Domingues, P. & Calado, A.J. (2019). Studies on woloszynskioid dinoflagellates X: ultrastructure, phylogeny and colour variation in *Tovellia rubescens* sp. nov. (Dinophyceae). *Journal of Eukaryotic Microbiology*, **66**: 937–953.

Pandeirada, M.S., Craveiro, S.C., Daugbjerg, N., Moestrup, Ø. & Calado, A.J. (2021). Fine-structural characterization and phylogeny of *Sphaerodinium* (Suessiales, Dinophyceae), with the description of an unusual type of freshwater dinoflagellate cyst. *European Journal of Protistology*, **78**: Article 125770.

Playfair, G.I. (1920). Peridineae of New South Wales. *Proceedings of the Linnean Society of New South Wales*, **44**: 793–818, pls XLI–XLIII.

Popovský, J. & Pfiester, L.A. (1986). A taxonomical note to the Section *umbonatum* of the genus *Peridinium* Ehrenberg, 1932 (Dinophyceae). *Archiv für Protistenkunde*, **132**: 73–77.

Popovský, J. & Pfiester, L.A. (1990). Dinophyceae (Dinoflagellida). In *Süßwasserflora von Mitteleuropa* (Ettl, H., Gerloff, J., Heynig, H. & Mollenhauer, D., editors), vol. 6. Gustav Fischer, Jena.

Roberts, K.R., Timpano, P. & Montegut, A.E. (1987). The apical fibrous complex: a new cytological feature of some dinoflagellates. *Protoplasma*, **137**: 65–69.

Ronquist, F. & Huelsenbeck, J.P. (2003). MrBayes 3: Bayesian phylogenetic inference under mixed models. *Bioinformatics*, **19**: 1572–1574.

Saldarriaga, J.F., Taylor, F.J.R., Keeling, P.J. & Cavalier-Smith, T. (2001). Dinoflagellate nuclear SSU rRNA phylogeny suggests multiple plastid losses and replacements. *Journal of Molecular Evolution*, **53**: 204–213.

Schiller, J. (1935). Dinoflagellatae (Peridineae) in monographischer Behandlung. In *Rabenhorst's Kryptogamen-flora von Deutschland, Österreich und der Schweiz*, 2nd edition, **10** (3). Part 2, Issue 2. (Kolkwitz, R., editor), pp 161–320. Akademische Verlagsgesellschaft, Leipzig.

Schilling, A.J. 1891. Die Süsswasser-Peridineen. *Flora*, **74**: 220–299, pls VIII-X.

Schnepf, E., Deichgräber, G. & Drebes, G. (1985). Food uptake and the fine structure of the dinophyte *Paulsenella* sp., an ectoparasite of marine diatoms. *Protoplasma*, **124**: 188–204.

Seo, K.S. & Fritz, L. (2002). Diel changes in pyrenoid and starch reserves in dinoflagellates. *Phycologia*, **41**: 22–28.

Starmach, K. (1974). Cryptophyceae, Dinophyceae, Raphidophyceae. In *Flora Słodkowodna Polski* (Starmach, K. & Siemińska, J., editors), vol. 4. Państwowe Wydawnictwo Naukowe, Warszawa, Kraków. 520 pp.

Stein, F. (1883). *Der Organismus der Infusionsthiere nach eigenen Forschungen in systematischer Reihenfolge bearbeitet. III. Abtheilung. Die Naturgeschichte der Flagellaten oder Geißelinfusorien. II. Hälfte. Die Naturgeschichte der arthrodelen Flagellaten. Einleitung und Erklärung der Abbildungen*. Wilhelm Engelmann, Leipzig. 30 pp, XXV pls.

Stern, R.F., Andersen, R.A., Jameson, I., Küpper, F.C., Coffroth, M.-A., Vaulot, D., Le Gall, F., Véron, B., Brand, J.L., Skelton, H., Kasai, F., Lilly, E.L. & Keeling, P.J. (2012). Evaluating the ribosomal Internal Transcribed Spacer (ITS) as a candidate dinoflagellate barcode marker. *PloS ONE*, **7**: Article e42780.

Swofford, D.L. (2002). PAUP*. Phylogenetic Analysis Using Parsimony (* and Other Methods). Version 4. Sinauer Associates, Sunderland, MA.

Takano, Y. & Horiguchi, T. (2005). Acquiring scanning electron microscopical, light microscopical and multiple gene sequence data from a single dinoflagellate cell. *Journal of Phycology*, **42**: 251–256.

Waterhouse, A.M., Procter, J.B., Martin, D.M.A., Clamp, M. & Barton, G.J. (2009). Jalview Version 2 - a multiple sequence alignment editor and analysis workbench. *Bioinformatics*, **25**: 1189–1191.

Zhang, Q., Liu, G-X. & Hu, Z-Y. (2011) Morphological observation of a freshwater *Peridinium* strain and phylogenetic analysis of *Peridinium*. *Plant Science Journal*, **29**: 1–10.

Supplementary Table S1. Size measurements of cells of *Parvodinium* in culture from Buçaco, Portugal.

Cell	Length (µm)	Width (µm)	Thickness (µm)
1	14.4	10.8	-
2	18.7	12.7	-
3	18.7	13.3	-
4	18.0	-	10.7
5	19.3	12.7	-
6	19.3	-	-
7	18	-	-
8	17.6	-	10.4
9	16.5	-	9.9
10	17	10.7	-
11	17.6	13.2	-
12	20	14.7	-
13	16.7	10.7	-
14	20	14	-
15	19.3	-	12
16	16.7	12	-
17	16	11.3	-
18	18.7	13.3	-
19	16.4	-	10.4
20	16.5	11.5	-
21	14.8	12.1	-
22	15.9	-	10.2
23	15.9	11.5	-
24	12.6	8.5	8.2
25	17.6	12.6	-
26	18.1	13.7	-
27	19.2	13.7	-
28	17	-	10.4
29	16.7	11.3	-
30	19.3	12.7	-
31	20	-	12.7
32	15.3	10.7	-
33	18.7	13.3	-
34	17.3	-	10.7
35	20.7	13.3	-
36	20	14	-
37	15.9	11	-
38	20	14.7	-
39	19.3	14	-

Cell	Length (µm)	Width (µm)	Thickness (µm)
40	16.7	12	-
41	18	12.7	-
42	18	-	11.3
43	20	12.7	-
44	17.3	12	-
45	18	14	-
46	18.7	13.3	-
47	17.3	-	-
48	20	12.7	-
49	16.7	12	-
50	14.7	11.3	-
51	15.3	12	-
52	16.7	13.3	-
53	17.3	11.3	-
54	18.7	12	-
55	18.7	-	10.7
56	16.5	11	-
57	17	11	-
58	17.6	12.1	-
59	10.9	6.6	-
60	16.5	11.5	-
61	17.5	-	10.9
62	16.4	10.4	9.9
63	15.9	11.5	-
64	19.8	14.8	-
65	10.4	-	7.7
66	17	12.6	-
67	15.9	12.1	-
68	17	-	10.4
69	-	11.3	-

Supplementary Table S2. Comparative overview of fine-structural characters in the Peridiniopsidaceae members, described for the type species of *Peridiniopsis*, *Palatinus*, *Joshia*, two species of *Parvodinium*: *P. umbonatum-inconspicuum* from this study (closely related to the type species) and *P. parvulum*, and "*Scrippsiella*" *hexapraecingula*.

Taxon	Chloroplast morphology	Eyespot type	Apical pore complex	Peduncle/MSP
Peridiniopsis borgei	lobes radiating from round central pyrenoid, with starch sheath	type B; up to 6 layers of globules	present, with apical fibrous complex	present/long MSP extending to the back of the cell and curving back to the ventral side, subdivided distally
Palatinus apiculatus	lobes radiating from central pyrenoid penetrated by cytoplasmic channels	type A; 1–2 layers of globules, the inner bending obliquely inward	absent	absent/short microtubular strand homologous to MSP not attached to cell surface
Johsia chumphonensis	lobes radiating from round central pyrenoid, with starch sheath	type B; 2 layers of globules	present; apical fibrous complex unknown	unknown
Parvodinium umbonatum-inconspicuum species complex	lobes peripheral or radiating from cell centre; central pyrenoid absent	type A; 2 layers of globules	present, with apical fibrous complex	present/long MSP extending to the back of the cell and curving back to the ventral side, subdivided distally
Parvodinum parvulum	lobes radiating; central pyrenoid not reported	type A; up to 4 layers of globules	present; apical fibrous complex unknown	unknown
"*Scrippsiella*" *hexapraecingula*	numerous chloroplasts; round central pyrenoid, with starch sheath	type A; 2 layers of globules	present; apical fibrous complex unknown	present/unknown

Supplementary Table S2. – Continued

Pusule	Flagellar apparatus (selected features)	Sources
rounded and flat vesicles extending from a large sac pusule connecting to the LFC; TFC with pusular tubes	proximal end of LMR/r1 linked by 2 fibres to 2 triplets of TB; TMR/r3 extending around TFC, nucleating a cylindrical TMRE with fibrous core in distal end	1
flat vesicles and cylindroid tubes; one large sac pusule connecting to the LFC and a smaller one to the TFC	proximal end of LMR/r1 linked by 3 fibres to 3 triplets of TB; TMR/r3 extending around TFC, nucleating a TMRE of 1–2 rows of 20 microtubules	2
unknown	unknown	3
large system of ramifying flat and tubular vesicles; sac pusule absent	proximal end of LMR/r1 linked by 3 fibres to 3 triplets of TB; TMR/r3 relatively short, nucleating a TMRE of single row of 11 microtubules	this study; 4
unknown	unknown	3
unknown	unknown	5, 6

1, Calado & Moestrup (2002); 2, Craveiro *et al.* (2009); 3, Luo *et al.* (2020); 4, Seo & Fritz (2002); 5, Horiguchi & Chihara (1983); 6, Horiguchi *et al*. (1999).

CHAPTER 5

ULTRASTRUCTURE AND PHYLOGENY OF *PARVODINIUM CUNNINGTONII* COMB. NOV. (SYN. *PERIDINIOPSIS CUNNINGTONII*) AND DESCRIPTION OF *P. CUNNINGTONII* VAR. *INERME* VAR. NOV. (PERIDINIOPSIDACEAE, DINOPHYCEAE)

Inclusion in this thesis is not intended as effective publication of nomenclatural acts included in the manuscript.

ABSTRACT

Two strains of peridinioids were isolated from a flooded stream near Aveiro, central Portugal, and examined by light microscopy, scanning electron microscopy and serial-section transmission electron microscopy. The two strains showed the same tabulation and cell shape as *Peridiniopsis cunningtonii*. One of the strains had lightly reticulated plates and spines in most hypothecal plates, matching the features of typical *P. cunningtonii*. The other strain showed smooth plates and consistently lacked spines in the apiculate hypotheca. The strains were similar in fine structure, and had a central pyrenoid with a starch sheath and perforated by cytoplasmic channels. Details of the flagellar apparatus matched those known from *Parvodinium*, as did the remarkably long microtubular strand leading to an extruded peduncle that was visible in serial sections. Phylogenetic analyses based on partial LSU rDNA and the concatenated ribosomal operon placed the strain with the smooth hypotheca in a clade with *Parvodinium* species; and the two strains grouped as closely related sister taxa in the partial LSU rDNA phylogeny. A new combination is proposed, *Parvodinium cunningtonii* comb. nov. and a new variety, *Parvodinium cunningtonii* var. *inerme* var. nov., is described.

Key words: dinoflagellates, flagellar apparatus, microtubular strand of the peduncle (MSP), SSU-ITS-LSU rDNA, *Peridiniopsis*, pusule

INTRODUCTION

The genus *Peridiniopsis* Lemmermann, as currently circumscribed in the most recent flora on freshwater dinoflagellates, is recognized as polyphyletic (Moestrup and Calado 2018). Fifteen species of *Peridiniopsis* are recognized in the flora, which are set apart from other peridinin-containing peridinioids by having a combination of six cingular plates and zero or one intercalary plates in the epitheca (Moestrup and Calado 2018). The general plate formula given for *Peridiniopsis* in Moestrup and Calado (2018) is po, x, 3–5′, 0–1a, 6–7″, 6c, 4–6s, 5‴, 2⁗. The formula allows for different combinations of numbers in different plate series and provides a practical but artificial means of classification of the group. As an example, molecular-based phylogenies recently revealed that the common freshwater species previously known as

Peridiniopsis elpatiewskyi (Ostenfeld) Bourrelly, which has no anterior intercalary plates, is a member of *Parvodinium* Carty (Kretschmann et al. 2019). With the transfer of *P. elpatiewskyi* to the genus *Parvodinium* the circumscription of that genus has stretched to include species without intercalary plates, in contrast to the presence of two anterior intercalary plates in all its previously recognized species (Carty 2008; Kretschmann et al. 2019; Moestrup and Calado 2018). Both *Parvodinium* and *Peridiniopsis* are currently assigned to the Peridiniopsidaceae, a monophyletic family that includes also the freshwater genus *Palatinus* Craveiro, Calado, Daugbjerg & Moestrup and the marine genus *Joshia* Z. Luo, Na Wang, K.N. Mertens & H. Gu (Gottschling et al. 2017; Luo et al. 2020; Pandeirada et al. 2022). An additional species, the marine dinoflagellate currently designated '*Scrippsiella*' *hexapraecingula* because of its three anterior intercalary plates, has also been shown to be a close relative of species of Peridiniopsidaceae; reinvestigation of this species may perhaps reveal a new genus of this family (Horiguchi and Chihara 1983; Luo et al. 2020).

In the original description of the Peridiniopsidaceae, the combined presence of six plates in the cingulum and up to two intercalary plates in the epitheca were two of the main features considered to discriminate members of this family from members of the Peridiniaceae (Gottschling et al. 2017). The internal cell features of the Peridiniopsidaceae were summarized by Pandeirada et al. (2022) based on detailed fine structure descriptions available for several of the members of the family. This included *Peridiniopsis borgei* Lemmermann (the type species of *Peridiniopsis*), *Palatinus apiculatus* (Ehrenberg) Craveiro, Calado, Daugbjerg & Moestrup (the type of *Palatinus*) and a species of the complex *Parvodinium umbonatum–P. inconspicuum* (which includes the type of *Parvodinium*; hereafter designated *P. umbonatum–inconspicuum*); and was complemented with more limited information available from *Joshia chumphonensis* Z. Luo, Na Wang, K.N. Mertens & H. Gu, *Parvodinium parvulum* (Wołoszyńska) Na Wang, K.N. Mertens & H. Gu and '*Scrippsiella*' *hexapraecingula* (Calado and Moestrup 2002; Craveiro et al. 2009; Horiguchi and Chihara 1983; Luo et al. 2020; Pandeirada et al. 2022). Currently known ultrastructural features of the Peridiniopsidaceae may be summarized as follows: the eyespot is of type A (with several layers of carotenoid-rich globules included in a chloroplast lobe) or B (like type A but covered on the sulcus side by a layer of vesicles with crystalloid

contents); the chloroplast lobes often show thylakoid-free areas and are arranged in an extensive radial network, usually extending from a large central pyrenoid (which is sometimes penetrated by cytoplasmic channels), surrounded or not by starch; an apical pore complex is usually present with an underlying apical fibrous complex (absent in *Palatinus*); an extruded peduncle is often present (visible in TEM; absent in *Palatinus*); an extensive, internally divided microtubular strand of the peduncle (MSP) is often present and extends to the peduncle (reduced and not reaching the cell surface in *Palatinus*); the pusule is variable, with different combinations of flat vesicles, cylindroid tubes and ramifying flat and tubular vesicles, with or without sac pusules; the basal bodies form an angle of 80–90º, each basal body associated with two microtubular roots; a layered connective (LC) links the dorsal side of the longitudinal microtubular root (root 1; LMR/r1) with the proximal posterior side of the transverse basal body (TB) and with a transverse striated root; the proximal end of the LMR/r1 connects, by two or three small fibres, to two or three triplets of the TB; the right-hand side of the longitudinal basal body (LB) associates with a single microtubule (single-straded microtubular root; SMR/r2); the transverse microtubular root (root 3; TMR/r3) nucleates variable numbers of microtubules (the microtubular extension of the TMR; TMRE/r3E) with variable paths and sometimes associated with fibrous material (forming a circle with a fibrous core in *P. borgei*); the proximal ends of the two basal bodies are usually not directly linked by a fibre (present only in *Palatinus*); the exit points of both flagella and peduncle are surrounded by prominent striated collars that are usually connected to one another by striated fibres (Pandeirada et al. 2022).

Herein we report on the external morphology and fine structure of two slightly different strains of peridinioids isolated from a flooded area of a stream located near Aveiro, central Portugal, both matching in shape and tabulation *Peridiniopsis cunningtonii* Lemmermann. Phylogenetic analyses based on rRNA gene sequences revealed that both these strains are closely related to *Parvodinium* species. A new combination in *Parvodinium* is proposed and a new variety described.

MATERIAL AND METHODS

Biological Material

Two cultures of dinoflagellates, preliminarily identifiable as *Peridiniopsis cunningtonii*, were started from cells isolated from plankton samples collected in Ribeiro da Palha (40°33.240′N, 8°34.095′W), a flooded stream near the village of Nariz, Aveiro, Portugal, on two different dates. One culture line, *P. cunningtonii* strain 1, was started from a single cell isolated into MBL culture medium (Nichols 1973) from a sample collected on 16 July 2015. Cells from strain 1 had the plate tabulation of *Peridiniopsis cunningtonii* but did not have the hypothecal spines characteristic of typical *P. cunningtonii*. A second culture line, *P. cunningtonii* strain 2, was started from a single cell, isolated from a sample collected on 17 October 2016, into quadruple concentration L16 medium supplemented with vitamins (Lindström 1991; Popovský and Pfiester 1990). Cells of strain 2 came from a field population that displayed the plate tabulation and hypothecal spines characteristic of typical *P. cunningtonii*, and cultured cells maintained these features until the culture was lost six months later. Both cultures were kept at 18°C and a 12:12 light:dark photoperiod with a photon flux density of ca. 25 µmol m^{-2} s^{-1}.

Light microscopy (LM)

Photographs were taken with a Zeiss Axioplan 2 imaging light microscope (Zeiss, Oberkochen, Germany) equipped with DP70 or ColorView IIIu Olympus cameras (Olympus, Tokyo, Japan). Cell division in *P. cunningtonii* strain 1 was recorded with a JVC TK-C1481BEG colour video camera (Norbain SD, Reading, UK) mounted on a Leitz Labovert FS inverted light microscope (Leica Microsystems, Wetzlar, Germany).

Scanning electron microscopy (SEM)

Three fixation protocols were used to observe different aspects of motile cells of *P. cunningtonii* strain 1. For clear observation of amphiesmal plates, cells were fixed by 1) mixing equal volumes of culture and ethanol 50%, for 40 min and 2) by mixing 0.95 ml of culture and 0.05 ml 2% aqueous OsO$_4$, for 5 min. Cells with the flagella in situ were obtained by fixing 3) a mixture of two volumes of culture and one volume of a 3:1 (v/v) mixture of aqueous 2% OsO$_4$ and saturated HgCl2, for 1 h. Fixed cells from all fixation

protocols were retained on Nuclepore polycarbonate filters with 5-μm pore size (Whatman, GE Healthcare Life Sciences, Maidstone, UK). Filters from fixations 2 and 3 were washed with distilled water for 30–45 min before dehydration in a graded ethanol series, together with filters from fixation 1. The dehydrated filters were critical-point-dried in a Baltec CPD-030 (Balzers, Liechtenstein), glued onto stubs and sputter-coated with gold-palladium. Cells were observed in the scanning electron microscopes Hitachi S-4100 (Hitachi High-Technologies, Tokyo, Japan) and JEOL JSM 6335F (Jeol, Tokyo, Japan).

Transmission electron microscopy (TEM)

Swimming cells from both cultures were fixed for 40–75 min in 2% glutaraldehyde made in phosphate buffer 0.1 M, pH 7.2 (final concentration). In addition, swimming cells from the culture of *P. cunningtonii* strain 2 were fixed in a mixture of 1% glutaraldehyde and 0.5% OsO_4 (final concentrations) in phosphate buffer 0.1 M, pH 7.2, for 25 min. The fixed cells were washed in phosphate buffer, included into 1.5% agar blocks, and postfixed with 0.5% or 1% OsO_4 (final concentrations) in the same buffer. After being washed in phosphate buffer and distilled water, the blocks were dehydrated through a graded ethanol series and propylene oxide, and embedded in low viscosity resin (Agar Scientific, Stansted, Essex, UK). The blocks were sectioned with an EM UC6 ultramicrotome (Leica Microsystems, Wetzlar, Germany). Ribbons of serial sections (70 nm thick) were transferred with slot grids to Formvar film and stained with uranyl acetate and lead citrate. Sections of three cells of *P. cunningtonii* strain 2 and three cells of strain 1 were observed in a JEM 1010 electron microscope (JEOL, Tokyo, Japan), equipped with a Gatan Orius digital camera (Gatan Inc., Pleasanton, California, USA).

Single-cell PCR amplification of LSU rDNA

Seven swimming cells from culture of *P. cunningtonii* strain 1 were isolated into a 0.2-ml PCR tube and frozen at –8ºC for 2 days. PCR amplification of partial LSU rDNA involved external primers D1R (Scholin et al. 1994) and 28-1483R (Daugbjerg et al. 2000), and a bead of illustraTM puReTaq Ready-To-Go PCR Beads kit (GE Healthcare, UK). The reaction was conducted in a thermocycler Biometra-Tprofessional (Biometra GmbH, Göttingen, Germany), with thermal profile as in Pandeirada et al.

(2014). The amount of amplified LSU rDNA was increased through nested PCR using 2 µl of the first PCR products and two primer combinations: D1R with D3A and D3B with 28-1483R. The thermal profile was the same as in Pandeirada et al. (2017). The nested-PCR products were purified using the QIAquick PCR Purification Kit (Qiagen, Hilden, Germany), and sent to Macrogen Europe (Amsterdam, Netherlands) for sequence determination with primers D1R, D2C, D3A, D3B and 28-1483R (Daugbjerg et al. 2000; Nunn et al. 1996; Scholin et al. 1994).

DNA extraction and PCR amplifications of SSU rDNA, ITS rDNA and LSU rDNA

About 50 swimming cells from each *P. cunningtonii* culture were submitted to DNA extraction with the QuickExtract^TM FFPE DNA Extraction Kit (epicentre, Illumina, San Diego, California, USA), following the manufacturer's instructions. Two microlitres of extracted DNA were used in all PCR amplifications conducted. Amplification of LSU rDNA of *P. cunningtonii* strain 2 was as described above for strain 1 with the single modification of using the specific Dino-ND primer (Hansen and Daugbjerg 2004) instead of the 28-1483R primer, in both initial and nested PCRs. Amplifications of SSU rDNA and ITS rDNA of *P. cunningtonii* strain 1 were based on Takano and Horiguchi (2005) but going directly to the second round of PCR amplification. The products from all PCR amplifications were purified with the QIAquick PCR Purification Kit (Qiagen, Hilden, Germany), and sent to Macrogen Europe (Amsterdam, The Netherlands) for sequencing of SSU rDNA and ITS rDNA from *P. cunningtonii* strain 1, with primers as in Takano and Horiguchi (2005), and for sequencing of LSU rDNA from *P. cunningtonii* strain 2 using D1R, D2C, D3A, D3B and Dino-ND (Hansen and Daugbjerg 2004; Nunn et al. 1996; Scholin et al 1994).

Sequence divergence

PAUP* (ver. 4.0a, build 169) was used to estimate the divergence between the partial sequences of the nuclear-encoded LSU rDNA of the two strains (Swofford 2002).

Phylogeny

Two sequence data matrices were prepared to infer the phylogeny of the two isolates of *P. cunningtonii*. The first comprised partial sequences of nuclear-encoded

LSU rDNA (1,635 base pairs including introduced gaps) from *P. cunningtonii* strain 2 and *P. cunningtonii* strain 1 together with a diverse assemblage of dinoflagellates (52 genera, 84 different taxa). Ciliates, apicomplexans and *Perkinsus* formed the outgroup taxa. For the second analysis based on concatenation of the ribosomal operon (3,923 base pairs including introduced gaps of partial SSU rDNA, ITS 1, 5.8S rDNA, ITS 2 and partial LSU rDNA) only the strain 1 was included together with some of the most closely related lineages inferred from the LSU rDNA-based phylogeny. However, due to lack of sequence data, '*Peridinium inconspicuum*' and '*Peridinium centenniale*' were replaced with *Parvodinium trawinskii* Kretschmann, Owsianny, Zerdoner & Gottschling and *P. marciniakii* Kretschmann, Owsianny, Zerdoner & Gottschling. Therefore, the LSU rDNA phylogeny comprised a total of 12 *Parvodinium* sequences whereas the concatenated included 10 *Parvodinium* sequences. Other included dinoflagellates belonged to e.g., *Palatinus*, *Peridinium* Ehrenberg, *Johsia* and *Scrippsiella* Balech. Two species of *Heterocapsa* F.Stein formed the outgroup. See Pandeirada et al. (2022) for information on alignments and sequence editing. Two approaches were applied for phylogenetic inference: Bayesian analysis (BA) and RAxML as implemented in Geneious (ver. 2022.1.1). Common for both BA (ver. 3.2.6 of MrBayes by Huelsenbeck and Ronquist (2001)) 5 million generations were run with a tree sampled every 1,000 generations. The burn-in length was set at 500,000 leaving 4,501 trees for consensus trees. Specifically for the concatenated data matrix, each genetic marker was divided into five partitions (SSU, ITS1, 5.8S, ITS2 and LSU) and allowed to evolve under different models of sequence evolution by applying the 'unlink' option in the command script. For RAxML (ver. 8, Stamatakis 2014) the GTR GAMMA I option was used with both alignments and 1,000 bootstrap replications were included to evaluate the robustness of the tree topologies. These values were mapped onto BA trees.

RESULTS

The external morphology of strain 2 agrees with the morphology of typical *Peridiniopsis cunningtonii*. In contrast, strain 1 shows a slight difference in LSU rDNA sequence and a constant, apparently inheritable, difference in morphology from strain 2, which we consider worthy of formal recognition at variety level within *P. cunningtonii*. In our phylogenetic analyses both strains resolved in the same clade as *Parvodinium*

species, justifying a new combination in *Parvodinium*. To avoid confusion in referring to the two strains in the following text we will use the names formally established later in the article: *Parvodinium cunningtonii* for strain 2, and *P. cunningtonii* var. *inerme* var. nov. for strain 1 (see Taxonomic summary).

The cultures of both strains were unialgal and presumably monoclonal since they both resulted from single cells. These cultures diverged markedly in asexual growth. Gamete fusion was not detected in either strain, despite the observation of cysts in cultures of *Parvodinium cunningtonii* var. *inerme* var. nov. Cyst formation and germination were not followed. *Parvodinium cunningtonii* var. *inerme* has been in culture for about seven years and has usually high numbers of motile cells. *Parvodinium cunningtonii* var. *cunningtonii* persisted in culture only for about half a year, always with very low numbers of motile cells and without the formation of cysts.

Cell morphology of *Parvodinium cunningtonii* var. *inerme* var. nov.

Motile cells and cysts are shown in Figs. 1 and 2. Cells were ovoid to pyriform and somewhat compressed dorsoventrally (Figs. 1A–D; 2A–C). The epicone was conical, with an apical pore complex (apc) in the prominent apex, and was longer than the round to conical, antapically pointed hypocone (Figs. 1A–D; 2A–F). The submedian cingulum was almost circular (Figs. 1A–D; 2A–C; 2F). The sulcus penetrated somewhat the epicone, and extended also toward the antapex (Fig. 2A, B, F). Cells were 24.1 ± 2.9 μm long (range 17.7–30.0 μm; n = 60), 17.1 ± 2.4 μm wide (range 11.8–20.7 μm; n = 41), and 14.4 ± 0.9 μm thick (range 12.7–16.4 μm; n = 14).

Chloroplast lobes were yellowish-brown and radiated from a central pyrenoid to the cell periphery (Fig. 1A–D). One accumulation body (ac) was sometimes notorious above the central pyrenoid (Fig. 1B). The nucleus was ellipsoid and occupied most of the hypocone (Fig. 1B, D). A rectangular, orange eyespot, somewhat slanted relative to the longitudinal axis of the cell, 3.0–4.5 μm long (n = 12), was present in the upper part of the sulcus (Fig. 1A, C).
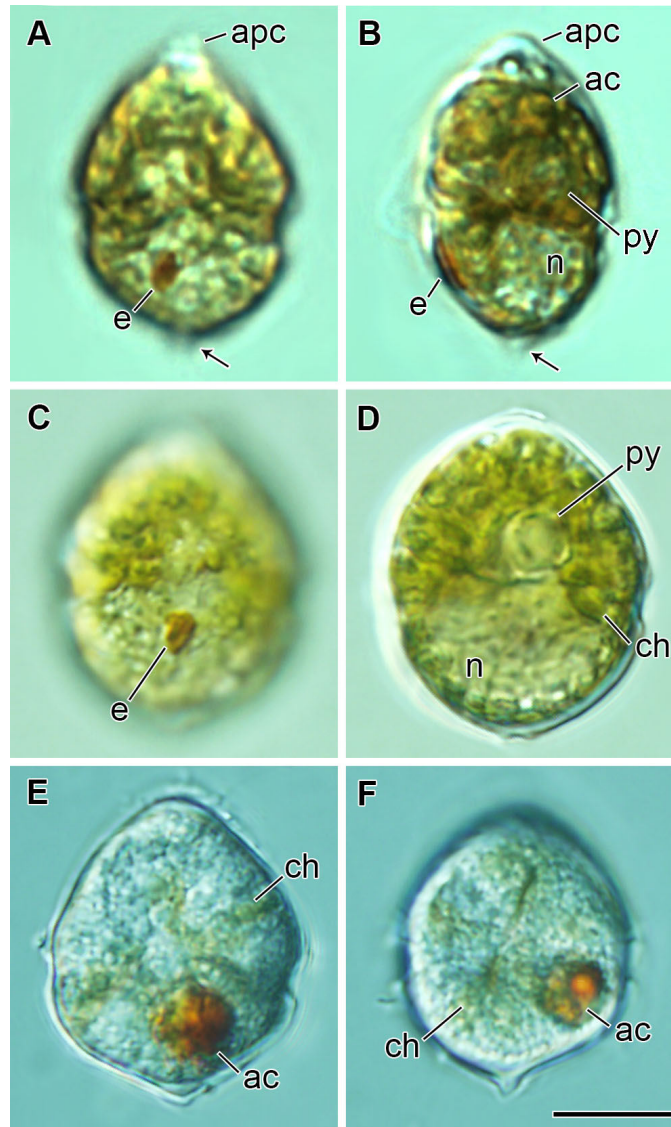
Fig. 1. *Parvodinium cunningtonii* var. *inerme* var. nov., LM. (**A, B**) Ventral and left-lateral views of vegetative cell showing the pointed antapical end (arrow), the apical pore complex (apc), the eyespot (e), the nucleus (n) in the hypocone, and the pyrenoid (py) and accumulation body (ac) in the epicone. (**C, D**) Vegetative cell focused in different planes showing the eyespot (e), the nucleus (n) and chloroplast lobes (ch) radiating from the central pyrenoid (py). (**E, F**) Cysts smooth-walled, with similar shape as the vegetative cells. Cyst contents are predominantly colourless with faint traces of chloroplast lobes (ch) and a large accumulation body (ac). All to the same scale. Scale bar: 10 μm.

The plate tabulation was po, cp, x, 4′, 1a, 6″, 6c, 5s, 5‴, 2⁗ (Kofoidian notation). The epitheca included four apical plates, six precingular plates, and a single intercalary plate (1a) on the left-dorsal side (Fig. 2A–D). Some variation of the epithecal tabulation was observed; out of 27 cells analysed, 21 had the usual plate tabulation (4′, 1a), two cells had four apical and zero intercalary plates (4′, 0a; not shown) and four cells had

five apical and zero intercalary plates (5′, 0a; Fig. 2E). Three plates formed the apc: a central cover plate (cp) encircled by the pore plate (po), and a rectangular canal plate (x) tightly appressed to the ventral side of po (Fig. 2D, E). On the hypotheca there were two antapical plates (1⁗ and 2⁗) of similar size, and five postcingular plates, of which 3‴ was the largest and 5‴ the smallest (Fig. 2A–C, F). The sulcus was composed by five plates: an anterior sulcal plate (as) extending somewhat into the epitheca; a larger, posterior sulcal plate (ps) extending to the antapex; a right sulcal (rs) plate extending as a flap, hiding the exit pores of the flagella and peduncle, and partially overlapping the left (ls) and the small accessory sulcal plates (acs) (Fig. 2A, B, F). Six plates formed the cingulum, of which the first plate (c1) was shorter and partially included in the anterior-left side of the sulcus (Fig. 2A–C, F). The sixth cingular plate (c6) descended slightly distally by nearly half the cingulum width (Fig. 2A, B). The limits of this plate (c6) coincided roughly with the limits of the sixth precingular (6″) and fifth postcingular (5‴) plates; similarly, the limits of plates c4 and c5 were coincident with those of postcingular plates 3‴ and 4‴, respectively (Fig. 2A–C, F). An antapical projection (apiculus), 0.5–1.8 μm long (n = 15), typically occurred in plate 1⁗, near the suture with plate 2⁗, or right at the suture between antapical plates (Fig. 2B, C, F).

Plates were smooth and the observed sutures were thin. Trichocyst pores occurred throughout the cell surface but were absent from the apc and from the right and left sulcal plates (Fig. 2B–F). Cells that stopped swimming exited the theca through the dorsal side, with at least the fourth precingular plate being discarded (not shown).

Cyst walls were smooth and matched the shape of the motile cells (a pointed cyst with submedian paracingulum); they were almost colourless with faint traces of chloroplast lobes and contained an orange-red accumulation body (Fig. 1E, F). Cysts were 20.5–28.0 μm long and 13.5–24.0 μm wide (n = 27).
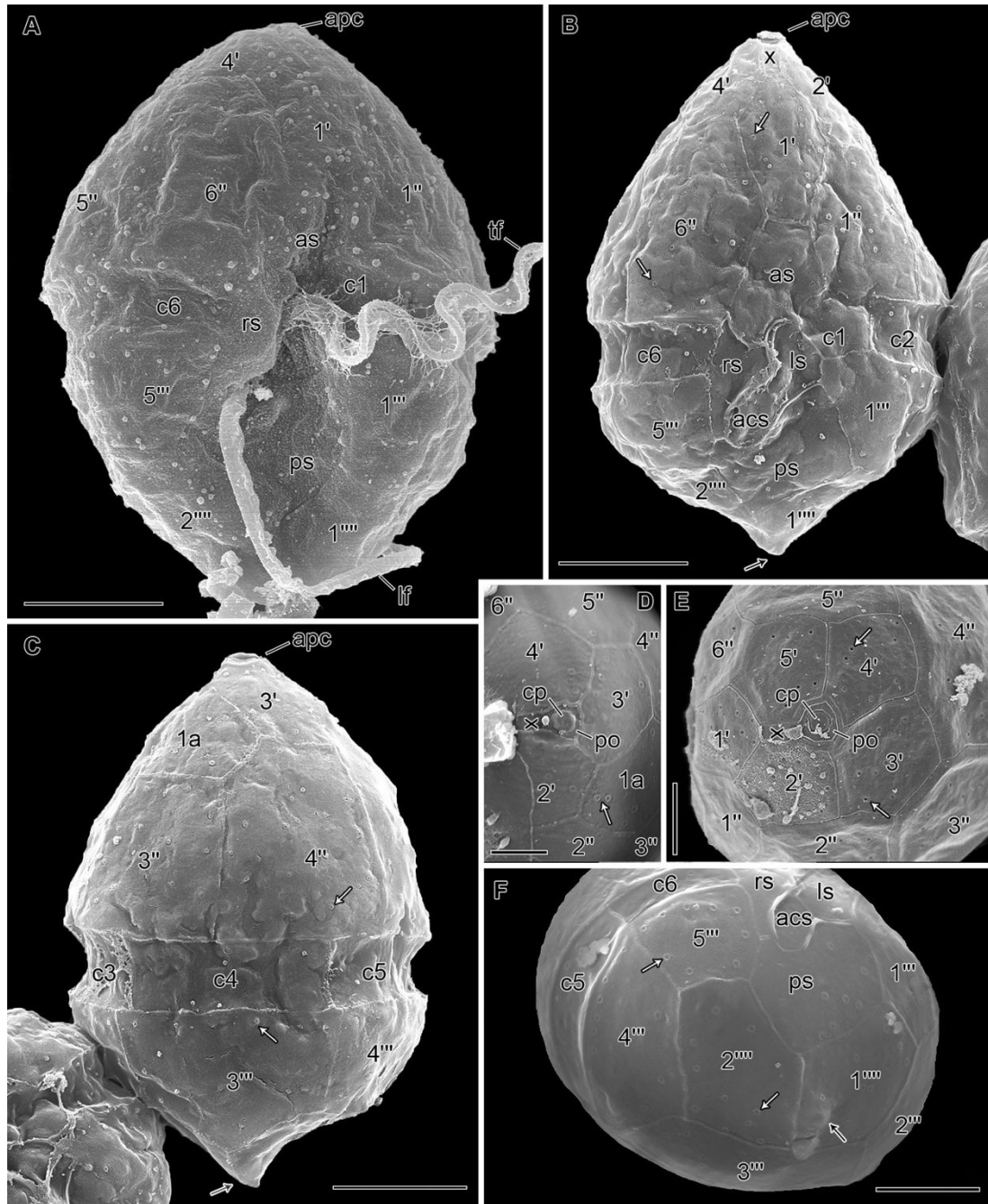
Fig. 2. *Parvodinium cunningtonii* var. *inerme* var. nov., SEM. Plates are labelled in Kofoidian notation. (**A**) Ventral view of a cell with preserved outer membranes and transverse (tf) and longitudinal flagella (lf), prepared with fixation 3. (**B–C**) Ventral and dorsal/right view of cells prepared with fixation protocol 2. Five plates form the sulcus: anterior (as), right (rs), left (ls) and posterior (ps) sulcal plates, plus smaller accessory sulcal plate (acs) (seen in A, B, F). (**D–E**) Apical views of cells prepared with fixation 1, showing the typical tabulation with one intercalary plate (in D) and one variation with five apical plates and no intercalary plate (in E). Apical pore complex (apc) with pore plate (po), cover plate (cp) and canal plate (x). (**F**) Antapical view of a cell prepared with fixation 2. The pointed antapical end is indicated by a black arrow and trichocysts pores by white arrows. Scale bars: 5 μm (A–C, F); 3 μm (D, E).

Cell division in *Parvodinium cunningtonii* var. *inerme* var. nov.

Division stages were observed in immobile cells that were isolated from the bottom of the culture batches into separate wells with culture medium and followed under the inverted microscope. These immobile cells were morphologically similar to motile cells, except for the absence of flagella (Fig. 3A), and were more abundant during the first two or three hours of the light phase. The nucleus of these cells migrated from the hypocone to the epicone over a period of 1–3 h (Fig. 3A, B), followed by nuclear division that progressed for about 4 h (Fig. 3C, D). Cytokinesis started shortly after the two separated nuclei were clearly visible in the cell, with a cleavage furrow progressively extending to the area between the nuclei (Fig. 3D, E). About 1.5 h since the cleavage furrow started to become visible, the incompletely divided daughter cells emerged, with a gentle amoeboid movement, through the dorsal side of the theca, at the level of the cingulum (Fig. 3F–H). The released, incompletely divided cells showed two separate hypocones, each one with a nucleus and an eyespot (e), and only one epicone and one cingulum (Fig. 3F, H). Two longitudinal flagella and one or two transverse flagella were usually present, but they were not in the furrows at this stage. The dividing cell remained motionless for a few seconds and sunk; it started to swim after the flagella were accommodated in the cingulum and both sulci (Fig. 3G, H). This swimming stage continued for about 6 h, up to the first 3–4 h of the dark phase. The division and final separation of the two cells was never observed, showing that the complete process of division was very long (more than 15 h). Similar swimming stages were observed in the culture throughout the light and dark phases, with more or less developed thecal plates that were shed during temporary stops (Fig. 3I). No evidence of fusion of cells, or planozygotes (flagellated cells with two sulcal flagella) was ever observed in this culture. The cysts that were observed were perhaps of asexual origin.

Cell morphology of *Parvodinium cunningtonii* var. *cunningtonii*

Motile cells and empty thecae, with plates marked in Kofoidian notation, are shown in Fig. 4. Cells were ovoid and somewhat compressed dorsoventrally (Fig. 4A–J, L, M). The epicone was conical, topped with an apical pore complex (apc) and slightly longer than the rounded-trapezoidal hypocone, which presented antapical and postcingular spines (Fig. 4). The cingulum was almost circular (Fig. 4C–E, M). The sulcus

penetrated the epicone and extended toward the antapex (Fig. 4E, H, M). Cells were 26–32 μm long (n = 12) and 19–25 μm wide (n = 10).

Chloroplast lobes were yellowish-brown and radiated from the centre of the cell to the periphery; a pyrenoid was not clearly visible in LM. One accumulation body (ac) was usually prominent in the epicone (Fig. 4A–D). In the upper part of the sulcus, there was a rectangular dark-orange eyespot (e) somewhat slanted relative to the cell axis, 3.5–4.0 μm long (n = 5) (Fig. 4A–D). The nucleus (n) was ellipsoid and occupied part of the hypocone (Fig. 4D).

The plate tabulation was po, cp, x, 4′, 1a, 6″, 6c, 5s, 5‴, 2⁗. No variations were detected in the number of intercalary and apical plates in the cells observed. All plates were lightly reticulated, and sometimes separated by wide sutures; the hypothecal plates were ornamented with spines. In most cells all postcingular and antapical plates, except plate 3‴, had at least one spine (Fig. 4E–J, L, M). The longest spines were in the antapical plates (1⁗ and 2⁗) and were up to 5 μm long.
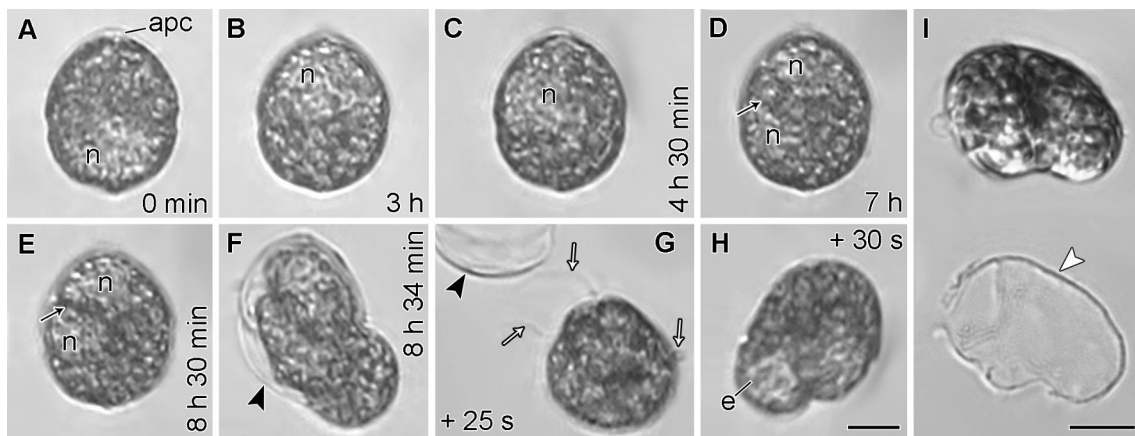
Fig. 3. *Parvodinium cunningtonii* var. *inerme* var. nov., LM. (**A–H**) Division of an immobile cell. Image-series from video recording, with elapsed time indicated. (**A**) Cell without flagella with the nucleus (n) in the hypocone. apc, apical pore complex. (**B–E**) Nuclear migration to the epicone, where mitosis took place. A cleavage furrow is seen (D, E) between the two nuclei formed. (**F–H**) Incompletely divided daughter cells exited the theca (arrowhead). Arrows point two longitudinal flagella and transverse flagellum in G. The eyespot in one hypocone is visible (e, in H). (**I**) Another cell in division that stopped swimming and exited the theca (arrowhead). Scale bars: 10 μm.
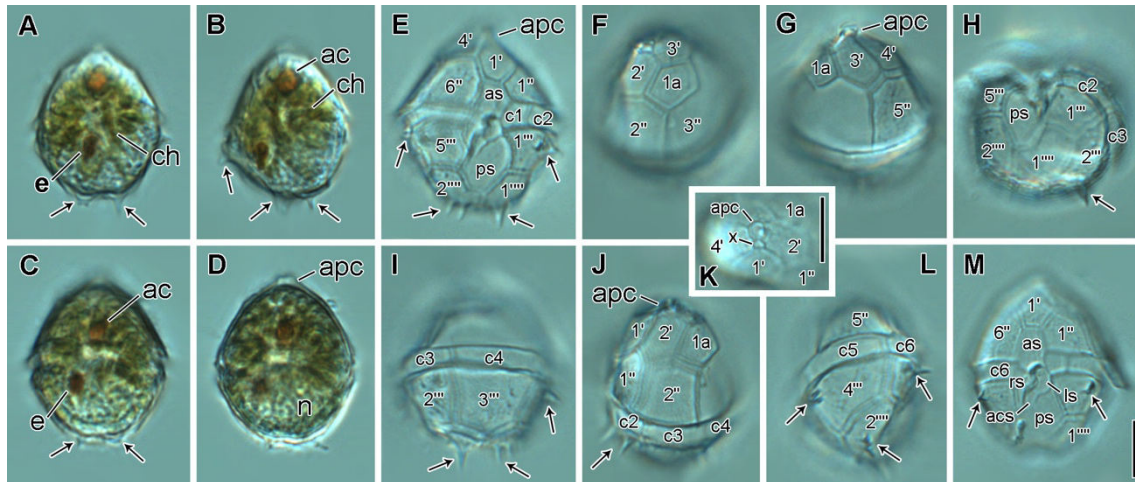
Fig. 4. *Parvodinium cunningtonii* var. *cunningtonii*, LM. (**A, B**) Ventral and left-ventral views of one cell with chloroplast lobes (ch) radiating from the centre, an accumulation body (ac) in the epicone and the eyespot in the sulcal region. Antapical and postcingular spines are prominent (arrows). apc, apical pore complex. (**C, D**) Ventral view and optical section of a cell with short spines in the hypotheca, the nucleus (n) in the hypocone, the eyespot (e) and accumulation body (ac); the apical pore complex (apc) is indicated. (**E–L**) Empty theca in different views showing plates labelled in Kofoidian notation. Antapical and postcingular plates with prominent spines (arrows). The apical pore complex (apc) includes a short canal plate (x). (**M**) Ventral view of a different theca with two postcingular spines (arrows) visible. The five sulcal plates are indicated: anterior (as), right (rs), left (ls), posterior (ps) and the smaller accessory sulcal plate (acs). Scale bars: 10 μm; (A–J, L, M) to the same scale.

General fine structure (TEM)

The general fine structure observed in cells of the two strains was similar (Fig. 5). The ellipsoid nucleus was in the mid-dorsal side of the hypocone (Fig. 5A). Chloroplast lobes (ch), with thylakoids in groups of three per lamella, radiated in all directions from a prominent pyrenoid (py) located in the epicone; at the periphery of the cell, the chloroplast lobes extended tangentially, covering most of the cell surface (Fig. 5A, D, E). The pyrenoid was surrounded by starch (st) and its matrix was perforated by numerous, scattered cytoplasmic channels, mostly ca. 40 nm in diameter; pusular elements were also observed in a few, wider cytoplasmic channels (Fig. 5E, F). Trichocysts (t) were usually present in the peripheral cytoplasm (Fig. 5A, C, E). Starch grains were scattered in the cell but were more numerous in the hypocone, whereas oil droplets (o) were more abundant in the epicone (Fig. 5A). An eyespot, consisting of four to five layers of globules inside the ventral surface of a chloroplast lobe, was

present in the sulcus (Fig. 5A, B). Each individual globule measured 100 to 120 nm in diameter.

Longitudinal sections through the apical pore complex (apc) exposed an apparently continuous fibrous layer (Fig. 6A–D) underlying the pore plate (po). The posterior portion of the fibrous layer subdivided into several somewhat striated fibers that extended along the peripheral cytoplasm for about 500 nm (arrowheads in Fig. E). The cytoplasm of this apical region was rich in irregularly shaped vesicles with clear contents and elongated necks that extended toward the cover plate (white arrows in Fig. 6A–C).

Pusular system

In both *Parvodinium cunningtonii* strains, two sets of pusular elements (membrane-bounded compartments wrapped in a vesicle) were observed, each one associated with one of the flagellar canals (Figs. 7; 8E; 9B, C; 10A, B, H; 11E; 12A). One pusular tube (pu), more or less flattened in some regions, opened at the transverse flagellar canal (TFC) and extended to the dorsal-right side of the cell with several ramifications (Figs. 7A, C–E; 10A, B). At least one of these ramified pusular tubes extended into the pyrenoid and was visible inside cytoplasmic channels that penetrated chloroplast lobes and the pyrenoid (Figs. 5E, F; 7A, F). This pusular tube, near the connection to the TFC, was ca. 300 nm wide and had the three pusular membranes usually closely appressed (Figs. 9B, C; 10A, B); in other portions, along the extension of the ramified pusular tube, the surrounding vesicle had numerous fenestrations, resulting from links between its outer and inner membranes, which left the inner membrane of the pusule in contact with the cytoplasm (arrows, Fig. 7B). Some portions of the pusular tube were internally lined by electron-opaque granules ca. 15 nm in diameter (Figs. 5F; 7E, F). Connected to the longitudinal flagellar canal (LFC), there was a pusular vesicle (puv), slightly collapsed and with an irregular shape, that ramified and extended c. 3.5 µm toward the centre of the cell (Figs. 7G; 8E; 10H). The lumen of this puv included several vesicles with irregularly-shaped granulated bodies (arrowheads in Figs. 7G; 8E; 10H).
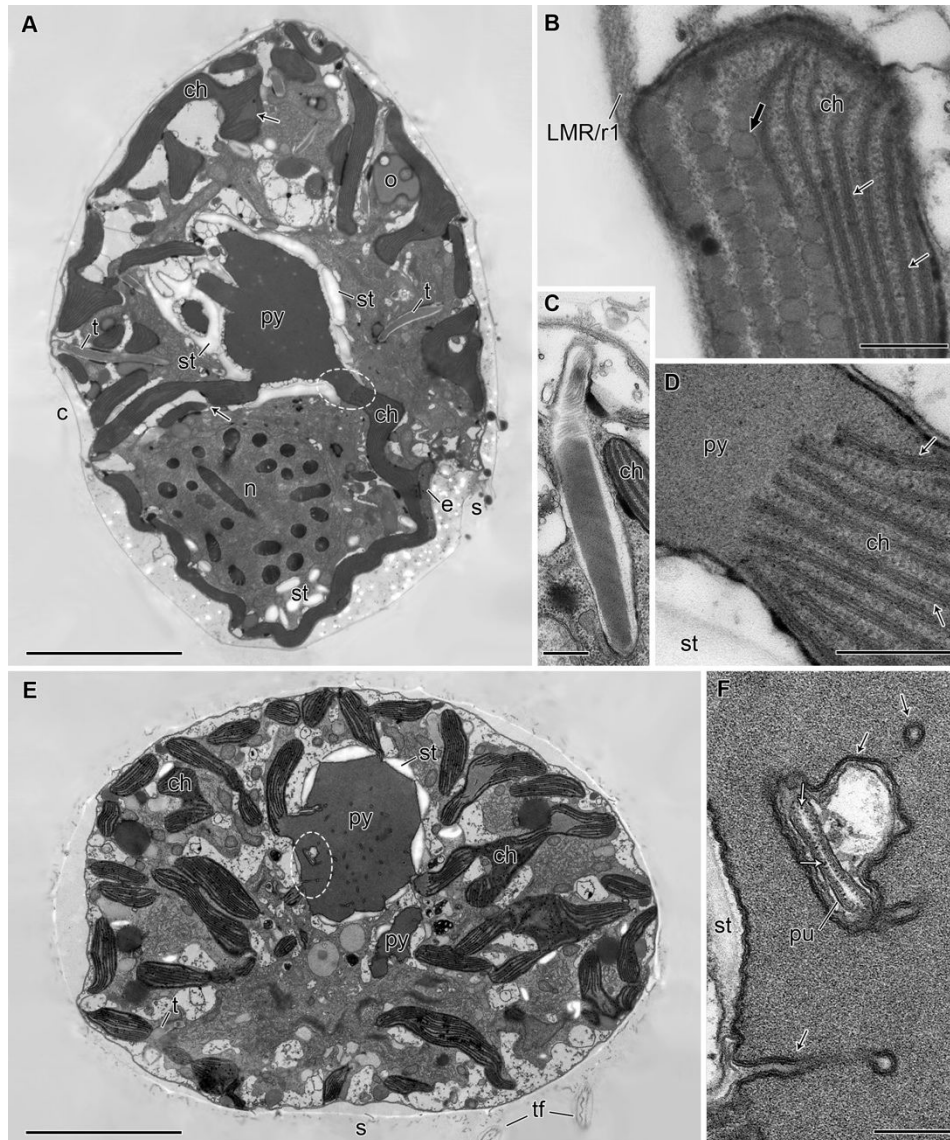
Fig. 5. *Parvodinium cunningtonii* var. *inerme* var. nov. (**A–D**) and *P. cunningtonii* var. *cunningtonii* (**E, F**), general ultrastructural features, TEM. (**A**) Longitudinal section of a cell view from the right side, showing the position of the nucleus (n) and chloroplast lobes (ch) radiating from the central pyrenoid (py). Ramifications and thylakoid-free areas visible in radiating lobes (arrows). e, eyespot; t, trichocysts; o, oil droplets; st, starch; c, cingulum; s, sulcus. (**B**) Detail of eyespot with four adjacent rows of globules (thick arrow) disposed along the ventral surface of a chloroplast lobe, in front of the thylakoids (thin arrows). The longitudinal microtubular root (LMR/r1) lays between the cell surface and the chloroplast lobe. (**C**) Longitudinal section of a trichocyst. (**D**) Chloroplast lobe (ch) radiating from the central pyrenoid (py) complex (ellipse in A), showing the three-thylakoid lamella (arrows). (**E**) Transverse section in apical view of a cell sectioned above the cingulum level showing the chloroplast lobes (ch) radiating from the pyrenoid (py) surrounded by starch (st). s, sulcal area; tf, transverse flagella. (**F**) Magnification of pyrenoid matrix (ellipse in E) traversed by cytoplasmic channels (black arrows); the larger cytoplasmic channel includes a pusular element (pu) with dotted lumen (white arrows). Scale bars: 5 µm (A, E); 300 nm (B–D, F).

190
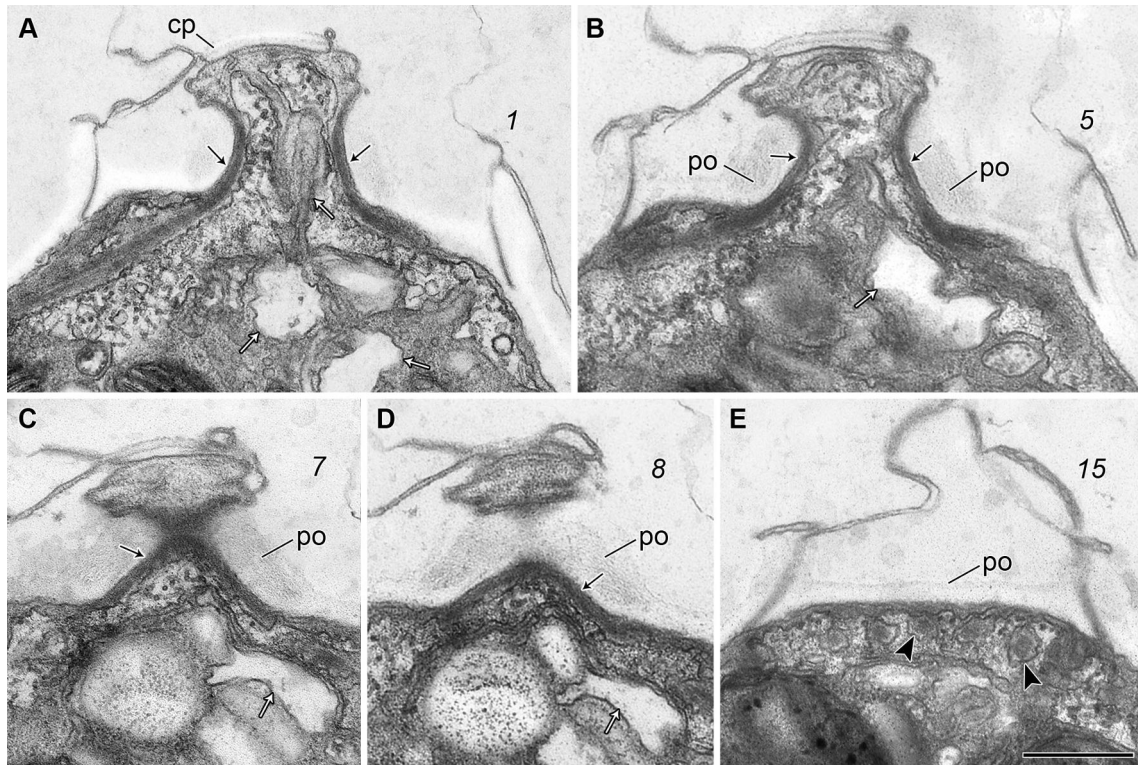
Fig. 6. *Parvodinium cunningtonii* var. *cunningtonii*, apical pore complex, TEM (initial fixative containing OsO₄). Non-adjacent oblique-longitudinal serial sections, proceeding from the anterior-right side of the cell. Slanted numbers represent section numbers. (**A, B**) Sections through the pore plate (po) with enclosed cytoplasm, and the cover plate (cp). Fibrous layer is marked (black arrows) underneath the po and extending to the apical-most cytoplasm. Several vesicles extend towards the cp (white arrows). (**C, D**) Tangential sections through the pore plate (po) and the cover plate (cp), showing fibers (black arrows) and vesicles (white arrows). (**E**) Individualized fibers (arrowheads) in cross section underneath the Po. Scale bar: 500 nm.

Flagellar apparatus

The flagellar apparatus of the two strains was identical and is here shown in series of sections from a cell of *Parvodinium cunningtonii* var. *inerme*, advancing from the apex to the antapex of the cell (Fig. 8A–H) and from two cells of *P. cunningtonii* var. *cunningtonii*, one also sectioned from the apex to the antapex but slightly tilted to the right (Fig. 10A–H) and a second one sectioned from right to left (Fig. 11A–E). The two basal bodies formed an angle of about 90º, as inferred from serial sections, and had their proximal ends almost touching (Fig. 8E). The points of emergence of the transverse and longitudinal flagella (TF and LF, respectively) were surrounded by rings of striated material (the TSC and LSC, transverse and longitudinal striated collar, respectively).

The transverse basal body (TB) was associated with two microtubular roots. A single microtubule, the transverse microtubular root (TMR/r3), curved along the anterior-ventral side of the transverse flagellar canal (TFC), near a small row of collared pits (arrowheads in Fig. 8B, C), and associated with the anterior-dorsal base of the TB (Figs. 8B–D; 10B; 11B). In its distal end, the TMR nucleated a strand of ca. 22 microtubules, the so-called transverse microtubular root extension (TMRE/r3E), which followed the anterior side of the TFC and then curved along its dorsal side into a posterior direction (for about 1.5 μm), until it suddenly turned to the dorsal side of the cell (Figs. 9A–C; 11C–E; 12A). The second microtubular root associated with the TB was a single microtubule running alongside a striated fibre (TSR and TSRM/r4); the TSR was ca. 40 nm thick and together with the TSRM/r4 extended from the proximal-dorsal side of the TB for about 400 nm toward the TSC (Figs. 8G, H; 9A; 10B, C). The longitudinal basal body (LB) was also linked to two microtubular roots: a single-stranded microtubular root (SMR/r2) that started near the proximal-right side of the LB and curved slightly into a dorsal-posterior direction for about 550 nm; the second microtubular root was a strand of ca. seven microtubules (the longitudinal microtubular root, LMR/r1) that associated with the proximal-left side of the LB and curved slightly into a dorsal-posterior direction, in a roughly parallel route to the SMR/r2; the number of microtubules increased posteriorly to about 30, which came to lie underneath the cell surface down to the level of the eyespot (Figs. 5B; 7D, G; 8F–H; 9A–C; 10E–H; 11B). The two basal bodies were indirectly linked by a layered structure, the so-called layered connective (LC), which in transverse section was ca. 74 nm thick, 105 nm wide and 280 nm long. The LC was made of two electron-opaque layers separated by a more electron-translucent layer, and contacted with its anterior surface the TB, and with the posterior surface an electron-opaque layer of material that covered the dorsal side of the LMR/r1 (Figs. 8G–H; 11B). The proximal end of the TSR and TSRM/r4 also contacted the anterior layer of the LC. Two or three small fibres linked the dorsal face of the proximal end of the LMR to two or three triplets of the posterior side of the TB (Fig. 11B).
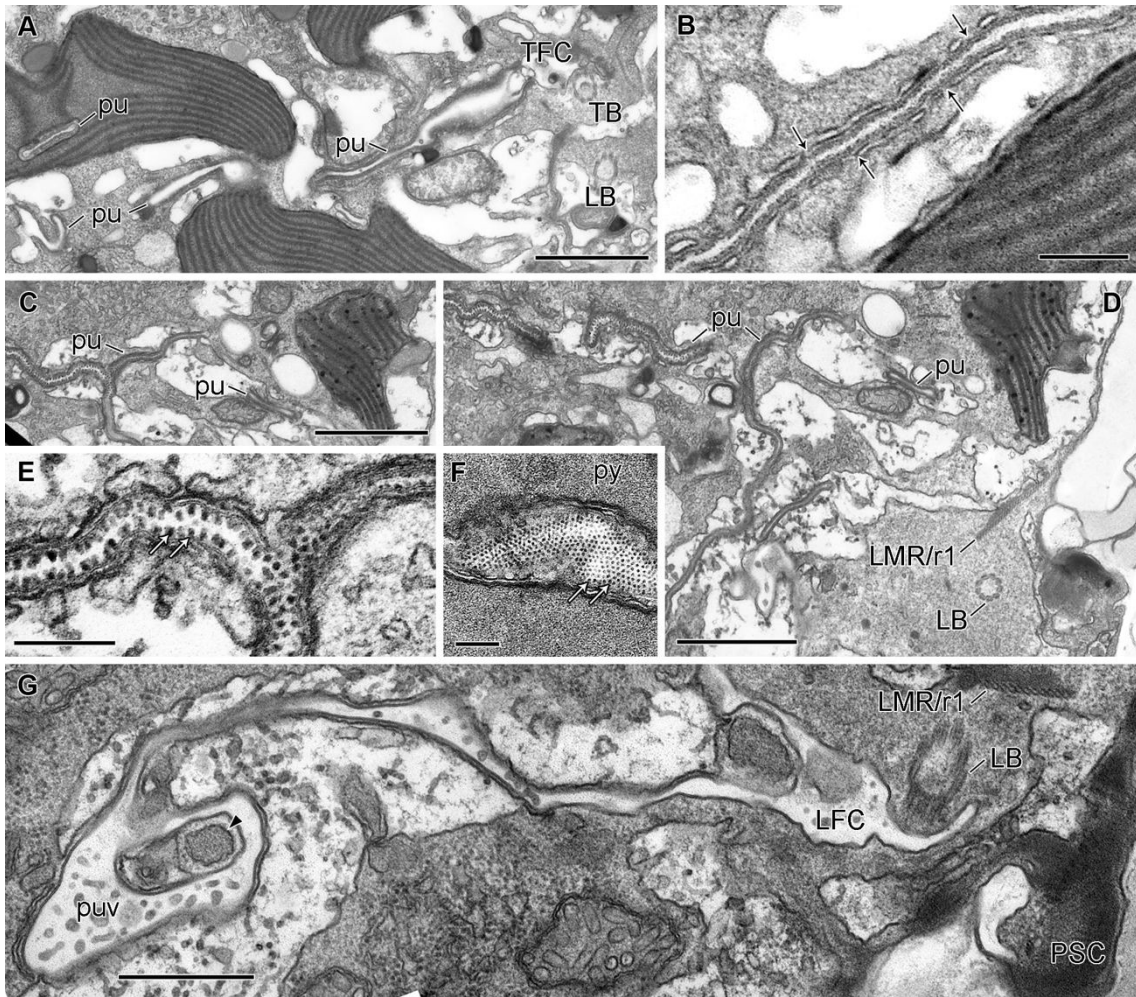
Fig. 7. *Parvodinium cunningtonii* var. *inerme* var. nov. (**A, B**) and *P. cunningtonii* var. *cunningtonii* (**C–F**), pusular system, TEM. (**A**) Pusular tube (pu) connecting to the transverse flagellar canal (TFC) and extending from the ventral area to the centre of the cell. A portion of the pusular tube is seen included in a chloroplast lobe. TB, transverse basal body. (**B**) Detail of pusular tube with the enveloping vesicle, showing fenestrations (black arrows). (**C, D**) Pusular flattened tubes (pu) ramify and extend from the ventral region to the interior of the cell. (**E**) Detail of ramified portion of the pusular tube with dotted contents (arrows). (**F**) Tangential section through a pusular tube with dotted content (arrows) that penetrates the pyrenoid (py). (**G**) Pusular vesicle (puv) with vesicle including a granulated body (arrowhead), associated to the longitudinal flagellar canal (LFC). LB, longitudinal basal body; LMR/r1, longitudinal microtubular root; PSC, peduncle striated collar. Scale bars: 1 μm (A, C, D); 200 nm (B, E, F); 500 nm (G).
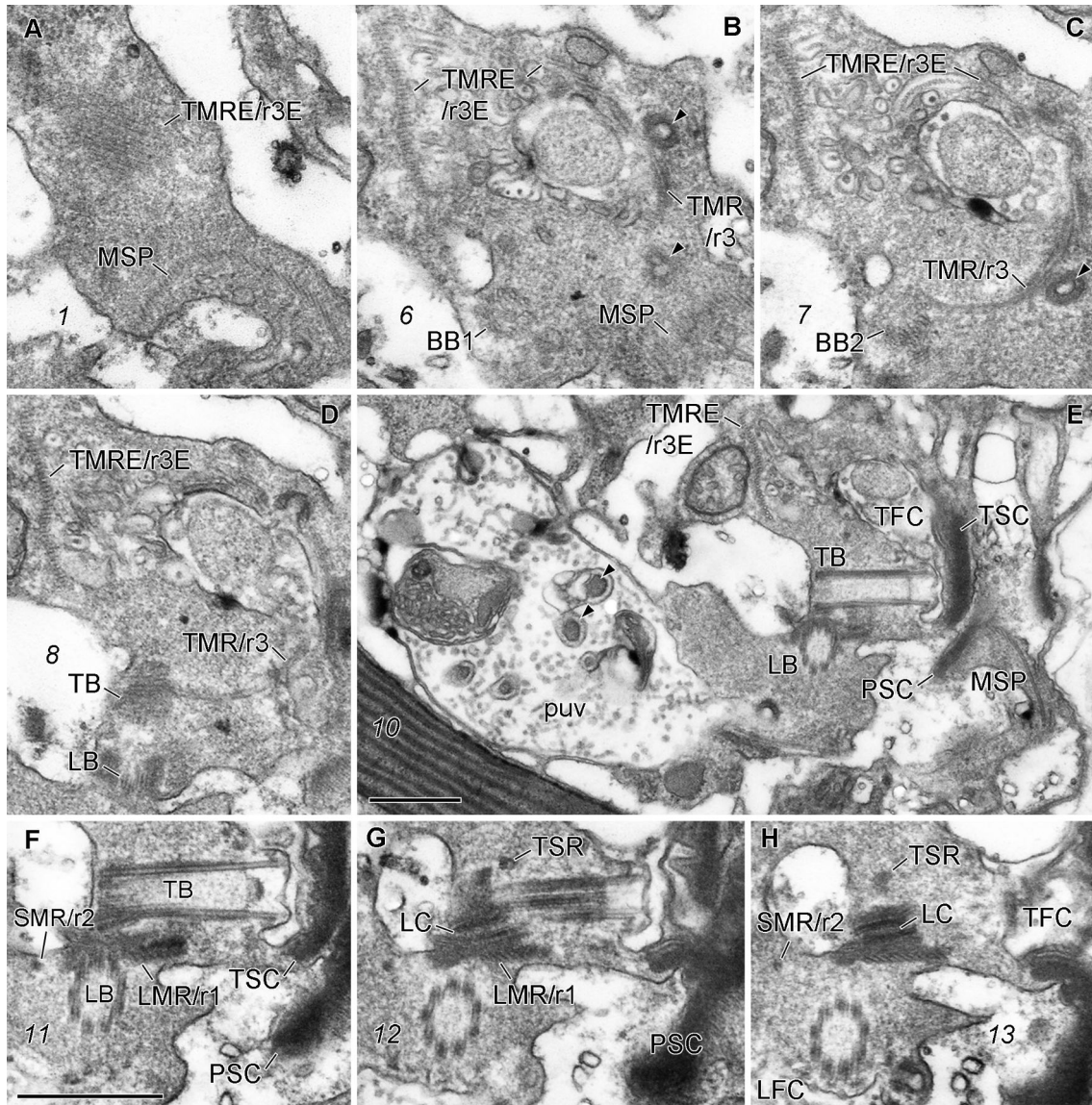
Fig. 8. *Parvodinium cunningtonii* var. *inerme* var. nov., flagellar apparatus, TEM. Non-adjacent serial sections progressing from the apex to the antapex of a cell slightly tilted to the dorsal side. Slanted numbers indicate the section number. (**A–D**) The microtubular strand of the peduncle (MSP) and the transverse microtubular root extension (TMRE/r3E) are seen progressing to the basal bodies. The transverse microtubular root (TMR/r3) that nucleates the TMRE/r3E, is seen near collared pits (arrowheads) and ending near the transverse basal body (TB). Two replicated basal bodies (BB1, BB2) are visible in B and C. (**E**) Both basal bodies, the TB and the longitudinal basal body (LB), and the MSP are visible as well as the transverse striated collar (TSC) and the peduncle striated collar (PSC). A large pusular vesicle (puv), emerging from the longitudinal flagellar canal and including vesicles with granulated bodies (arrowheads), is shown. (**F–H**) The single-stranded microtubular root (SMR/r2) and the longitudinal microtubular root (LMR/r1) are present on the left and right side of the LB, respectively. The layered connective (LC) appears between the LB and TB. TSR, transverse striated root. Scale bars: 500 nm; (A–D, F–H) to the same scale.

Peduncle and microtubular strand of the peduncle (MSP)

An extruded peduncle was observed in sections of both *Parvodinium cunningtonii* var. *cunningtonii* and *P. cunningtonii* var. *inerme* (Figs. 9A; 10G; 11D). The peduncle was composed by cytoplasm lined by a single-membrane, and included a group of ca. 20 microtubules, the so-called microtubular strand of the peduncle (MSP). The peduncle extruded through a collar of fibrous material, the so-called peduncular striated collar (PSC) and extended to the exterior of the cell through a narrow canal, ca. 1.3 µm long x 0.4 µm high x 0.25 µm wide, lined by 4–6 platelets with a somewhat fibrous aspect, different from that of larger plates (Fig. 10G, H). Outside the cell, the peduncle was up to 3.5 µm long and 1.5 µm wide. The MSP extended to the interior of the cell, arranged as two slightly overlapping rows of about 20 and 15 microtubules each, accompanied in this ventral area of the cell by several tubular vesicles with clear contents (arrows in Fig. 10A, D); electron-opaque bodies were not detected along the MSP. The MSP had an estimated path in the cell of 15–20 μm, ascending on the ventral right side of the basal bodies, slightly curving to the ventral-left side of the central pyrenoid and up to near an accumulation body (Figs. 10A–G; 11A, B; 12B), where it curved and extended back to the right side of the cell, passing on the ventral side of the pyrenoid (Fig. 12A, B) and ending between pyrenoid and nucleus, almost reaching the distal end of the TMRE/r3E (not shown).

Sequence divergence and phylogeny

The genetic distance (sequence divergence) between the two strains of *P. cunningtonii* was calculated based on the Kimura-2-parameter model and it had a value of 0.0032. This estimate was based on four substitutions out of 1,260 base pairs of the nuclear-encoded LSU rDNA, in the comparison.

The tree topology based on partial LSU rDNA included a diverse assemblage of dinoflagellates in addition to the two newly determined sequences of *Parvodinium cunningtonii* var. *cunningtonii* (GenBank access ON980538) and *P. cunningtonii* var. *inerme* (GenBank access ON980539). Figure 13 shows 12 strains of *Parvodinium* (three of them referred as '*Peridinium*' as in the original articles where they were sequenced) forming a monophyletic clade with high support from posterior probability (PP = 0.99) and moderate support from bootstrap (BS = 78%). The two strains of *P. cunningtonii*

were sister taxa with maximum support. Together they formed a sister group to a clade that included *Parvodinium parvulum*, *P. elpatiewskyi* (Ostenfeld) Kretschmann, Zerdoner & Gottschling, *P. mixtum* Kretschmann, Owsianny, Zerdoner & Gottschling,
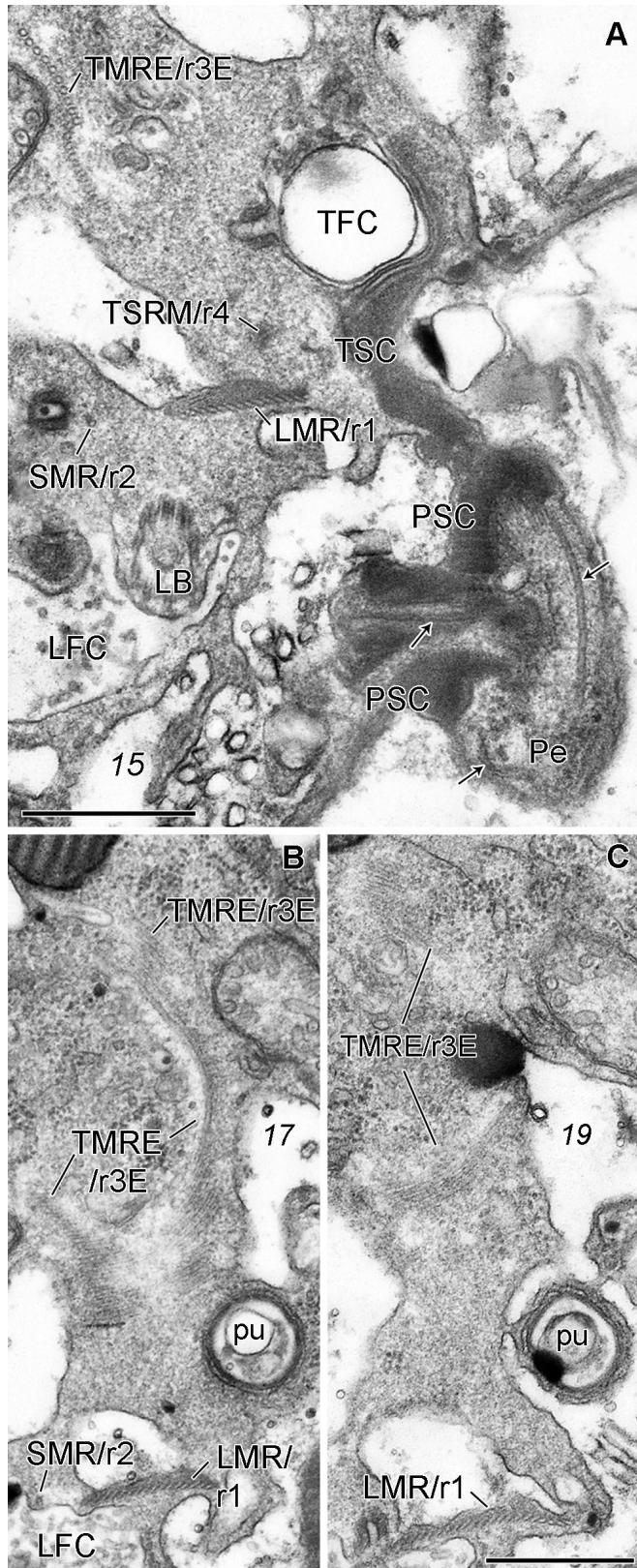
Fig. 9. *Parvodinium cunningtonii* var. *inerme* var. nov., flagellar apparatus and peduncle, TEM. Continuation of series from Fig. 8. Slanted numbers indicate the section number. (**A**) A small peduncle (Pe) surrounded by the peduncle striated collar (PSC) is extruded; the microtubules forming the Pe are marked by arrows. The longitudinal microtubular root (LMR/r1), the single-stranded microtubular root (SMR/r2) and the transverse striated root microtubule (TSRM/r4) are still visible. TMRE/r3E, transverse microtubular root extension; TFC, transverse flagellar canal; LFC, longitudinal flagellar canal. (**B, C**) The TMRE/r3E curves and extends to the dorsal side of the cell. Note the pusular tube (pu) that emerges from the TFC. Scale bars: 500 nm; (B, C) to the same scale.

'*P. inconspicuum*' and one unidentified strain. The support for this branching pattern was PP = 1.0 and BS = 90%. The earliest diverging lineage within *Parvodinium* consisted of '*Peridinium umbonatum* var. *inaequale*', '*P. centenniale'* and two strains with uncertain identity. Following the LSU rDNA-based phylogeny the closest sister lineage to *Parvodinium* encompassed *Palatinus* spp., *Peridiniopsis borgei* and *Johsia chumphonensis*. However, this branching pattern was not well supported (PP = 0.78 and BS < 50%). As is typical for gene trees based on LSU rDNA sequences the backbone of dinoflagellates lineages was unresolved (polytomy) leaving us with no possibility to infer their evolutionary history.

In the concatenated analysis which only comprised the most closely related dinoflagellate lineages based on the LSU rDNA data matrix, both BA and RaxML suggested *Parvodinium* to be monophyletic (PP = 0.98 and BS = 77%). With respect to *Parvodinium cunningtoniii* var. *inerme* it branched off as the second deepest lineage among *Parvodinium* spp. and thus formed a sister taxon to most species except '*Parvodinium* cf. *umbonatum*' (Fig. 14). The phylogenetic position of *P. cunningtonii* var. *inerme* also received high branch support (PP = 1.0 and BS = 99%). Furthermore, the branch length to *P. cunningtonii* var. *inerme* was relatively long indicating that the species was genetically distinct. Contrary, the branch lengths (genetic distances) between congeners (*P. parvulum*, *P. elpatiewskyi*, *P. mixtum* and *P. trawinskii*) were comparatively short.

DISCUSSION

Identity and phylogenetic affinities

The general morphology, plate arrangement and spine distribution of the culture line designated above as 'strain 2'/*P. cunningtonii* identifies it as *Peridiniopsis cunningtonii*, as described by Lemmermann in West (1907) and represented in freshwater dinoflagellate floras (Lefèvre 1932, as *Peridinium cunningtonii* (Lemmermann) Lemmermann; Moestrup and Calado 2018; Popovský and Pfiester 1990). The epithecal tabulation observed in cells of this strain corresponds to the one described for *Peridinium cunningtonii* var. *pseudoquadridens* Er. Lindemann (1919); we follow Lefèvre (1932), who regarded this as a tabulation variant, and take Lindemann's variety as a synonym of *Peridiniopsis cunningtonii*, pending further

research on these variations (Kretschmann et al. 2019). The presence of spines in the major hypothecal plates, except on plate 3‴, agrees with the original drawings and description, and with several later representations of the species (West 1907; Lindemann 1919, as *Peridinium cunningtonii* var. *pseudoquadridens*; Bourrelly 1970; Couté and Iltis 1984; Hansen and Flaim 2007).
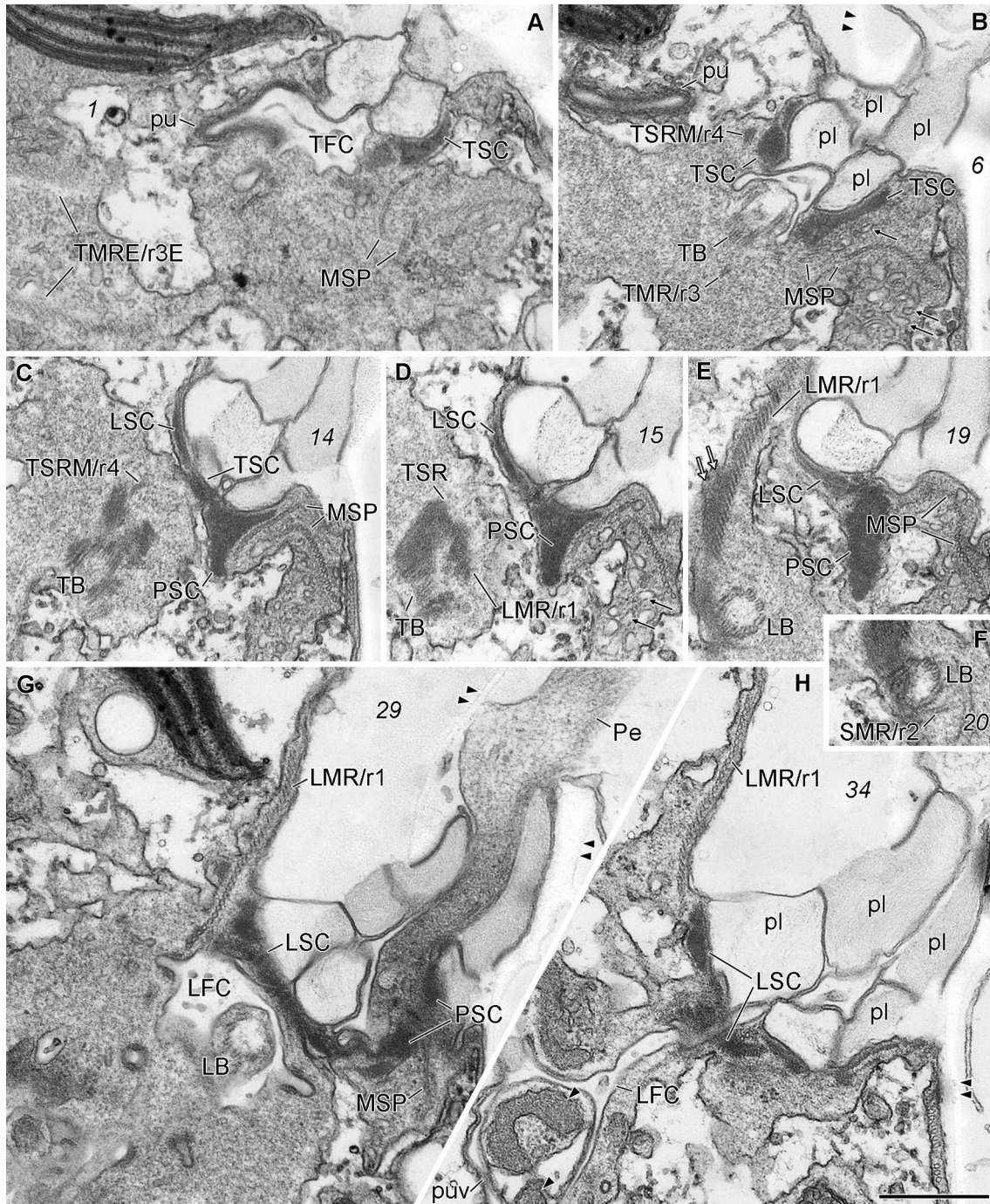
The absence of spines in the hypotheca of cells of the population from which strain 1 originated, and the constancy of this feature in culture, would impede the morphological identification of this material as typical *P. cunningtonii*, despite the similarity in epithecal tabulation of the two strains. The variations in the position of plate 1a (contacting the apical pore in a few of the cells examined) seen in strain 1 further suggest that such tabulation variants carry a reduced taxonomic signal. The very small genetic distance found between the two strains studied herein indicates close relatedness, and we therefore describe strain 1 as a variety within the same species. The new variety is distinguished from other varieties of *Peridiniopsis cunningtonii* recognized in Moestrup and Calado (2018) – *P. cunningtonii* var. *excavata* (M. Lefèvre) Moestrup and *P. cunningtonii* var. *treubii* (Wołoszyńska) Moestrup – by the pointed antapex and the absence of hypothecal spines.

The LSU rDNA-based phylogeny resolved the two strains herein reported on as sister taxa; and both this and the concatenated phylogeny place the species in a clade that includes species of *Parvodinium*, whereas the type of *Peridiniopsis* appears in a different clade together with the genera *Johsia* and *Palatinus*. The corresponding transfer to the genus *Parvodinium* of *P. cunningtonii* is effected below (see Taxonomic summary).

←

Fig. 10. *Parvodinium cunningtonii* var. *cunningtonii*, flagellar apparatus and peduncle, TEM. Non-adjacent serial sections progressing from the apex to the antapex of a cell slightly tilted to the right. Slanted numbers indicate the section number. (**A–D**) The transverse microtubular root extension (TMRE/r3E), sectioned after its curvature, and two rows of the microtubular strand of the peduncle (MSP) accompanied by vesicles (black arrows) are visible. A pusular tube (pu) extends from the transverse flagellar canal (TFC) to the dorsal side of the cell. The transverse striated root (TSR), with its associated transverse striated root microtubule (TSRM/r4), and the transverse microtubular root (TMR/r3) are seen approaching the transverse basal body (TB). Note the different aspect of the platelets (pl), that form the exiting canal of the transverse flagellum, from the outer thecal plates (double arrowheads). (**E, F**) The longitudinal microtubular root (LMR/r1) and the single-stranded microtubular root (SMR/r2) are seen joining the longitudinal basal body (LB). Note the electron-opaque material covering the dorsal side of the LMR/r1 (white arrows). (**G, H**) The peduncle (Pe), surrounded by the peduncle striated collar (PSC) at its base, extrudes through a narrow canal made by platelets (pl). The longitudinal flagellar canal (LFC) extends into the pusular vesicle (puv) that includes granulated bodies (arrowheads). Double arrowheads point the outer thecal plates. TSC, transverse striated collar; LSC, longitudinal striated collar. All to the same scale. Scale bar: 500 nm.

Cyst and cell division

The cyst produced by *Parvodinium cunningtonii* var. *inerme* is smooth-walled, with the same shape of the swimming cell, similarly to what was found in species of the *P. umbonatum–inconspicuum* complex (Chu et al. 2008; Tardio et al. 2009; Wall et al. 1973). Spherical to ovoid cysts with smooth wall were described from several *Parvodinium* species, e.g. *P. marciniakii*, *P. mixtum, P. elpatiewskyi* (Kretschmann et al. 2018, 2019) as well as from *P. cunningtonii* (Lemmermann 1910; Sako et al. 1984). The spherical cyst described for *P. cunningtonii* by Sako et al. (1984) resulted from transformation of a sexually produced planozygote. However, sexual reproduction was not detected in our cultures.
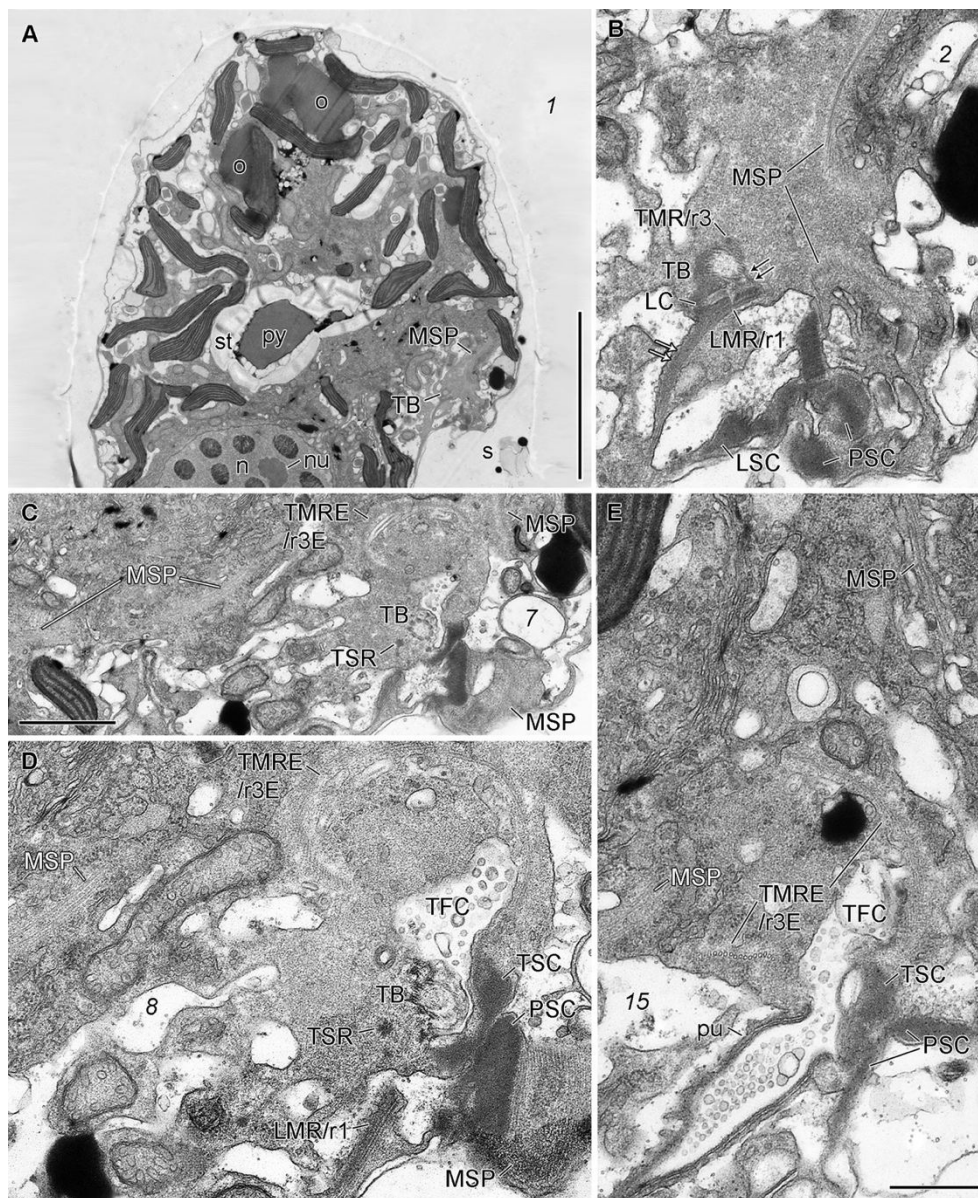
Cell division in Peridiniales commonly occurs after the cell stops swimming and two daughter cells form inside the old amphiesma, from which the cells emerge, in most cases, completely separated (Fensome et al. 1993; Moestrup and Calado 2018). Although complete separation of daughter cells was never observed in *P. cunningtonii* var. *inerme*, it is noteworthy that the process leading to cell division in this taxon somewhat resembles the one described from some members of the Peridiniopsidaceae, such as *Palatinus apiculatus* and '*Scrippsiella*' *hexapraecingula*. In the latter two taxa, an incompletely divided daughter cells exits the parental amphiesma and remains swimming for some time in this semi-divided stage before completing division (Craveiro et al. 2009; Horiguchi and Chihara 1983; West 1909). The formation of thecal plates in the incompletely divided stage, which resulted in a compound theca, was described by Lindemann (1919, as *Peridinium cunningtonii* var. *pseudoquadridens*).

←

Fig. 11. *Parvodinium cunningtonii* var. *cunningtonii*, flagellar apparatus and microtubular strand of the peduncle (MSP), TEM. Non-adjacent longitudinal serial sections proceeding toward the left side of the cell, view from the right side. Slanted numbers indicate the section number. (**A**) General view of the cell showing the position of the nucleus (n) with one nucleolus (nu), the pyrenoid (py) surrounded by starch (st), and the somewhat retracted ventral region with the transverse basal body (TB) and position of the microtubular strand of the peduncle (MSP). (**B**) The transverse basal body (TB) connects to the proximal-dorsal side of the longitudinal microtubular root (LMR/r1) through two short fibers (two arrows). The layered connective (LC) is between the electron-opaque material (white arrows) on the dorsal side of the LMR/r1 and the TB. The microtubular strand of the peduncle (MSP, black letters) extends to the anterior side of the cell. (**C–E**) The transverse microtubular root extension (TMRE/r3E) shows its curving path around the anterior side of the transverse flagellar canal (TFC). Note the ascending path of the MSP (black letters) in the ventral side of the cell and the descending path of the MSP (white letters) to the dorsal side. LMR/r1, longitudinal microtubular root; TMR/r3, transverse microtubular root; PSC, peduncular striated collar. Scale bars: 5 μm (A); 1 μm (C); 500 nm (B, D, E).

General fine structure and apical pore complex

The general fine-structural features of *Parvodinium cunningtonii* and var. *inerme* are the typical for photosynthetic dinoflagellates with an apical pore, including: a nucleus with condensed chromosomes; chloroplast lobes with thylakoids arranged in groups of three; a pusular system; trichocysts, oil droplets and starch grains scattered in the cytoplasm; and a complex of fibres associated with the apical pore. This complex of fibres resembles the apical pore complex recently described from a strain of the *Parvodinium umbonatum–inconspicuum* complex and those of several other peridinioids with an apical pore, e.g. *Scrippsiella sweeneyae* Balech, *Peridiniopsis borgei*, *Chimonodinium lomnickii* (Wołoszyńska) Craveiro, Calado, Daugbjerg, Gert Hansen & Moestrup and *Theleodinium calcisporum* Craveiro, Pandeirada, Daugbjerg, Moestrup & Calado (Calado and Moestrup 2002; Craveiro et al. 2011, 2013; Roberts et al. 1987). Although the aspect of the apical fibrous complex is dependent upon the fixation method used (here shown from material fixed with a mixture containing osmium tetroxide), the basic arrangement of a fibrous cylinder that lines the inside of the pore plate and extends posteriorly into several peripheral fibres seems to be common to all of these species (Pandeirada et al. 2022; Roberts et al. 1987).

The presence in both strains of *P. cunningtonii* of a pyrenoid surrounded by a starch sheath in the middle of the epicone, from which the chloroplast lobes extend to the periphery, differs from what was found in *Parvodinium* umbonatum–*inconspicuum* and in *P. parvulum*, but resembles what was found in *Peridiniopsis borgei* and *Johsia chumphonensis* (Calado and Moestrup 2002; Luo et al. 2020; Pandeirada et al. 2022). The presence of numerous cytoplasmic channels of irregular shape within the pyrenoid matrix is a relatively uncommon feature shared with *Palatinus apiculatus*, in which the central pyrenoid differs from that of *P. cunningtonii* in being somewhat stellate and by lacking a starch sheath (Craveiro et al. 2009). A pyrenoid penetrated by cytoplasmic channels is also present in *Bysmatrum arenicola* T. Horiguchi & Pienaar (Horiguchi and Pienaar 1988, as '*Scrippsiella arenicola*' nom. inval.) and in species of *Heterocapsa*, two genera distantly related to the Peridiniopsidaceae (Tamura et al. 2005; Tillmann et al. 2017).

The eyespot in both strains of *P. cunningtonii* is of type A, as observed in all *Parvodinium* species for which ultrastructural features are known (Luo et al. 2020; Pandeirada et al. 2022).

Pusule and flagellar apparatus

Long, well-defined pusular tubes were found associated with the transverse flagellar canal (TFC) in *Palatinus apiculatus* (two tubes) and in *Parvodinium umbonatum–inconspicuum* (one tube) but are absent in *Peridiniopsis borgei* (Calado and Moestrup 2002; Craveiro et al. 2009; Pandeirada et al. 2022). *Parvodinium cunningtonii* and *P. cunningtonii* var. *inerme* also showed one pusular tube connected to the TFC, which branched distally and was internally lined by electron-opaque granules in some portions of its extension; this part of the pusular apparatus is reminiscent of the one found in *Parvodinium umbonatum–inconspicuum* (Pandeirada et al. 2022). *Peridiniopsis borgei* and *Palatinus apiculatus* have a sac pusule associated with the longitudinal flagellar canal (LFC), in contrast to *P. umbonatum–inconspicuum* and *P. cunningtonii*, which lack a sac pusule; instead, there is in the former a complex system that includes a flat vesicle that ramifies into tubular portions, and a complex network of tubes; and in the latter, a simple flat pusular vesicle with several ramifications (Pandeirada et al. 2022; present work). Despite their complexity, which makes them difficult to compare, the pusular systems so far described from *Parvodinium* species seem to display more affinities with one another than with the pusular arrangements described from other Peridiniopsidaceae (particularly *Peridiniopsis borgei* and *Palatinus apiculatus*).

In general, the flagellar apparatus of the two varieties of *Parvodinium cunningtonii* is similar to what was recently described from *Parvodinium umbonatum–inconspicuum*. The differences that stand out are mainly quantitative, particularly in the number of microtubules in the TMRE/r3E (one row of ca. 22 in *P. cunningtonii* and one row of ca. 11 in *P. umbonatum–inconspicuum*) and in the path they describe (Pandeirada et al. 2022). In *P. umbonatum–inconspicuum* the TMRE/r3E is relatively short and extends to the dorsal-left side of the cell, over the TFC, whereas in *P. cunningtonii* the path is longer and more complex, with the TMRE/r3E curving around the anterior edge of the TFC and continuing in a posterior direction until it turns and extends to the dorsal side of the cell. Among the species of Peridiniopsidaceae so far examined in detail, the

TMRE/r3E of *Peridiniopsis borgei* is the most distinct, with 23 microtubules branching off from a larger microtubular strand to make a cylindrical arrangement around an axial fibre; the arrangement is stable along a path of over 10 μm around a large sac pusule, toward the dorsally located pyrenoid (Calado and Moestrup 2002). The TMRE/r3E of *Palatinus apiculatus* is much simpler, consisting of one or two strands of microtubules that curve around the ventral and the anterior surfaces of the TFC (Craveiro et al. 2009). Features like the angle and relative position of basal bodies, the four microtubule-containing roots and the layered connective linking LMR/r1 to TSR and TB (and the absence of a longer connective between these two roots) do not seem to provide distinctive characters between the genera of Peridiniopsidaceae. In addition, a two- or three-armed fibrous connective between LMR/r1 and triplets of the TB seems to be shared by members of the Peridiniopsidaceae (see Pandeirada et al. 2022).
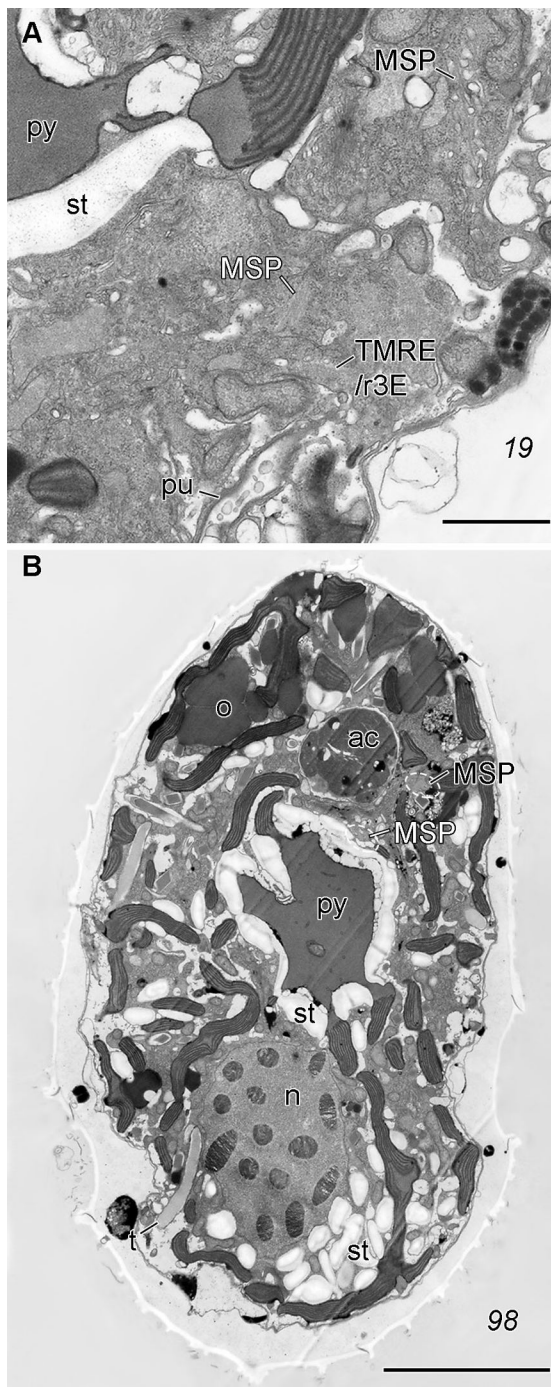
Fig. 12. *Parvodinium cunningtonii* var. *cunningtonii*, microtubular strand of the peduncle (MSP) and ransverse microtubular root extension (TMRE/r3E), TEM. Continuation of series of sections from Fig. 11. Slanted numbers indicate the section number. (**A**) The position of the MSP is indicated in the ascending path (black letters) on the ventral side of the pyrenoid (py) and on the descending path (white letters) passing near the TMRE/r3E. (**B**) Longitudinal section showing the relative position of the MSP on the ascending path, near the accumulation body (ac), and also in the descending path on the anterior-ventral side of the pyrenoid. n, nucleus; o, oil globule; pu, pusule; st, starch grains; t, trichocyst. Scale bars: 1 μm (A); 1 μm (D); 500 nm (B, C, E).

Peduncle and microtubular strand of the peduncle

In dinoflagellates, a cytoplasmic extension protruding from the ventral surface, near the insertion area of the flagella (commonly referred to as a peduncle, or sometimes a feeding tube, or a pallium), is usually supported internally by a microtubular strand (MSP) or a microtubular basket (MB) (Calado and Moestrup 1997, 2002). Although the use of the peduncle, feeding tube or pallium for feeding is well-documented (e.g. Calado et al. 1998; Calado and Moestrup 1997; reviewed in Hansen and Calado 1999) no unequivocal evidence of the use of extracellular organic particles as food by species of Peridiniopsidaceae is available, and the use of MSP and peduncle in the group is uncertain. In spite of this, an extruded peduncle has been found in several species of Peridiniopsidaceae. Whereas in both *P. cunningtonii* and *Peridiniopsis borgei* an extruded peduncle was detected only in TEM sections, in *P. umbonatum–inconspicuum* it was also visible in SEM (Pandeirada et al. 2022). The path of the MSP inside the cell is rather extensive and complex in all these *Parvodinium* strains and is reminiscent of what was described for *P. borgei*, which has however a larger number of microtubules (ca. 80) (Calado and Moestrup 2002; Pandeirada et al. 2022). Electron-opaque bodies have been typically associated with all types of microtubular apparatuses known to be involved in supporting, or driving, food uptaking peduncles, feeding tubes and palliums, whether large or small (Calado et al. 1998; Calado and Moestrup 1997; Jacobsen and Anderson 1992). Electron-opaque bodies, and sometimes also electron-translucent elongated vesicles, have also been found in association with the MSP or MB in several photosynthetic dinoflagellates that are not known to feed on organic particles (e.g. *P. borgei* and *Naiadinium polonicum* (Wołoszyńska) Carty, respectively; Calado and Moestrup 2002; Craveiro et al. 2015). The absence of the electron-opaque bodies in *Parvodinium cunningtonii* contrasts with the observation of electron-opaque vesicles in the extruded peduncle of *P. umbonatum–inconspicuum* (Pandeirada et al. 2022). *Palatinus apiculatus* is so far the only Peridiniopsidaceae examined in fine structural detail that did not show a peduncle and has a relatively small MSP without associated vesicles (Craveiro et al. 2009). Whether these differences reflect different stages in a progressive loss of feeding-related characters inherited from a heterotrophic or mixotrophic ancestor is not clear.

The addition of *P. cunningtonii* to the family Peridiniopsidaceae adds variation in two series of plates to the previously known range of epithecal tabulations: the variants 4′, 1a and 5′ in the apical region, and six precingular plates (rather than seven) on the base of the epitheca. This underlines the unreliability of tabulation formulas for establishing a classification, and the uncertainty about the phylogenetic affinities of other taxa currently classified as *Peridiniopsis* or *Parvodinium* that have not yet been analysed by modern methods.
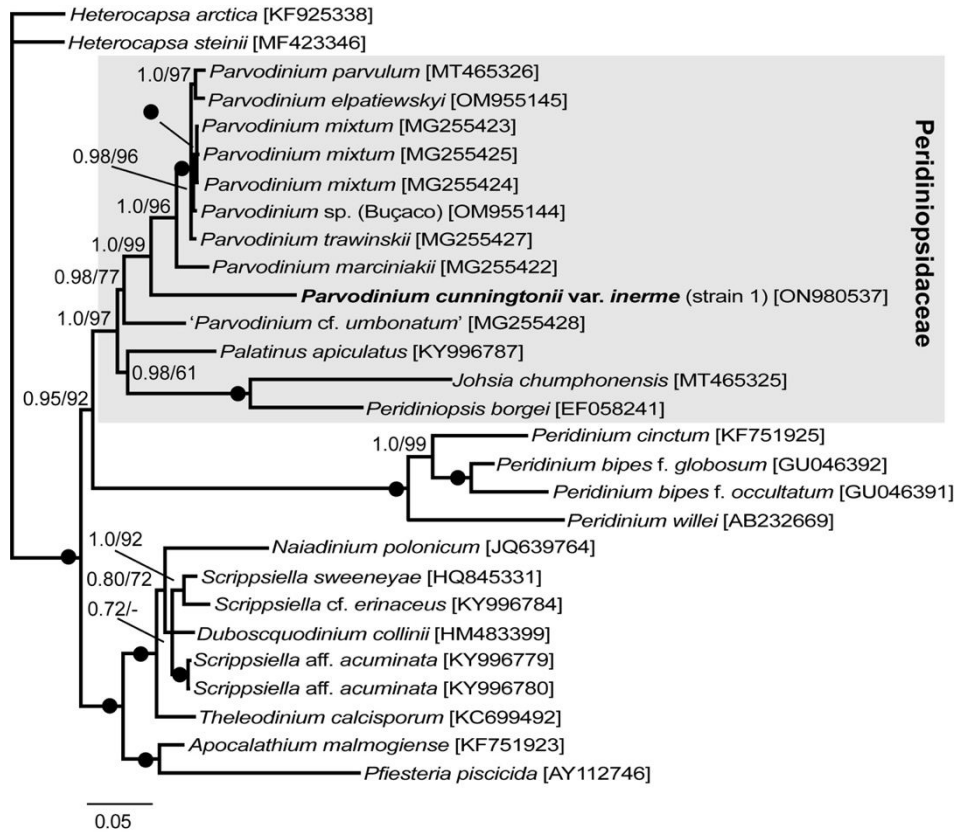
Fig. 14. Phylogeny of *Parvodinium cunningtonii* var. *inerme* based on concatenation of SSU rDNA, ITS 1, 5.8S rDNA, ITS 2 and partial LSU rDNA totaling 3,923 base pairs. The phylogeny was inferred from Bayesian analysis (BA) and included 27 other dinoflagellate sequences and of these 10 belonged to *Parvodinium* spp. *Heterocapsa* spp. formed the outgroup. Robustness of the tree topology (branch support) was obtained from posterior probabilities (PP ≥ 0.5; BA) and bootstrap (BS ≥ 50%; 1,000 replications in RAxML). These values are written at internodes. PP < 0.5 and BS < 50% are denoted by a dash (-). Filled circles indicate the highest possible support: 1.0 in BA and 100% in BS. GenBank accession numbers follow the names of species. The branch lengths are proportional to the number of character changes, see scale bar.

←

Fig. 13. Phylogeny of *Parvodinium cunningtonii* var. *cunningtonii* and *P. cunningtonii* var. *inerme* based on nuclear-encoded partial LSU rDNA (1,635 base pairs, including introduced gaps). The phylogeny was inferred from Bayesian analysis (BA) and included a diverse assemblage of dinoflagellates (83 sequences and 52 genera). Ciliates, apicomplexans and *Perkinsis* formed the outgroup. Robustness of the tree topology (branch support) was obtained from posterior probabilities (PP ≥ 0.5; BA) and bootstrap (BS ≥ 50%; 1,000 replications in RAxML). These values are written at internodes. PP < 0.5 and BS < 50% are denoted by a dash (-). Filled circles indicate the highest possible support: 1.0 in BA and 100% in BS. GenBank accession numbers follow the names of species. The branch lengths are proportional to the number of character changes, see scale bar.

TAXONOMIC SUMMARY

Meeting the requirements of the ICN 2018 (Turland et al. 2018).

***Parvodinium cunningtonii* (Lemmermann) Pandeirada, Craveiro, Daugbjerg, Moestrup and Calado comb. nov.**

Basionym: *Peridiniopsis cunningtonii* Lemmermann in West 1907, J. Linn. Soc., Bot. 38, p. 189, pl. 9, fig. 2.

Homotypic synonym: *Peridinium cunningtonii* (Lemmermann) Lemmermann 1910, p. 671.

***Parvodinium cunningtonii* var. *inerme* Pandeirada, Craveiro, Daugbjerg, Moestrup and Calado var. nov.**

Diagnosis: Differs from *Parvodinium cunningtonii* var. *cunningtonii* in the shape of the hypocone, which tapers into an antapical apiculum, and by lacking spines in the hypotheca; the amphiesmal plates are generally smooth; cells, on average, slightly smaller than the typical variety, mostly 18–30 μm long, 12–21 μm wide and 13–16 μm thick. The genetic distance (sequence divergence) from the strain of *P. cunningtonii* var. *cunningtonii* described herein is 0.0032, representing four substitutions out of 1260 base pairs of the nuclear-encoded LSU rDNA.

Holotype: SEM stub with critical-point-dried cells from a culture batch, fixed in ethanol 25% (final concentration). Deposited at the University of Aveiro Herbarium, registered as AVE-A-T-15. Fig. 2B, C illustrate cells from this stub. GenBank accession ON980537.

Type locality: Flooded area of the freshwater stream Ribeiro da Palha near the village of Nariz, Aveiro, Portugal (40°33.240′N, 8°34.095′W), collected 16 July 2015 by M. Pandeirada.

Etymology: Infraspecific epithet from Latin *inermis*, *-e*, unarmed, without spines or prickles.

ACKNOWLEDGEMENTS

REFERENCES

Bourrelly, P., 1970. Les algues d'eau douce 3: les algues bleues et rouges, les Eugléniens, Peridiniens et Cryptomonadines. Boubée, Paris, 512 pp.

Calado, A.J., Moestrup, Ø., 1997. Feeding in *Peridiniopsis berolinensis* (Dinophyceae): new observations on tube feeding by an omnivorous, heterotrophic dinoflagellate. Phycologia 36, 47–59.

Calado, A.J., Moestrup, Ø., 2002. Ultrastructural study of the type species of *Peridiniopsis*, *Peridiniopsis borgei* (Dinophyceae), with special reference to the peduncle and flagellar apparatus. Phycologia 41, 567–584.

Calado, A.J., Craveiro, S.C., Moestrup, Ø., 1998. Taxonomy and ultrastructure of a freshwater, heterotrophic *Amphidinium* (Dinophyceae) that feeds on unicellular protists. J. Phycol., 34: 536–554.

Carty, S., 2008. *Parvodinium* gen. nov. for the Umbonatum group of *Peridinium* (Dinophyceae). Ohio J. Sci. 108, 103–107.

Chu, G., Sun, Q., Rioual, P., Boltovskoy, A., Liu, Q., Sun, P., Han, J., Liu, J., 2008. Distinct microlaminations and freshwater "red tides" recorded in Lake Xiaolongwan, northeastern, China. J. Paleolimnol. 39, 319–333.

Couté, A., Iltis, A., 1984. Mise au point sur la flore péridiniale (Algae, Pyrrhophta) d'eau douce de Côte d'Ivoire. Rev. Hydrobiol. Trop. 17, 53–64.

Craveiro, S.C., Calado, A.J., Daugbjerg, N., Moestrup, Ø., 2009. Ultrastructure and LSU rDNA-based revision of *Peridinium* group palatinum (Dinophyceae) with the description of *Palatinus* gen. nov. J. Phycol. 45, 1175–1194.

Craveiro, S.C., Calado, A.J., Daugbjerg, N., Hansen, G., Moestrup, Ø. 2011. Ultrastructure and LSU rDNA-based phylogeny of *Peridinium lomnickii* and description of *Chimonodinium* gen. nov. (Dinophyceae). Protist 162, 590–615.

Craveiro, S.C., Pandeirada, M.S., Daugbjerg, N., Moestrup, Ø., Calado, A.J. 2013. Ultrastructure and phylogeny of *Theleodinium calcisporum* gen. et sp. nov., a freshwater dinoflagellate that produces calcareous cysts. Phycologia 52, 488–507.

Craveiro, S.C., Daugbjerg, N., Moestrup, Ø., Calado, A.J., 2015. Fine-structural characterization and phylogeny of *Peridinium polonicum*, type species of the recently described genus *Naiadinium* (Dinophyceae). Eur. J. Protistol. 51, 259–279.

Daugbjerg, N., Hansen, G., Larsen, J., Moestrup, Ø., 2000. Phylogeny of some of the major genera of dinoflagellates based on ultrastructure and partial LSU rDNA sequence data, including the erection of three new genera of naked dinoflagellates. Phycologia 39, 302–317.

Fensome, R.A., Taylor, F.J.R., Norris, G., Sarjeant, W.A.S., Wharton, D.I., Williams, G.L., 1993. A classification of living and fossil dinoflagellates. Micropaleontology, Special Publication 7: 1–351.

Gottschling, M., Kretschmann, J., Žerdoner Čalasan, A., 2017. Description of Peridiniopsidaceae, fam. nov. (Peridiniales, Dinophyceae). Phytotaxa 299, 293–296.

Hansen, G., Daugbjerg, N., 2004. Ultrastructure of *Gyrodinium spirale*, the type species of *Gyrodinium* (Dinophyceae), including a phylogeny of *G. dominans*, *G. rubrum* and *G. spirale* deduced from partial LSU rDNA sequences. Protist 155, 271–294.

Hansen, G., Flaim, G., 2007. Dinoflagellates of the Trentino Province, Italy. J. Limnol. 66, 107–141.

Horiguchi, T., Chihara, M., 1983. *Scrippsiella hexapraecingula* sp. nov. (Dinophyceae), a tide pool dinoflagellate from the Northwest Pacific. Bot. Mag., Tokyo 96, 351–358.

Horiguchi, T., Pienaar, R.N., 1988. Ultrastructure of a new sand-dwelling dinoflagellate, *Scrippsiella arenicola* sp. nov. J. Phycol. 24, 426–438.

Huelsenbeck, J.P., Ronquist, F., 2001. MRBAYES: Bayesian inference of phylogenetic trees. Bioinformatics 17, 754–755.

Jacobson, D.M., Anderson, D.M., 1992. Ultrastructure of the feeding apparatus and myonemal system of the heterotrophic dinoflagellate *Protoperidinium spinulosum*. J. Phycol. 28, 69–82.

Kretschmann, J., Owsianny, P.M., Žerdoner Čalasan, A., Gottschling, M., 2018. The hot spot in a cold environment: puzzling *Parvodinium* (Peridiniopsidaceae, Peridiniales) from the polish Tatra mountains. Protist 169, 206–230.

Kretschmann, J., Žerdoner Čalasan, A., Meyer, B., Gottschling, M., 2019 (2020). Zero intercalary plates in *Parvodinium* (Peridiniopsidaceae, Peridiniales) and phylogenetics of *P. elpatiewskyi*, comb. nov. Protist 171, Article 125700.

Lefèvre, M., 1932. Monographie des espèces d'eau douce du genre *Peridinium* Ehrb. Arch. Bot. Mém. 2 (Mémoire 5), 1–210, pls 1–6.

Lemmermann, E., 1910. Algen I (Schizophyceen, Flagellaten, Peridineen). Kryptogamenflora der Mark Brandenburg, Bd. 3. Gebrüder Borntraeger, Leipzig, 712 pp.

Lindemann, E., 1919. Untersuchungen über Süßwasserperidineen und ihre Variationsformen. Arch. Protistenk. 39, 209–262 + pl 17.

Lindström, K., 1991. Nutrient requirements of the dinoflagellate *Peridinium gatunense*. J. Phycol. 27, 207–219.

Luo, Z., Mertens, K.N., Gu, H., Wang, N., Wu, Y., Uttayarnmanee, P., Pransilpa, M., Roeroe, K.A., 2020. Morphology, ultrastructure and molecular phylogeny of *Johsia chumphonensis* gen. et sp. nov. and *Parvodinium parvulum* comb. nov. (Peridiniopsidaceae, Dinophyceae). Eur. J. Phycol. 56, 324–336.

Moestrup, Ø., Calado, A.J., 2018. Dinophyceae. In: Büdel, B., Gärtner, G., Krienitz, L., Schagerl, M. (Eds.), Süßwasserflora von Mitteleuropa – Freshwater Flora of Central Europe, vol. 6, 2nd ed. Springer-Verlag, Berlin. XII + 561 pp.

Nichols, H.W., 1973. Growth media — freshwater. In: Stein, J.R. (Ed.), Handbook of phycological methods. Culture methods & growth measurements. Cambridge University Press, Cambridge, pp. 7–24.

Nunn, G.B., Theisen, B.F., Christensen, B., Arctander, P., 1996. Simplicity-correlated size growth of the nuclear 28S ribosomal RNA D3 expansion segment in the crustacean order Isopoda. J. Mol. Evol. 42, 211–223.

Pandeirada, M.S., Craveiro, S.C., Daugbjerg, N., Moestrup, Ø., Calado, A.J., 2014. Studies on woloszynskioid dinoflagellates VI: description of *Tovellia aveirensis* sp. nov. (Dinophyceae), a new species of Tovelliaceae with spiny cysts. Eur. J. Phycol. 49, 230–243.

Pandeirada, M.S., Craveiro, S.C., Daugbjerg, N., Moestrup, Ø., Calado, A.J., 2017. Studies on woloszynskioid dinoflagellates VIII: life cycle, resting cyst morphology and phylogeny of *Tovellia rinoi* sp. nov. (Dinophyceae). Phycologia 56, 533–548.

Pandeirada, M.S., Craveiro, S.C., Daugbjerg, N., Moestrup, Ø., Calado, A.J., 2022. Cell fine structure and phylogeny of *Parvodinium*: towards an ultrastructural characterization of the Peridiniopsidaceae (Dinophyceae). Eur. J. Phycol. in press.

Popovský, J., Pfiester, L.A., 1990. Dinophyceae (Dinoflagellida). In: Ettl, H., Gerloff, J., Heynig, H., Mollenhauer, D. (Eds.), Süßwasserflora von Mitteleuropa, vol. 6. Gustav Fischer, Jena.

Roberts, K.R., Timpano, P., Montegut, A.E., 1987. The apical fibrous complex: a new cytological feature of some dinoflagellates. Protoplasma, 137: 65–69.

Sako, Y., Ishida, Y., Kadota, H., Hata, Y., 1984. Sexual reproduction and cyst formation in the freshwater dinoflagellate *Peridinium cunningtonii*. Nippon Suisan Gakkaishi 50, 743–750. [Bulletin of the Japanese Society of Scientific Fisheries]

Scholin, C.A., Herzog, M., Sogin, M., Anderson, D.M., 1994. Identification of group- and strain-specific genetic markers for globally distributed *Alexandrium* (Dinophyceae). II. Sequence analysis of a fragment of the LSU rRNA gene. J. Phycol. 30, 999–1011.

Stamatakis, A., 2014. RAxML version 8: a tool for phylogenetic analysis and post-analysis of large phylogenies. Bioinformatics 30, 1312–1313. doi.org/10.1093/bioinformatics/btu033.

Swofford, D.L., 2002. Phylogenetic Analysis Using Parsimony (*and other methods). Version 4. Sinauer Associates, Sunderland, Massachuetts.

Takano, Y., Horiguchi, T., 2005. Acquiring scanning electron microscopical, light microscopical and multiple gene sequence data from a single dinoflagellate cell. J. Phycol. 42, 251–256.

Tamura, M., Iwataki, M., Horiguchi, T., 2005. *Heterocapsa psammophila* sp. nov. (Peridiniales, Dinophyceae), a new sand-dwelling marine dinoflagellate. Phycol. Res. 53, 303–311.

Tardio, M., Ellegaard, M., Lundholm, N., Sangiorgi, F., Di Giuseppe, D., 2009. A hypocystal archeopyle in a freshwater dinoflagellate from the *Peridinium umbonatum* group (Dinophyceae) from Lake Nero di Cornisello, South-East Alps, Italy. Eur. J. Phycol. 44, 1–10.

Tillmann, U., Hopperanth, M., Gottschling, M., Kusber, W., Elbrächter, M., 2017. Plate pattern clarification of the marine dinophyte *Heterocapsa triquetra* sensu Stein (Dinophyceae) collected at Kiel Fjord (Germany). J. Phycol. 53, 1305–1324.

Wall, D., Dale, B., Harada, K., 1973. Descriptions of new fossil dinoflagellates from the Late Quaternary of the Black Sea. Micropaleontology 19, 18–31.

West, G.S., 1907. Report on the freshwater algae, including phytoplankton, of the third Tanganyika Expedition conducted by Dr. W.A. Cunnington, 1904–1905. J. Linn. Soc., Bot. 38, 81–197. [Class Peridineae studied by E. Lemmermann].

West, G.S., 1909. A biological investigation of the Peridineae of Sutton Park, Warwickshire. New Phytol. 8, 181–196.

CHAPTER 6

CONCLUDING REMARKS

CONCLUDING REMARKS

The classification of peridinioids was traditionally based on thecal features and was not oriented by phylogenies inferred from the analysis of DNA sequences (Saldarriaga et al. 2004; Logares et al. 2007). The ultrastructural analysis of the type species of the genera *Peridinium* (Calado et al. 1999) and *Peridiniopsis* (Calado & Moestrup 2002), and the inclusion of sequences of these species in DNA-based phylogenies, led to taxonomic changes among the peridinioids, some of them unexpected (Craveiro et al. 2009, 2011, 2015, 2016; Gottschling et al. 2017; Moestrup & Calado 2018; Kretschmann et al. 2018, 2019; Luo et al. 2020). Further molecular-ultrastructural comparisons among peridinioid (and non-peridinioid) dinoflagellates still holds promise of providing important insights into unresolved dinoflagellate systematics. Detailed ultrastructural examination of other peridinioid species hitherto not analysed is required to establish phylogenetically relevant characters in the group, and to provide a more accurate portrait of character evolution in dinoflagellates. In the present work, several freshwater dinoflagellates were assessed ultrastructurally and added to ribosomal DNA-based phylogenetic hypotheses. One species proved to be an undescribed member of the genus *Tovellia* (woloszkyinskoid); and another gave us the opportunity to verify the stability of several unusual characters previously found in the genus *Sphaerodinium*, and constituted the first demonstration with modern methods of species-level diversity in that genus (Chapters 2, 3). Other analysed taxa were selected among well-known peridinioid species. The separation of species of the 'umbonatum' group from the genus *Peridinium* by Carty (2008) left only the presence to two anterior intercalary plates as characters of the new genus *Parvodinium*. The fine-structural examination of peridinioid specimens identifiable as members of the *Parvodinium umbonatum–inconspicuum* species complex (taken as representative of the type of the genus) was undertaken to establish a wider basis of features potentially characteristic of the genus, at a level of detail comparable to the one available for type species of several other peridinioid genera – *Peridinium*, *Peridiniopsis*, *Palatinus*, *Chimonodinium*, *Theleodinium*, *Apocalathium*, *Naiadinium*, *Tyrannodinium* (Chapter 4). Recent analyses of peridinioid species underlined that plate formulas may not be taken as reliable guidelines to phylogenetic/taxonomic affinities. This was clearly shown by the demonstrated affinity of *Peridiniopsis elpatiewskyi* with species of *Parvodinium* (Kretschmann et al. 2019; confirmed by our unpublished analyses based on

rDNA and ultrastructure). The presence of two somewhat different populations identifiable as *Peridiniopsis cunningtonii* in a nearby lake afforded the opportunity to reassess the affinities of this species, which also revealed a closer relationship with *Parvodinium* than with *Peridiniopsis* (Chapter 5).

Phylogenetic scenarios that include the peridinioids and related groups (with orders or families indicated) are given in Figs 1, 2. These speculative views of relationships involving dinoflagellate orders containing peridinioids, and others that appear closely related, were modified from published phylogenies (see below), and provide a basis for a tentative mapping of cell features (Figs 1b, 2). A comparative overview of fine-structural characters of a relevant selection of dinoflagellate groups is given in Table 1.
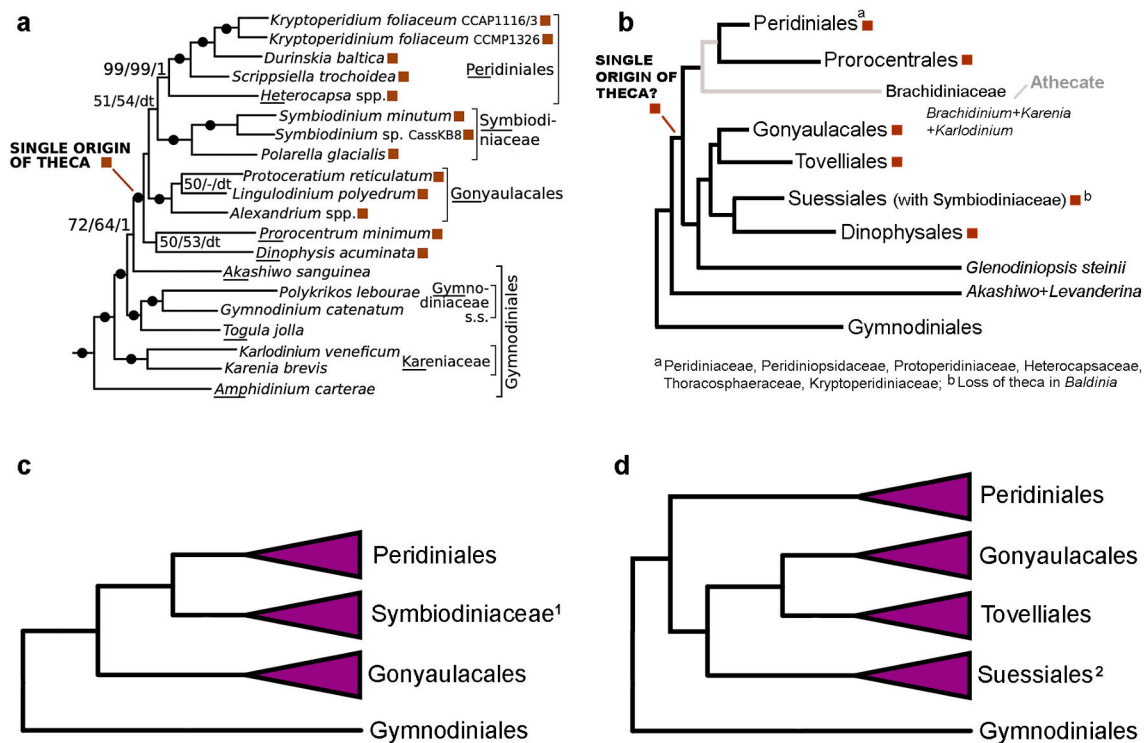
Fig. 1. Phylogenetic scenarios adapted from (a) a multiprotein-based phylogeny by Janouškovec et al. (2017) and (b) an rDNA-based phylogeny by Chácon & Gottschling (2020), with relative position and branching order of thecate dinoflagellates. Orange squares indicate thecate groups. In (c) and (d) are simplified versions of (a) and (b), respectively, with only the orders indicated.

Taylor's (2004) morpho-molecular hypotheses: evolution of thecate dinoflagellates from athecate forms, and segregation of the Gonyaulacales from the Peridiniales (or, more generally, gonyaulacoids from peridinioids), have been supported by taxa-enriched phylogenetic analyses with broad taxonomic sampling, based on rDNA and multiprotein

sequences, onto which morphological, biochemical and life-cycle aspects have been mapped (e.g., Janouškovec et al. 2017; Price & Bhattacharya 2017; Chácon & Gottschling 2020). However, a consensual phylogenetic scheme displaying the order-level affinities of dinoflagellates remains to be achieved. Figs 1a, 1b exemplify phylogenetic scenarios obtained by Janouškovec et al. (2017) and Chácon & Gottschling (2020), respectively, with the relative position of several currently recognized orders of thecate dinoflagellates.

The part of a well-supported pattern from Janouškovec et al.'s (2017) multiprotein-based tree that includes the thecate dinoflagellates is reproduced here as Fig. 1a. Four dinoflagellate orders are included: Gymnodiniales at the basis (athecate dinoflagellates) and all thecate dinoflagellates diverging later. The Gonyaulacales branch out as a sister group of a clade containing the Symbiodiniaceae (Suessiales) and the Peridiniales. *Heterocapsa* spp. appears as a sister group of the rest of the Peridiniales. The single origin of the dinoflagellate theca is mapped by Janouškovec et al. (2017); the presence of a theca is marked in Fig. 1a by orange squares. An easier perception of the branching pattern of Fig. 1a may be gathered from Fig. 1c, in which only orders and the family Symbiodiniaceae (Suessiales) are marked.

Figure 1b was based on an extensive rDNA-based phylogenetic tree published by Chácon & Gottschling's (2020). It displays a somewhat different assemblage of families and orders, including the thin-covered Tovelliales (Chácon & Gottschling 2020). Just as Figs 1a and 1c, Figs 1b and 1d show the Gymnodiniales as a basal group, with the thecate dinoflagellates arising later. However, the branching pattern of dinoflagellate orders is different (nearly inverted) compared with that shown in Janouškovec et al. (2017): the Peridiniales resolve as sister to a clade containing the Gonyaulacales (thecate) and two thin-covered groups, the Suessiales and the Tovelliales (Chácon & Gottschling 2020). The distribution of groups with a theca (marked by orange squares in Fig. 1b) still suggests a single origin, and implies the loss of this feature by the ancestor of the Brachidiniaceae (including the Kareniaceae; Chácon & Gottschling 2020). In contrast, the Brachidiniaceae form a basal clade in a sister group to the Gymnodiniales in other rDNA-based phylogenies with a large taxon sampling (Gottschling et al. 2019, 2020). Although a branching order is explicit for all groups in Gottschling et al. (2019, 2020) and Chácon & Gottschling (2020) statistical support for many of order-level clades is

rather limited, highlighting a large level of uncertainty that persists concerning the deep branches of the dinoflagellate group.
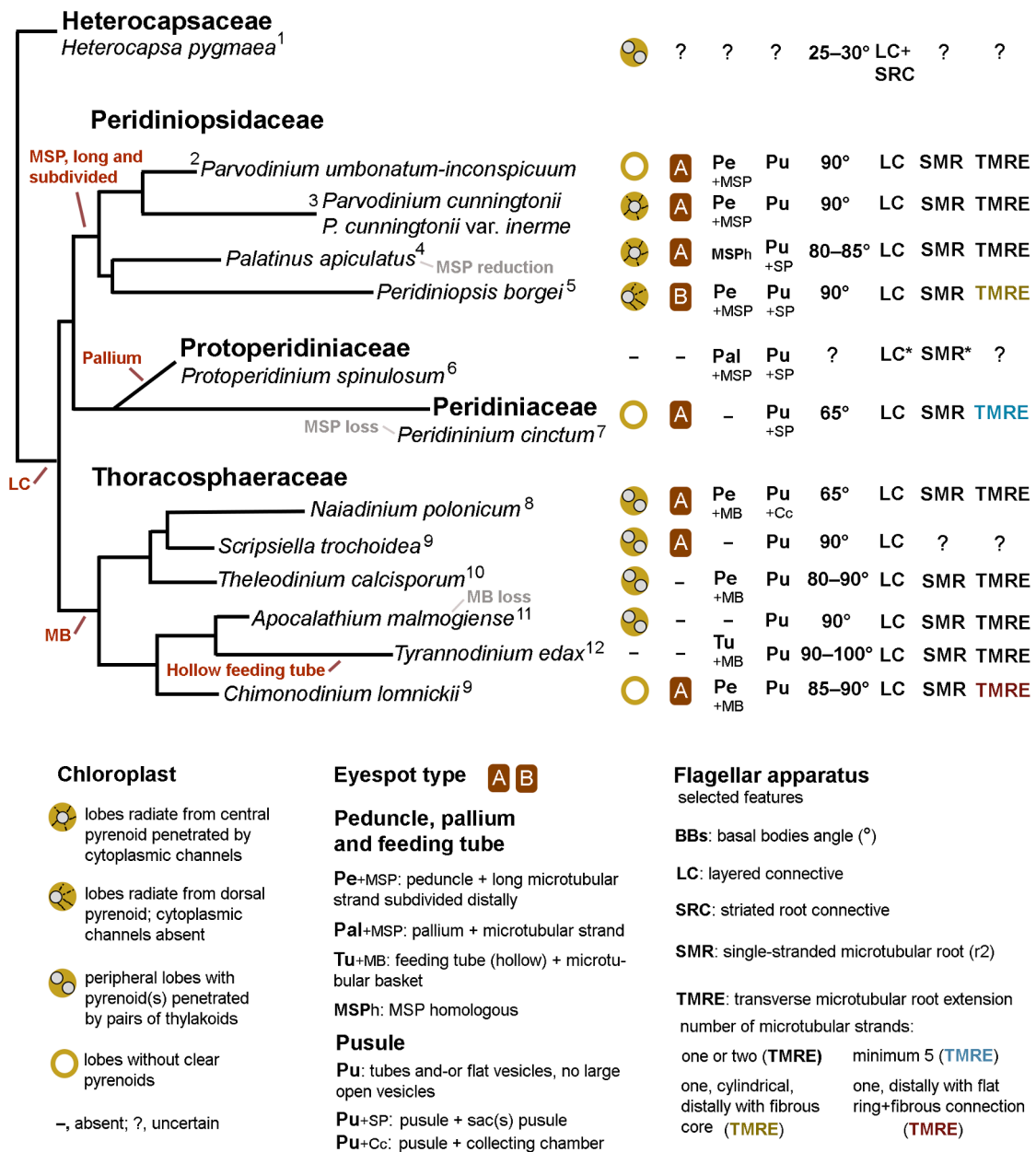
Fig. 2. Model for character evolution in the order Peridiniales (including Thoracosphaerales). A phylogenetic scenario with the relative position of the families Peridiniaceae, Peridiniopsidaceae, Thoracosphaeraceae and Protoperidiniaceae (adapted from recently published phylogenies, see text). Some structural and fine-structural attributes are indicated at particular nodes or on the right-hand side of the phylogenetic tree. Numbers indicate the original references: 1, Bullman & Roberts (1986); 2, Chapter 4, this work; 3, Chapter 5, this work; 4, Craveiro et al. (2009); 5, Calado & Moestrup (2002); 6, Jacobson & Anderson (1992); 7, Calado et al. (1999); 8, Craveiro et al. (2015); 9, Craveiro et al. (2011); 10, Craveiro et al. (2013); 11, Craveiro et al. (2016); 12, Calado et al. (2009). LC*, SMR*, presence of SMR and LC inferred from unpublished observations in another Protoperidiniaceae by Craveiro et al.

The lack of consensus concerning the evolution of order-level (and, in part, family-level) groups hinders our understanding of character evolution in dinoflagellates. In Table 1 a comparative overview of fine-structural features is attempted, with representatives of Peridiniales, Gonyaulacales, Tovelliales and Suessiales. The thecate orders Prorocentrales and Dinophysales, although relevant in the context of thecate dinoflagellates, are not included because too little is known about fine-structural details of members of these orders. Table 1 is based on previously published ultrastructural information combined with new results provided here, and aims to summarize important information about potential key ultrastructural features that may be recognized under a more solid understanding of evolutionary steps in dinoflagellates. Features that appear to this author likely to be phylogenetically relevant (on the basis of published data) were given preference: chloroplast arrangement; eyespot type; organization of the cell apex; peduncle and microtubular strand(s); pusule; and selected features of the flagellar apparatus (Moestrup & Daugbjerg 2007; Moestrup & Calado 2018).

The family Peridiniopsidaceae has received consistent support in published phylogenies, where it resolves as a close relative of the Peridiniaceae and the Thoracosphaeraceae (including the Pfiesteriaceae) (Gottschling et al. 2017; Kretschmann et al. 2018, 2019; Luo et al. 2020; this work). A tentative branching pattern of families Peridiniopsidaceae, Peridiniaceae, Protoperidiniaceae and Thoracosphaeraceae, with Heterocapsaceae as outgroup, is shown in Fig. 2; it was adapted from (mainly) concatenated rDNA-based phylogenies (Gottschling et al. 2017; Kretschmann et al. 2018, 2019; Žerdoner Čalasan et al. 2019; Chácon & Gottschling 2020; Luo et al. 2020; Holzer et al. 2021; Ott et al. 2022; this work). Selected internal cell features were marked in Fig. 2 in a way analogous to Fig. 1A, 1B.

Table 1. Comparative overview of fine-structural characters of the taxa examined in this thesis (marked in bold) with other representatives of Peridiniales (including the type species of *Peridinium*, *Peridiniopsis* and *Palatinus*), Gonyaulacales (*Gonyaulax spinifera* and *Alexandrium catenella*), Tovelliales (*Tovellia coronata*) and Suessiales (*Sphaerodinium cracoviense*).

Group and taxa	Chloroplast	Eyespot type	Cell apex structure	Peduncle/MSP	Pusule	Flagellar apparatus (selected features)
PERIDINIALES *Peridinium cinctum*[1]	lobes radiating from near cell centre; central pyrenoid absent	A	absent	absent	pusular tubes and vesicles with irregular shape; one sac pusule connected to each flagellar canal	BBs at 65°; LC; LMR of 10–24 microtubules; TMRE of several rows of 7–22 microtubules; SMR
Palatinus apiculatus[2]	lobes radiating from central pyrenoid penetrated by cytoplasmic channels	A	absent	absent/short microtubular strand homologous to MSP not attached to cell surface	pusular flat vesicles and cylindroid tubes; one sac pusule connected to each flagellar canal	BBs at 80–85°; LC; LMR of 5–40 microtubules; TMRE of 1–2 rows of 20 microtubules; SMR; TB–LMRc
Peridiniopsis borgei[3]	lobes radiating from dorsal pyrenoid with starch sheath	B	fibrous complex underlying the apical pore	present/long MSP extending to the back of the cell and curving back to the ventral side, subdivided distally; with electron-opaque bodies	rounded and flat pusular vesicles extending from a large sac pusule connecting to the LFC; TFC with pusular tubes	BBs at 90°; LC; LMR of 6–30 microtubules, connected to LSC; TMRE cylindrical, with fibrous core in distal end; SMR; TB–LMRc
***Parvodinium umbonatum-inconspicuum* species complex (including type)[4]**	lobes peripheral or radiating from cell centre; central pyrenoid absent	A	fibrous complex underlying the apical pore	like *P. borgei*	large system of ramifying flat and tubular pusular vesicles; sac pusule absent	BBs at 90°; LC; LMR of 10–30(40) microtubules; TMRE of single row of 11 microtubules; SMR; TB–LMRc
***Parvodinium cunningtonii* and var. *inerme* var. ined.**[5]	lobes radiating from starch-sheathed central pyrenoid penetrated by cytoplasmic channels	A	fibrous complex underlying the apical pore	like *P. borgei* but lacking electron-opaque bodies	pusular vesicle connecting to the LFC; ramifying tube connecting to the TFC; tube lumen partially lined by electron-opaque granules; sac pusule absent	BBs at 90°; LC; LMR of 7–30 microtubules; TMRE of single row of 22 microtubules; SMR; TB–LMRc

SUESSIALES *Sphaerodinium cracoviense*[6]	lobes radiating from cell centre; central pyrenoid absent	F	apical furrow with 3 platelets	absent/short MSP homologous, not attached to cell surface	pusule canal connects TFC and one collecting chamber with numerous pusular tubules; LFC with small pusular vesicles	BBs at 90 or 140°; SRC; LMR of 8–36 microtubules; TMRE of 6 or 7 rows of 4–8 microtubules; LB–LMRc, VF, lamellar body
Sphaerodinium polonicum var. *tatricum*[7]	like *S. cracoviense* [a]	F	like *S. cracoviense*	like *S. cracoviense*	like *S. cracoviense*	BBs at 120°; SRC; LMR of 10–40 microtubules; TMRE of several microtubular rows; LB–LMRc, VF, lamellar body
TOVELLIALES *Tovellia coronata*[8]	numerous peripheral lobes[b]	C	Apical Line of Plates (ALP)	unknown/MSP with electron-opaque vesicles	pusular tube opens at the LFC, tubules and sacs exist to the cell inner; tubules lumen lined by electron-opaque bodies	unknown
Tovellia rubescens[9]	lobes radiating from central pyrenoid[b]	C	Apical Line of Plates (ALP)	unknown/MSP with electron-opaque vesicles extending to the ventral ridge	pusular tube extends from the flagellar base area; forms external diverticula	BBs at 120°; SRC; TMRE of 12 microtubules; LMR?
GONYAULACALES *Gonyaulax spinifera*[10]	lobes radiating from central pyrenoid	absent	fibrous complex underlying the apical pore	unknown/short MSP homologous, not attached to cell surface	two large pusular sacs with tubules; each attached to a flagellar canal	BBs at 145°; sbc; SRC; LMR of 35 microtubules; TMRE?; SMR?; LMR–TSCc
Alexandrium catenella[11]	lobes radiating from central pyrenoid	absent	fibrous complex underlying the apical pore	unknown/short MSP homologous reaching ventral ridge; lacks electron-opaque vesicles	two large pusular sacs associated with the flagellar canals	BBs at 90°; sbc; SRC; LMR of 14 to over 30 microtubules; TMRE and SMR; LMR–LSCc

a, number and shape of lobes differed in two strains analyzed; one strain had pseudograna-like thylakoid stacks. b, reddish cells in *T. coronata* and sometimes also in *T. rubescens*: greenish or yellowish-green chloroplast lobes always or sometimes masked by red to brown granules; astaxanthin and astaxanthin-related pigments identified in *T. rubescens* by HPLC-MS/MS.

1, Calado et al. 1999; 2, Craveiro et al. 2009; 3, Calado & Moestrup 2002; 4, this thesis, Chapter 4; 5, this thesis, Chapter 5; 6, Craveiro et al. 2010; 7, Pandeirada et al. 2021 (this thesis, Chapter 3); 8, Lindberg et al. 2005; 9, Pandeirada et al. 2019 (this thesis, Chapter 2); 10, Hansen et al. 1996; 11, Hansen & Moestrup 1998.

Within the confines of Fig. 2, several features associated with the organization of the chloroplast (and, if present, pyrenoid), ventral cytoplasmic extensions (peduncle, pallium or feeding tube) and pusular elements, appear to be associated exclusively with the Peridiniopsidaceae. These include a chloroplast arrangement with lobes radiating from a large, central or dorsal pyrenoid, sometimes with cytoplasmic channels penetrating the pyrenoid – and contrasts with pairs of thylakoids penetrating pyrenoids in the family Thoracosphaeraceae (Craveiro et al. 2009, 2015, 2016; this work). A combination of a peduncle with a very long microtubular strand (MSP) that subdivides into several smaller strands in its inner portion also seems exclusive of the family Peridiniopsidaceae. This type of MSP was observed in *Peridiniopsis borgei*, *Parvodinium umbonatum–inconspicuum* and *P. cunningtonii* and var. *inerme* (Calado & Moestrup 2002; this work); although vesicles with electron-opaque contents accompanied the MSP in the ventral area of at least *P. borgei* and *P. umbonatum–inconspicuum*, these species have not been documented feeding on particulate matter and the function of the MSP and associated peduncle is unknown.

Pusular organization is quite variable in dinoflagellates and therefore has the potential to be a phylogenetic significant feature. However, pusule morphology is rather sensitive to fixation protocols and complete descriptions of pusular elements are quite difficult to achieve. It appears that large, open vesicles, connected directly or indirectly to the flagellar canals and linked to typical pusular elements, have a limited distribution; those not surrounded by distinctive, presumably fibrous, material (so-called sac pusules) are noted in Fig. 2 only in the clade formed by Peridiniopsidaceae, Protoperidiniaceae and Peridiniaceae (Jacobson & Anderson 1992; Calado et al. 1999; Calado & Moestrup 2002; Craveiro et al. 2009; this work).

A few characters pertaining to the flagellar apparatus are also tentatively marked in Fig. 2. More than the contribution they may provide for the characterization of the groups included, they highlight the need for increasing the number of comparison points within the peridinioids and phylogenetically related groups. Relatively few details are available from Heterocapsaceae, which occupies a sister-group position relative to the peridinioids included in Fig. 2, and nearly no information is available from the phylogenetically related Prorocentrales and Dinophysales. On the other hand, the recognition of meaningful character states for the strutural and ultrastructural features available is not

straighforward and would benefit from a review of current knowledge of the fine-structure of dinoflagellates.

REFERENCES

Bullman V. & Roberts K.R. 1986. Structure of the flagellar apparatus in *Heterocapsa pygmaea* (Pyrrophyta). *Phycologia* 25: 558–571.

Carty S. 2008. *Parvodinium* gen. nov. for the Umbonatum group of *Peridinium* (Dinophyceae). *Ohio Journal of Science* 108: 103–107.

Chacón J. & Gottschling M. 2020. Dawn of the dinophytes: a first attempt to date origin and diversification of harmful algae. *Harmful Algae* 97: Article 101871.

Calado A.J. & Moestrup Ø. 2002. Ultrastructural study of the type species of *Peridiniopsis*, *Peridiniopsis borgei* (Dinophyceae), with special reference to the peduncle and flagellar apparatus. *Phycologia* 41: 567–584.

Calado A.J., Hansen G. & Moestrup Ø. 1999. Architecture of the flagellar apparatus and related structures in the type species of *Peridinium*, *P. cinctum* (Dinophyceae). *European Journal of Phycology* 34: 179–191.

Calado A.J., Craveiro S.C., Daugbjerg N. & Moestrup Ø. 2009. Description of *Tyrannodinium* gen. nov., a freshwater dinoflagellate closely related to the marine Pfiesteria-like species. *Journal of Phycology* 45: 1195–1205.

Craveiro S.C., Calado A.J., Daugbjerg N. & Moestrup Ø. 2009. Ultrastructure and LSU rDNA-based revision of *Peridinium* group palatinum (Dinophyceae) with the description of *Palatinus* gen. nov. *Journal of Phycology* 45: 1175–1194.

Craveiro S.C., Moestrup Ø., Daugbjerg N. & Calado A.J. 2010. Ultrastructure and large subunit rDNA-based phylogeny of *Sphaerodinium cracoviense*, an unusual freshwater dinoflagellate with a novel type of eyespot. *Journal of Eukaryotic Microbiology* 57: 568–585.

Craveiro S.C., Calado A.J., Daugbjerg N., Hansen G. & Moestrup Ø. 2011. Ultrastructure and LSU rDNA-based phylogeny of *Peridinium lomnickii* and description of *Chimonodinium* gen. nov. (Dinophyceae). *Protist* 162: 590–615.

Craveiro S.C., Pandeirada M.S., Daugbjerg N., Moestrup Ø. & Calado A.J. 2013. Ultrastructure and phylogeny of *Theleodinium calcisporum* gen. et sp. nov., a freshwater dinoflagellate that produces calcareous cysts. *Phycologia* 52: 488–507.

Craveiro S.C., Daugbjerg N., Moestrup Ø. & Calado A.J. 2015. Fine-structural characterization and phylogeny of *Peridinium polonicum*, type species of the recently described genus *Naiadinium* (Dinophyceae). *European Journal of Protistology* 51: 259–279.

Craveiro S.C., Daugbjerg N., Moestrup Ø. & Calado A.J. 2016. Studies on *Peridinium aciculiferum* and *Peridinium malmogiense* (=*Scrippsiella hangoei*): comparison with *Chimonodinium lomnickii* and description of *Apocalathium* gen. nov. (Dinophyceae). *Phycologia* 56: 21–35.

Gottschling M., Kretschmann J. & Žerdoner Čalasan A. 2017. Description of Peridiniopsidaceae, fam. nov. (Peridiniales, Dinophyceae). *Phytotaxa* 299: 293–296.

Gottschling M., Chacón J., Žerdoner Čalasan A., Neuhaus S., Kretschmann J., Stibor H. & John U. 2019. Phylogenetic placement of environmental sequences using taxonomically reliable databases helps to rigorously assess dinophyte biodiversity in Bavarian lakes (Germany). *Freshwater Biology* 65: 193–208.

Gottschling M., Czech L., Mahé F., Adl S. & Dunthorn M. 2020. The windblown: possible explanation for dinophyte DNA in forest soils. *Journal of Eukaryotic Microbiology* 68: Article e12833.

Hansen G. & Moestrup Ø. 1998. Fine-structural characterization of *Alexandrium catenella* (Dinophyceae) with special emphasis on the flagellar apparatus. *European Journal of Phycology* 33: 281–91.

Hansen G., Moestrup Ø. & Roberts K.R. 1996. Fine structural observations on *Gonyaulax spinifera* (Dinophyceae), with special emphasis on the flagellar apparatus. *Phycologia* 35: 354–366.

Holzer V.J.C., Kretschmann J., Knechtel J., Owsianny P. & Gottschling M. 2021. Morphological and molecular variability of *Peridinium volzii* Lemmerm. (Peridiniaceae, Dinophyceae) and its relevance for infraspecific taxonomy. *Organisms Diversity and Evolution* 22: 1–15.

Jacobson D.M. & Anderson D.M. 1992. Ultrastructure of the feeding apparatus and myonemal system of the heterotrophic dinoflagellate *Protoperidinium spinulosum*. *Journal of Phycology* 28: 69–82.

Janouškovec J., Gavelis G.S., Burki F., Dinh D., Bachvaroff T.R., Gornik S.G., Bright K.J., Imanian B., Strom S.L., Delwiche C.F. et al. 2017. Major transitions in dinoflagellate evolution unveiled by phylotranscriptomics. *PNAS* 114: E171-E180.

Kretschmann J., Owsianny P.M., Žerdoner Čalasan A. & Gottschling M. 2018. The hot spot in a cold environment: puzzling *Parvodinium* (Peridiniopsidaceae, Peridiniales) from the Polish Tatra Mountains. *Protist* 169: 206–230.

Kretschmann J., Žerdoner Čalasan A., Meyer B. & Gottschling M. 2019 ('2020'). Zero intercalary plates in *Parvodinium* (Peridiniopsidaceae, Peridiniales) and phylogenetics of *P. elpatiewskyi*, comb. nov. *Protist* 171: Article 125700.

Lindberg K., Moestrup Ø. & Daugbjerg N. 2005. Studies on woloszynskioid dinoflagellates I: *Woloszynskia coronata* re-examined using light and electron microscopy and partial LSU rDNA sequences, with description of *Tovellia* gen. nov. and *Jadwigia* gen. nov. (Tovelliaceae fam. nov.). *Phycologia* 44: 416–440.

Logares R. 2007. *Microbial evolution: patterns of diversity in aquatic protists*. PhD thesis, Lund University, Sweden. 160 pp.

Luo Z., Mertens K.N., Gu H., Wang N., Wu Y., Uttayarnmanee P., Pransilpa M. & Roeroe K.A. 2020 ('2021'). Morphology, ultrastructure and molecular phylogeny of *Johsia chumphonensis* gen. *et* sp. nov. and *Parvodinium parvulum* comb. nov. (Peridiniopsidaceae, Dinophyceae). *European Journal of Phycology* 56: 324–336.

Moestrup Ø. & Calado A.J. 2018. Dinophyceae. In: *Süßwasserflora von Mitteleuropa — Freshwater Flora of Central Europe*, vol. 6, ed. 2 (Ed. by B. Büdel, G. Gärtner, L. Krienitz & M. Schagerl), Springer-Verlag, Berlin, 560 pp.

Moestrup Ø. & Daugbjerg N. 2007. On dinoflagellate phylogeny and classification. In: *Unravelling the algae: the past, present, and future of algal systematics* (Ed. by J. Brodie & J. Lewis), CRC Press, Boca Raton, pp. 215–230. (Systematics Association Special Volume No. 75).

Ott B.M., Litaker R.W., Holland W.C. & Delwiche C.F. 2022. Using RDNA sequences to define dinoflagellate species. *PLOS One* 17: Article e0264143.

Pandeirada M.S., Craveiro S.C., Daugbjerg N., Moestrup Ø., Domingues P. & Calado A.J. 2019. Studies on woloszynskioid dinoflagellates X: ultrastructure, phylogeny and colour variation in *Tovellia rubescens* sp. nov. (Dinophyceae). *Journal of Eukaryotic Microbiology* 66: 937–953.

Pandeirada M.S., Craveiro S.C., Daugbjerg N., Moestrup Ø. & Calado A.J. 2021. Fine-structural characterization and phylogeny of *Sphaerodinium* (Suessiales, Dinophyceae), with the

description of an unusual type of freshwater dinoflagellate cyst. *European Journal of Protistology* 78: Article 125770.

Price D.C. & Bhattacharya D. 2017. Robust dinoflagellate phylogeny inferred from public transcriptome databases. *Journal of Phycology* 53: 725–729.

Saldarriaga J.F., Taylor F.J.R., Cavalier-Smith T., Menden-Deuer S. & Keeling P.J. 2004. Molecular data and the evolutionary history of dinoflagellates. *European Journal of Protistology* 40: 85–111.

Taylor F.J.R. 2004. Illumination or confusion? Dinoflagellate molecular phylogenetic data viewed from a primarily morphological standpoint. *Phycological Research* 52: 308–324.

Žerdoner Čalasan A., Kretschmann J. & Gottschling M. 2019. They are young, and they are many: dating freshwater lineages in unicellular dinophytes. *Environmental Microbiology* 21: 4125–4135.